LINEAR AND NONLINEAR VIBRATIONAL CHARACTERISTICS OF OIL LUBRICATED JOURNAL BEARINGS.

by

C. J. Myers, B.Sc.

A thesis submitted in fulfilment of the requirements for the degree of Doctor of Philosophy.

Department of Applied Mathematical Studies,
The University of Leeds.

November, 1981.

Abstract.

This thesis is concerned with an investigation of the vibrational characteristics of oil lubricated journal bearings and, in particular, the instability known as oil whirl, which is a self-excited oscillation induced by the hydrodynamic forces generated in the bearing. The thesis is divided into two parts. In Part 1, linear stability theory is used to determine the critical parameter values at which oil whirl is initiated. This information is conveniently expressed on a two dimensional stability chart, separating regions of stability from those of instability. The vibrational characteristics of a variety of bearing models are contrasted with particular emphasis on the effect of adopting different cavitation boundary conditions at film rupture and the effect of oil film behaviour during journal vibration. An analysis of the single axial groove journal bearing is presented and the effects of groove location and oil supply pressure on the vibrational characteristics of the bearing are examined.

In Part 2, attention is focused on the nonlinear aspects of oil whirl, one objective being to determine the motion of the journal beyond its stability threshold. Several nonlinear techniques are employed to analyse the nonlinear equations of motion and to identify different features (bifurcation theory, multiple scaling, the method of averaging and numerical integration). Particular emphasis is placed on examining the structure of periodic solutions of the equations of motion at and close to the position of neutral stability. It is shown that the onset of oil whirl is a bifurcation phenomenon in which the equilibrium position gives way to a small amplitude whirl orbit (limit cycle). Two different types of bifurcation behaviour are possible, depending on the operating parameters of the bearing. Results obtained from the different nonlinear techniques are contrasted and an assessment is made of how suitable these methods are for examining the phenomenon of oil whirl.

TO SUSAN

and LOUISE

ACKNOWLEDGEMENTS.

The completion of a work of this nature is not possible without a great deal of assistance from many people, to whom I am very grateful. I should like to thank Dr. M. D. Savage and Dr. C. M. Taylor for their supervision, help and encouragement throughout the work and also for their friendship, which I value highly. I should like to express my gratitude to Mr. D. Knapp for his help with the nonlinear aspects of the work, particularly with the Hopf bifurcation theorem discussed in Chapter 5. Thanks are also due to the Science Research Council for their financial support. My wife deserves a special mention, not only for her skill and patience in the typing of this thesis, but also for her support over the last three years, for which I am very grateful.

Chris. Myers. Nov 1981.

Contents

NOTATION

A	journal centre
B_{xx}, B_{xy} B_{yx}, B_{yy}	non-dimensional bearing velocity coefficients
D	bearing diameter
F	bearing load
K_{xx}, K_{xy} K_{yx}, K_{yy}	non-dimensional bearing displacement coefficients
F_r, F_t	radial and tangential hydrodynamic force components
$\bar{F}_r, \bar{F}_t$	non-dimensional force components ($\bar{F}_r = F_r/SF$, etc.)
F_X, F_Y	Cartesian force components
$\bar{F}_X, \bar{F}_Y$	non-dimensional force components ($\bar{F}_X = F_X/SF$, etc.)
L	axial bearing length
O	bearing centre
R	bearing radius
S	Sommerfeld number ($LR^3\omega\mu/Fc^2$)
S_s	modified Sommerfeld number ($RL^3\omega\mu/Fc^2$)
X^1, Y^1	journal centre co-ordinates
X, Y	non-dimensional co-ordinates ($X = X^1/c$, etc.)
$a_1, a_2 \ldots a_{34}$ $b_1, b_2 \ldots b_{34}$	Taylor expansion coefficients
c	bearing radial clearance (R-r)
d	logarithmic decrement
e	journal eccentricity
h	fluid film thickness
2m	journal mass
$\bar{m}$	non-dimensional mass ($mc\omega^2/F$)
p	hydrodynamic pressure
$\bar{p}$	non-dimensional pressure ($c^2p/R^2\omega\mu$)

r	journal radius
t	time
x^1, y^1	journal centre co-ordinates
x, y	non-dimensional co-ordinates ($x=x^1/c$, etc.)
z	axial co-ordinate
α	real part (λ)
θ	angular co-ordinate
λ	eigenvalue
$\bar{\lambda}$	non-dimensional eigenvalue ($\bar{\lambda}=\lambda/\omega$)
μ	lubricant viscosity
$\bar{\mu}$	small parameter
ν	stability parameter ($F/mc\omega^2$)
σ	system parameter ($S/\bar{\omega}$)
τ	non-dimensional time (ωt)
ϕ	attitude angle
ω	rotational speed
$\bar{\omega}$	non-dimensional speed $((mc/F)^{1/2}\omega)$
Ω	whirl frequency
$\bar{\Omega}$	whirl frequency ratio (Ω/ω)

Subscripts

s	refers to steady state conditions
crit	denotes the threshold of instability
$\cdot$	time derivative (d/dt)
$'$	non-dimensional time derivative ($d/d\tau$)

Note

Where the use of a symbol is confined to a short section of the thesis it is defined when it is introduced.

INTRODUCTION.

A basic requirement of any piece of rotating machinery is that it should operate in a stable manner. This is equally true of a shaft of diameter 6mm in a dentist's drill rotating at half a million rpm and a 500MW steam turbine rotating at 3000rpm with a shaft diameter of 600mm. In recent years, with modern technology demanding larger machines operating at greater speeds, much attention has focused on the vibrational characteristics of rotating machinery. A major factor influencing the vibrational characteristics of such machinery is the support bearings which are usually of the journal bearing type.

This thesis is concerned with an investigation of the vibrational characteristics of a simple rotor system mounted symmetrically on two plain, cylindrical, oil lubricated journal bearings. This type of machinery may, under certain conditions, develop an instability due to the oil film in the bearings. The hydrodynamic forces so generated are capable of sustaining a self excited oscillation in which energy is transferred from the rotation of the rotor into a whirling motion of the journal.

Oil whirl, which is the name given to the type of instability mentioned above, occurs above a specific rotor speed (the threshold speed). Once initiated, the instability may take either of two different forms. One possibility is for large amplitude motion in which the journal whirls around the bearing centre at a frequency close to half the running speed (for this reason the instability is often referred to as "half frequency whirl"). This is a dangerous operating condition for the machine since it may result in contact between the bearing and journal surfaces causing excessive wear and a sharp rise in temperature. The second possibility for whirling is a small amplitude motion in which the journal centre whirls around the steady state equilibrium position in a stable closed orbit (limit cycle). Providing the amplitude is not too large this may well be an acceptable operating

condition for the machine. The parameters which determine the form of oil whirl are unclear, this being one of the objectives of the present investigation.

The model under investigation is of a rotor supported on two plain, cylindrical journal bearings (Figure 1). It is assumed that:

i) the rotor is rigid, symmetric and perfectly balanced.

ii) the rotor spins with constant angular velocity about its axis.

iii) the load supported by the bearings is due to gravity and is divided equally between the two bearings.

iv) the bearings are identical and have rigid supports.

v) the hydrodynamic pressure generated in the bearings may be determined by solving the lubrication equation - the Reynolds equation. The assumptions made in deriving the Reynolds equation are given in Chapter 1. To examine the qualitative features of oil whirl two approximate analytic solutions to the Reynolds equation are used throughout this work (see Chapter 1).

A rigid rotor may whirl in two different modes:- cylindrical whirling, in which the two ends of the rotor are in phase (Figure 2(a)) and conical whirling, in which the two ends of the rotor are 180 degrees out of phase (Figure 2(b)). This investigation is confined to cylindrical whirling, which is the most frequently encountered form of whirling. This additional assumption means that every point on the rotor performs the same planar motion, perpendicular to the rotor axis and it is sufficient to consider only one bearing.

The objectives of the investigation are:

i) to examine the role which cavitation plays in determining the vibrational characteristics of the journal with particular emphasis on:

a) the effect of using different cavitation boundary conditions at film rupture.

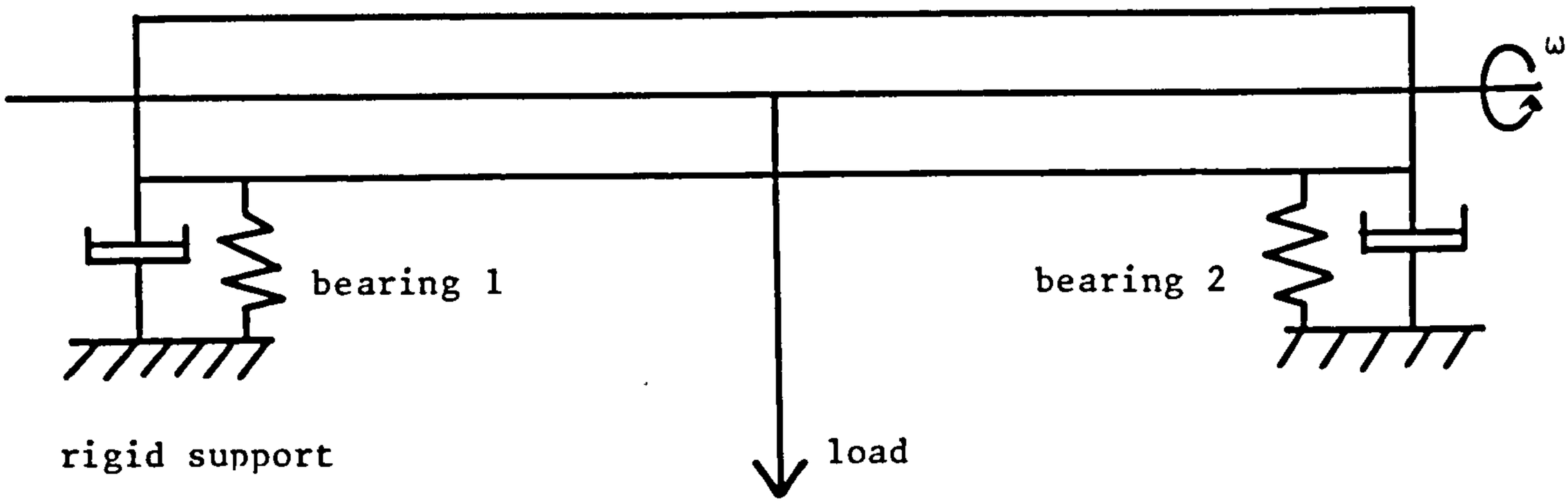

Figure 1. A rigid rotor supported in fluid film bearings. The fluid in the bearings is represented by a spring-dashpot system.

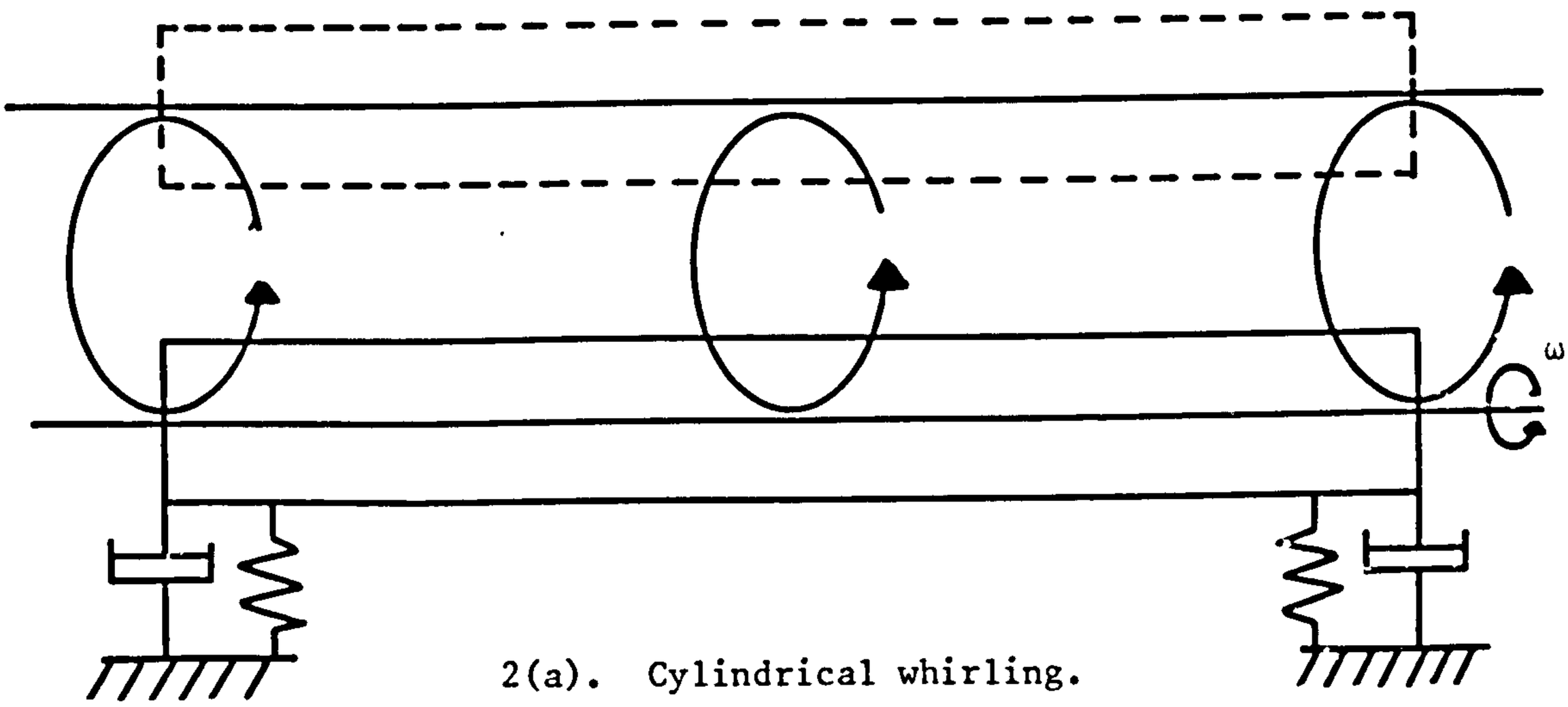

2(a). Cylindrical whirling.

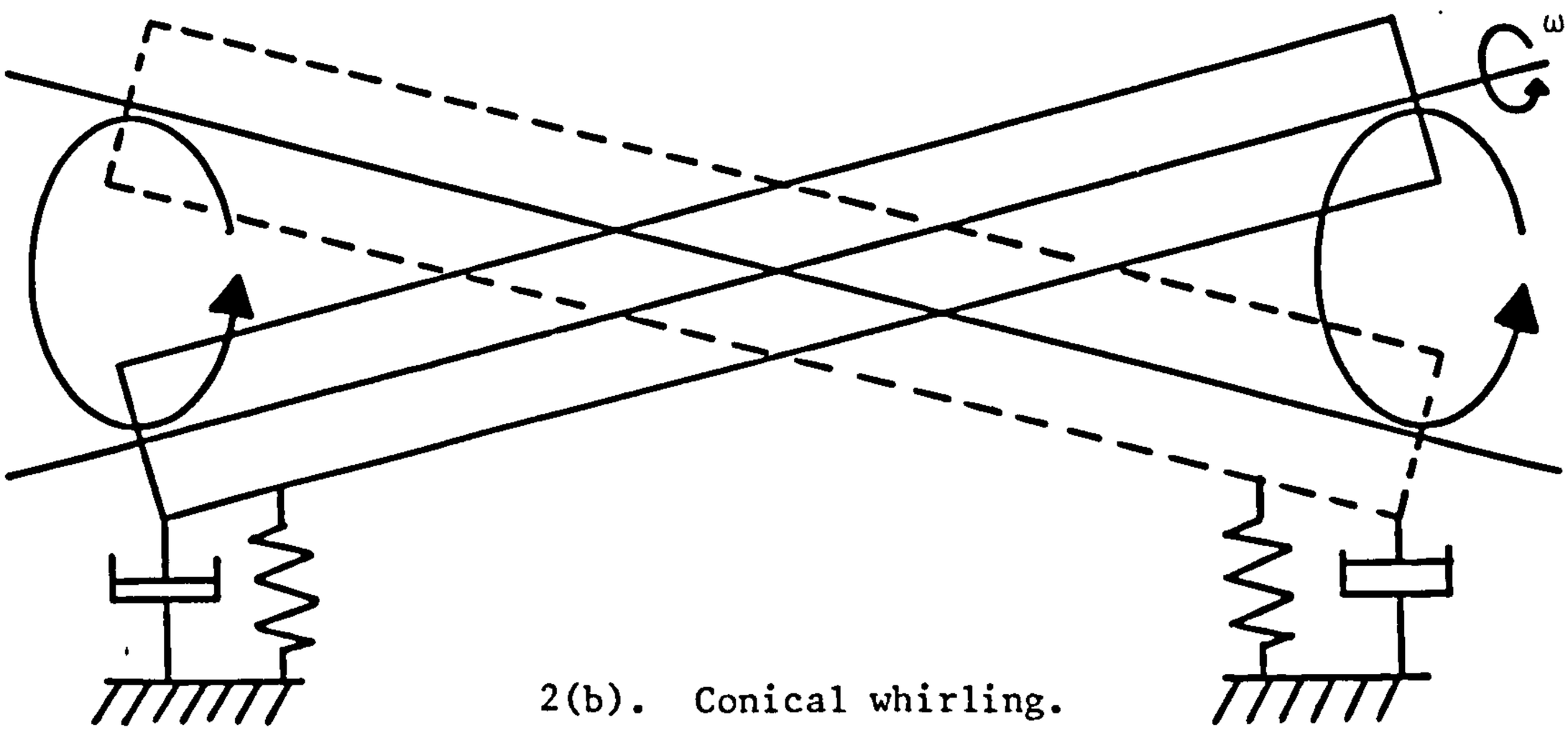

2(b). Conical whirling.

Figure 2. Whirling modes of a rigid rotor supported in fluid film bearings.

b) the behaviour of the oil film during journal vibration.

ii) to investigate the influence of groove position and oil supply pressure on the vibrational characteristics of the single axial groove journal bearing.

iii) to determine the motion of the journal once oil whirl has been initiated and to investigate the factors governing the size and shape of any closed whirl orbits.

This thesis is divided into two parts. Part 1 involves the use of linear stability theory to achieve objectives (i) and (ii). In part 2 the following nonlinear techniques are used to pursue objective (iii):- bifurcation theory, multiple scaling, the method of averaging and numerical integration.

Two further objectives of the present work are:

iv) to assess the limitations of a purely linear approach.

v) to determine the applicability of the various non-linear techniques to the investigation of the phenomenon of oil whirl.

Part 1.

INVESTIGATION OF THE VIBRATIONAL CHARACTERISTICS OF OIL LUBRICATED JOURNAL BEARINGS USING LINEAR STABILITY THEORY.

CHAPTER I

BASIC CONCEPTS AND HISTORICAL REVIEW.

1.1 DESCRIPTION OF A PLAIN JOURNAL BEARING.

A plain journal bearing is shown in Figure 1.1. It consists of a circular shaft rotating within a stationary, circular bearing shell. Under normal operating conditions the journal takes up a position in the bearing which is eccentric to the bearing centre. Thus, the annulus, which is wholly or partially filled with lubricant, is divided into a converging and a diverging region. Lubricant, which is generally forced into the bearing under a small supply pressure, is dragged into the converging film section by the rotation of the journal. Since the lubricant has progressively less space to occupy, fluid film pressure forces are generated which in turn support the applied load. This pressure generating mechanism is the principle upon which hydrodynamic lubrication is based.

The various parameters required to specify the bearing geometry are;

the bearing radius R — the journal radius r

the radial clearance c = R-r — the axial bearing length L.

Two co-ordinates are required to specify the position of the journal centre. They are normally taken to be the eccentricity (e) of the journal centre with respect to the bearing centre and the attitude angle (ϕ), the angle between the direction in which the applied load acts and the line connecting the centres of the journal and the bearing. The eccectricity ratio (ε) is defined as the eccentricity normalised with respect to the radial clearance ($\varepsilon = e/c$). An angular co-ordinate θ is used to locate positions round the bearing relative to the line of centres:-

$\theta = 0(\pi)$ corresponds to the position of maximum (minimum) film thickness.

The film thickness (h) is very small (the ratio c/R is typically 1/1000) and to a good approximation it can be shown that;

$$h = c(1+\varepsilon\cos\theta)$$

1.2 THE REYNOLDS EQUATION.

The equation describing the pressure distribution in a thin film

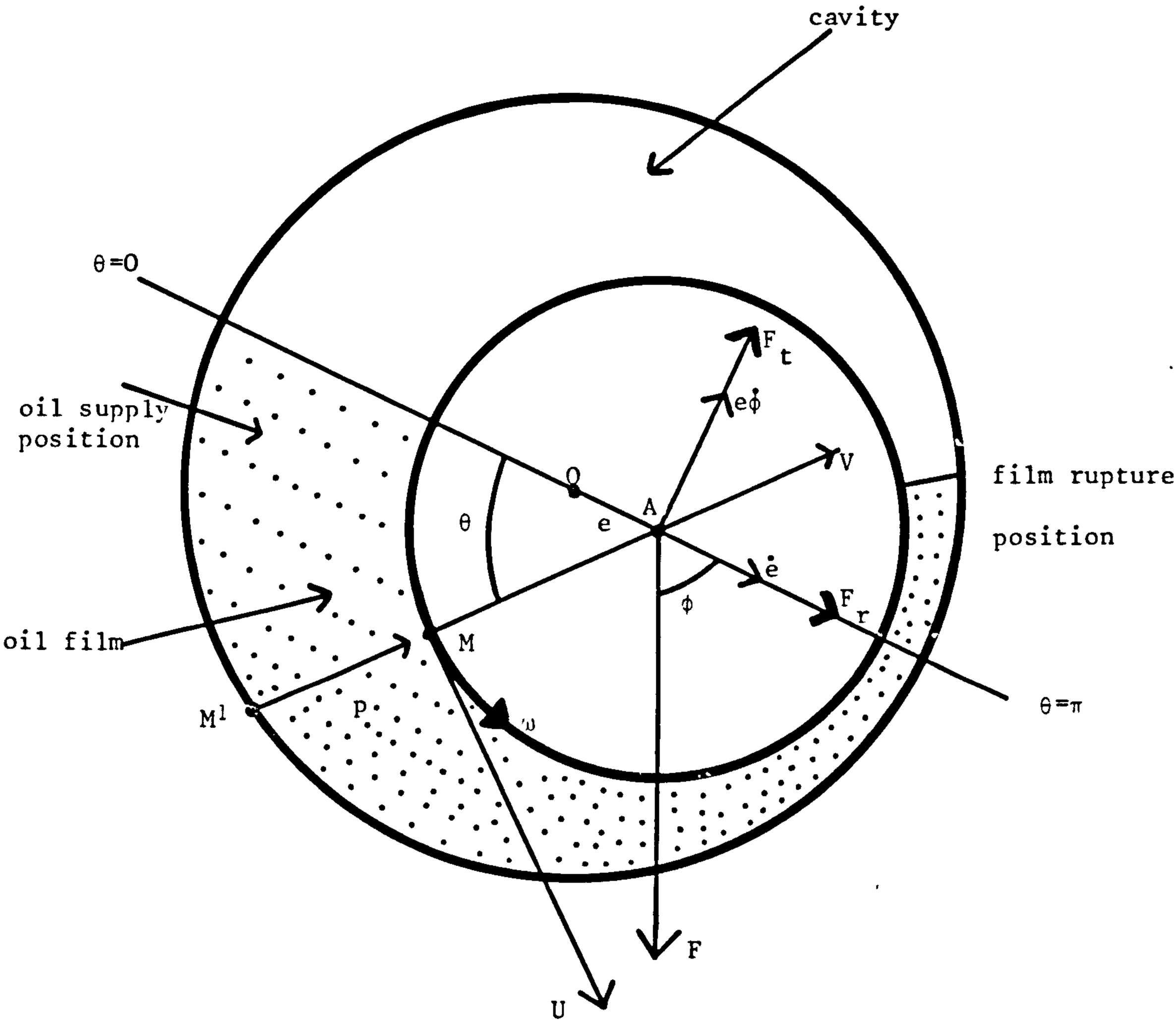

O = bearing centre

A = journal centre

ω = rotational speed

θ = angular co-ordinate

e = journal eccentricity

φ = attitude angle

p = hydrodynamic pressure

F = load

F_r, F_t = hydrodynamic force components

Figure 1.1. Journal bearing under dynamic conditions.

was first derived by Reynolds (1886) and is known as the Reynolds equation. The full Reynolds equation for an incompressible lubricant in the lubrication situation shown in Figure 1.2 is:

$$\frac{\partial}{\partial x}\left(\frac{h^3}{\mu}\frac{\partial p}{\partial x}\right) + \frac{\partial}{\partial z}\left(\frac{h^3}{\mu}\frac{\partial p}{\partial z}\right) = 6U\frac{\partial h}{\partial x} + 12V \qquad (1.1)$$

The co-ordinate system is as shown in Figure 1.2 (with z into the paper); p is the hydrodynamic pressure, μ is the lubricant viscosity, U is the tangential surface velocity and V the normal surface velocity. The terms on the right hand side of equation (1.1) contribute to the generation of pressure in the bearing in different ways:

i) the first term represents the familiar "wedge-shaped" fluid film and arises because the film thickness varies with distance.

ii) the second term represents the variation of film thickness with respect to time and is referred to as the "squeeze film" effect.

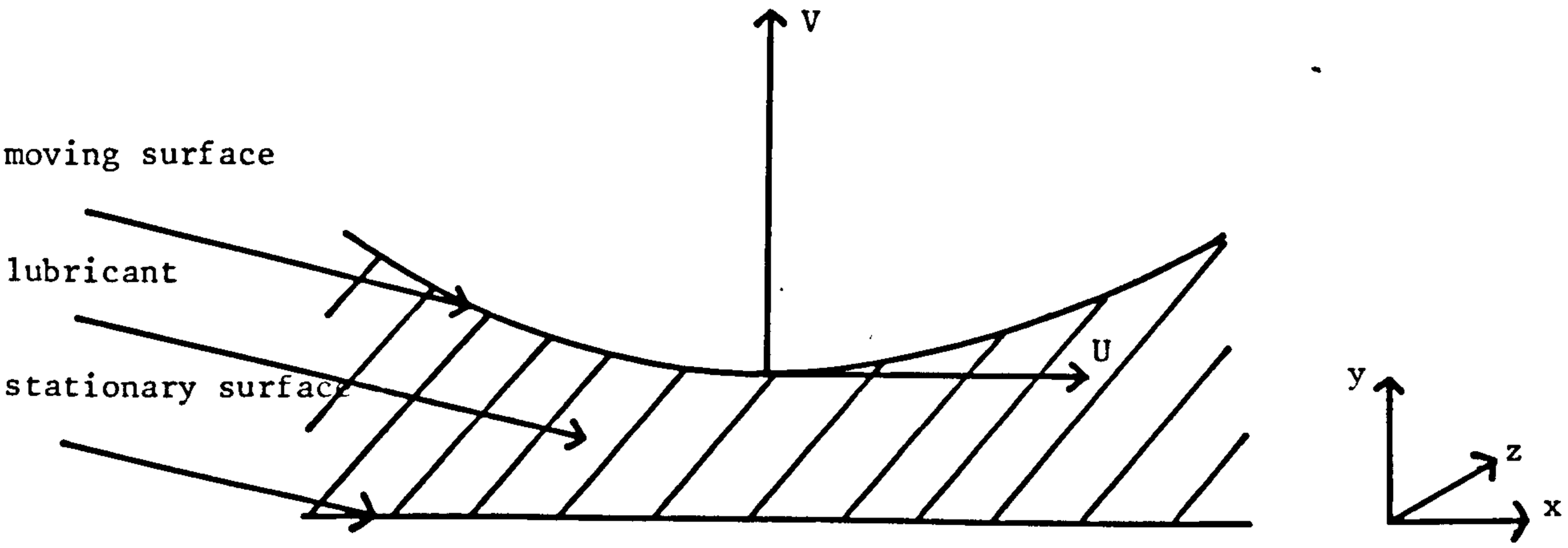

Figure 1.2. A typical lubrication situation.

Equation (1.1) may be derived from the full Navier Stokes equations of motion (Pinkus and Sternlicht (1961)). It is based upon the following assumptions:

i) the film thickness is small and the effect of film curvature may be neglected.

ii) fluid inertia is small compared to the viscous shear.

iii) no external body forces act on the film.

iv) there is no variation of pressure across the oil film ($\partial p/\partial y = 0$).

v) the flow is laminar.

In addition to the assumptions listed above it is assumed throughout this work that the lubricant viscosity remains constant.

To write down the Reynolds equation for a journal bearing, consider a point M on the journal surface at an angular co-ordinate θ (Figure 1.1). M has tangential and normal velocities relative to the point M^1 on the surface of the bearing. These velocities are made up of the components of the velocity of the shaft centre relative to the bearing centre plus the velocity of the surface of the shaft $R\omega$ about its own centre. Thus:

$$U = R\omega + \dot{e}\sin\theta - e\dot{\phi}\cos\theta$$

$$V = \dot{e}\cos\theta + e\dot{\phi}\sin\theta$$

$$\text{also } x = R\theta \text{ and } h = c(1+\varepsilon\cos\theta)$$

Substituting into equation (1.1) yields:

$$\frac{\partial}{\partial\theta}\left\{(1+\varepsilon\cos\theta)^3\frac{\partial p}{\partial\theta}\right\} + R^2\frac{\partial}{\partial z}\left\{(1+\varepsilon\cos\theta)^3\frac{\partial p}{\partial z}\right\}$$

$$= 6\mu\left(\frac{R}{c}\right)^2\left\{-\varepsilon(\omega-2\dot{\phi})\sin\theta + 2\dot{\varepsilon}\cos\theta + O(c/R)\right\} \quad (1.2)$$

The terms of order (c/R) inside the bracket on the right hand side of equation (1.2) are small compared with the remaining terms and are neglected.

Equation (1.2) is a second order partial differential equation for

$p(\theta,z)$. In its complete form it can only be solved numerically for all but the most special cases. The solution of equation (1.2) requires the specification of boundary conditions on pressure and it is here that problems arise since it is rarely clear where the fluid film starts and terminates. The geometry of a journal bearing, being typical of many hydrodynamic lubrication situations, is such that the bearing has a converging and a diverging film section. In general this means the fluid film pressure will be superambient over the converging film section, but will fall below atmospheric in the diverging film section. Consequently the oil film will not be continuous: film rupture will occur and the space between the position of film rupture and film reformation will be filled with a mixture of oil and air. Although a considerable amount of work has been done in this area the exact boundary conditions which determine the film rupture and film reformation positions are not known precisely. Some of the models which have been developed to describe the oil film in the bearing are used in this thesis (see Chapters 2,3 and 4).

There are two approximations of the full Reynolds equation which enable analytic solutions to be obtained.

The Long Bearing Approximation.

This approximation is due to Sommerfeld (1904). It is assumed that the bearing is of sufficient length in the axial direction to neglect the z dependence in equation (1.2), which then reduces to:

$$\frac{d}{d\theta}\left\{(1+\varepsilon\cos\theta)^3 \frac{dp}{d\theta}\right\} = 6\mu\left(\frac{R}{c}\right)^2\left\{-\varepsilon(\omega-2\dot{\phi})\sin\theta + 2\dot{\varepsilon}\cos\theta\right\} \qquad (1.3)$$

The assumption is equivalent to neglecting side leakage in the bearing.

The Short Bearing Approximation.

Short bearing theory was developed by Ocvirk (1953). It is based on the fact that in many applications the bearing is rather short ie. the length to diameter ratio L/D is small (L/D $\simeq \frac{1}{4}$ to $\frac{1}{2}$). Ocvirk assumed

that the pressure gradient in the circumferential direction can be ignored in comparison with the pressure gradient in the axial direction.

$$\text{ie.}\quad \frac{\partial}{\partial\theta}\left[h^3\,\frac{\partial p}{\partial\theta}\right] << \frac{\partial}{\partial z}\left[h^3\,\frac{\partial p}{\partial z}\right]$$

Based on this assumption the Reynolds equation (1.2) reduces to:

$$\frac{\partial}{\partial z}\left\{(1+\varepsilon\cos\theta)^3\,\frac{\partial p}{\partial z}\right\} = 6\,\frac{\mu}{c^2}\left\{-\varepsilon(\omega-2\dot{\phi})\sin\theta + 2\dot{\varepsilon}\cos\theta\right\} \qquad (1.4)$$

Although equations (1.3) and (1.4) are only approximations to the real situation they do provide analytic expressions for the pressure distribution and the force components which are valuable, not only in checking numerical procedures, but in examining the qualitative features of oil whirl. Both long and short bearing theory are used in this thesis.

Having solved a particular version of the Reynolds equation, the hydrodynamic forces are calculated by integrating the pressure distribution over the oil film domain (Ar). It is usual to resolve the forces into two perpendicular components:

i) a radial force component F_r acting along the line connecting the centres of the journal and the bearing.

ii) a tangential force component F_t perpendicular to the line of centres:

Referring to Figure 1.1:

$$F_r = \iint_{Ar} p\cos\theta\; d(Ar) \qquad F_t = \iint_{Ar} p\sin\theta\; d(Ar) \qquad (1.5)$$

1.3 DIFFERENT TYPES OF FLUID FILM INSTABILITY.

Newkirk and Lewis (1956), Pinkus (1956), Hori (1959) and Tondl (1961) have classified unstable whirling of rotor-bearing systems into two different types of motion:

i) half frequency whirl

ii) resonant whip

Sternlicht (1962) has classified three different types of rotor whirl motions:

i) half frequency whirl

ii) fractional frequency whirl

iii) resonant whip

Smith (1970) also found three different types of fluid film instability:

i) light load instability

ii) half frequency whirl

iii) low frequency whirl (similar to resonant whip)

There is general agreement that light load instability as well as fractional frequency whirl are of the same general nature as half frequency whirl. This type of instability is most commonly observed with rigid rotors in plain fluid film bearings and occurs above a specific rotor speed (the threshold speed), which is a function of the stiffness and damping properties of the oil film. The frequency of the whirling motion is typically one half of the rotor speed. This type of instability, which is the subject of this investigation, will be referred to as oil whirl throughout this work.

Resonant whip is a violent whirling of the rotor in its bearings. It is found with flexible rotors in plain fluid film bearings and occurs at rotor speeds above twice the first critical speed in bending of the rotor. The frequency of the whirling motion is typically the first critical speed in bending of the rotor. This type of instability is not investigated in this thesis.

It may therefore be concluded that there are two fundamentally different types of fluid film instability:

i) oil whip

ii) resonant whip

Unfortunately, owing mainly to confusion regarding the names given to these types of instability, they are sometimes confused in the literature.

1.4 HISTORICAL REVIEW.

Fluid film instability was first identified by Newkirk (1924), who subsequently carried out a detailed experimental program involving a parametric study of both rigid and flexible rotor instability (Newkirk (1930,1956,1957), Newkirk and Taylor (1925), Newkirk and Grobel (1934), Newkirk and Lewis (1956).

Both types of fluid film instability were encountered and it is clear that Newkirk was able to distinguish between them. Newkirk (1956) contrasted results obtained previously with a flexible rotor and a rigid rotor. The flexible rotor had a first critical speed in bending of 1210rpm. The rotor whirled over the speed range 2300-5000rpm with a frequency around 1250rpm. The amplitude of the whirl orbit increased with increasing speed. The results were compared with those obtained using a very stiff rotor for which there were no discernible (bending) critical speeds up to 30,000rpm. This shaft whirled at low speeds with a frequency slightly less than half the running speed. It was also noted that the rigid rotor whirl died out at higher speed, which varied from 7,000 to 18,000rpm, an effect which defies a simple explanation.

The first attempt to investigate the motion of a rigid journal within a bearing using hydrodynamic theory was made by Harrison (1919), who derived expressions for the radial and tangential components of the fluid film forces. These expressions were based on the Reynolds assumptions applied to an infinitely long bearing operating with a complete film. Harrison neglected the inertia of the rotor in formulating the equations of motion of the journal and concluded that stable whirl orbits were possible once the journal was displaced from its steady state equilibrium position.

Robertson (1933) reconsidered Harrison's work and formulated the equations of motion for a journal supported in very long bearings, including the inertia of the rotor. Although Robertson was unable to solve the equations of motion to determine the path of the journal, he was able to show qualitatively that the journal was inherently unstable and once whirling commenced the journal spiralled outwards towards the bearing side with a frequency approaching one half of the running speed.

Around the time that oil whip was identified by Newkirk in 1924, Stodola (1925) undertook a theoretical investigation of the influence of the journal bearings on the critical speeds of the rotor. In the course of this investigation both he and Hummel (1926) arrived independently at the conclusion that the fluid film forces in a bearing induce rotor instabilitywhen the journal eccentricity is less than 0.7.

Stodola's model, which neglected subambient pressures in the bearing, was based upon a linearisation of the fluid film forces. It was then possible to calculate the stability of the equilibrium position. The linearisation procedure has subsequently been greatly developed. To illustrate Stodola's analysis let the journal have a mass m and let the journal centre position have Cartesian co-ordinates (x,y). The fluid film force components F_x and F_y depend on the instantaneous position and velocity of the journal centre such that the linearised equations of motion become:

$$m\ddot{x} = F_x(x,y,\dot{x},\dot{y}) = \left(\frac{\partial F_x}{\partial x}\right)x + \left(\frac{\partial F_x}{\partial y}\right)y + \left(\frac{\partial F_x}{\partial \dot{x}}\right)\dot{x} + \left(\frac{\partial F_x}{\partial \dot{y}}\right)\dot{y} \qquad (1.6)$$

$$m\ddot{y} = F_y(x,y,\dot{x},\dot{y}) = \left(\frac{\partial F_y}{\partial x}\right)x + \left(\frac{\partial F_y}{\partial y}\right)y + \left(\frac{\partial F_y}{\partial \dot{x}}\right)\dot{x} + \left(\frac{\partial F_y}{\partial \dot{y}}\right)\dot{y}$$

where the partial derivatives are evaluated at the equilibrium position ($x = y = \dot{x} = \dot{y} = 0$). The equations are two simultaneous second order ordinary differential equations with constant coefficients which are readily tested for stability once the eight partial derivatives are known

(see section 1.5).

Although Stodola's method is correct and simple it presents the problem of obtaining accurate values for the eight Taylor expansion coefficients (the bearing coefficients). Stodola neglected the four velocity coefficients ($\partial F_x/\partial \dot{x}, \partial F_x/\partial \dot{y}$ etc.) and arrived at values for the four displacement coefficients ($\partial F_x/\partial x, \partial F_x/\partial y$ etc.) from an estimate of the functional relationship between the applied load and the steady state equilibrium position of the journal centre.

The interest in the problem of hydrodynamic instability increased considerably after World War II, beginning with Hagg (1946), and has grown ever since, primarily because of the trend towards high-speed machinery. This interest was reflected in a number of experimental investigations carried out in the 1950's (Pinkus (1956), Newkirk and Lewis (1956), Hori (1959), Tondl (1961)). However, experimental investigations are not so numerous as the analytic studies and frequently they are somewhat inconclusive owing to the lack of adequate instrumentation, or failure to recognise the governing system parameters. Furthermore, it is not always clear if extraneous factors have been eliminated totally from the test apparatus (eg. external damping and external vibration sources).

An important contribution to the understanding of hydrodynamic instability was made by Poritsky (1953). He analysed a flexible rotor operating in fluid film bearings. In the first part of his paper he used the long bearing, full film solution to the Reynolds equation, but confined his attention to small eccentricities. He reached the same conclusion as Robertson (1933) that the journal was inherently unstable and would whirl at all rotor speeds. However, Poritsky, unlike Robertson and many of the other early investigators, appreciated the significance of film rupture in the bearings. He postulated that the inclusion of cavitation would introduce a radial force component which is absent when

cavitation is neglected. Poritsky showed that when this term was incorporated into the equations of motion stability was predicted provided:

$$m\omega^2 \left(\frac{1}{K_r} + \frac{1}{K_s}\right) < 4 \text{ or } \omega < 2\omega_1 \qquad (1.7)$$

where K_r and K_s are the rotor stiffness and oil film stiffness respectively, m is the rotor mass, ω the rotational speed and ω_1 the first critical speed of the rotor supported on the oil film. For $\omega > 2\omega_1$, Poritsky showed that the rotor was unstable and would whirl at a frequency equal to ω_1 in accordance with observed performance. This is an important result since it suggests that cavitation, which is generally considered to be an undesirable feature of journal bearings, is nevertheless crucial in providing stability.

Poritsky's analysis neglected the influence of fluid film damping and no attempt was made to determine the value of the fluid film stiffness except to postulate that these would be linear with displacement for small amplitude motions. Later investigations into the elastic and damping properties of the cavitated fluid film (Sternlicht (1959)) verified the existence of the radial force component and also provided values for the velocity and displacement coefficients.

Poritsky's work was extended by Hori (1959) in a particularly lucid investigation of hydrodynamic instability in fluid film bearings. Hori's model was similar to Poritsky's. Hori used the long bearing approximation to solve the Reynolds equation and allowed for cavitation by assuming that the oil film only occupied the converging film section of the bearing. Having formulated the equations of motion of the rotor, Hori analysed small amplitude vibrations by linearising the equations about the steady state equilibrium position. The linearised equations were then tested for stability by using Routh's criterion which led to the condition:

$$\frac{F}{mc\omega^2} > K_1(\varepsilon_s)\left[K_2(\varepsilon_s) + \frac{1}{\omega_1^2}\left(\frac{F}{mc}\right)\right] \quad \text{for stability} \qquad (1.8)$$

where F is the load supported by the bearing

m is the rotor mass

c is the radial clearance

ε_s is the steady state value of the eccentricity ratio

ω_1 is the first critical speed in bending of the rotor (by itself).

The quantities K_1 and K_2 are functions only of the steady state eccentricity ratio. The stability condition described by equation (1.8) may be expressed as a two dimensional stability chart with axes $F/mc\omega^2$ and ε_s. A different stability borderline, which separates regions of stability from those of instability, is obtained for each value of $1/\omega_1^2$ (F/mc). Hori's stability chart is reproduced in Figure 1.3. Such a stability chart may be used to determine whether or not a rotor will run stably at a given rotor speed. It can also be seen that a rotor is always stable above an eccentricity ratio of 0.8 and that the threshold of instability for a flexible rotor is lower than for a rigid rotor.

Hori then examined the stability of large amplitude vibrations such that the shaft bends considerably and the journal centre rotates about the bearing centre. He showed that large amplitude vibrations (resonant whip) could not occur below a speed of twice the first critical speed in bending of the rotor. Although Hori's analysis of the large amplitude motion is based on some dubious assumptions, his results did enable him to explain successfully several observations made by Newkirk and Lewis (1956) and Pinkus (1956). He also obtained modest agreement with his own experimental results.

Up to the 1950's the only available solution of the Reynolds equation was that for the long bearing approximation. Ocvirk's short bearing theory was developed in 1953 and it subsequently became fashionable to use short bearing solutions (eg. Holmes (1960), Huggins (1963-64),

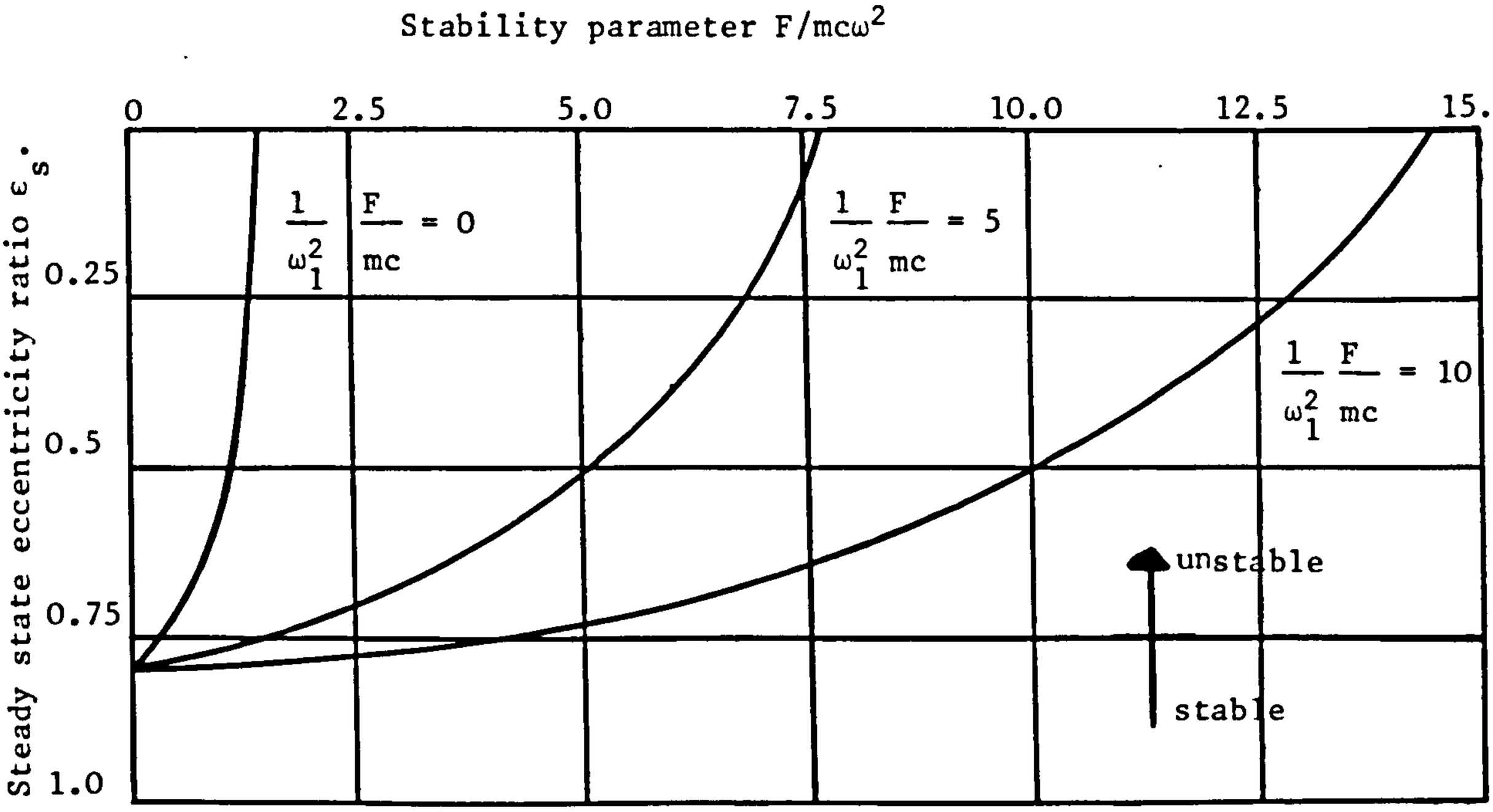

Figure 1.3. Hori's stability chart

Lund (1966)). In one of the first investigations, Holmes (1960) analysed the vibrational characteristics of a rigid rotor supported on two short journal bearings. He allowed for cavitation by assuming the lubricant only occupied the converging film section of the bearing. He adopted the now well-tested procedure of linearising the hydrodynamic forces about the steady state equilibrium position to obtain the eight bearing coefficients and tested for stability by using Routh's criterion. Holmes presented his results in terms of a two dimensional stability chart similar to the approach adopted by Hori (1959).

With the development of high-speed digital computers in the early 1960's it became possible to solve the full Reynolds equation by the finite difference method. The eight bearing coefficients and stability curves were presented by Lund (1966) for bearings with a range of L/D ratios. Several numerical methods were developed in the early 1970's to determine the bearing coefficients for bearings with finite L/D ratios

(Woodcock and Holmes (1970), Lundholm (1971), Lund and Thomsen (1978)). These methods are discussed in Chapter 4. This work has led to a wide variety of different bearing geometries being examined (Allaire (1980), Ruddy (1980)).

Most of the recent experiments on rotor stability have been performed in connection with the validation of computer programs for stability analysis. One such experimental study was made by Lund and Tonnesen (1978). Experiments were conducted on two rotor systems having the following details:

	Rotor 1	Rotor 2
Rotor mass	40kg	187.5kg
Rotor length	1040mm	1190mm
Bearing span	880mm	880mm
Shaft diameter	80mm	80mm
Journal diameter	62.7mm	62.7mm

Two types of bearings and supports were tested:

i) rigid bearing with axial grooves.

ii) cylindrical bearing mounted on a flexible support with a squeeze film damper.

Lund and Tonnesen calculated the stability threshold and whirl frequency ratio by a computer program and verified the predicted results experimentally with the two rotors described above. For the heavier rotor, the stability threshold in rigidly mounted bearings was found to be 12,600rpm. The use of flexible foundations with a squeeze film damper enabled the same rotor to be operated at its maximum speed of 20,000rpm without any indication of instability.

Lund and Tonnesen obtained the following conclusions from their test program:

i) the experiments confirmed the general validity of using an analytic

model to predict the threshold speed and whirl frequency of a rotor-bearing system. The linear model predicted the instability threshold in good agreement with the experimental findings. Discrepancies can more readily be ascribed to other causes than deficiencies in the analytic model.

ii) unbalance vibrations were found to initiate a self-excited whirl, with the result that the instability threshold speed was lowered.

iii) unstable whirling was itself found to excite a spectrum of frequencies in the rotor system but the whirl orbit was a stationary limit cycle, associated with a single frequency. If a large limit cycle amplitude can be accepted it is feasible to operate the test rotors past the onset of instability. In practice, however, the threshold speed should be considered the maximum acceptable speed.

iv) the addition of flexibility and damping to the foundation is the crucial point in the suppression of instability for a rotor-bearing system.

In recent years attention has also focused on the nonlinear aspects of oil whirl. This interest has arisen from the observation that several machines have operated successfully at speeds considerably in excess of the instability threshold speed (Newkirk and Lewis (1956), Mitchell, Holmes and Byrne (1965-66), Tondl (1965)). It has been suggested that the nonlinearity of the hydrodynamic forces may be the stabilizing factor in the sense that, even if the steady state equilibrium position becomes unstable and therefore whirl is initiated, the whirl amplitude does not grow without bounds, but whirls in a closed orbit (limit cycle).

Most of the investigations which have included nonlinear effects have been based upon numerical integration of the equations of motion using either:

i) standard step-by-step marching techniques (eg. Runge-Kutta) on a digital computer (Reddi and Trumpler (1962), Mitchell, Holmes and Byrne (1965-66), Tolle and Muster (1969), Badgley and Booker (1969), McKay (1981)).

ii) an analogue computer (Jennings (1960), Huggins (1963-64), Mitchell, Holmes and Byrne (1965-66)).

Mitchell, Holmes and Byrne (1965-66) performed a numerical investigation of the nonlinear equations of motion using both long and short bearing theory. They assumed the oil film was complete and integrated the equations using both an analogue and a digital computer. Whirl orbits were shown for a large range of parameter values. From their detailed investigations the authors concluded that the journal was inherently unstable for all rotor speeds and spiralled outwards towards the bearing side at a frequency close to half the running speed. This work confirmed the much earlier work of Robertson (1933) and Poritsky (1953), who had reached the same conclusion using linear techniques.

It is of interest to note, however, that both Reddi and Trumpler (1962) and Tolle and Muster (1969), who both analysed a bearing with a complete film, did not reach this conclusion. Under certain conditions they found that stable whirl orbits did exist for $\varepsilon < 1$. The vibrational characteristics of bearings with complete films are discussed in Chapter 2 as a starting point for this investigation. This work confirmed the results of Mitchell, Holmes and Byrne (1965-66) and McKay (1981).

These discrepancies illustrate the limitations of a purely numerical approach. The difficulties of using a digital computer are that many time steps are needed to determine the journal path with the result thaterrors accumulate. The difficulty of using an analogue computer is that it is difficult to simulate exactly the fluid film forces. It is evident that where it is possible more rigorous mathematical techniques should be employed in order to verify the numerical results and to highlight the important regions of parameter space.

Surprisingly the author has found only a few numerical studies which have included nonlinear effects and allowed for cavitation. Badgley and Booker (1969) investigated the stability of plane cylindrical motion

of a rotor supported in plain, cylindrical journal bearings. They obtained expressions for the hydrodynamic forces by using long bearing theory, short bearing theory and Warner's finite length bearing approximation to the Reynolds equation (Warner (1963)). They included the effect of film rupture by considering only the superambient pressure region. The nonlinear equations of motion were solved on a digital computer. Results were presented only in terms of a two dimensional stability borderline. For given initial conditions they determined whether or not the journal spiralled into or away from the equilibrium position. Not surprisingly the stability borderlines which they presented were in very good agreement with those obtained using linear theory. Badgley and Booker did not address themselves to the more interesting problem as to the motion of the journal above the threshold speed.

Other nonlinear investigations which have included the effect of film rupture (Jennings (1960), Huggins (1963-64), Someya (1963-64)) are somewhat inconclusive owing to the difficulties already mentioned and the number of parameters involved.

An alternative technique to numerical integration was developed by Lund (1966). By employing the method of averaging to solve the nonlinear equations of motion he was able to determine the size and orientation of any closed whirl orbits directly, not as a result of transient growth or decay. Lund presented results for the short bearing although in principle it can be employed with any bearing type.

Broadly speaking the approach adopted by Lund is followed in this thesis, ie.:

i) determine the onset of instability using linear theory

ii) and then employ a combination of numerical and analytic techniques to solve the nonlinear equations of motion as the speed is altered away from the threshold speed.

Lund found that stable small amplitude whirl orbits could exist at

speeds both above and below the threshold speed, but were confined to a narrow speed range about the threshold speed. The method of averaging, together with Lund's results, is discussed fully in Chapter 7.

Summary.

The various investigations of fluid film instability cited above may be conveniently classified into four categories:

i) qualitative studies.

ii) evaluation of the threshold of instability by linearising the equations of motion.

iii) studies of nonlinear effects.

iv) experimental investigations.

The important contributions to each of these categories are listed in Table 1.1. The list is not meant to be a complete bibliography of the subject.

1.5 GENERAL THEORY OF LINEAR STABILITY ANALYSIS.

For a journal of mass 2m, with a load of 2F, the equations of motion are, in polar co-ordinates (e, ϕ):

$$m\left[\frac{d^2e}{dt^2} - e\left(\frac{d\phi}{dt}\right)^2\right] = F\cos\phi + F_r\left(e, \frac{de}{dt}, \phi, \frac{d\phi}{dt}\right) \qquad (1.9)$$

$$m\left[e\frac{d^2\phi}{dt^2} + 2\frac{de}{dt}\frac{d\phi}{dt}\right] = -F\sin\phi + F_t\left(e, \frac{de}{dt}, \phi, \frac{d\phi}{dt}\right)$$

(see Figure 1.1).

In general, the hydrodynamic force components are nonlinear functions of the journal centre's displacement and velocity.

The equations may be non-dimensionalised by substituting:

$$\varepsilon = \frac{e}{c} \quad \tau = \omega t \quad \bar{F}_r = \frac{F_r}{SF} \quad \bar{F}_t = \frac{F_t}{SF} \quad \nu = \frac{F}{mc\omega^2} \quad S = \frac{LR^3\omega\mu}{Fc^2} \qquad (1.10)$$

S is a non-dimensional bearing parameter referred to as the Sommerfeld number. The non-dimensional equations of motion are:

Qualitative studies	Evaluation of the threshold of instability by linearising the equations of motion	Studies of nonlinear effects	Experimental investigations
Robertson (1933)	Stodola (1925)	Jennings (1960)	Newkirk and Taylor (1925)
Hagg (1946)	Hummel (1926)	Reddi and Trumpler (1962)	Newkirk and Grobel (1934)
Poritsky (1953)	Hagg (1946)	Huggins (1963-64)	Newkirk and Lewis (1956)
Cameron (1955)	Hagg and Warner (1953)	Someya (1963-64)	Cameron and Solomon (1957)
Pinkus and Sternlicht (1961)	Poritsky (1953)	Mitchell, Holmes and Byrne (1965-66)	Boeker and Sternlicht (1956)
Smith (1963,1970)	Sternlicht (1959)	Lund (1966,1980)	Pinkus (1956)
Sternlicht and Rieger (1967-68)	Hori (1959)	Tolle and Muster (1969)	Hori (1959)
	Holmes (1960,1963,1966)	Badgley and Booker (1969)	Tondl (1965)
	Lund (1966)	Rieger and Thomas (1976)	Lund and Tonnesen (1978)
	Woodcock and Holmes (1970)	McKay (1981)	
	Lund and Thomsen (1978)		
	Lundholm (1969,1971,1973)		
	Craighead (1976)		
	Allaire (1980)		
	Ruddy (1980)		

Table 1.1. Summary of work on fluid film instability of rotors in bearings.

$$\ddot{\varepsilon} - \varepsilon\dot{\phi}^2 = \nu\left\{\cos\phi + S\bar{F}_r(\varepsilon,\dot{\varepsilon},\phi,\dot{\phi})\right\} \tag{1.11}$$

$$\varepsilon\ddot{\phi} + 2\dot{\varepsilon}\dot{\phi} = -\nu\left\{\sin\phi - S\bar{F}_t(\varepsilon,\dot{\varepsilon},\phi,\dot{\phi})\right\}$$

The steady state solution to equation (1.11) is:

$$\cos\phi_s = -S\bar{F}_{rs} \qquad \sin\phi_s = S\bar{F}_{ts} \tag{1.12}$$

$$\Rightarrow \quad \tan\phi_s = \bar{F}_{ts}/-\bar{F}_{rs} \qquad S = (\bar{F}_{rs}^2 + \bar{F}_{ts}^2)^{-1/2} \tag{1.13}$$

denoting steady state conditions by the subscript "s".

Since equations (1.11) are nonlinear, it is not possible to solve them analytically without first simplifying them. During a small amplitude vibration of the journal about its equilibrium position (Figure 1.4):

$$\varepsilon \to \varepsilon_s + \delta, \ \phi \to \phi_s + \gamma \quad (\delta << \varepsilon_s, \ \gamma << 1) \tag{1.14}$$

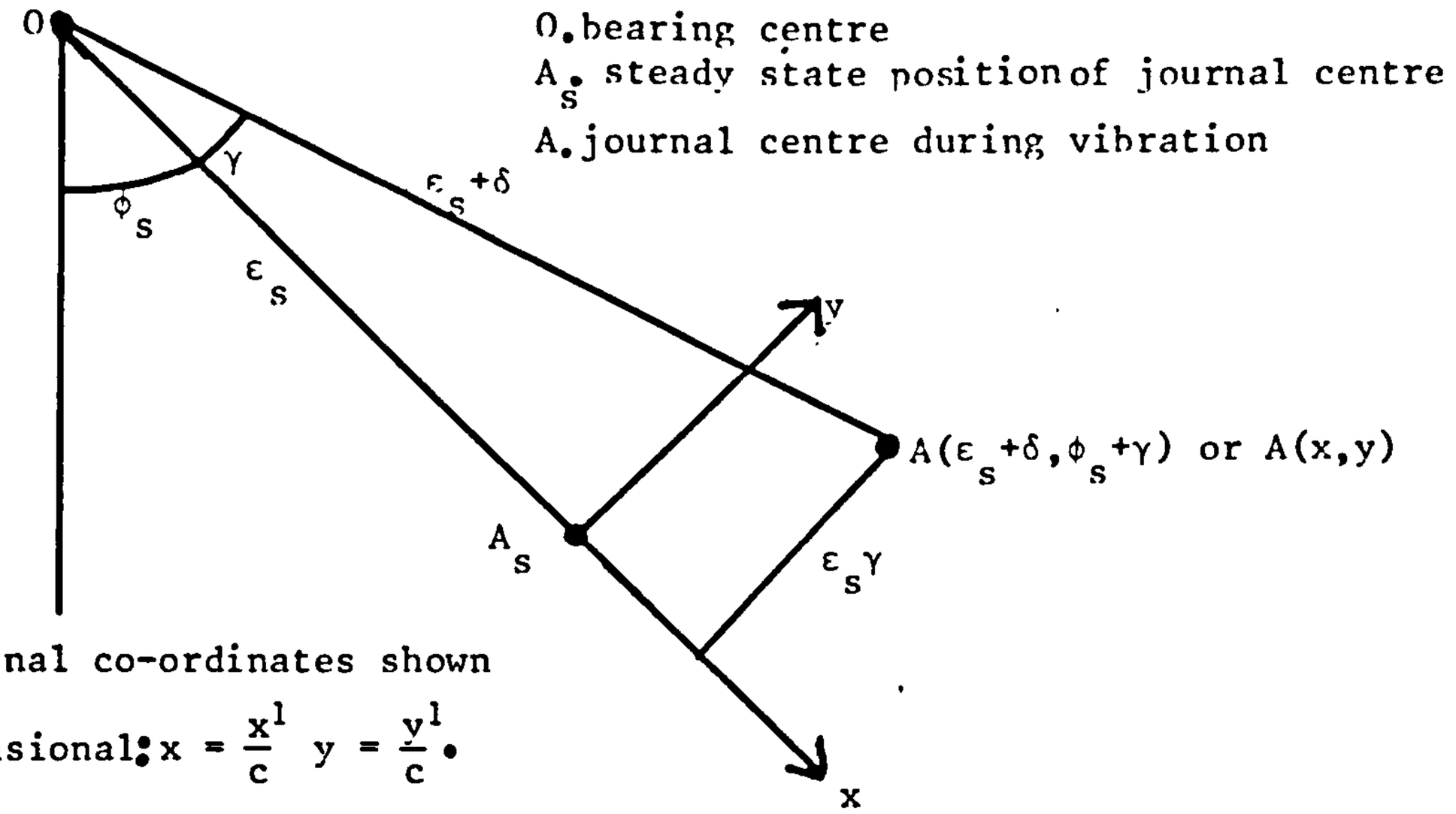

nb. the journal co-ordinates shown are nondimensional: $x = \frac{x^1}{c}$ $y = \frac{y^1}{c}$.

Figure 1.4. Journal centre during small amplitude vibration about its steady state equilibrium position.

Substituting equations (1.14) into equations (1.11), neglecting terms higher than the first order and expanding the force components in a first order Taylor expansion yields:

$$\delta'' - \nu S \left(\frac{\partial \bar{F}_r}{\partial \varepsilon}\right)_s \delta' - \nu \frac{S}{\varepsilon_s}\left(\frac{\partial \bar{F}_r}{\partial \phi}\right)_s (\varepsilon_s \gamma') - \nu S \left(\frac{\partial \bar{F}_r}{\partial \varepsilon}\right)_s \delta - \nu \frac{S}{\varepsilon_s}\left(-\bar{F}_{ts} + \frac{\partial \bar{F}_r}{\partial \phi}\right)_s (\varepsilon_s \gamma) = 0$$

$$\varepsilon_s \gamma'' - \nu S \left(\frac{\partial \bar{F}_t}{\partial \varepsilon}\right)_s \delta' - \nu \frac{S}{\varepsilon_s}\left(\frac{\partial \bar{F}_t}{\partial \phi}\right)_s (\varepsilon_s \gamma') - \nu S \left(\frac{\partial \bar{F}_t}{\partial \varepsilon}\right)_s \delta - \nu \frac{S}{\varepsilon_s}\left(\bar{F}_{rs} + \frac{\partial \bar{F}_t}{\partial \phi}\right)_s (\varepsilon_s \gamma) = 0 \quad (1.15)$$

It is convenient, at this stage, to introduce a Cartesian co-ordinate system (x,y), centred upon the steady state position of the journal centre. The x-axis is taken along the line connecting the centres of the bearing and the journal (in equilibrium) and the y-axis is perpendicular to this line. (Figure 1.4).

Thus $x \simeq \delta$ and $y \simeq \varepsilon_s \gamma$ for small journal displacements from the equilibrium position. (1.16)

Introduce the following notation:

$$B_{xx} = -S\left(\frac{\partial \bar{F}_r}{\partial \varepsilon}\right)_s \quad B_{xy} = -\frac{S}{\varepsilon_s}\left(\frac{\partial \bar{F}_r}{\partial \phi}\right)_s \quad B_{yx} = -S\left(\frac{\partial \bar{F}_t}{\partial \varepsilon}\right)_s \quad B_{yy} = -\frac{S}{\varepsilon_s}\left(\frac{\partial \bar{F}_t}{\partial \phi}\right)_s \quad (1.17)$$

$$K_{xx} = -S\left(\frac{\partial \bar{F}_r}{\partial \varepsilon}\right)_s \quad K_{xy} = -\frac{S}{\varepsilon_s}\left(-\bar{F}_{ts} + \frac{\partial \bar{F}_r}{\partial \phi}\right)_s \quad K_{yx} = -S\left(\frac{\partial \bar{F}_t}{\partial \varepsilon}\right)_s \quad K_{yy} = -\frac{S}{\varepsilon_s}\left(\bar{F}_{rs} + \frac{\partial \bar{F}_t}{\partial \phi}\right) \quad (1.18)$$

Equations (1.17) and (1.18) define the eight bearing coefficients, which consist of four velocity coefficients (equation 1.17) and four displacement coefficients (equation 1.18). The linearised equations of motion (equations 1.15) may now be written in the form:

$$\begin{aligned} x'' + \nu B_{xx} x' + \nu B_{xy} y' + \nu K_{xx} x + \nu K_{xy} y &= 0 \\ y'' + \nu B_{yx} x' + \nu B_{yy} y' + \nu K_{yx} x + \nu K_{yy} y &= 0 \end{aligned} \quad (1.19)$$

Seeking a solution of the form:

$$x = x_o e^{\bar{\lambda}\tau} \qquad y = y_o e^{\bar{\lambda}\tau} \quad (1.20)$$

leads to the characteristic equation:

$$\bar{\lambda}^4 + \nu(B_{xx}+B_{yy})\bar{\lambda}^3 + \nu\{(K_{xx}+K_{yy}) + \nu(B_{xx}B_{yy}-B_{xy}B_{yx})\}\bar{\lambda}^2 \qquad (1.21)$$

$$+ \nu^2\{B_{xx}K_{yy}+B_{yy}K_{xx}-B_{xy}K_{yx}-B_{yx}K_{xy}\}\bar{\lambda} + \nu^2\{K_{xx}K_{yy}-K_{xy}K_{yx}\} = 0$$

The equation may be written:

$$\bar{\lambda}^4 + B\bar{\lambda}^3 + C\bar{\lambda}^2 + D\bar{\lambda} + E = 0 \qquad (1.22)$$

The stability of the equilibrium position is determined by an application of Routh's criterion, which for a quartic equation is:

"A necessary and sufficient condition for the quartic equation (1.22) to have all four roots with negative real parts is:

i) $B > 0$.

ii) $C > 0$.

iii) $D > 0$.

iv) $E > 0$. (1.23)

v) $R = D(BC-D) - B^2E > 0$." Hartog (1947).

Thus, for equation (1.21), the stability conditions are:

i) $\nu(B_{xx}+B_{yy}) > 0$.

ii) $\nu\{(K_{xx}+K_{yy}) + \nu(B_{xx}B_{yy}-B_{xy}B_{yx})\} > 0$.

iii) $\nu^2\{B_{xx}K_{yy}+B_{yy}K_{xx}-B_{xy}K_{yx}-B_{yx}K_{xy}\} > 0$. (1.24)

iv) $\nu^2\{K_{xx}K_{yy}-K_{xy}K_{yx}\} > 0$.

v) $R = \nu^4\{B_{xx}K_{yy}+B_{yy}K_{xx}-B_{xy}K_{yx}-B_{yx}K_{xy}\}\{(K_{xx}+K_{yy})+\nu(B_{xx}B_{yy}-B_{xy}B_{yx})\}(B_{xx}+B_{yy})$

$$- \nu^4\{B_{xx}K_{yy}+B_{yy}K_{xx}-B_{xy}K_{yx}-B_{yx}K_{xy}\}^2 - \nu^4(B_{xx}+B_{yy})^2\{K_{xx}K_{yy}-K_{xy}K_{yx}\} > 0$$

In the vast majority of cases, the first four conditions are automatically satisfied and the fifth condition becomes a condition on ν for stability; namely that:

$$\nu > \frac{\dfrac{(B_{xx}+B_{yy})(K_{xx}K_{yy}-K_{xy}K_{yx})}{(B_{xx}K_{yy}+B_{yy}K_{xx}-B_{xy}K_{yx}-B_{yx}K_{xy})} - \dfrac{(B_{xx}K_{xx}+B_{yy}K_{yy}+B_{xy}K_{yx}+B_{yx}K_{xy})}{(B_{xx}+B_{yy})}}{(B_{xx}B_{yy}-B_{xy}B_{yx})} \qquad (1.25)$$

for stability

$$\text{or } \nu > \nu_{crit} \text{ for stability.} \qquad (1.26)$$

Extensive use of the stability condition described by equation (1.25) is made throughout Part 1 of this thesis.

At the position of neutral stability, two of the eigenvalues are purely imaginary:

$$\text{ie. at } \nu = \nu_{crit} \quad \bar{\lambda} = \pm i\bar{\Omega}_{crit}$$

Substituting into equation (1.21):

$$\Rightarrow \bar{\Omega}_{crit} = \left\{\frac{(B_{xx}K_{yy}+B_{yy}K_{xx}-B_{xy}K_{yx}-B_{yx}K_{xy})\nu_{crit}}{(B_{xx}+B_{yy})}\right\}^{1/2} \qquad (1.27)$$

from which the critical value of the whirl frequency ratio may be calculated.

For $\nu > \nu_{crit}$, the journal is stable to small perturbations from its equilibrium position. The degree of stability may be measured by calculating the logarithmic decrement associated with each mode of vibration. For example, suppose that:

$$\nu > \nu_{crit} \Rightarrow \bar{\lambda} = -\bar{\alpha} \pm i\bar{\Omega}, \ \bar{\lambda} = -\bar{\beta} \pm ib \text{ with } \bar{\beta} >> \bar{\alpha} > 0.$$

In this case, the degree of stability may be measured by calculating the logarithmic decrement associated with the first pair of roots:

$$\text{logarithmic decrement, } d = \frac{2\pi}{\bar{\Omega}}\ \bar{\alpha} \qquad (1.28)$$

The logarithmic decrement represents the logarithm of the decay in the amplitude of the vibration during one period of the oscillation ($2\pi/\bar{\Omega}$). The larger the value of d, the greater the stability of the journal. Conversely, if d is negative, it may be used to measure the degree of

instability.

Note.

It is important to remember that the linearised equations of motion are valid only for small amplitude journal motion about the equilibrium position.

CHAPTER 2

THE VIBRATIONAL BEHAVIOUR OF JOURNAL BEARINGS OPERATING WITH COMPLETE FILMS.

In this Chapter an investigation of the vibrational characteristics of a journal bearing operating with a complete film is made (Figure 2.1). Long and short bearing theory are used and it is shown that both models lead to the same conclusion - the steady state equilibrium position is unstable. This result is well known and has been shown several times (eg. Poritsky (1953), Holmes (1963)). The analysis is repeated here since it is appropriate to begin with a study of the simplest model. It is also important to understand the deficiencies of any mathematical model when compared to the real physical situation. It is the task of the applied mathematician to try and eliminate these deficiencies by refining the model.

2.1 AN ANALYSIS USING LONG BEARING THEORY.

The Reynolds equation for a long bearing was shown in Chapter 1 to be:

$$\frac{d}{d\theta}\left\{(1+\varepsilon\cos\theta)^3\frac{dp}{d\theta}\right\} = 6\mu\left(\frac{R}{c}\right)^2\left\{(2\dot{\phi}-\omega)\varepsilon\sin\theta+2\dot{\varepsilon}\cos\theta\right\} \qquad (2.1)$$

This equation may be integrated twice using:

i) the appropriate boundary conditions; $p=0$ at $\theta=0, 2\pi$, which model a complete film.

ii) the Sommerfeld substitution $1+\varepsilon\cos\theta = \frac{1-\varepsilon^2}{1-\varepsilon\cos\psi}$.

Details of the substitution, together with a list of integrals required throughout this work, may be found in Appendix I.

The pressure distribution may be re-written in terms of θ as:

$$\left(\frac{c}{R}\right)^2\frac{p}{\mu\omega} = \frac{6\varepsilon(1-2\dot{\phi})(2+\varepsilon\cos\theta)\sin\theta}{(2+\varepsilon^2)(1+\varepsilon\cos\theta)^2} + 6\left\{\frac{1}{(1+\varepsilon\cos\theta)^2} - \frac{1}{(1+\varepsilon)^2}\right\}\frac{\dot{\varepsilon}}{\varepsilon} \qquad (2.2)$$

The hydrodynamic forces generated in the bearing are calculated by integrating the pressure distribution over the bearing in two perpendicular directions (Figure 2.1).

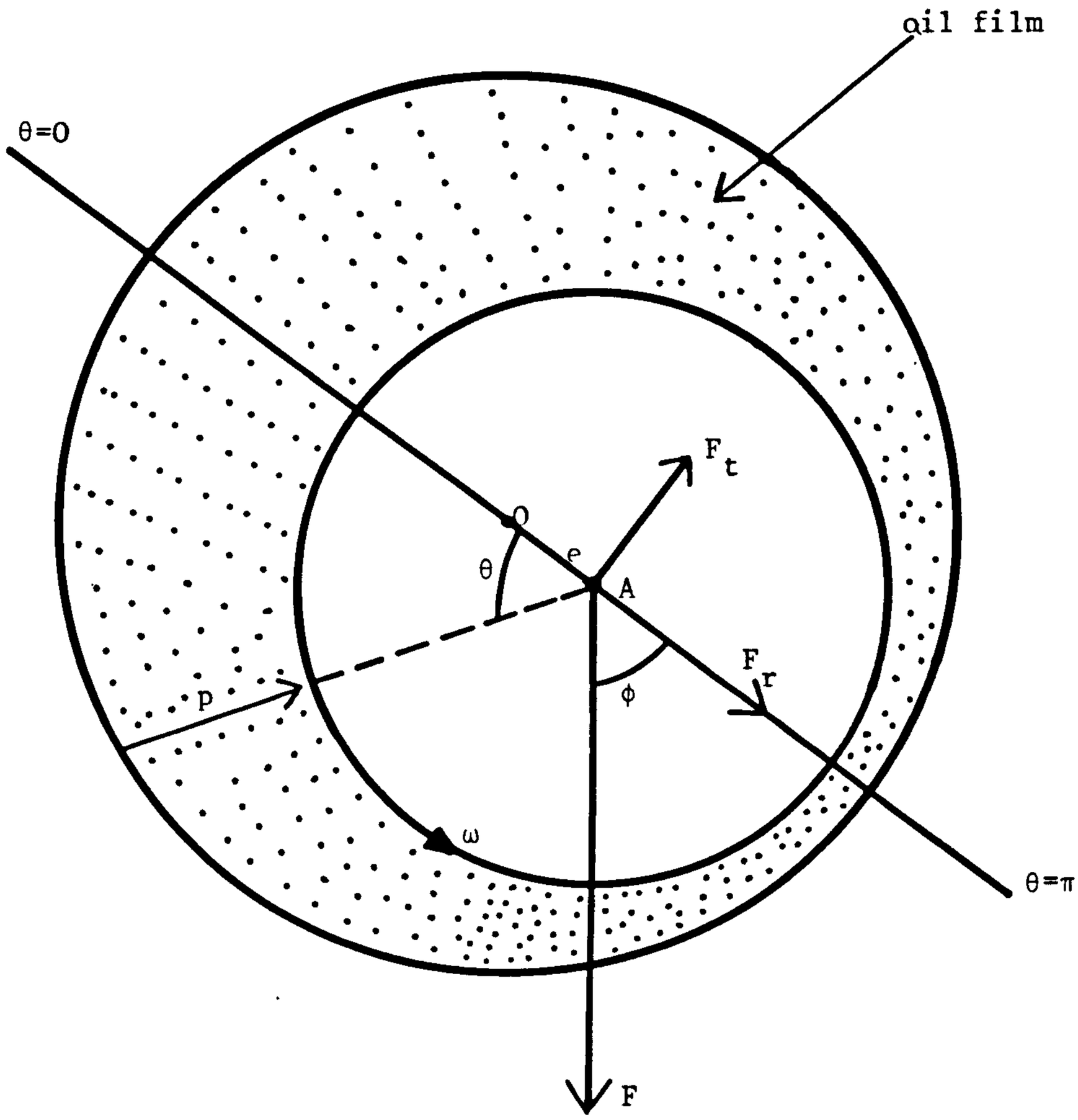

Figure 2.1. Journal bearing operating with a complete film.

$$F_r = \text{Radial Force} = LR\int_0^{2\pi} p(\theta)\cos\theta\, d\theta = -LR\int_0^{2\pi} \frac{dp}{d\theta}\sin\theta\, d\theta \quad \text{(By parts)}$$

$$F_t = \text{Tangential Force} = LR\int_0^{2\pi} p(\theta)\sin\theta\, d\theta = LR\int_0^{2\pi} \frac{dp}{d\theta}\cos\theta\, d\theta.$$

Substituting for $^{dp}/_{d\theta}$ and evaluating the integrals (Appendix I):

$$-\left(\frac{c}{R}\right)^2 \frac{F_r}{LR\omega\mu} = \frac{12\pi\varepsilon'}{(1-\varepsilon^2)^{3/2}} \qquad \left(\frac{c}{R}\right)^2 \frac{F_t}{LR\omega\mu} = \frac{12\pi\varepsilon(1-2\phi')}{(1-\varepsilon^2)^{1/2}(2+\varepsilon^2)} \tag{2.3}$$

The equations of motion of the journal in polar co-ordinates (ε,ϕ) are:

$$mc(\ddot{\varepsilon} - \varepsilon\dot{\phi}^2) = F\cos\phi + F_r \qquad \text{(Figure 2.1)} \tag{2.4}$$

$$mc(\varepsilon\ddot{\phi} + 2\dot{\varepsilon}\dot{\phi}) = -F\sin\phi + F_t$$

Substituting for F_r and F_t (equations 2.3) and putting $\tau=\omega t$ yields the non-dimensional form of the equations of motion.

$$\ddot{\varepsilon}-\varepsilon\phi'^2 = \nu\left\{\cos\phi - \frac{12S\pi\varepsilon'}{(1-\varepsilon^2)^{3/2}}\right\} \tag{2.5}$$

$$\varepsilon\ddot{\phi}+2\varepsilon'\phi' = -\nu\left\{\sin\phi - \frac{12S\pi\varepsilon(1-2\phi')}{(1-\varepsilon^2)^{1/2}(2+\varepsilon^2)}\right\}$$

where $\nu = \dfrac{F}{mc\omega^2}$, $S = \dfrac{LR^3\omega\mu}{Fc^2}$, the Sommerfeld number.

The equations have a unique steady state solution for each value of the Sommerfeld number denoted by (ε_s,ϕ_s) where:

$$\phi_s = \frac{\pi}{2} \quad \text{and} \quad S = \frac{(1-\varepsilon_s^2)^{1/2}(2+\varepsilon_s^2)}{12\pi\varepsilon_s} \tag{2.6}$$

Thus the theoretical locus of the journal centre under steady state conditions is a straight line with an attitude angle of 90° (Figure 2.2). Equation (2.6) establishes the relationship between the Sommerfeld number S and ε_s (Figure 2.3).

The non-dimensional steady state pressure distribution is found by substituting $\varepsilon'=\phi'=0$ in equation (2.2):

$$\bar{p}_s = \left(\frac{c}{R}\right)^2 \frac{p}{\mu\omega} = \frac{6\varepsilon_s(2+\varepsilon_s\cos\theta)\sin\theta}{(2+\varepsilon_s^2)(1+\varepsilon_s\cos\theta)^2} \qquad (2.7)$$

This is frequently referred to as the Sommerfeld pressure distribution. A typical profile is shown in Figure 2.4 for ε_s=0.6. It is anti-symmetric about $\theta=\pi$, the importance of which will be discussed later in this Chapter.

The steady state forces are:

$$\bar{F}_{rs} = \frac{F_{rs}}{SF} = 0 \qquad \bar{F}_{ts} = \frac{12\pi\varepsilon_s}{(2+\varepsilon_s^2)\ (1-\varepsilon_s^2)^{\ 1/2}} = \frac{1}{S} \qquad (2.8)$$

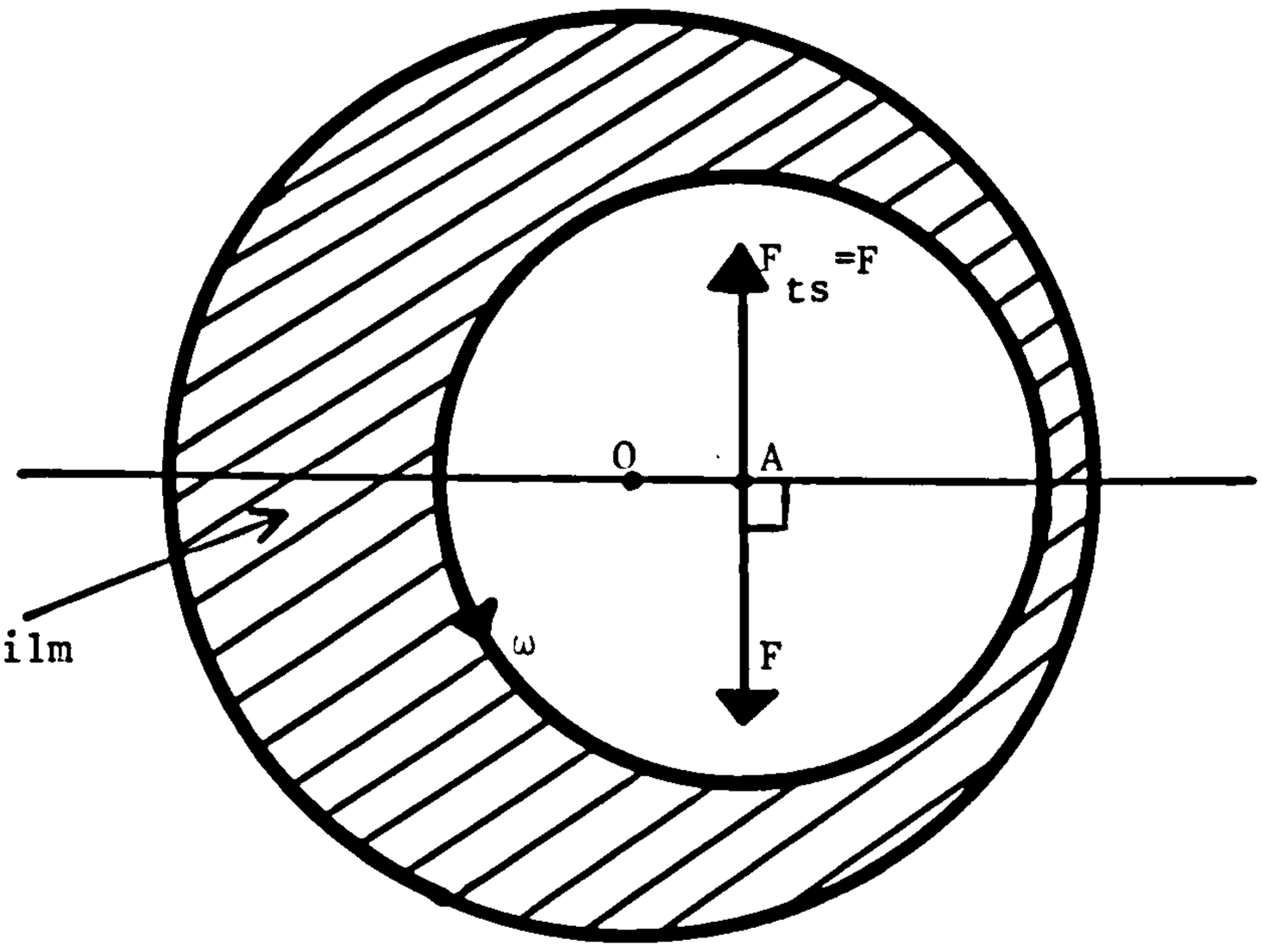

Figure 2.2. Theoretical steady state behaviour of a journal bearing operating with a complete film.

The absence of a radial force means the load is supported entirely by the tangential component (hence $\phi_s=\pi/2$).

The equations of motion (2.5) are nonlinear and cannot be solved analytically. However, following the procedure outlined in Chapter 1, the equations may be linearised about the equilibrium position. The linearised equations are:

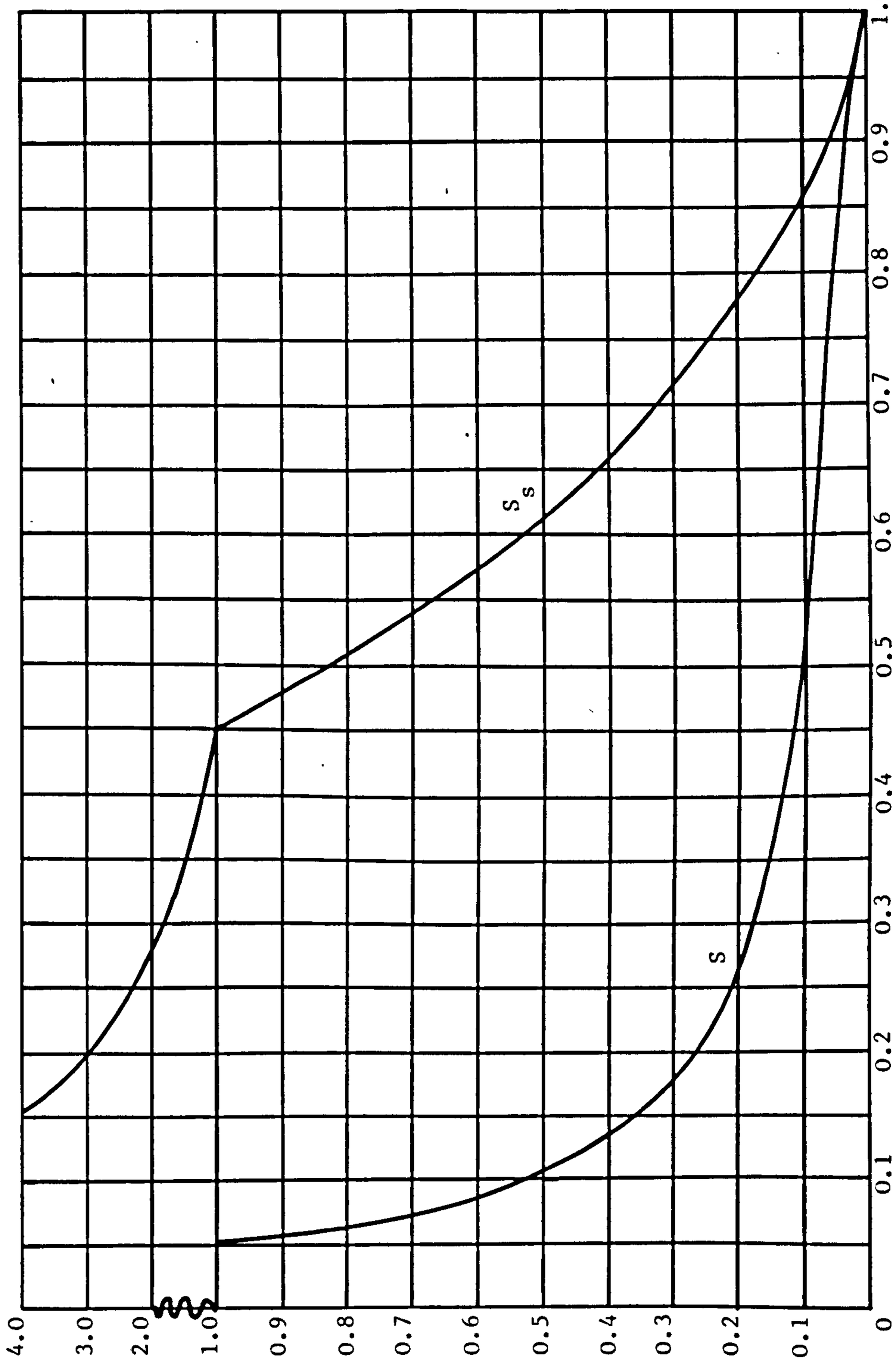

Figure 2.3. Comparison of the Sommerfeld numbers for bearings with complete films.

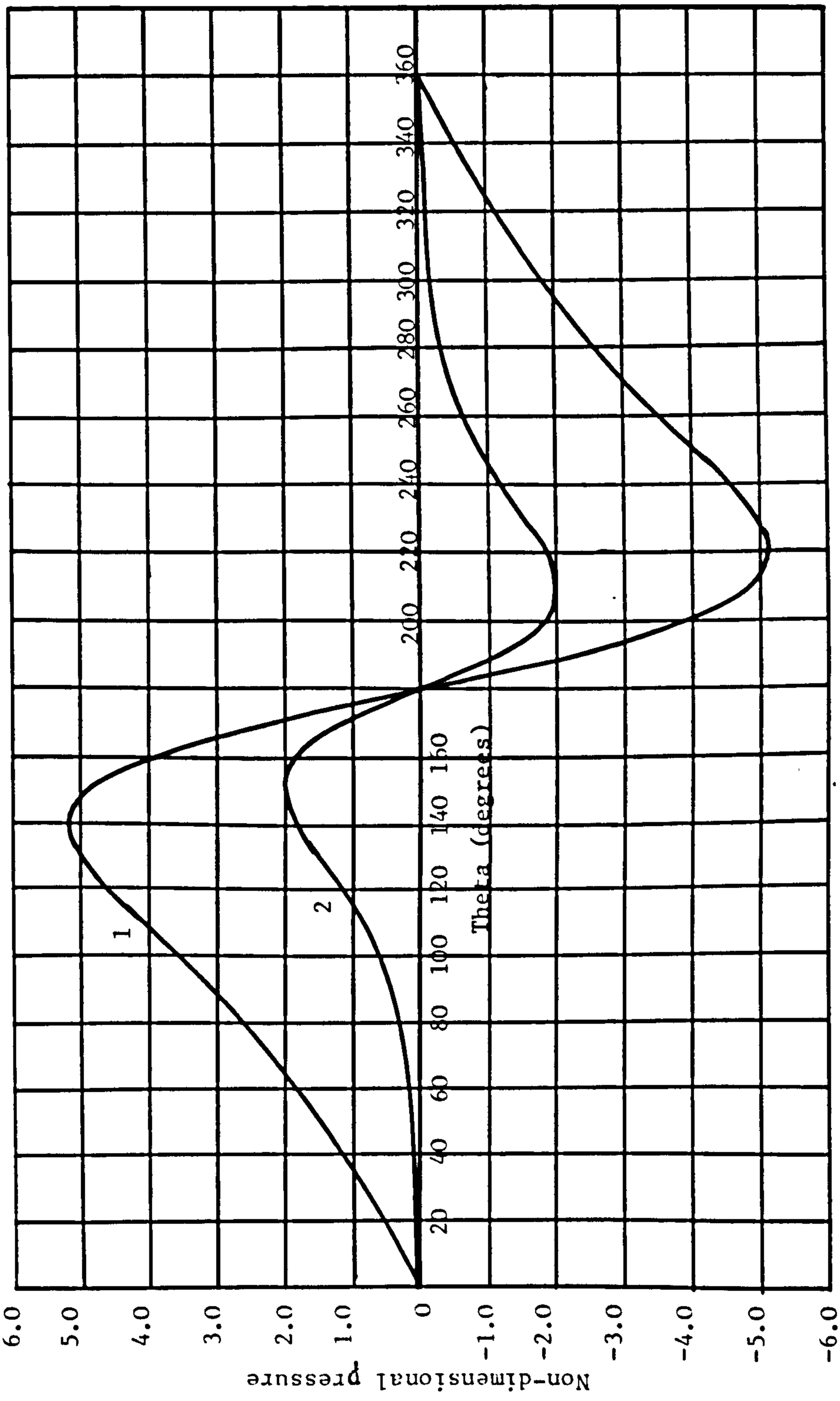

Figure 2.4. Steady state pressure profiles generated in bearings with complete films.

$$\ddot{x}+\nu\frac{(2+\epsilon_s^2)}{\epsilon_s(1-\epsilon_s^2)}\dot{x}+\frac{\nu}{\epsilon_s}y=0 \qquad (2.9)$$

$$\ddot{y}+2\frac{\nu}{\epsilon_s}\dot{y}-\frac{\nu(2-\epsilon_s^2+2\epsilon_s^4)y}{\epsilon_s(1-\epsilon_s^2)(2+\epsilon_s^2)}=0$$

The eight velocity and displacement coefficients are:

$$B_{xx}=\frac{(2+\epsilon_s^2)}{\epsilon_s(1-\epsilon_s^2)} \qquad B_{xy}=B_{yx}=0 \qquad B_{yy}=\frac{2}{\epsilon_s} \qquad (2.10)$$

$$K_{xx}=K_{yy}=0 \qquad K_{yx}=\frac{-(2-\epsilon_s^2+2\epsilon_s^4)}{\epsilon_s(1-\epsilon_s^2)(2+\epsilon_s^2)} \qquad K_{xy}=\frac{1}{\epsilon_s}$$

The characteristic or frequency equation is:

$$\bar{\lambda}^4+\frac{\nu(4-\epsilon_s^2)\bar{\lambda}^3}{\epsilon_s(1-\epsilon_s^2)}+2\nu^2\frac{(2+\epsilon_s^2)\bar{\lambda}^2}{\epsilon_s^2(1-\epsilon_s^2)}+\nu^2\frac{(2-\epsilon_s^2+2\epsilon_s^4)}{\epsilon_s^2(2+\epsilon_s^2)(1-\epsilon_s^2)}=0 \qquad (2.11)$$

B C E

Applying Routh's criterion to this equation it is easily seen that:

i) $B,C,E>0\ \forall$ non-zero values of ν and ϵ_s.

ii) $R=D(BC-D)-B^2E=-B^2E<0$.

Thus the condition, $R>0$, for stability cannot be satisfied. Therefore the equilibrium position is <u>unstable</u> for all values of ν and ϵ_s (apart from the special cases discussed below).

i) As $\epsilon_s\to 0$ the frequency equation (2.11) reduces to:

$$4\bar{\lambda}^2+1=0 \Rightarrow \bar{\lambda}\to\pm i/2 \quad \text{(neutrally stable)}.$$

ii) As $\epsilon_s\to 1$ equation (2.11) reduces to:

$$3\bar{\lambda}^3+6\nu\bar{\lambda}^2+\nu=0 \Rightarrow \text{as } \nu\to 0 \quad \bar{\lambda}\to 0$$

$$\text{as } \nu\to\infty \quad \bar{\lambda}\to\pm i/\sqrt{6}$$

iii) As $\nu \to \infty$ $\quad \bar{\lambda} \to \pm \left\{ \dfrac{2-\varepsilon_s^2+2\varepsilon_s^4}{2(2+\varepsilon_s^2)^2} \right\}^{1/2} i$ (neutrally stable).

The analysis above suggests that the parameters ν and ε_s may play a role in determining the degree of instability. This is discussed in more detail in section 2.3.

2.2 AN ANALYSIS USING SHORT BEARING THEORY.

The Reynolds equation for a short bearing was shown in Chapter 1 to be:

$$\frac{d}{dz}\left\{(1+\varepsilon\cos\theta)^3\frac{dp}{dz}\right\} = 6\frac{\mu}{c^2}\{\varepsilon(2\dot{\phi}-\omega)\sin\theta+2\dot{\varepsilon}\cos\theta\} \qquad (2.12)$$

Integrating twice with the boundary conditions:

$p = 0$ at $z = 0, L$

$$\Rightarrow \left(\frac{c}{L}\right)^2 \frac{p}{\omega\mu} = \frac{3z(z-L)}{L^2}\left\{\frac{-\varepsilon(1-2\phi')\sin\theta+2\varepsilon'\cos\theta}{(1+\varepsilon\cos\theta)^3}\right\} \qquad (2.13)$$

The pressure is zero (ie. ambient) when:

$$\theta = \theta_1,\ \pi+\theta_1,\ 2\pi \leftarrow \theta_1 \text{ where } \tan\theta_1 = \frac{2\varepsilon'}{\varepsilon(1-2\phi')} \qquad (2.14)$$

To investigate a short bearing operating with a complete film, the pressure distribution must be taken over 360°. Therefore the hydrodynamic forces are calculated by integrating the pressure over the bearing from $z = 0, L$ and $\theta = 0,\ 2\pi$ (which is equivalent to integrating from θ_1, to $2\pi + \theta_1$).

$$\Rightarrow F_r = R\int_0^L\int_0^{2\pi} p(\theta,z)\cos\theta\,d\theta\,dz \qquad F_t = R\int_0^L\int_0^{2\pi} p(\theta,z)\sin\theta\,d\theta\,dz$$

Substituting for $p(\theta,z)$ from equation (2.13) and evaluating the integrals:

$$-\left(\frac{c}{L}\right)^2\frac{F_r}{LR\omega\mu} = \frac{\pi(1+2\varepsilon^2)\varepsilon'}{(1-\varepsilon^2)^{5/2}} \qquad \left(\frac{c}{L}\right)^2\frac{F_t}{LR\omega\mu} = \frac{\pi\varepsilon(1-2\phi')}{2(1-\varepsilon^2)^{3/2}} \qquad (2.15)$$

The non-dimensional form of the equations of motion are:

$$\varepsilon'' - \varepsilon\phi'^2 = \nu\left\{\cos\phi - S_s \frac{\pi(1+2\varepsilon^2)\varepsilon'}{(1-\varepsilon^2)^{5/2}}\right\} \qquad (2.16)$$

$$\varepsilon\phi'' + 2\varepsilon'\phi' = -\nu\left\{\sin\phi - S_s \frac{\pi\varepsilon(1-2\phi')}{2(1-\varepsilon^2)^{3/2}}\right\}$$

Where $S_s = \frac{RL^3\omega\mu}{Fc^2} = 4\left(\frac{L}{D}\right)^2 S$, a modified Sommerfeld number.

The steady state solution to these equations is:

$$\phi_s = \frac{\pi}{2} \qquad S_s = \frac{2(1-\varepsilon_s^2)^{3/2}}{\pi\varepsilon_s} \qquad (2.17)$$

For each value of the modified Sommerfeld number S_s there is a unique steady state solution. The relationship between S_s and ε_s is illustrated in Figure 2.3.

The steady state pressure distribution is:

$$\bar{p}_s = \left(\frac{c}{L}\right)^2 \frac{p_s}{\mu\omega} = \frac{-3z(z-L)\varepsilon_s \sin\theta}{L^2(1+\varepsilon_s\cos\theta)^3} \qquad (2.18)$$

A typical pressure profile is shown in Figure 2.4 for $\varepsilon_s = 0.6$, $z = L/2$. It is similar to the Sommerfeld pressure profile, but with smaller magnitudes.

The steady state forces are:

$$\bar{F}_{rs} = \frac{F_{rs}}{S_s F} = 0 \qquad \bar{F}_{ts} = \frac{F_{ts}}{S_s F} = \frac{\pi\varepsilon_s}{2(1-\varepsilon_s^2)^{3/2}} = \frac{1}{S_s} \qquad (2.19)$$

There is a great similarity between the two models. Again the absence of a radial force means the theoretical steady state locus of the journal centre is at an attitude angle of 90^o (Figure 2.2).

The linearised form of the equations of motion are:

$$\ddot{x} + 2\nu\frac{(1+2\varepsilon_s^2)\dot{x}}{\varepsilon_s(1-\varepsilon_s^2)} + \frac{\nu}{\varepsilon_s}y = 0 \qquad (2.20)$$

$$\ddot{y} + 2\frac{\nu}{\varepsilon_s}\dot{y} - \frac{\nu(1+2\varepsilon_s^2)x}{\varepsilon_s(1-\varepsilon_s^2)} = 0$$

The eight velocity and displacement coefficients are:

$$B_{xx} = -2K_{yx} = \frac{2(1+2\varepsilon_s^2)}{\varepsilon_s(1-\varepsilon_s^2)} \qquad B_{yy} = 2K_{xy} = \frac{2}{\varepsilon_s} \qquad (2.21)$$

$$B_{xy} = B_{yx} = K_{xx} = K_{yy} = 0$$

The frequency equation is:

$$\bar{\lambda}^4 + 2\nu\frac{(2+\varepsilon_s^2)\bar{\lambda}^3}{\varepsilon_s(1-\varepsilon_s^2)} + 4\nu^2\frac{(1+2\varepsilon_s^2)\bar{\lambda}^2}{\varepsilon_s^2(1-\varepsilon_s^2)} + \nu^2\frac{(1+2\varepsilon_s^2)}{\varepsilon_s^2(1-\varepsilon_s^2)} = 0 \qquad (2.22)$$

This equation is very similar to equation (2.11). Again the absence of a $\bar{\lambda}$ term means Routh's criterion cannot be satisfied. Hence the journal always has an unstable equilibrium position (apart from the special cases discussed below). In fact the result is known to be true for a bearing with any L/D ratio operating with a complete film (Marsh (1965)).

As for the long bearing several limiting cases of the frequency equation may be discussed.

i) As $\varepsilon_s \to 0$ $\bar{\lambda} \to \pm i/2$ (neutrally stable)

ii) As $\varepsilon_s \to 1$ the frequency equation (2.22) reduces to:

$2\bar{\lambda}^3 + 4\nu\bar{\lambda}^2 + \nu = 0$ => as $\nu \to 0$ $\bar{\lambda} \to 0$

$\nu \to \infty$ $\bar{\lambda} \to \pm i/2$ (neutrally stable)

iii) As $\nu \to \infty$ $\bar{\lambda} \to \pm i/2$ (neutrally stable)

2.3 RESULTS AND DISCUSSION.

The two frequency equations (2.11 and 2.22) were solved numerically for a range of values of ν and ε_s ($0.02 \leq \nu \leq 1.5$, $0.05 \leq \varepsilon_s \leq 0.95$).

It was found for both equations that only one complex pair of roots had a positive real part. Typical roots were:

$$\bar{\lambda} = -1.17 \pm 0.25i \quad ; \quad \bar{\lambda} = 0.11 \pm 0.35i$$

STABLE UNSTABLE

Therefore, by calculating the logarithmic decrement associated with the unstable root, it is possible to determine the degree of instability. The logarithmic decrement will always be negative - the greater the value of its modulus the greater will be the instability (see Chapter 1).

Curves of constant logarithmic decrement are shown in Figure 2.5. Both models show the same trends (the two charts are in fact very similar). It can be seen that the parameter ν is an important factor influencing the degree of instability - the system becomes less unstable on increasing ν. The same effect, but to a smaller degree, is achieved by decreasing ε_s.

The imaginary part of the unstable root corresponds to the whirl frequency ratio. Frequency curves are shown in Figure 2.6, and it may be observed, that for the cases studied, the ratio is always less than 0.5.

It is interesting to note that for bearings with complete films the eight Taylor coefficients reduce to four. They are illustrated for both models in Figure 2.7. The corresponding coefficients are similar (in fact K_{xy} and B_{yy} are identical for the two models).

It is important to remember that the linearised analysis is valid only when the journal is close to its equilibrium position. The complete motion can only be found by solving the full equations (2.5 and 2.16). It is clear, however, that the journal cannot return to its equilibrium position since it would again become unstable. It must either continue to move outwards towards the bearing side, or go into a closed orbit about its equilibrium position. An investigation of the full equations of motion is made in section 2.4 by integrating the equations numerically.

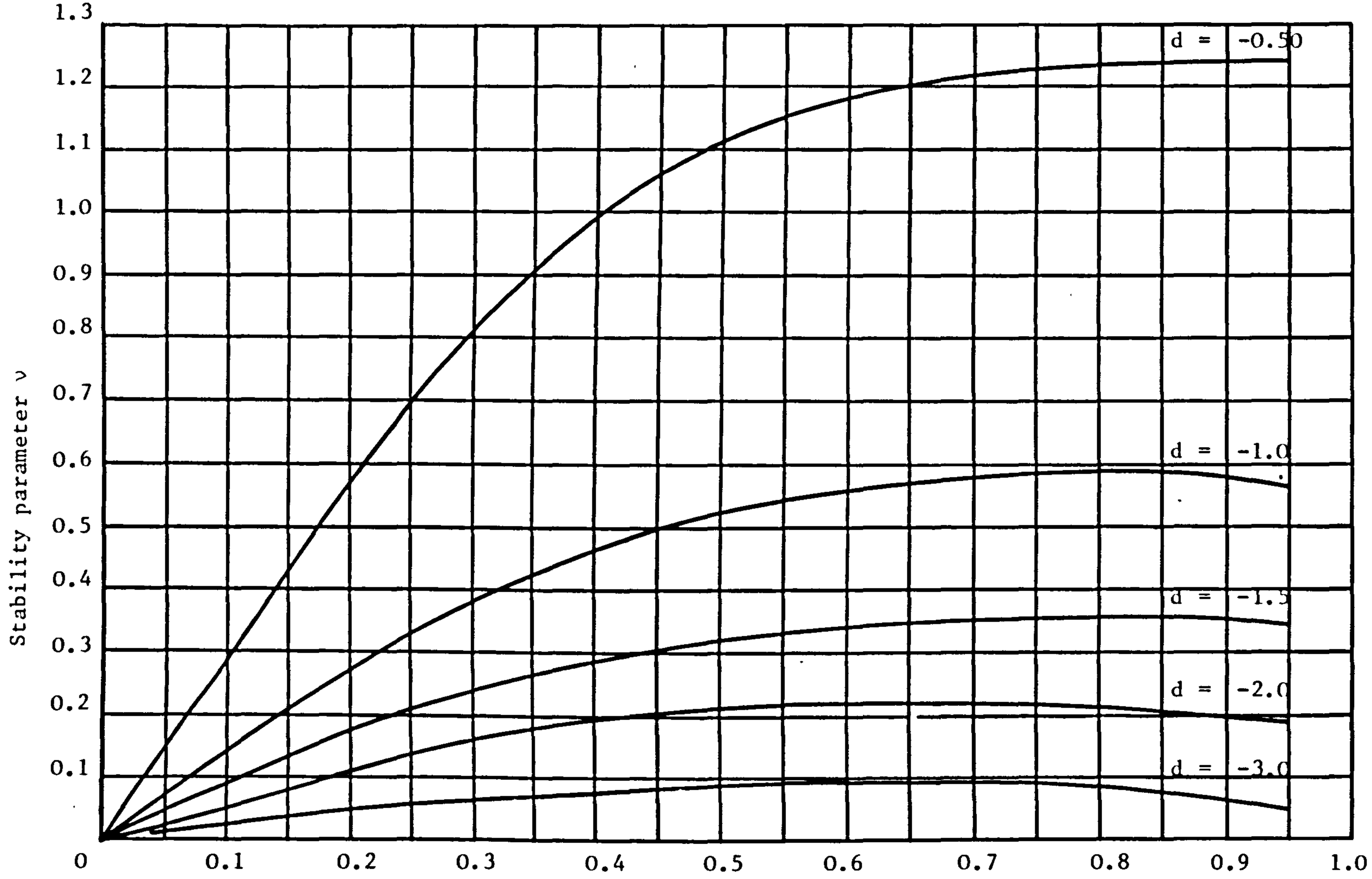

2.5(a). Long bearing (complete film).

Figure 2.5. Curves of constant logarithmic decrement.

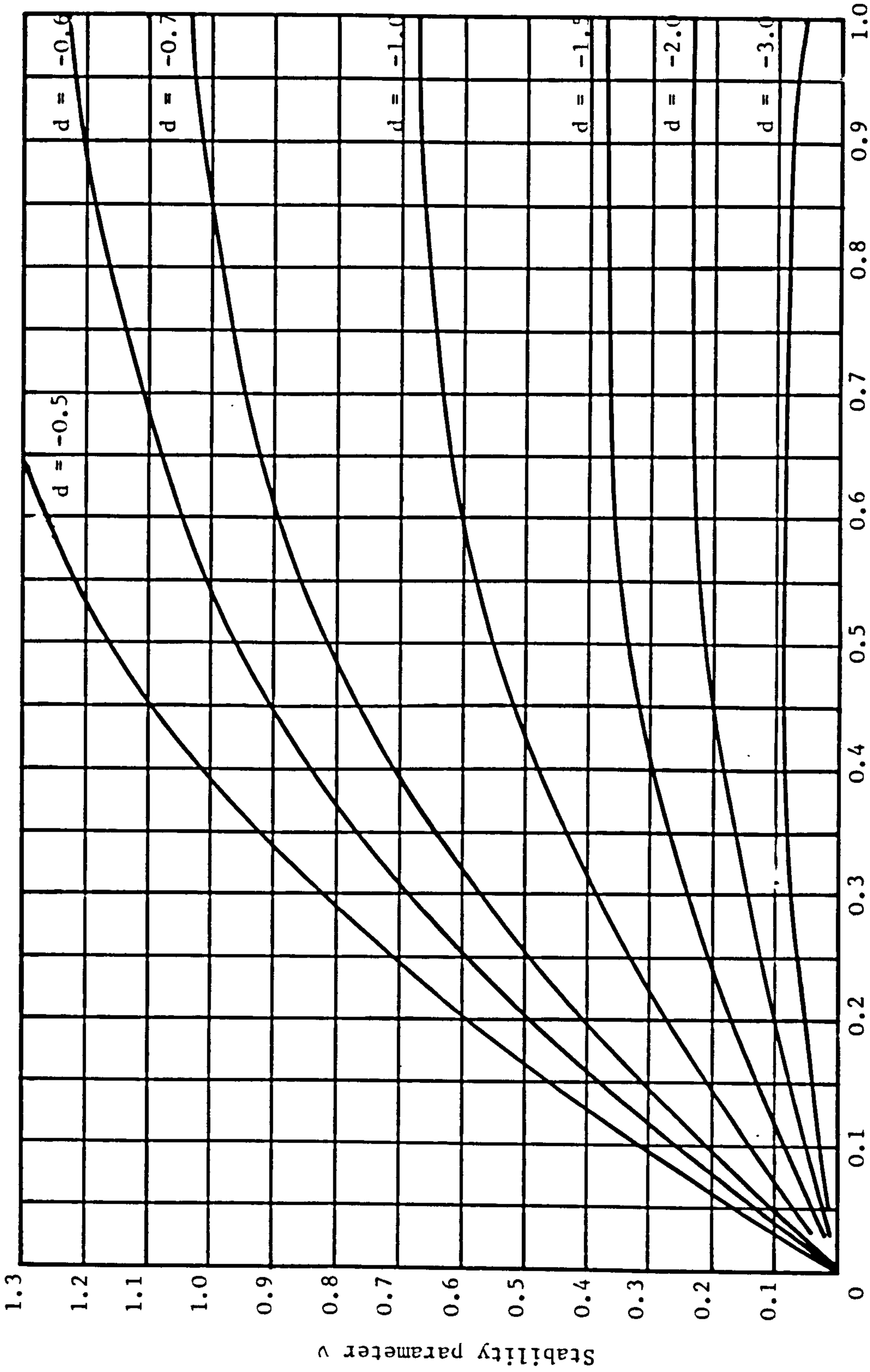

Figure 2.5. continued. Curves of constant logarithmic decrement.
2.5(b). Short bearing (complete film).

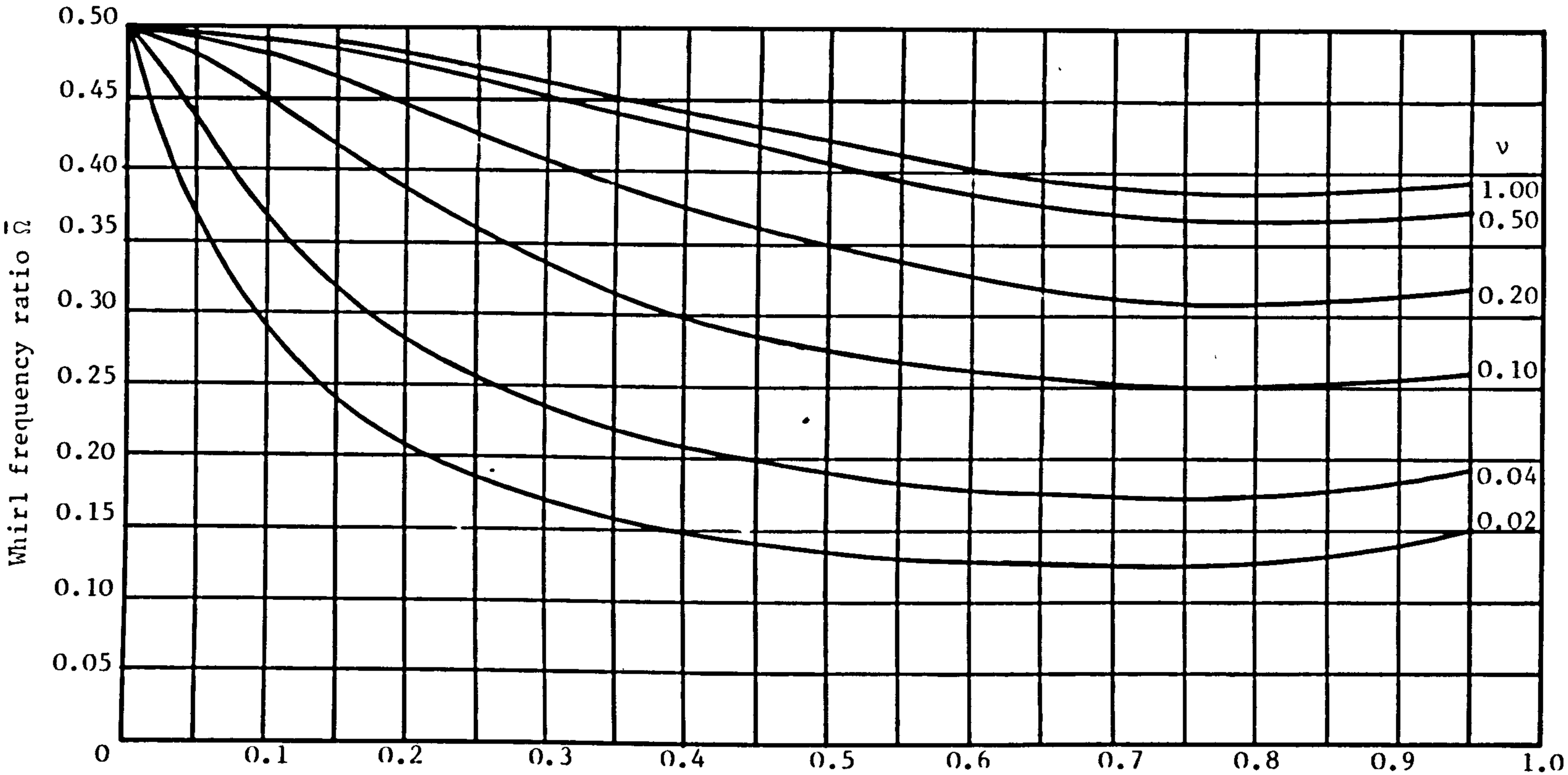

2.6(a). Long bearing (complete film).

Figure 2.6. Whirl frequency ratios.

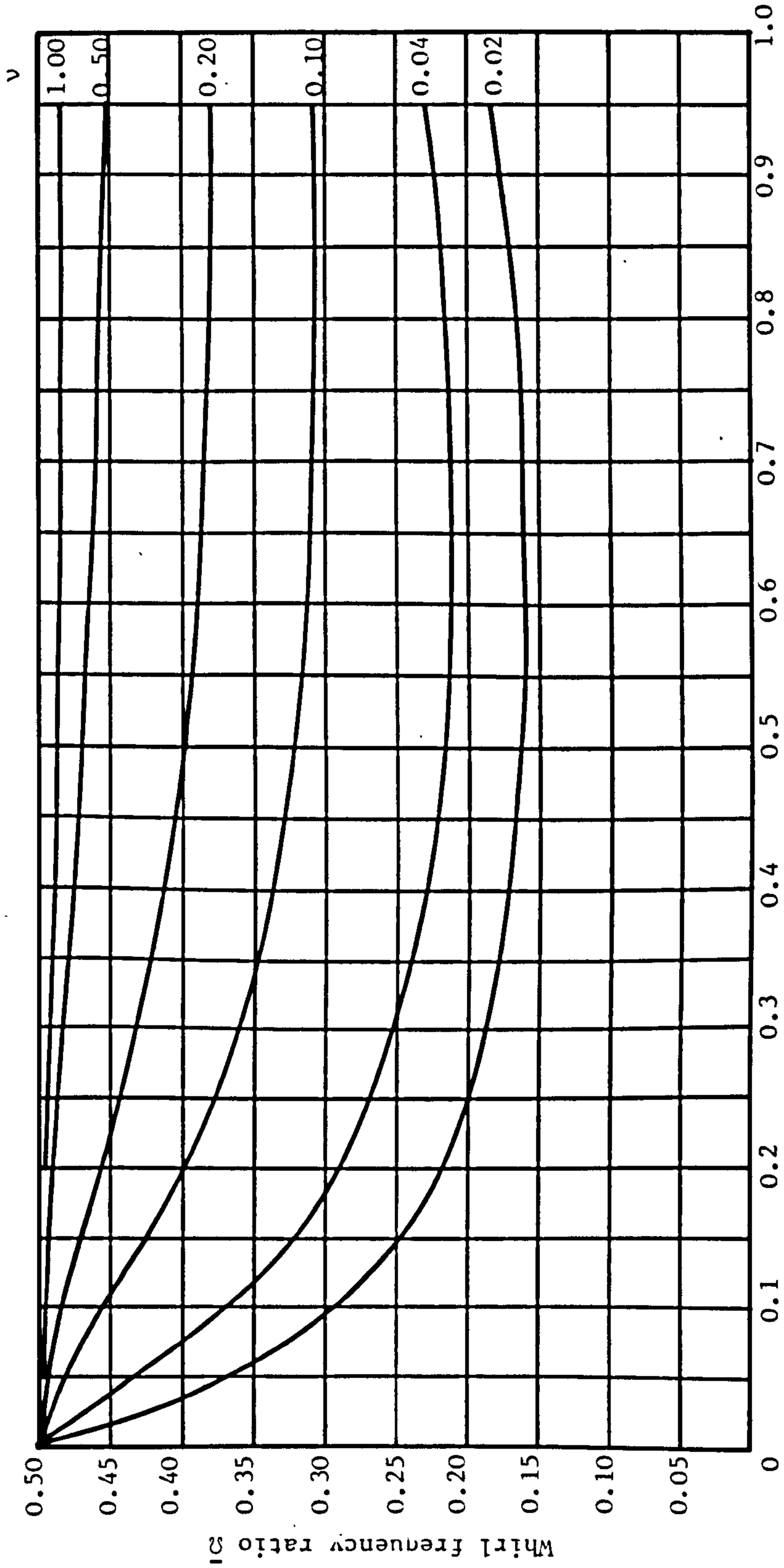

2.6(b). Short bearing (complete film).

Figure 2.6. continued. Whirl frequency ratios.

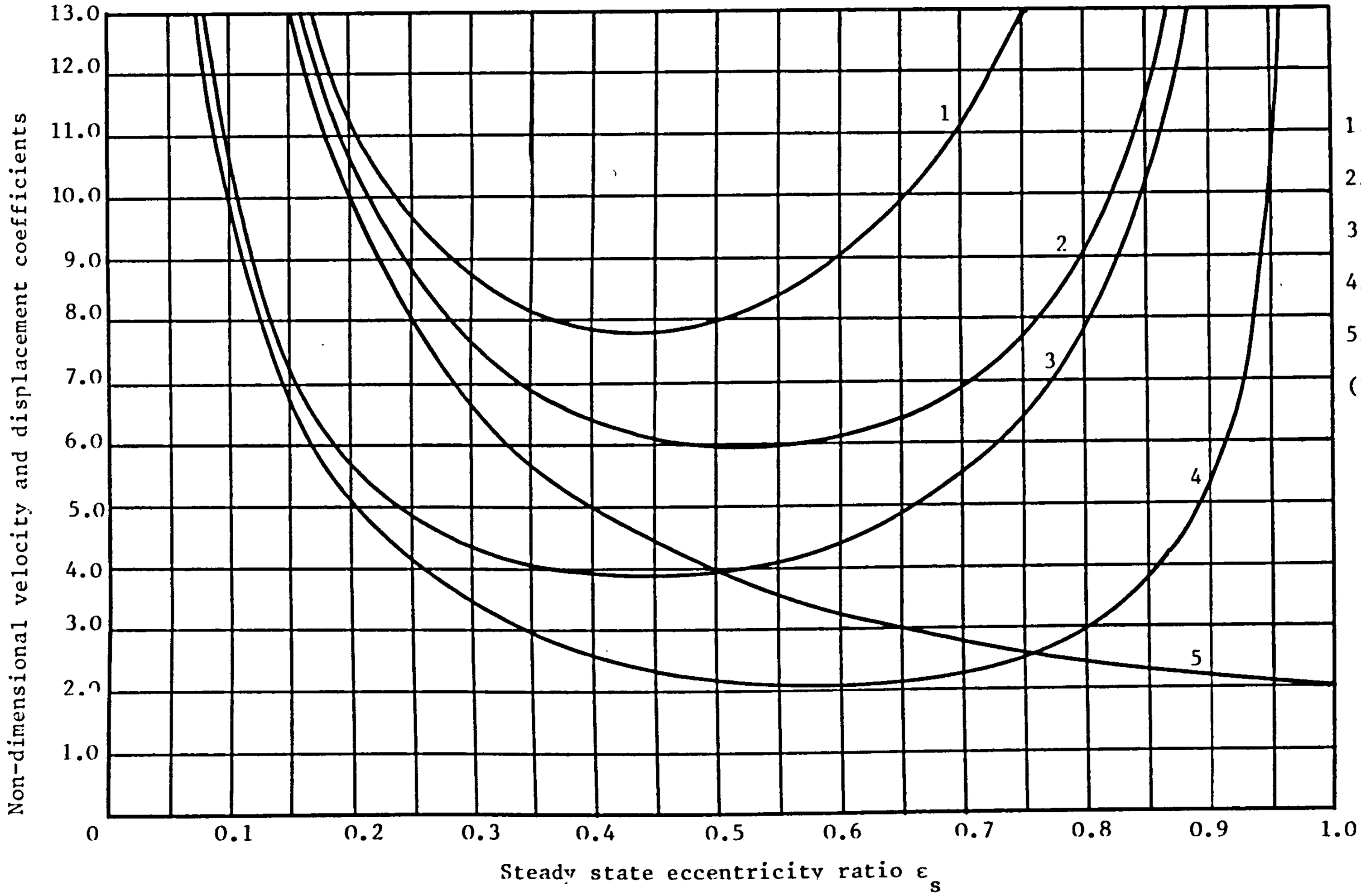

Figure 2.7. Velocity and displacement coefficients for bearings with complete films.

2.4 NUMERICAL INTEGRATION OF THE EQUATIONS OF MOTION.

The most suitable way of integrating the equations of motion numerically is to convert them to a system of first order equations. Consider, for example, the equations for a long bearing (equations 2.5):

Substituting $\varepsilon = Y_1$, $\dot{\varepsilon} = Y_2$, $\phi = Y_3$, $\dot{\phi} = Y_4$

the equations may be written as a system of four first order ordinary differential equations:

$$\dot{Y}_1 = Y_2$$

$$\dot{Y}_2 = \nu\left\{\cos Y_3 - \frac{12S(\varepsilon_s)\pi Y_2}{(1-Y_1^2)^{3/2}} + \frac{Y_1 Y_4^2}{\nu}\right\} \qquad (2.23)$$

$$\dot{Y}_3 = Y_4$$

$$\dot{Y}_4 = -\nu\left\{\frac{1}{Y_1}\sin Y_3 - \frac{12S(\varepsilon_s)\pi(1-2Y_4)}{(1-Y_1^2)^{1/2}(2+Y_1^2)} + \frac{2Y_2 Y_4}{Y_1 \nu}\right\}$$

with $S(\varepsilon_s)$ given by equation (2.6). Equations (2.23) are now in a suitable form for a step-by-step integration with:

i) suitable initial condition for Y_1, Y_2, Y_3, Y_4, (ie. ε_i, $\dot{\varepsilon}_i$, ϕ_i, $\dot{\phi}_i$,).

ii) values for the governing parameters ν and ε_s.

The equations were integrated using a standard Nottingham Algorithms Group library routine (number D02AHF), which advances the solution of a first order system of ordinary differential equations:

$$\frac{dy_i}{d\tau} = f_i(\tau, y_1, y_2, \ldots y_n) \qquad i=1,n$$

from $\tau = \tau_o$ to $\tau_o + \Delta\tau$ using a variable order Adams method (Hall and Watt (1976)). The routine obtains an estimate of the local error at each step and varies the order and step length automatically to keep this estimate below a given error bound. Since over a long range, errors may accumulate in various ways, the step length and error bound were varied initially

to see how this affected the overall result. A step length of 1 was finally used with an error bound of 10^{-8}. The required range of integration depended upon the various parameters ν and ε_s, but was never more than 600 time steps, this being achieved by repeated calls of the routine. The integration was terminated when the journal was close to the bearing side ($\varepsilon \to 1$) because of the singularity in equations (2.23) at $\varepsilon = 1$.

The equations were integrated for a range of values of ν, ε_s and $(\varepsilon_i - \varepsilon_s)$ (Table 2.1). The investigation had several objectives:

i) to determine the complete motion of the journal for selected parameter values. Of particular interest, in this respect, is whether or not there are any closed orbit solutions.

ii) to examine the effect of the governing parameters ν, ε_s and also the initial displacement $(\varepsilon_i - \varepsilon_s)$. (the initial values for the remaining dependent variables were put equal to their steady state values - $\phi = \pi/2$, $\varepsilon' = 0$, $\phi' = 0$).

ε_s	0.2	0.2	0.2	0.2	0.5	0.5	0.5	0.5	0.8	0.8	0.8	0.8
ν	0.1	0.5	1.0	2.5	0.1	0.5	1.0	1.0	0.1	0.5	1.0	2.5
ε	0.21	0.21	0.21	0.21	0.52	0.52	0.52	0.6	0.82	0.82	0.82	0.82
FIGURE 2.8					FIGURE 2.9				FIGURE 2.10			

Table 2.1 Table Showing Parameter Values For Which The Equations of Motion Were Solved.

The results are presented in graphic form (Figures 2.8, 2.9, 2.10). Each whirl orbit represents the motion of the journal centre. The broken circle, at $\varepsilon = 1$, is referred to as the clearance circle and represents the orbit of the journal centre when the journal makes contact with the bearing side (the largest amplitude vibration which is possible).

The following conclusions may be drawn from Figures 2.8, 2.9, 2.10.

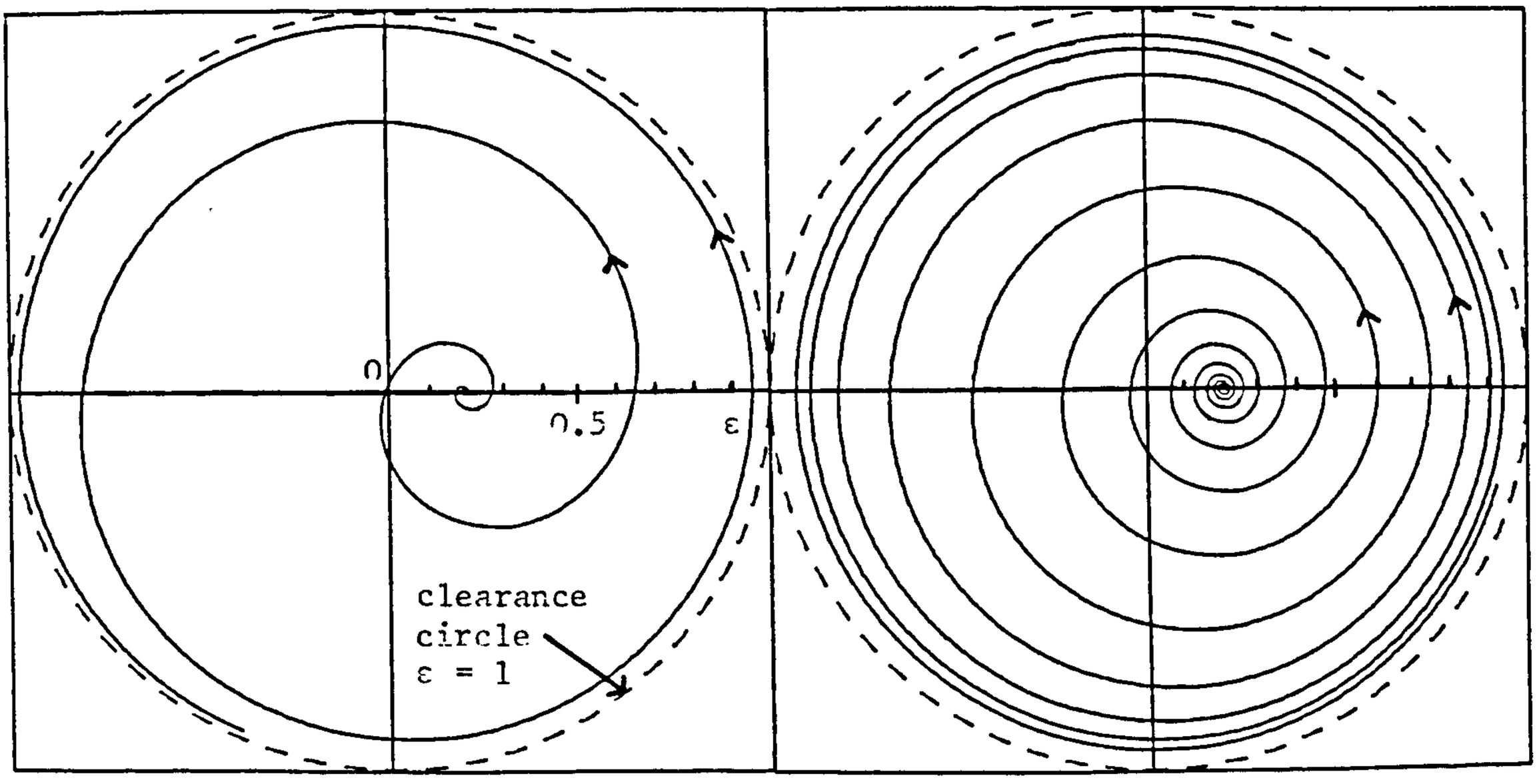

2.8(i) $\varepsilon_s = 0.2$ $\nu = 0.1$ $\varepsilon_i = 0.21$ 2.8(ii) $\varepsilon_s = 0.2$ $\nu = 0.5$ $\varepsilon_i = 0.21$

(arrows indicate the direction of whirling)

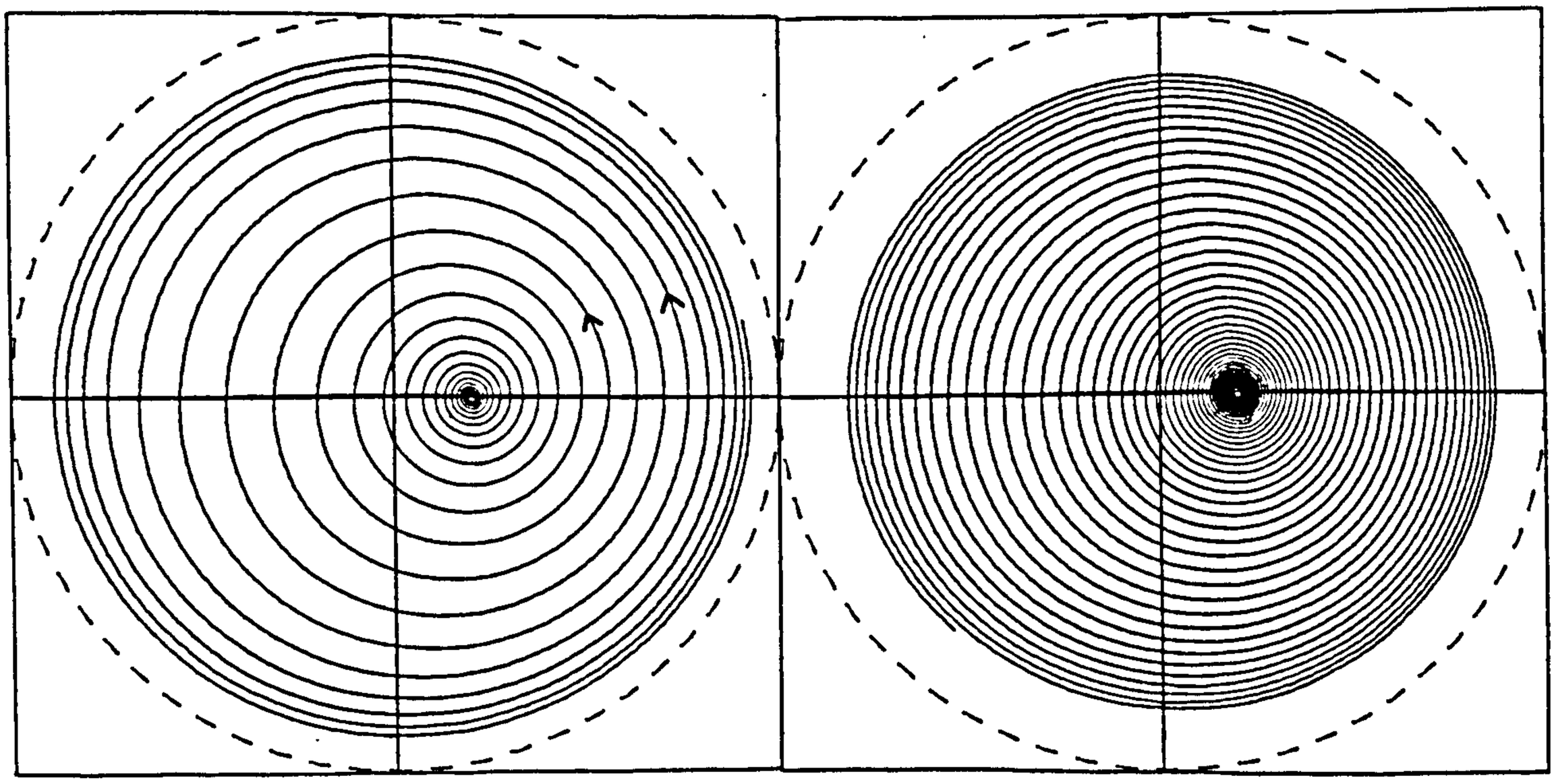

2.8(iii) $\varepsilon_s = 0.2$ $\nu = 1.0$ $\varepsilon_i = 0.21$ 2.8(iv) $\varepsilon_s = 0.2$ $\nu = 2.5$ $\varepsilon_i = 0.21$

Figure 2.8 Whirl Orbits For a Long Bearing Operating with a Complete Film.

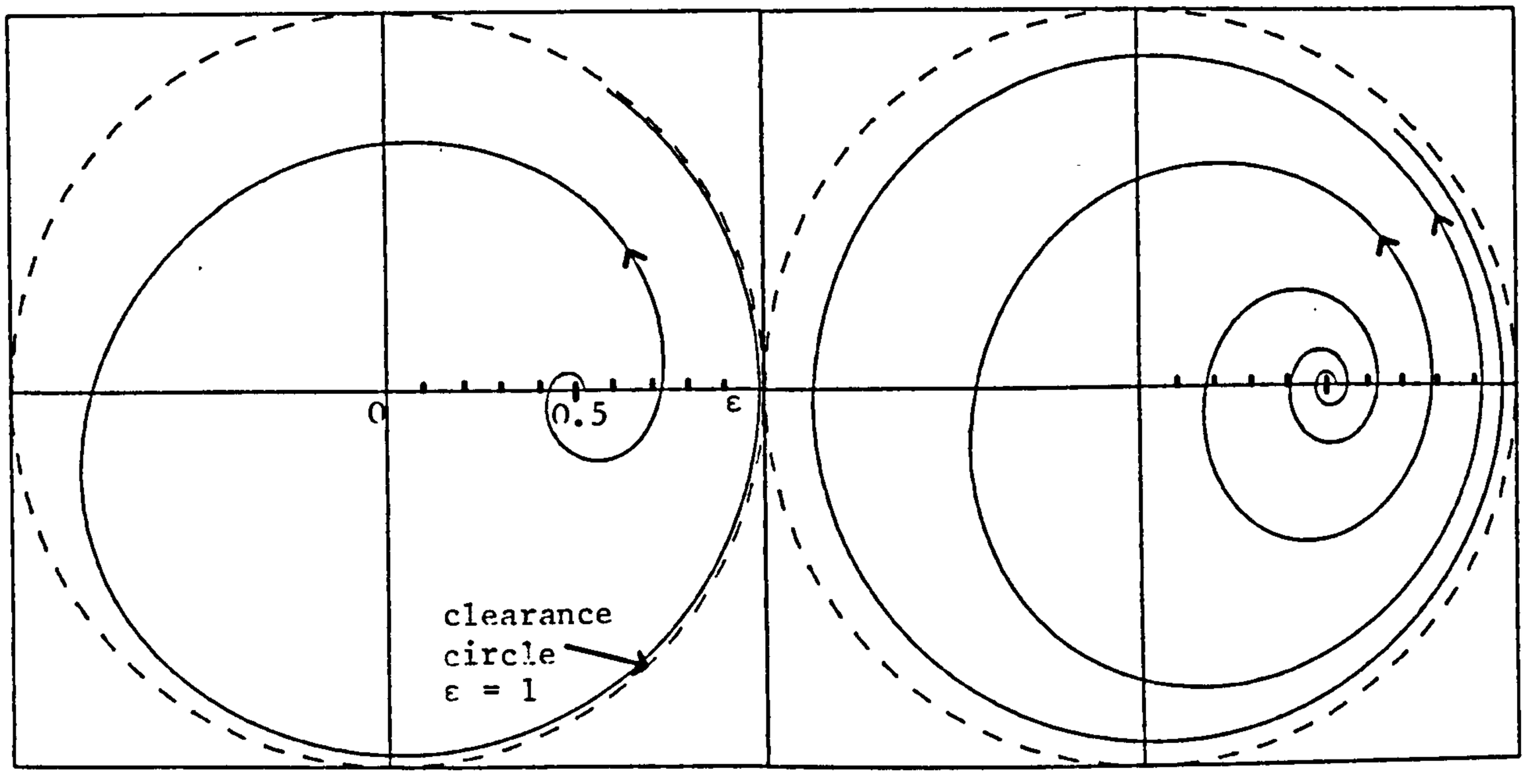

2.9(i) $\varepsilon_s = 0.5$ $\nu = 0.1$ $\varepsilon_i = 0.52$ 2.9(ii) $\varepsilon_s = 0.5$ $\nu = 0.5$ $\varepsilon_i = 0.52$

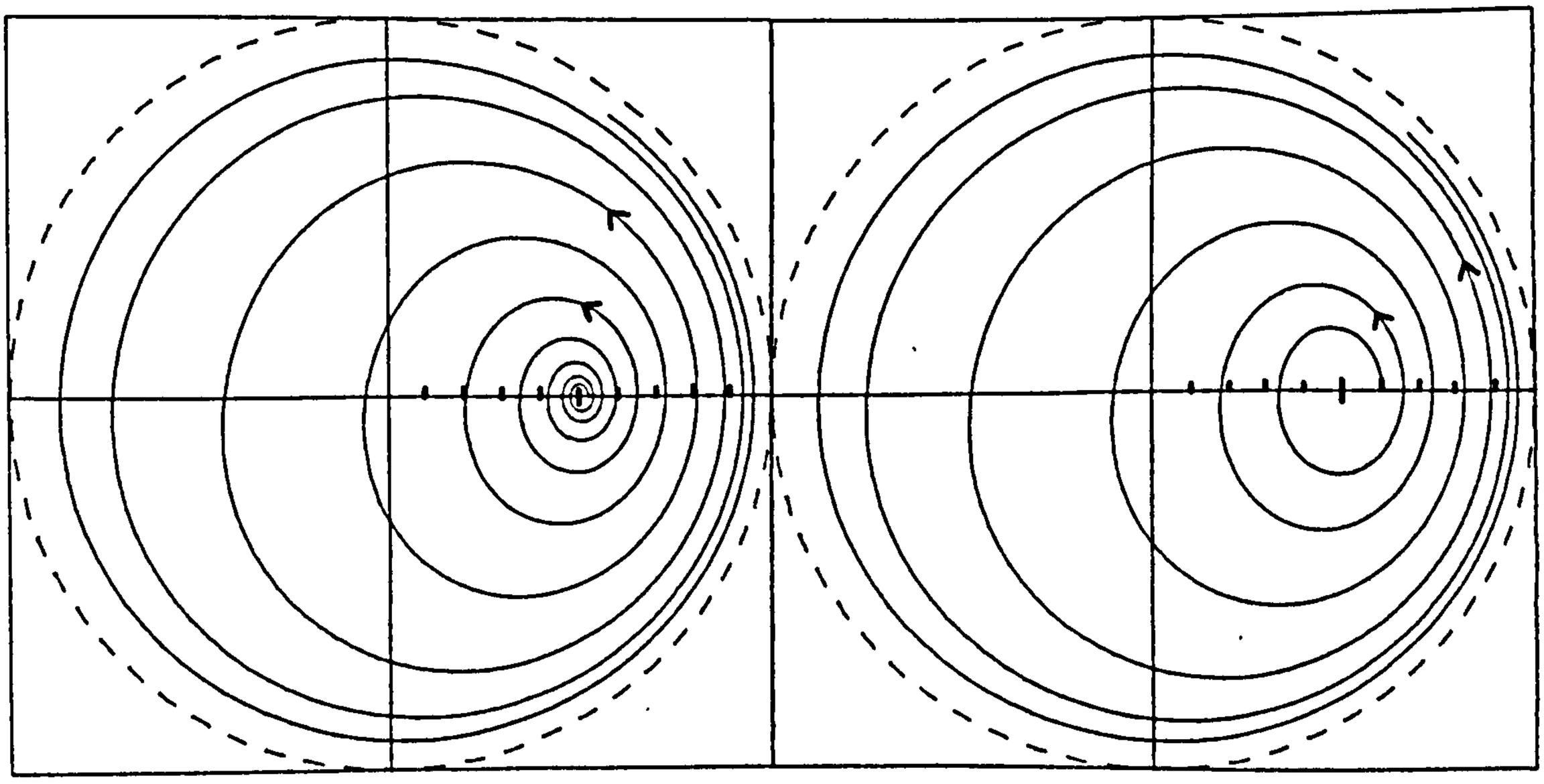

2.9(iii) $\varepsilon_s = 0.5$ $\nu = 1.0$ $\varepsilon_i = 0.52$ 2.9(iv) $\varepsilon_s = 0.5$ $\nu = 1.0$ $\varepsilon_i = 0.6$

Figure 2.9 Whirl Orbits For a Long Bearing Operating with a Complete Film.

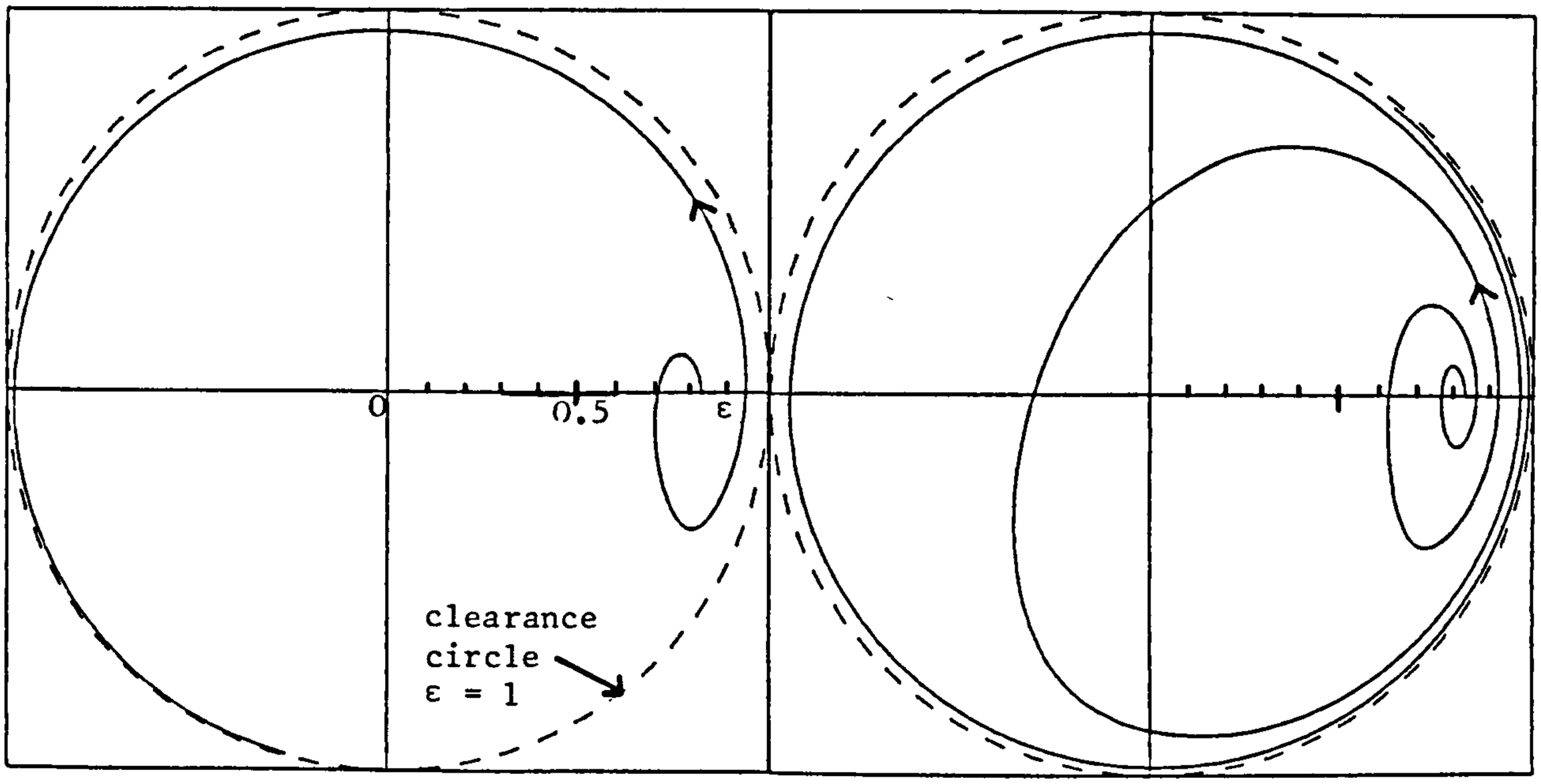

2.10(i) $\varepsilon_s = 0.8 \quad \nu = 0.1 \quad \varepsilon_i = 0.82$ 2.10(ii) $\varepsilon_s = 0.8 \quad \nu = 0.5 \quad \varepsilon_i = 0.82$

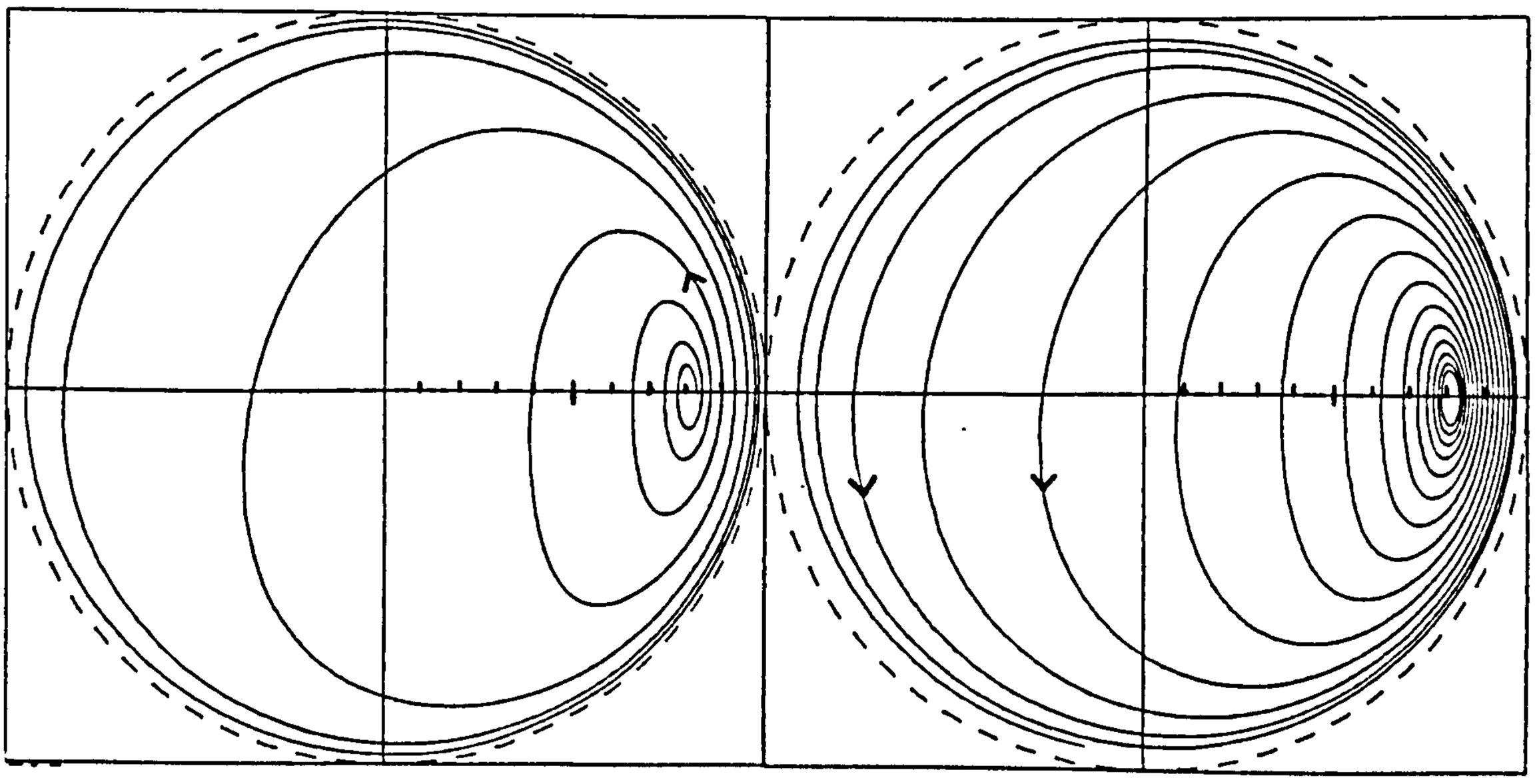

2.10(iii) $\varepsilon_s = 0.8 \quad \nu = 1.0 \quad \varepsilon_i = 0.82$ 2.10(iv) $\varepsilon_s = 0.8 \quad \nu = 2.5 \quad \varepsilon_i = 0.82$

Figure 2.10 Whirl Orbits For a Long Bearing Operating with a Complete Film.

i) All the results suggest that the journal approaches the bearing side asymptotically with time ($\varepsilon \to 1$ as $\tau \to \infty$). Apart from this limiting case there are no closed orbit solutions- the journal is unstable. It was also observed that as $\varepsilon \to 1, \dot{\phi} \to 1/2$, which may be deduced from the equations of motion (2.5).

ii) The paramter ν has an important effect on the number of loops within a given radius of the static eccentricity ratio; the number increasing with ν (compare Figures 2.8(i) with 2.8(ii)). A similar effect, though to a lesser extent, is obtained by decreasing ε_s (compare Figures 2.10 (ii) with 2. 8(ii)). Once the orbit has enclosed the bearing centre the loops tend to close up, particularly for larger values of ν (Figure 2.8(iv)) and in these cases the journal approaches the bearing side very slowly.

iii) Although the initial displacement $(\varepsilon_i - \varepsilon_s)$ affects the solution for the first few loops it does not alter the final motion of the journal (Figures 2.9(iii) and 2.9 (iv)). The shape of the initial loops is governed by ε_s. As ε_s is increased these loops become more elongated in the direction of the external load (Figure 2.10).

As investigation of the equations of motion for a short bearing (equations 2.16) revealed very similar features to the ones described above. To conclude this secion it may be noted that, for both models with a complete film, an investigation of the full nonlinear equations of motion has not revealed any significant information about the vibration of the journal which has not already been deduced from the linearised analysis. This is certainly <u>not</u> true of later models analysed in this thesis.

2.5 THE LIMITATIONS OF THE MODEL.

The findings of this Chapter are in agreement with Holmes (1963 and 1965), who used both linear and nonlinear analyses to investigate the vibrational characteristics of journal bearings operating with

complete films. The work described in this Chapter may also be related to that of Capriz (1963), and Reddi and Trumpler (1962). Capriz, in a detailed mathematical analysis of the whirling of a journal operating in a long bearing with a complete film and zero load (F = 0), has shown that the journal approaches the bearing side asymptotically with time, at a whirl frequency equal to half the rotational speed ($\varepsilon \to 1$, $\dot{\phi} \to 1/2$ as $\tau \to \infty$). Reddi and Trumpler, however, in considering the nonlinear whirling of a long bearing have concluded that for some cases a final closed orbit is possible (with $\varepsilon < 1$). No such closed orbits were found in this work, nor in the work mentioned above.

Given any mathematical model it is necessary to compare it with the real physical situation and to examine critically its validity. Through this examination it is possible to discover how the model may be improved.

The most obvious deficiency in this work is the failure to account for rupture of the oil film. The assumption that the oil film is complete generates a pressure profile in the bearing which is anti-symmetric about the line of minimum film thickness (Figure 2.4). The subambient pressures are therefore as high in magnitude as the superambient ones. Under normal operating conditions, but possibly not with light loading, the oil film cannot withstand these subambient pressures and will rupture. A cavity will form somewhere in the diverging film section of the bearing. For steady state conditions the cavity may form in two ways:

i) by ventilation from the surrounding atmosphere whenever subambient pressures occur.

ii) by the emission of dissolved gases from solution when the lubricant pressure falls below the saturation pressure.

In Chapter 3 the model is improved to account for cavitation and its effect on the vibrational characteristics of the journal will be analysed. In this work no distinction is made between the different

forms of cavitation. The pressure in the cavity is assumed to be ambient.

2.6 CONCLUSIONS.

i) A journal bearing operating with a complete film has an unstable equilibrium position. As whirling proceeds the journal spirals outwards towards the bearing surface at a frequency close to half the rotational speed.

ii) The parameter ν is an important factor governing the degree of instability.

iii) Under normal operating conditions the model is deficient because it does not take account of cavitation.

CHAPTER 3

THE SENSITIVITY OF THE VIBRATIONAL CHARACTERISTICS OF JOURNAL BEARINGS TO DIFFERENT CAVITATION BOUNDARY CONDITIONS AT FILM RUPTURE.

The effect of cavitation on the vibrational behaviour of the journal is investigated. Many different boundary conditions have been proposed to model the rupture of the oil film in a journal bearing (Dowson and Taylor (1979)). This is an indication of the complexity of the phenomenon of cavitation in bearings and it is true to say that the present understanding of the cavitation mechanism is still incomplete. In this Chapter, the vibrational characteristics of bearings operating with oil films satisfying different cavitation boundary conditions are contrasted. It is shown that an important additional factor is the behaviour of the oil film during a vibration of the journal.

3.1 A LONG BEARING OPERATING WITH AN OSCILLATING HALF FILM.

In this model, the oil film is assumed to extend from the line of maximum film thickness ($\theta = 0$) to the line of minimum film thickness ($\theta = \pi$). Since this line moves during any motion of the journal this means the film swings round with the line of centres (Figure 3.1(a)). This is an assumption which is made about the behaviour of the oil film and is important since it is shown in this Chapter that such behaviour has a significant effect on the vibrational characteristics of the journal. A cavity is assumed to exist over the remaining, diverging film section of the bearing. The pressure in the cavity is assumed to be ambient and therefore to make no contribution to the hydrodynamic forces. The appropriate boundary conditions are:

$$p = 0 \text{ at } \theta = 0,\pi \; ; \quad p \equiv 0 \text{ for } \pi < \theta < 2\pi \tag{3.1}$$

These boundary conditions were first proposed by Gümbel (1921) and used by Hori (1959) in his work on flexible rotors.

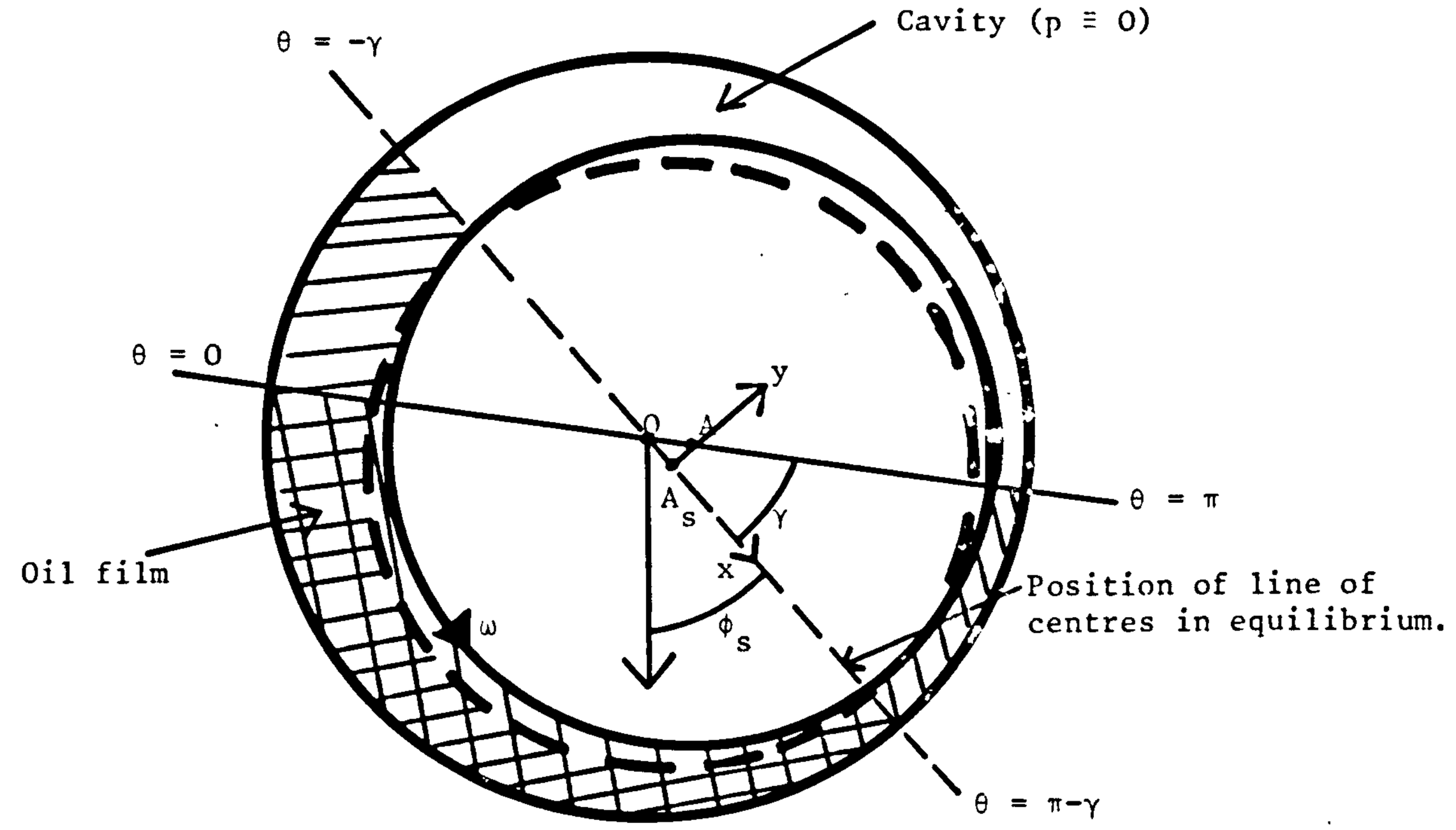

Figure 3.1(a). A journal bearing operating with an oscillating half film.

A = Journal centre

A_s = Equilibrium position of the journal centre.

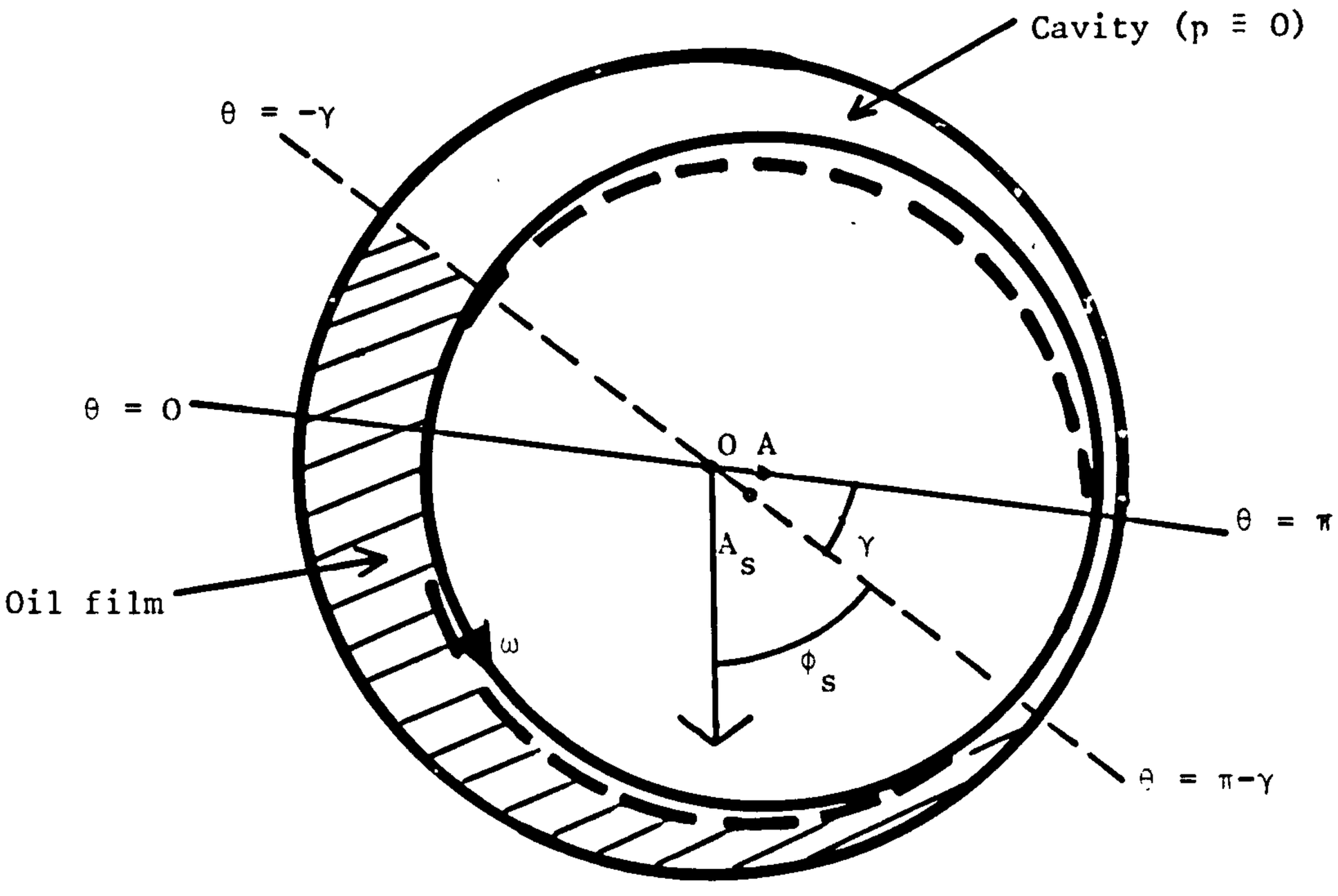

Figure 3.1(b). A journal bearing operating with a static half film.

Integrating the Reynolds equation for a long bearing (equation 2.1) with the above boundary conditions yields the pressure distribution:

$$\left(\frac{c}{R}\right)^2 \frac{p}{\omega\mu} = \frac{6\varepsilon(1-2\dot{\phi})(2+\varepsilon\cos\theta)\sin\theta}{(2+\varepsilon^2)(1+\varepsilon\cos\theta)^2} \tag{3.2}$$

$$+ 6\dot{\varepsilon}\left\{\frac{4}{\pi}\left[\frac{4-\varepsilon^2+3\varepsilon\cos\theta}{(1-\varepsilon^2)^{3/2}(2+\varepsilon^2)(1+\varepsilon\cos\theta)^2}\right]\sin\theta - \frac{4\cos^{-1}u}{\pi(1-\varepsilon^2)^2} + \left[\frac{1}{(1+\varepsilon\cos\theta)^2} - \frac{1}{(1+\varepsilon)^2}\right]\frac{1}{\varepsilon}\right\}$$

where $u = \dfrac{\varepsilon+\cos\theta}{1+\varepsilon\cos\theta}$

The hydrodynamic forces are:

$$F_r = LR\int_o^{\pi} p(\theta)\cos\theta d\theta \qquad F_t = LR\int_o^{\pi} p(\theta)\sin\theta d\theta$$

Integrating by parts, substituting for $dp/d\theta$ and evaluating the integrals (Appendix I):

$$-\left(\frac{c}{R}\right)^2 \frac{F_r}{LR\omega\mu} = \frac{12\varepsilon^2(1-2\dot{\phi})}{(2+\varepsilon^2)(1-\varepsilon^2)} + \frac{6\{\pi^2(2+\varepsilon^2)-16\}\dot{\varepsilon}}{\pi(2+\varepsilon^2)(1-\varepsilon^2)^{3/2}} \tag{3.3}$$

$$\left(\frac{c}{R}\right)^2 \frac{F_t}{LR\omega\mu} = \frac{6\pi\varepsilon(1-2\dot{\phi})}{(1-\varepsilon^2)^{1/2}(2+\varepsilon^2)} + \frac{24\varepsilon\dot{\varepsilon}}{(1-\varepsilon^2)(2+\varepsilon^2)}$$

The equations of motion are:

$$\ddot{\varepsilon}-\varepsilon\dot{\phi}^2 = \nu\left\{\cos\phi - S\left[\frac{12\varepsilon^2(1-2\dot{\phi})}{(2+\varepsilon^2)(1-\varepsilon^2)} + \frac{6\{\pi^2(2+\varepsilon^2)-16\}\dot{\varepsilon}}{\pi(2+\varepsilon^2)(1-\varepsilon^2)^{3/2}}\right]\right\} \tag{3.4}$$

$$\varepsilon\ddot{\phi}+2\dot{\varepsilon}\dot{\phi} = -\nu\left\{\sin\phi - S\left[\frac{6\pi\varepsilon(1-2\dot{\phi})}{(2+\varepsilon^2)(1-\varepsilon^2)^{1/2}} + \frac{24\varepsilon\dot{\varepsilon}}{(2+\varepsilon^2)(1-\varepsilon^2)}\right]\right\}$$

The steady state solution to these equations is:

$$\cos\phi_s = -S\bar{F}_{rs} = \frac{12S\varepsilon_s^2}{(2+\varepsilon_s^2)(1-\varepsilon_s^2)} \qquad \sin\phi_s = S\bar{F}_{ts} = \frac{6S\pi\varepsilon_s}{(2+\varepsilon_s^2)(1-\varepsilon_s^2)^{1/2}} \tag{3.5}$$

$$\Rightarrow \tan \phi_s = \frac{\pi(1-\varepsilon_s^2)^{1/2}}{2\varepsilon_s} \quad (3.6) \qquad S = \frac{(2+\varepsilon_s^2)(1-\varepsilon_s^2)}{6\varepsilon_s\{\pi^2(1-\varepsilon_s^2)+4\varepsilon_s^2\}^{1/2}} \quad (3.7)$$

The relationship between the Sommerfeld number S and the steady state eccentricity ratio (equation 3.7) is illustrated in Figure 3.2. The presence of a steady state force in the radial direction means the locus of the journal centre (equation 3.6) is now approximately semicircular (Figure 3.3). The steady state pressure is equal to the Sommerfeld pressure (equation 2.7) taken over the range $0 < \theta < \pi$ (Figure 3.4).

The equations of motion (3.4) may be linearised about the equilibrium position following the precedure outlined in Chapter 1. The eight velocity and displacement coefficients are:

$$B_{xx} = \frac{\{\pi^2(2+\varepsilon_s^2) - 16\}}{\pi\varepsilon_s(1-\varepsilon_s^2)^{1/2}(\pi^2(1-\varepsilon_s^2)+4\varepsilon_s^2)^{1/2}} \qquad B_{xy} = B_{yx} = \frac{-4}{(\pi^2(1-\varepsilon_s^2)+4\varepsilon_s^2)^{1/2}} \quad (3.8)$$

$$B_{yy} = 2K_{xy} = \frac{2\pi(1-\varepsilon_s^2)^{1/2}}{\varepsilon_s(\pi^2(1-\varepsilon_s^2)+4\varepsilon_s^2)^{1/2}} \qquad K_{xx} = \frac{4(2+\varepsilon_s^4)}{(2+\varepsilon_s^2)(1-\varepsilon_s^2)(\pi^2(1-\varepsilon_s^2)+4\varepsilon_s^2)^{1/2}}$$

$$K_{yx} = \frac{-\pi(2-\varepsilon_s^2+2\varepsilon_s^4)}{\varepsilon_s(2+\varepsilon_s^2)(1-\varepsilon_s^2)^{1/2}(\pi^2(1-\varepsilon_s^2)+4\varepsilon_s^2)^{1/2}} \qquad K_{yy} = \frac{2}{(\pi^2(1-\varepsilon_s^2)+4\varepsilon_s^2)^{1/2}}$$

The frequency equation is:

$$\bar{\lambda}^4 + \frac{\nu(4\pi^2-16-\pi^2\varepsilon_s^2)\bar{\lambda}^3}{\pi\varepsilon_s(1-\varepsilon_s^2)^{1/2}(\pi^2(1-\varepsilon_s^2)+4\varepsilon_s^2)^{1/2}} + 2\nu\left\{\frac{(6-\varepsilon_s^2+\varepsilon_s^4)}{(1-\varepsilon_s^2)(2+\varepsilon_s^2)(\pi^2(1-\varepsilon_s^2)+4\varepsilon_s^2)^{1/2}}\right.$$

$$\left. + \frac{\nu(\pi^2-8)(2+\varepsilon_s^2)}{\varepsilon_s^2(\pi^2(1-\varepsilon_s^2)+4\varepsilon_s^2)}\right\}\bar{\lambda}^2 \quad (3.9)$$

$$+ \frac{2\nu^2(6\pi^2-16-\pi^2\varepsilon_s^2)\bar{\lambda}}{\pi\varepsilon_s(1-\varepsilon_s^2)^{1/2}(\pi^2(1-\varepsilon_s^2)+4\varepsilon_s^2)} + \nu^2\left\{\frac{2\pi^2+(16-3\pi^2)\varepsilon_s^2+3\pi^2\varepsilon_s^4+(8-2\pi^2)\varepsilon_s^6}{\varepsilon_s^2(1-\varepsilon_s^2)(2+\varepsilon_s^2)(\pi^2(1-\varepsilon_s^2)+4\varepsilon_s^2)}\right\} = 0$$

Unlike the frequency equations for the two models with complete films (equations 2.11 and 2.22), there is now a $\bar{\lambda}$ term in this equation. An

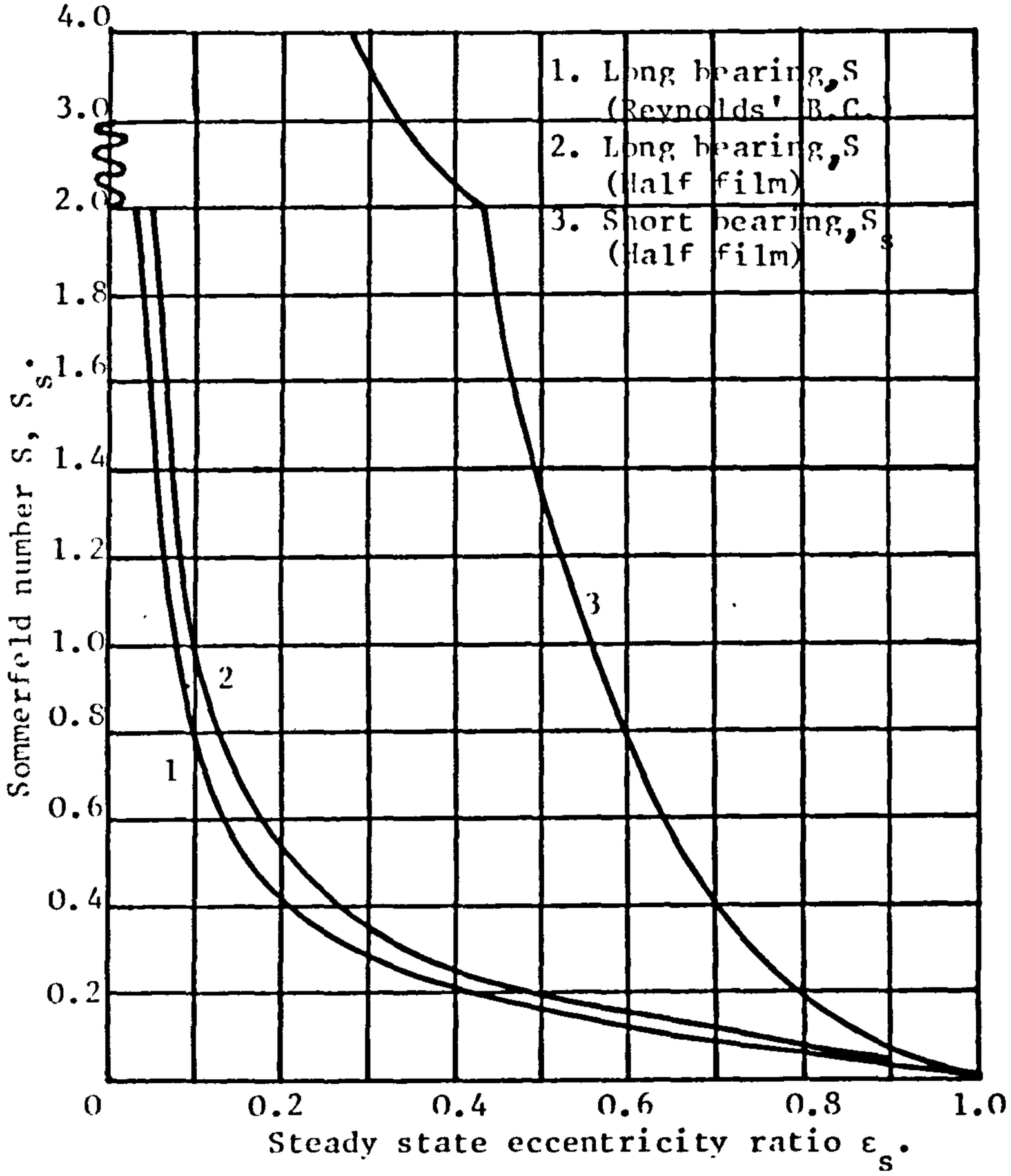

Figure 3.2. Relationship between the Sommerfeld number and the steady state eccentricity ratio for models with different cavitation boundary conditions at film rupture.

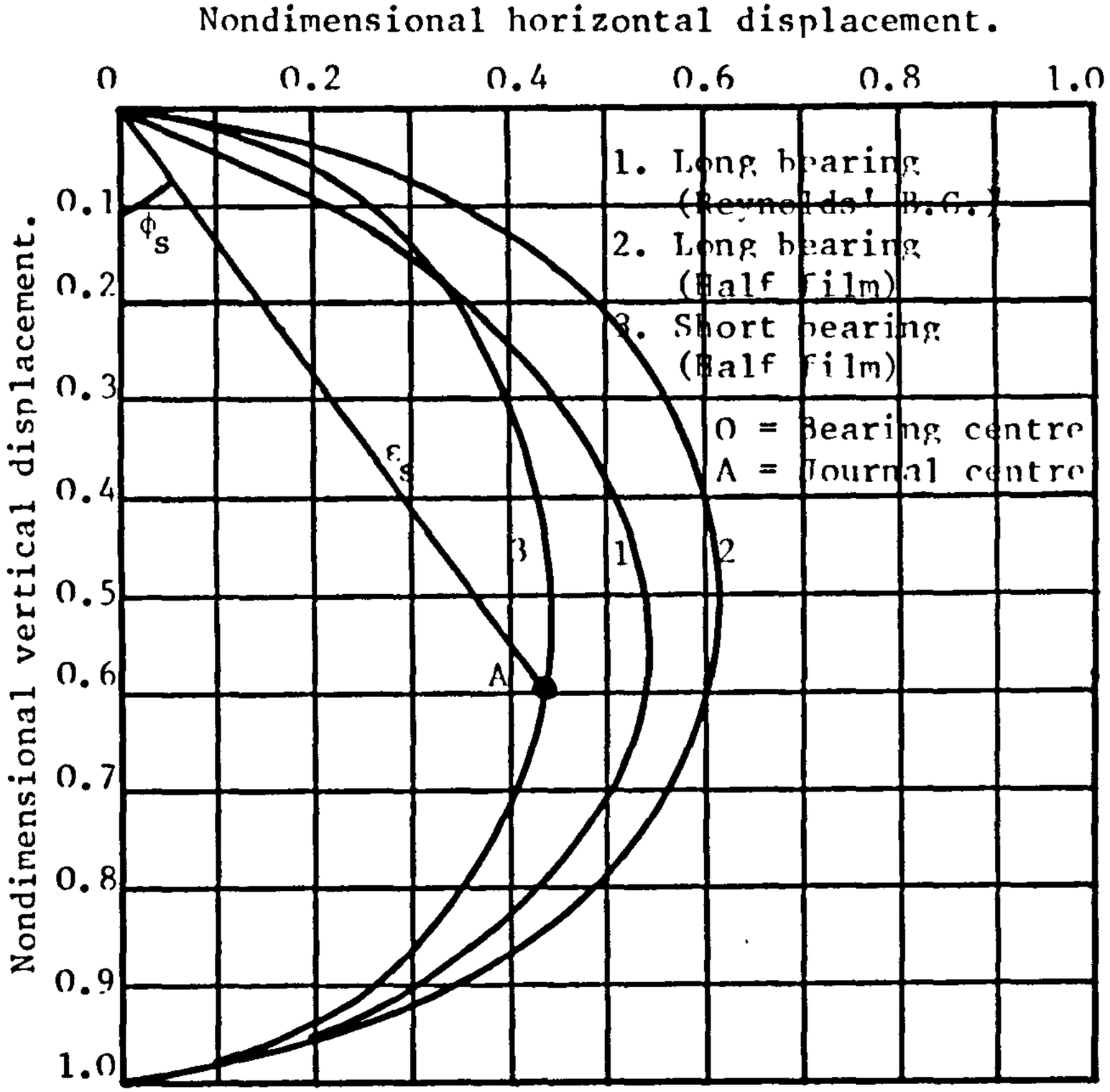

Figure 3.3. Theoretical steady locus of the journal centre for models with different cavitation boundary conditions at film rupture.

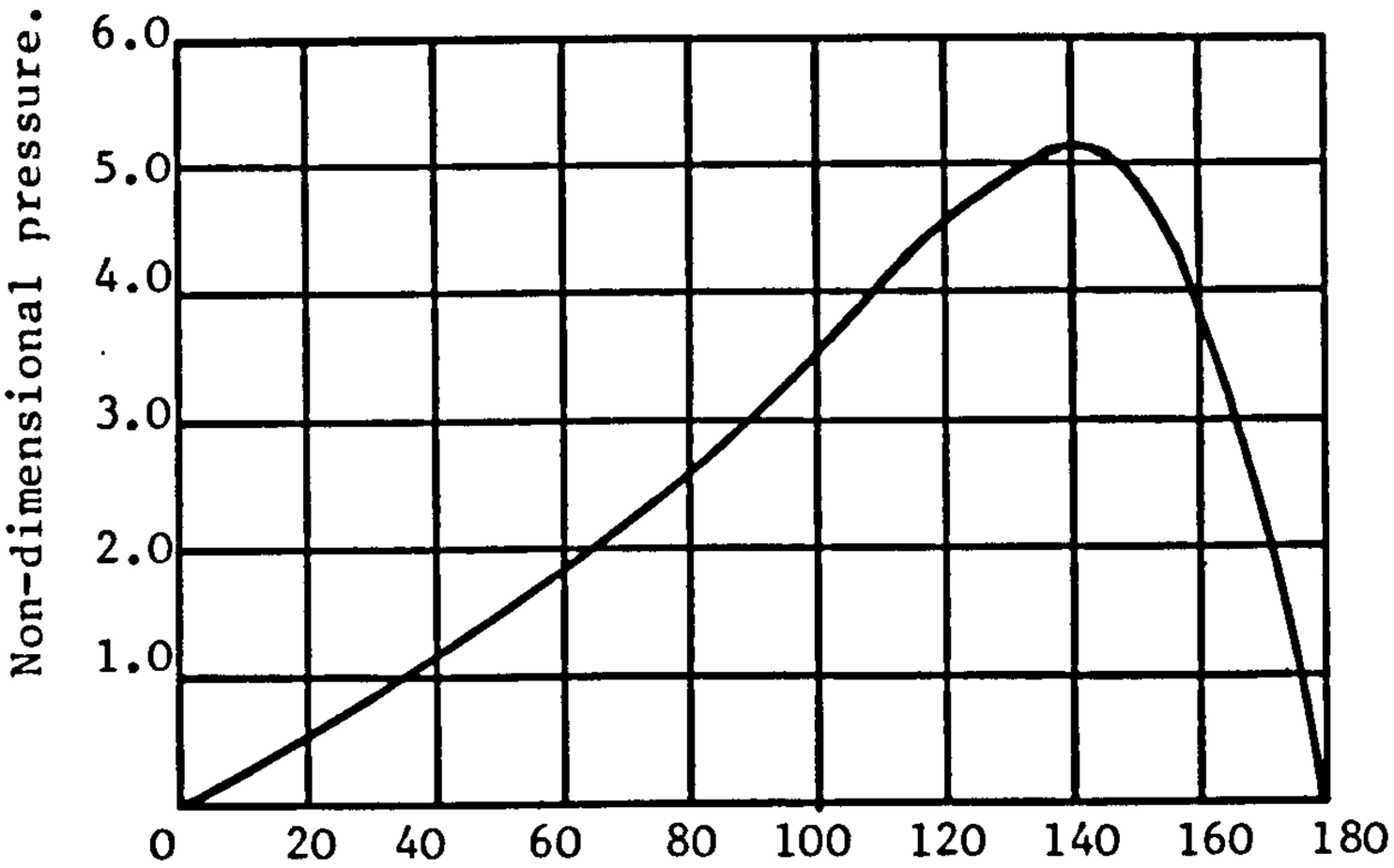

3.4(a). Long bearing (Half film), $\varepsilon_s = 0.6$

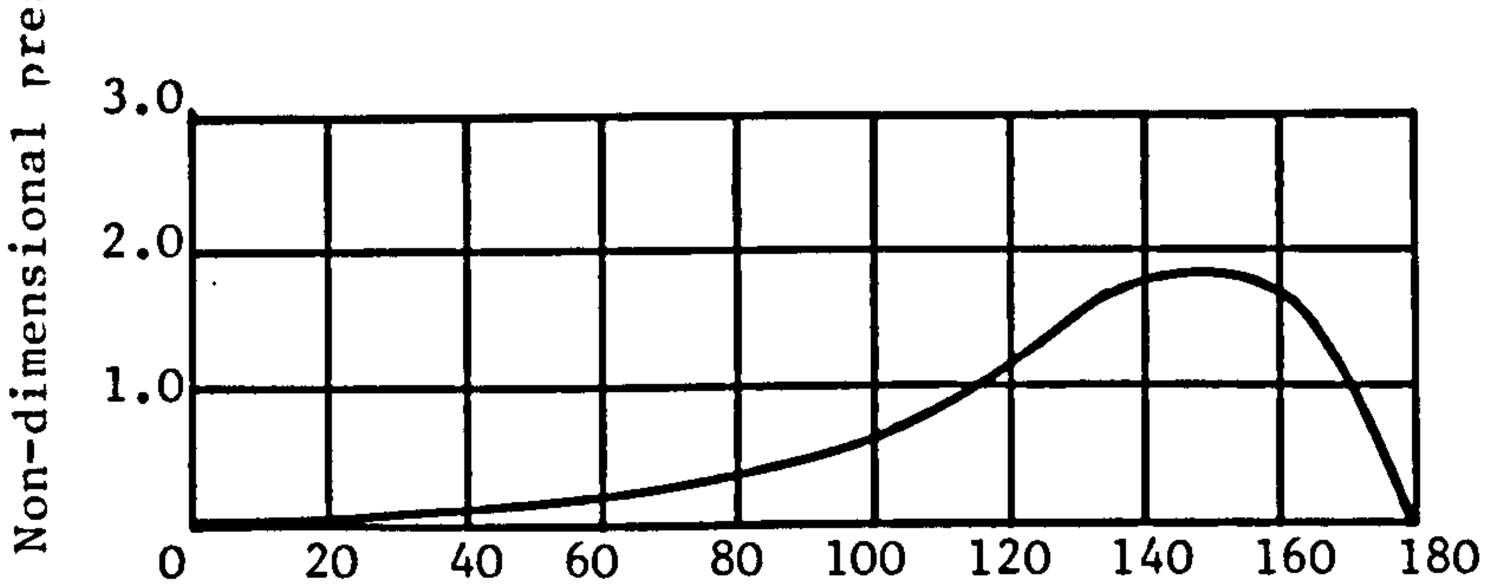

3.4(b). Short bearing (Half film), $\varepsilon_s = 0.6$, $z = L/2$

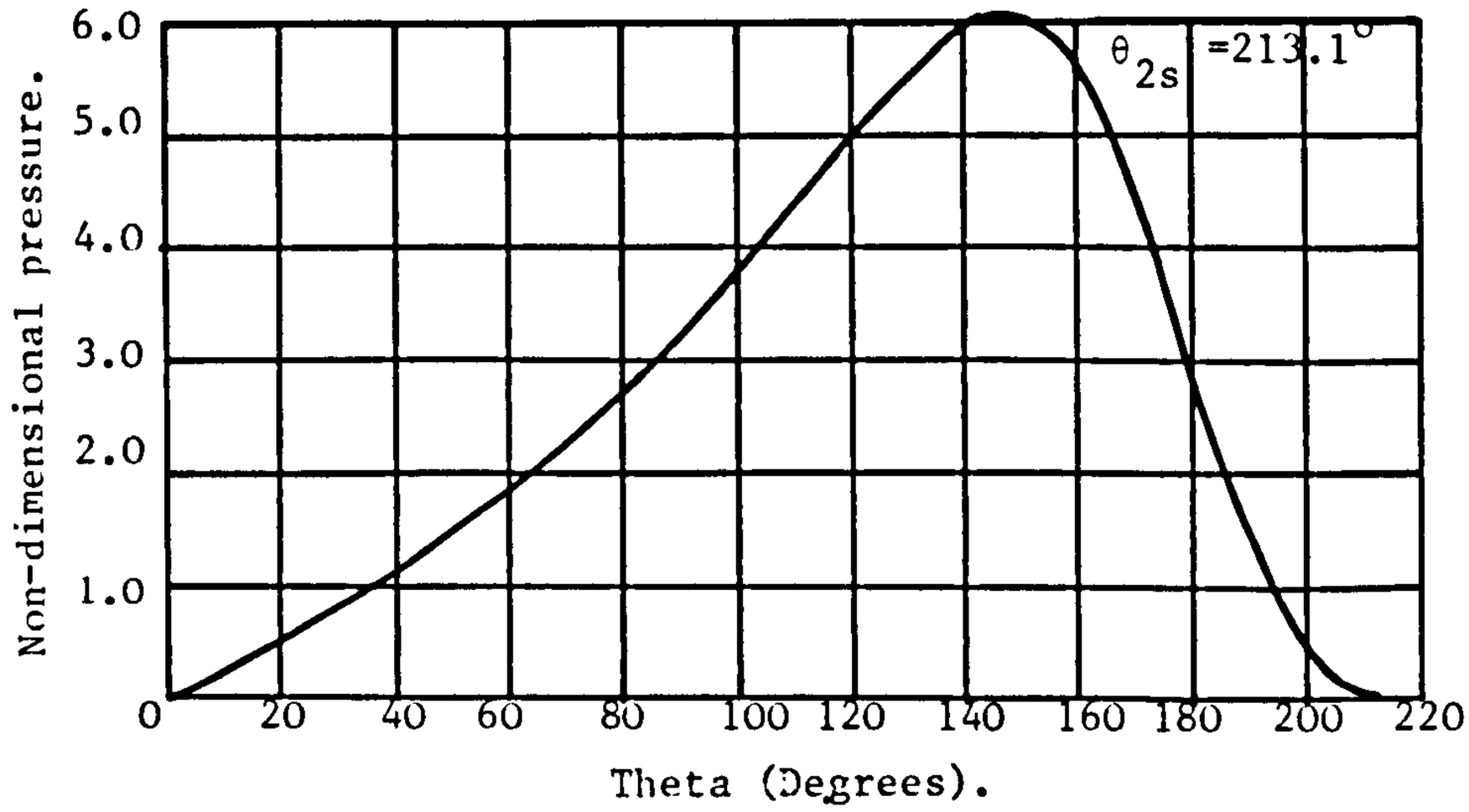

3.4(c). Long bearing (Reynolds' B.C.), $\varepsilon_s = 0.6$

Figure 3.4. Steady state pressure distributions for different models.

application of Routh's criterion now leads to the condition:

$$\nu > \nu_{crit.}(\varepsilon_s) \quad \text{for stability} \tag{3.10}$$

(see Chapter 1, equation 1.25)

The critical frequency (non-dimensional) is:

$$\bar{\Omega}_{crit.} = \left\{ \frac{2(6\pi^2-16-\pi^2\varepsilon_s^2)\nu_{crit.}}{(4\pi^2-16-\pi^2\varepsilon_s^2)(\pi^2(1-\varepsilon_s^2)+4\varepsilon_s^2)^{1/2}} \right\}^{1/2} \quad \text{(see equation 1.27)} \tag{3.11}$$

A stability curve of $\nu_{crit.}/\varepsilon_s$ is shown in Figure 3.5. The stability chart may be used to determine whether or not the journal will be stable for any given parameter values (ν,ε_s). The critical frequency curve is shown in Figure 3.6. A full discussion of these curves is presented in section 3.6, where a comparison is made with the predictions of the other models investigated in this Chapter.

With this simple model, which assumes an oscillating film, it has been shown that cavitation is a stabilizing mechanism (a bearing operating with a complete film is unstable for all values of ν and ε_s). The next objective is to investigate the effect of oil film behaviour on the vibrational characteristics of the journal.

3.2 A LONG BEARING OPERATING WITH A STATIC HALF FILM.

In this model the oil film is again taken to be 180^o in extent, but to begin and end along the equilibrium position of the line of centres. Therefore the film is assumed to remain static during any motion of the journal (Figure 3.1(b)). With γ equal to the change in the attitude angle from its equilibrium value, ϕ_s, the appropriate boundary conditions are:

$$p = 0 \text{ at } \theta = -\gamma, \pi - \gamma \; ; \quad p \equiv 0 \text{ for } \pi - \gamma < \theta < 2\pi - \gamma \tag{3.12}$$

The Reynolds equation for a long bearing (equation 2.1) may be integrated twice together with the above boundary conditions to obtain the

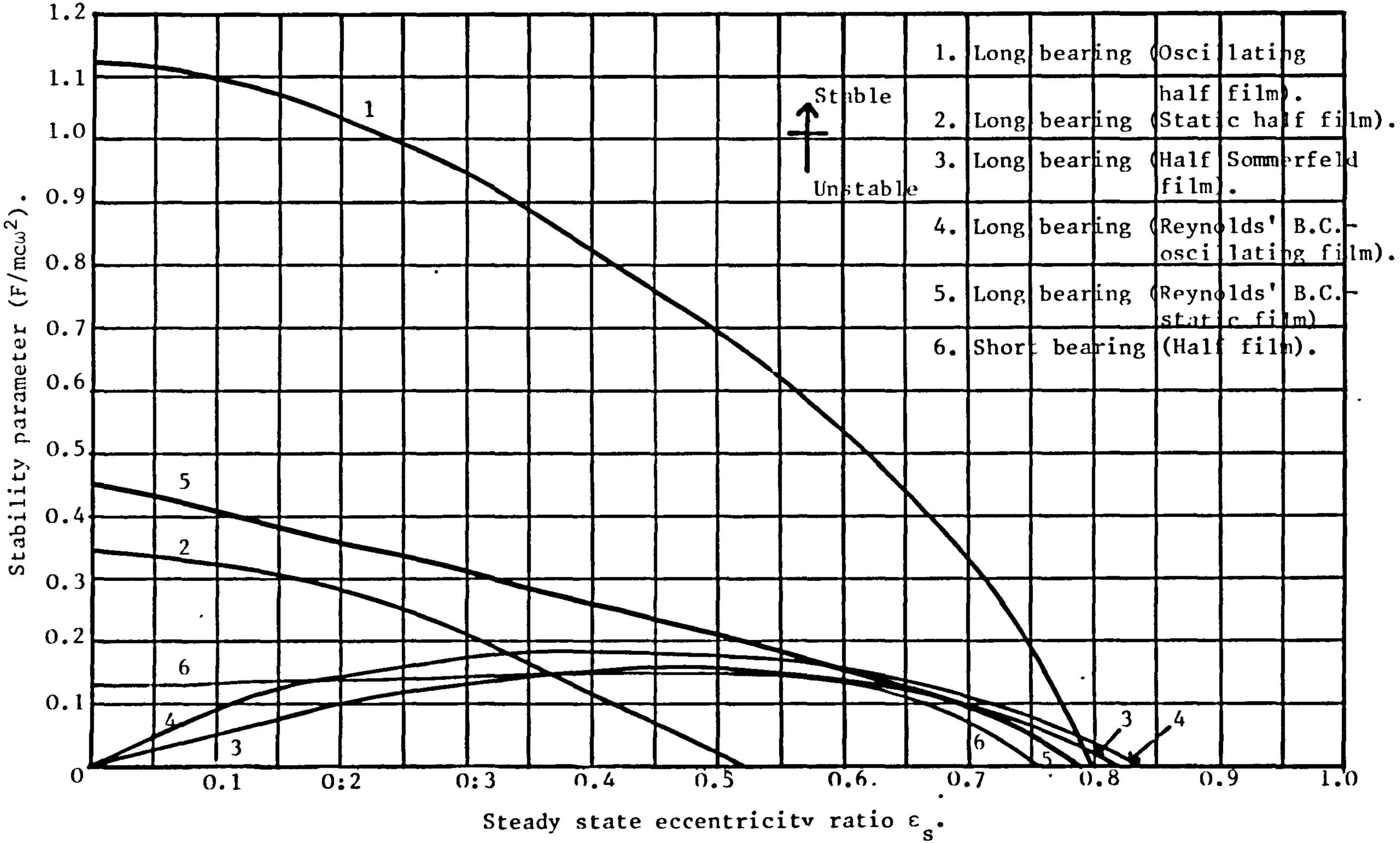

Figure 3.5. Stability borderlines for models with different cavitation boundary conditions at film rupture.

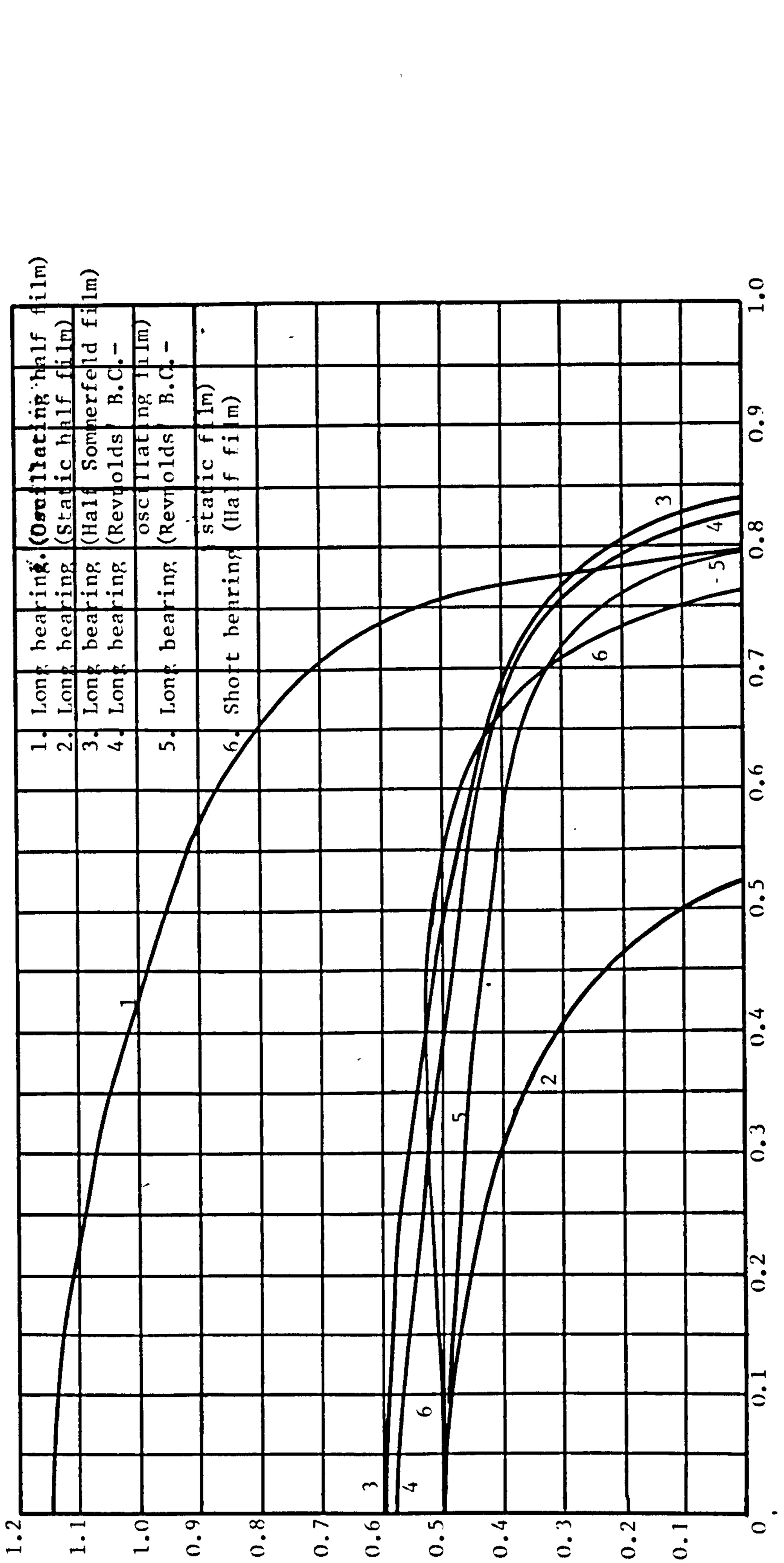

Figure 3.6. Critical frequency curves for models with different cavitation boundary conditions at film runture.

pressure distribution, which may then be integrated to obtain the force components:

$$F_r = LR\int_{-\gamma}^{\pi-\gamma} p(\theta)\cos\theta d\theta \qquad F_t = LR\int_{-\gamma}^{\pi-\gamma} p(\theta)\sin\theta d\theta$$

The expressions for the pressure p and the force components F_r, F_t, are rather lengthy and are given in Appendix II. The equations of motion may then be formulated as in the previous cases.

Under steady state conditions $\gamma = 0$ and hence the equilibrium solution is identical with that of the previous model (see equations 3.5, 3.6, 3.7). However, the linearised equations will not be the same because of the additional γ terms. The eight velocity and displacement coefficients are calculated following the procedure outlined in Appendix II. They are:

$$B_{xx} = \frac{\{\pi^2(2+\epsilon_s^2)-16\}}{\pi\epsilon_s(1-\epsilon_s^2)^{1/2}(\pi^2(1-\epsilon_s^2)+4\epsilon_s^2)^{1/2}} \qquad B_{xy} = B_{yx} = \frac{-4}{(\pi^2(1-\epsilon_s^2)+4\epsilon_s^2)^{1/2}}$$

$$B_{yy} = \frac{2\pi(1-\epsilon_s^2)^{1/2}}{\epsilon_s(\pi^2(1-\epsilon_s^2)+4\epsilon_s^2)^{1/2}} \qquad (3.13)$$

$$K_{xx} = \frac{4(2+\epsilon_s^4)}{(2+\epsilon_s^2)(1-\epsilon_s^2)(\pi^2(1-\epsilon_s^2)+4\epsilon_s^2)^{1/2}}$$

$$K_{xy} = \frac{\{\pi^2(2+\epsilon_s^2)(1-\epsilon_s^2)-16\}}{\pi\epsilon_s(2+\epsilon_s^2)(1-\epsilon_s^2)^{1/2}(\pi^2(1-\epsilon_s^2)+4\epsilon_s^2)^{1/2}}$$

$$K_{yx} = \frac{-\pi(2-\epsilon_s^2+2\epsilon_s^4)}{\epsilon_s(2+\epsilon_s^2)(1-\epsilon_s^2)^{1/2}(\pi^2(1-\epsilon_s^2)+4\epsilon_s^2)^{1/2}} \qquad K_{yy} = \frac{4(1+\epsilon_s^2)}{(2+\epsilon_s^2)(\pi^2(1-\epsilon_s^2)+4\epsilon_s^2)^{1/2}}$$

The coefficients are identical with those of the first model (equations 3.8), except for K_{xy} and K_{yy}. This is to be expected since the only difference between the two models is the additional γ terms (see Appendix II).

The eight coefficients may be used to calculate the frequency equation. The stability borderline is then calculated from an application of Routh's criterion (Figure 3.5). The critical frequency curve is shown in Figure 3.6. It is easily seen that there is a dramatic difference between the stability characteristics of the two models examined so far. The bearing operating with the static film is much more stable than the oscillating film. It must be emphasized again that the only difference between the two models is in the behaviour of the oil film during a vibration of the journal.

3.3 A LONG BEARING OPERATING WITH A HALF SOMMERFELD FILM.

A third alternative model of a journal bearing operating with a half film is to take the Sommerfeld pressure and neglect the subambient pressures predicted by it (the cavity is assumed to exist in this region). Under dynamic conditions the Sommerfeld pressure is (equation 2.2):

$$\left(\frac{c}{R}\right)^2 \frac{p}{\omega\mu} = \frac{6\varepsilon(1-2\phi')(2+\varepsilon\cos\theta)\sin\theta}{(2+\varepsilon^2)(1+\varepsilon\cos\theta)^2} + 6\left\{\frac{1}{(1+\varepsilon\cos\theta)^2} - \frac{1}{(1+\varepsilon)^2}\right\}\frac{\varepsilon'}{\varepsilon}$$

$\Rightarrow$ $p = 0$ at $\theta = 0$, 2π and $\pi+\alpha$ where α satisfies the equation:

$$\frac{-\varepsilon(1-2\phi')(2-\varepsilon\cos\alpha)\sin\alpha}{(2+\varepsilon^2)(1-\varepsilon\cos\alpha)} + \left\{\frac{1}{(1-\varepsilon\cos\alpha)^2} - \frac{1}{(1+\varepsilon)^2}\right\}\frac{\varepsilon'}{\varepsilon} = 0 \qquad (3.14)$$

The pressure is superambient for $0 < \theta < \pi + \alpha$ and subambient for $\pi + \alpha < \theta < 2\pi$. Therefore the cavity is assumed to exist in the region $\pi + \alpha < \theta < 2\pi$ (Figure 3.7).

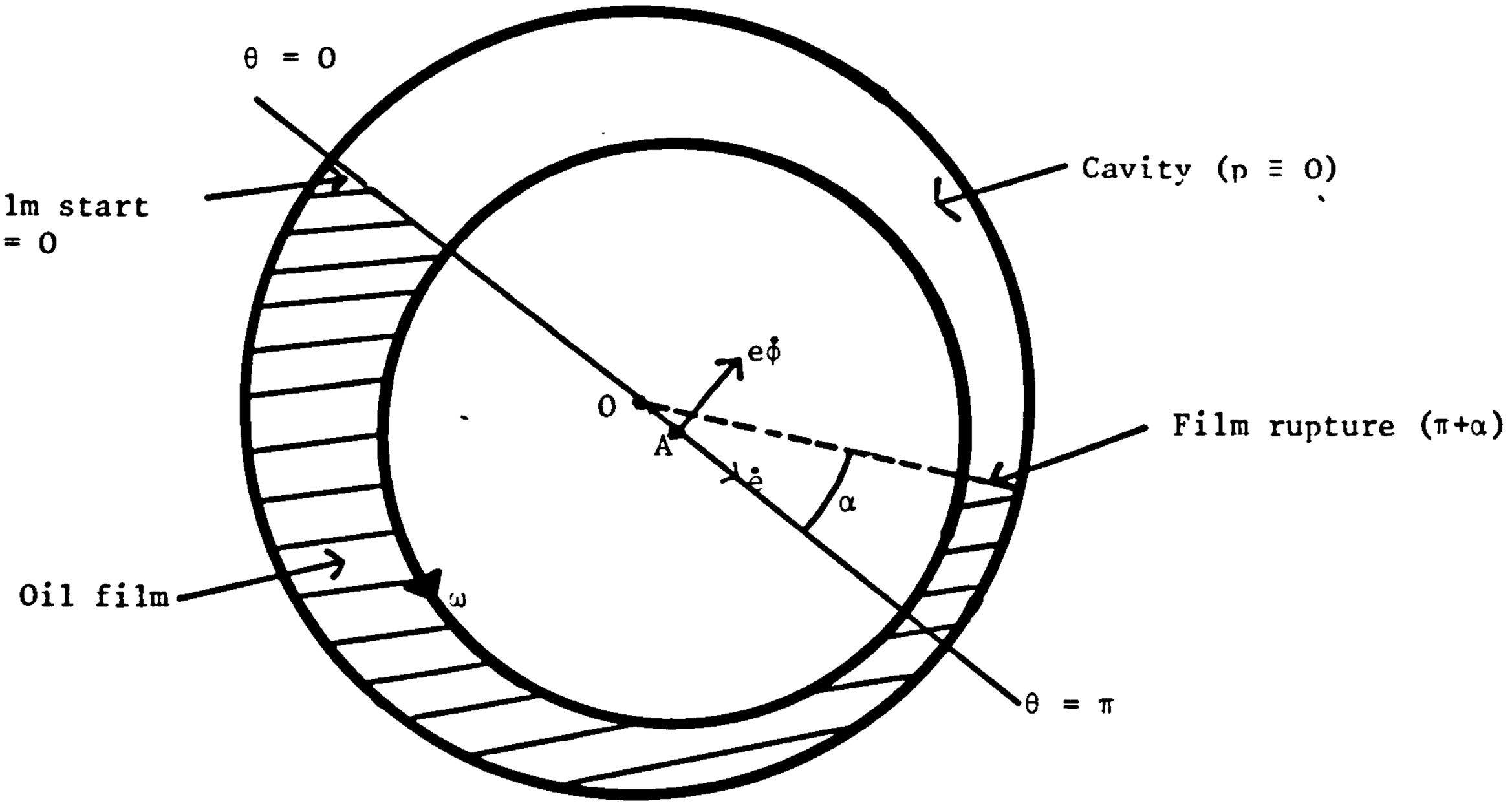

Figure 3.7 A long bearing operating with a half Sommerfeld film.

The hydrodynamic forces are:

$$-\left(\frac{c}{R}\right)^2 \frac{F_r}{LR^3\omega\mu} = \frac{\varepsilon(1-2\dot{\phi})}{4(1-\varepsilon^2)(2+\varepsilon^2)} \{4\varepsilon(\cos\psi_2-1)-(\cos 2\psi_2-1)\}$$

$$+ \frac{2\dot{\varepsilon}}{4(1-\varepsilon^2)^{3/2}} \{2\psi_2-\sin 2\psi_2\} \qquad (3.15)$$

$$\left(\frac{c}{R}\right)^2 \frac{F_t}{LR^3\omega\mu} = \frac{\varepsilon(1-2\dot{\phi})}{4(1-\varepsilon^2)^{3/2}(2+\varepsilon^2)} \{2\sin 2\psi_2-4\varepsilon\sin\psi_2+4(1-\varepsilon^2)\psi_2\}$$

$$+ \frac{2\dot{\varepsilon}}{4(1-\varepsilon^2)^2} \{4\varepsilon(\cos\psi_2-1)-(\cos 2\psi_2-1)\}$$

where ψ_2 is the Sommerfeld angle corresponding to $\pi + \alpha$.

The equations of motion of the journal are:

$$\ddot{\varepsilon} - \varepsilon\dot{\phi}^2 = \nu(\cos\phi+S\bar{F}_r) \qquad \varepsilon\ddot{\phi} + 2\dot{\varepsilon}\dot{\phi} = -\nu(\sin\phi-S\bar{F}_t) \qquad (3.16)$$

These equations together with equation (3.14) describe the full motion of the journal which can only be determined numerically in a step by step integration which solves equation (3.14) for α after each step. Under steady state conditions $\alpha = 0$ and hence the equilibrium solution

to equations (3.16) is identical with the previous two models (see equations 3.5, 3.6, 3.7 and Figures 3.2, 3.3, 3.4).

The first stage in linearising equations (3.16) is to obtain an expression for α from equation (3.14). During a small amplitude vibration of the journal about its equilibrium position α will be a small quantity (see equation 3.14). Substituting $\varepsilon = \varepsilon_s + \delta$ and $\phi = \phi_s + \gamma$ into equation (3.14) and retaining only first order terms:

$$\Rightarrow \alpha = \frac{4(2+\varepsilon_s^2)\dot{\delta}}{(1+\varepsilon_s)^2(2-\varepsilon_s)} \qquad (3.17)$$

Using the Sommerfeld relation (Appendix I) and the fact that α is a small angle the following expressions may be derived:

$$\cos\psi_2 = -1 \qquad \sin\psi_2 = \frac{-(1-\varepsilon_s^2)^{1/2}\alpha}{(1-\varepsilon_s)} \qquad \psi_2 = \pi + \frac{(1-\varepsilon_s^2)^{1/2}\alpha}{(1-\varepsilon_s)}$$

$$\cos 2\psi_2 = 1 \qquad \sin 2\psi_2 = \frac{2(1-\varepsilon_s^2)^{1/2}\alpha}{(1-\varepsilon_s)} \qquad (3.18)$$

The procedure for linearising equation (3.16) is:

i) Substitute $\varepsilon = \varepsilon_s + \delta$, $\phi = \phi_s + \gamma$.

ii) Use equations (3.18) to eliminate ψ_2.

iii) Use equation (3.17) to eliminate α.

iv) Neglect terms higher than the first order.

v) Collect like terms and put $\delta = x$, $\varepsilon_s\gamma = y$.

The eight velocity and displacement coefficients are:

$$B_{xx} = \frac{\pi(2+\varepsilon_s^2)}{\varepsilon_s(1-\varepsilon_s^2)^{1/2}(\pi^2(1-\varepsilon_s^2)+4\varepsilon_s^2)^{1/2}} \qquad B_{xy} = -2K_{yy} = \frac{-4}{(\pi^2(1-\varepsilon_s^2)+4\varepsilon_s^2)^{1/2}}$$

$$B_{yx} = \frac{-4(1-\varepsilon_s)(2+\varepsilon_s^2)}{\varepsilon_s(1-\varepsilon_s^2)(\pi^2(1-\varepsilon_s^2)+4\varepsilon_s^2)^{1/2}} \qquad B_{yy} = 2K_{xy} = \frac{2\pi(1-\varepsilon_s^2)^{1/2}}{\varepsilon_s(\pi^2(1-\varepsilon_s^2)+4\varepsilon_s^2)^{1/2}} \qquad (3.19)$$

$$K_{xx} = \frac{4(2+\varepsilon_s^4)}{(2+\varepsilon_s^2)(1-\varepsilon_s^2)(\pi^2(1-\varepsilon_s^2)+4\varepsilon_s^2)^{1/2}}$$

$$K_{yx} = \frac{-\pi(2-\varepsilon_s^2+2\varepsilon_s^4)}{\varepsilon_s(2+\varepsilon_s^2)(1-\varepsilon_s^2)^{1/2}(\pi^2(1-\varepsilon_s^2)+4\varepsilon_s^2)^{1/2}}$$

The eight coefficients may be used to derive the frequency equation. The stability borderline is then calculated from an application of Routh's criterion (Figure 3.5). The critical frequency curve is shown in Figure 3.6. A full discussion of these curves is postponed until section 3.6. However, it is evident from Figures 3.5 and 3.6 that the three models investigated so far have very different stability characteristics even though superficially they appear to be very similar.

The assumption that the film terminates at or close to the line of minimum film thickness with ambient pressure is not an accurate description of the physical situation. It is used for mathematical convenience as a simple way of modelling cavitation. A more accurate boundary condition is the one attributed to Reynolds (1886). It is most easily formulated from considerations of flow continuity. For a two dimensional flow situation the lubricant flow rate just before film rupture is (Figure 3.8):

$$-\frac{h^3}{12\mu}\frac{dp}{dx} + \frac{Uh}{2} \qquad (3.20)$$

In the cavitating region, assuming a finger pattern of air cavities, the pressure is assumed to be ambient, and so only Couette flow need be considered. Just after film rupture, assuming that the cavities occupy only a very small fraction of the total bearing width (ie. the cavities are "pointed") the flow rate per unit width is:

$$\frac{Uh}{2} \qquad (3.21)$$

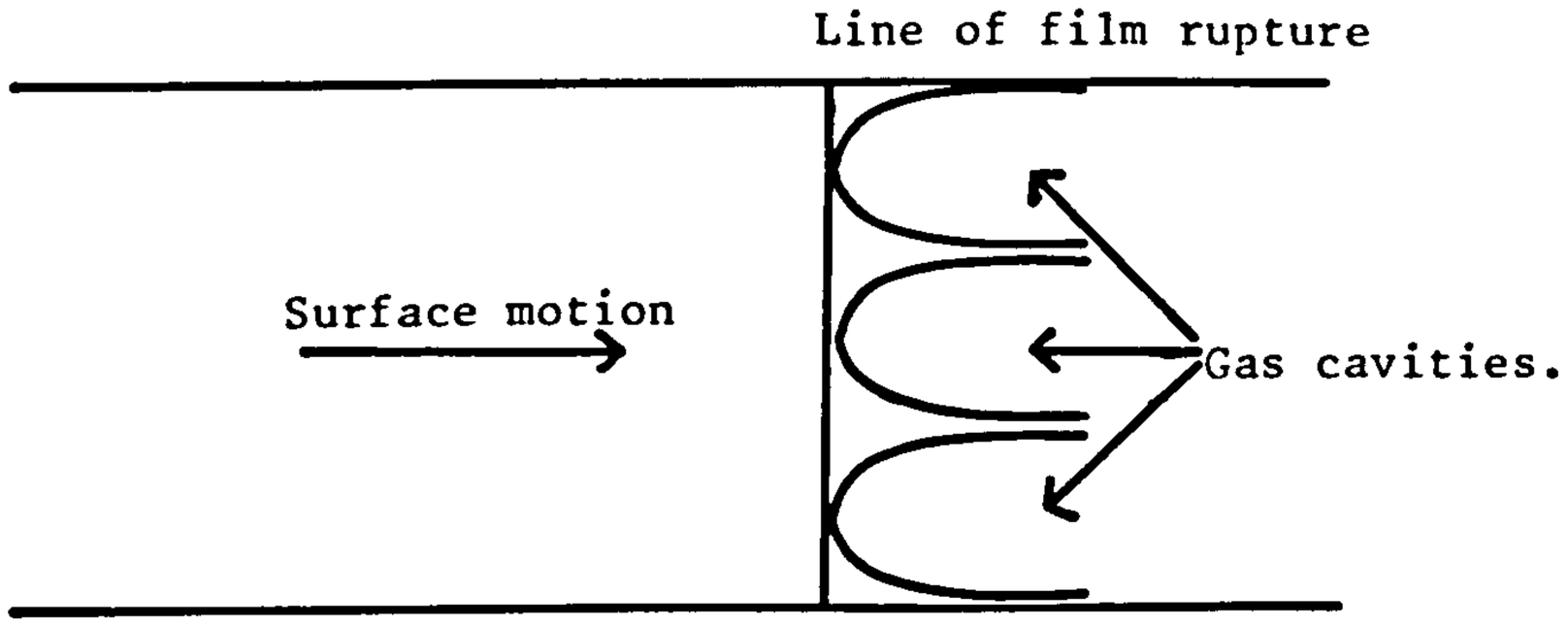

Figure 3.8 Plan view of two dimensional film rupture.

Equating the flow rates before and after rupture leads to the boundary condition:

$$p = \frac{dp}{dx} = 0 \qquad \text{at film rupture} \tag{3.22}$$

This analysis shows the incorrectness of Gümbel's boundary condition which has a negative pressure gradient at the cavity interface (Figure 3.4). In the next section the vibrational behaviour of a bearing operating with an oil film satisfying the Reynolds boundary condition is investigated.

3.4 A LONG BEARING (FILM SATISFYING THE REYNOLDS BOUNDARY CONDITION).

In this model the oil film is assumed to begin at or around the line of maximum film thickness with zero (ambient) pressure and to end beyond the line of minimum film thickness where both the pressure and the pressure gradient are zero (Figure 3.9). The boundary conditions are:

$$p = 0 \text{ at } \theta = \theta_1, \text{ film formation} \tag{3.23}$$

and $p = \frac{dp}{d\theta} = 0$ at $\theta = \theta_2$, film rupture

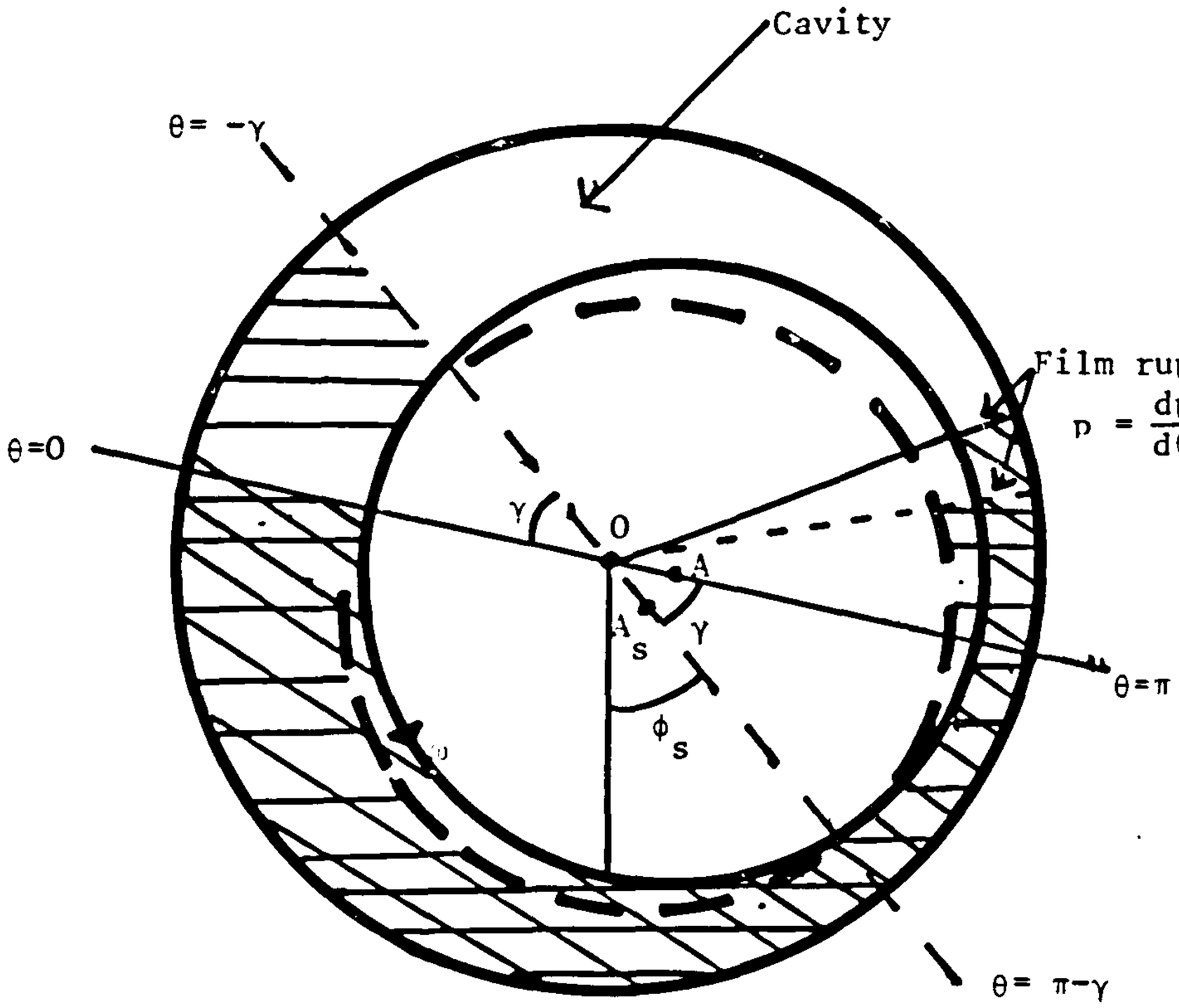

3.9(a): Oscillating film model.

A. Journal centre during vibration

A_s. Steady state position of journal centre

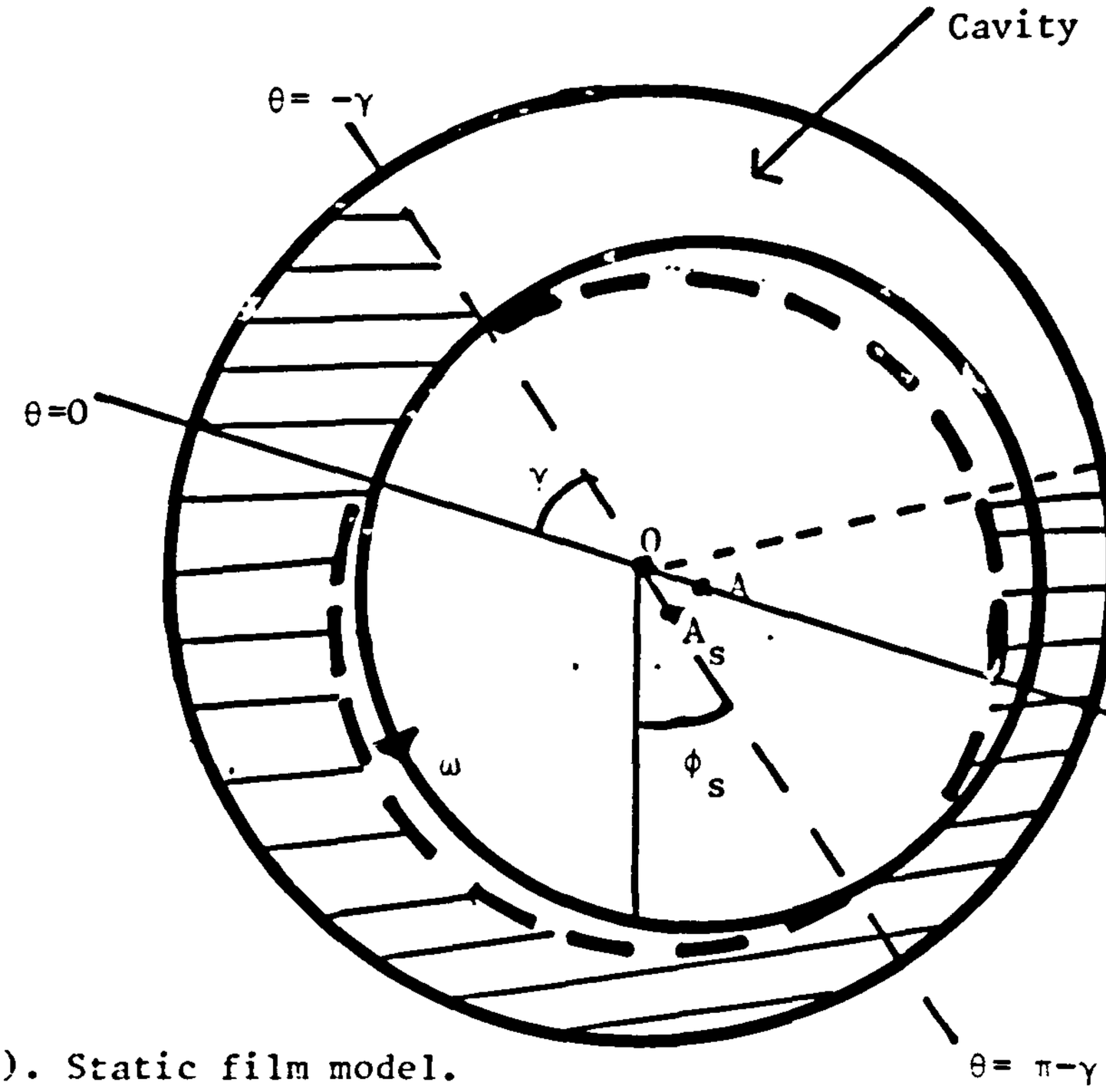

3.9(b). Static film model.

Figure 3.9. Journal bearing operating with a film satisfying the Reynolds boundary condition at film rupture.

Integrating the Reynolds equation (2.1):

$$\left(\frac{c}{R}\right)^2 \frac{1}{\mu\omega}\frac{dp}{d\theta} = 6\left\{\frac{\varepsilon(1-2\dot{\phi})(\cos\theta-\cos\theta_2)+2\dot{\varepsilon}(\sin\theta-\sin\theta_2)}{(1+\varepsilon\cos\theta)^3}\right\} \tag{3.24}$$

(which satisfies $(dp/d\theta)_{\theta_2} = 0$)

$$\Rightarrow \left(\frac{c}{R}\right)^2 \frac{p}{\mu\omega} = \frac{3\varepsilon(1-2\dot{\phi})F(\varepsilon,\psi,\psi_1,\psi_2)}{2(1-\varepsilon^2)^{3/2}(1-\varepsilon\cos\psi_2)} + \frac{3\dot{\varepsilon}Q(\varepsilon,\psi,\psi_1,\psi_2)}{(1-\varepsilon^2)^2(1-\varepsilon\cos\psi_2)} \tag{3.25}$$

(which satisfies $p(\theta_1)=0$)

ψ_1, ψ_2 are the Sommerfeld angles corresponding to θ_1, θ_2, respectively.

The location of film rupture at $\theta = \theta_2$ is determined from the equation:

$$\varepsilon(1-\varepsilon^2)^{1/2}(1-2\dot{\phi})F(\varepsilon,\psi_1,\psi_2) + 2\dot{\varepsilon}Q(\varepsilon,\psi_1,\psi_2) = 0 \tag{3.26}$$

The hydrodynamic forces are calculated by integrating the above pressure distribution. Throughout this work there are many lengthy algebraic expressions and it is necessary to introduce some notation to represent them (eg. F, Q). The full expression including the hydrodynamic forces may be found in Appendix II .

The equations of motion are:

$$\ddot{\varepsilon} - \varepsilon\dot{\phi}^2 = \nu\{\cos\phi + S\bar{F}_r(\varepsilon,\dot{\varepsilon},\dot{\phi},\psi_1,\psi_2)\} \tag{3.27}$$

$$\varepsilon\ddot{\phi} + 2\dot{\varepsilon}\dot{\phi} = -\nu\{\sin\phi - S\bar{F}_t(\varepsilon,\dot{\varepsilon},\dot{\phi},\psi_1,\psi_2)\}$$

where ψ_2 and hence θ_2 is determined from equation (3.26)

The steady state solution to these equations provides the relationship between the Sommerfeld number S and the steady state eccentricity ratio (Figure 3.2) and the locus of the journal centre (Figure 3.3). The steady state pressure profile for $\varepsilon_s = 0.6$, $\theta_1 = 0$ is shown in Figure 3.4 (the expressions are given in Appendix II).

To compute the complete motion of the journal for given initial conditions it would be necessary to integrate the equations of motion

numerically in a step by step routine which solves equation (3.26) for ψ_2 (θ_2) after each step. It is evident from equation (3.26) that even during a small amplitude vibration of the journal ψ_2 will not remain at its steady state value but will become $\psi_{2s}+\delta\psi_2$. The first stage in linearising the equations of motion is to obtain an expression for $\delta\psi_2$ by linearising equation (3.26) (see Appendix II).

After some tedious algebra it is possible to obtain expressions for the eight velocity and displacement coefficients as functions of $\varepsilon_s, \psi_{1s}, \psi_{2s}$ (see Appendix II). A computer program was written to calculate the eight coefficients. Once values of ε_s and ψ_{1s} had been specified, ψ_{2s} was determined by solving equation (3.26) numerically using the Newton-Raphson method (with $\varepsilon' = \phi' = 0$). The stability borderline and critical frequencywere then calculated from Routh's criterion (Figures 3.5 and 3.6).

An investigation was carried out into how the position of the oil film build up at $\theta = \theta_1$ influenced the vibrational characteristics of the journal. It was found that, for values of θ_1 close to the line of maximum film thickness ($-15^o < \theta_1 < 15^o$) the effect was insignificant and hence results are shown only for $\theta_1 = 0$. A more detailed examination is made in Chapter 4 for the axial groove bearing.

It was found, however, that the behaviour of the oil film during a vibration of the journal was important. Two different models may be examined - an oscillating film, or a static film (Figure 3.9).

Substituting $\theta_1 = 0$ into the preceding analysis models an oscillating film which swings to and fro with the vibration (Figure 3.9(a)). In the static film model the oil film is assumed to begin at the equilibrium position of the line of maximum film thickness (and continue to do so during the vibration) ie. at $\theta_1 = -\gamma$ (Figure 3.9(b)). This will alter the film rupture position at $\theta = \theta_2$ since θ_2 depends upon θ_1 (equation 3.26). The details of the analysis for this model may be

found in Appendix II. Under steady state conditions the two models are identical but they have different stability characteristics (Figures 3.5 and 3.6). Data for the Reynolds boundary condition is not widely available in the literature and so is presented in Table 3.1 for the two models.

3.5 A SHORT BEARING OPERATING WITH A HALF FILM.

The final model examined in this Chapter is a short bearing operating with a half film. It was shown in Chapter 2 (equation 2.12) that the pressure generated in a short bearing is:

$$\left(\frac{c}{L}\right)^2 \frac{p}{\mu\omega} = \frac{3z(z-L)}{L^2} \left\{ \frac{-\varepsilon(1-2\phi')\sin\theta+2\varepsilon'\cos\theta}{(1+\varepsilon\cos\theta)^3} \right\} \tag{3.28}$$

$$\Rightarrow p = 0 \quad \text{at } z = 0,L \quad \text{and at} \quad \theta = \theta_1, \pi+\theta_1, 2\pi+\theta_1$$

$$\text{where } \tan\theta_1 = \frac{2\varepsilon'}{\varepsilon(1-2\phi')} \tag{3.29}$$

The assumptions made in simplifying the Reynolds equation for a short bearing are so drastic that the pressure distribution cannot be altered. The subambient pressures are neglected in this model by assuming a cavity exists in the region $\pi+\theta_1<\theta<2\pi+\theta_1$ (Figure 3.10). This model was also considered by Holmes (1960) and Lund (1966).

The hydrodynamic forces are:

$$F_r = R\int_o^L \int_{\theta_1}^{\pi+\theta_1} p(\theta,z)\cos\theta d\theta dz \qquad F_t = R\int_o^L \int_{\theta_1}^{\pi+\theta_1} p(\theta,z)\sin\theta d\theta dz$$

$$\Rightarrow -\left(\frac{c}{L}\right)^2 \frac{F_r}{LR\omega\mu} = -\frac{\varepsilon}{2}(1-2\phi')I4+I6\varepsilon' \qquad \left(\frac{c}{L}\right)^2 \frac{F_t}{LR\omega\mu} = \frac{\varepsilon}{2}(1-2\phi')I5-I4\varepsilon' \tag{3.30}$$

(see Appendix I).

and the equations of motion are:

ε_s	S	ϕ_s^o	θ_{2s}^o	B_{xx}	$B_{xy}=B_{yx}$	B_{yy}	K_{xx}	K_{xy}	K_{yx}	K_{yy}	ν_{crit}	$\bar{\Omega}_{crit}$
0.1	0.76	69.0	249.2	16.42	-7.16	18.68	3.80	9.34	-8.95	3.58	0.0866	0.5720
0.2	0.39	66.9	241.3	8.66	-3.92	9.20	2.25	4.60	-4.25	1.96	0.1393	0.5515
0.3	0.26	64.5	233.8	6.25	-2.87	6.02	1.81	3.01	-2.73	1.44	0.1654	0.5278
0.4	0.20	61.6	226.6	5.21	-2.38	4.40	1.70	2.20	-2.02	1.19	0.1727	0.5030
0.5	0.15	58.3	219.7	4.77	-2.10	3.40	1.77	1.70	-1.66	1.05	0.1671	0.4774
0.6	0.12	54.2	213.1	4.71	-1.95	2.70	2.06	1.35	-1.51	0.97	0.1500	0.4465
0.7	0.09	49.1	206.6	5.01	-1.87	2.16	2.69	1.08	-1.54	0.94	0.1136	0.3906
0.8	0.07	42.2	200.2	5.87	-1.85	1.68	4.14	0.84	-1.81	0.93	0.0243	0.1848
0.9	0.04	31.7	193.2	8.22	-1.89	1.17	8.89	o.58	-2.66	0.95	0.0	0.0

3.1. (a) Oscillating film model

K_{xy}	K_{yy}	ν_{crit}	$\bar{\Omega}_{crit}$
8.13	-2.70	0.4093	0.4936
4.11	-0.99	0.3597	0.4808
2.75	-0.38	0.3078	0.4632
2.05	-0.04	0.2571	0.4422
1.61	0.19	0.2085	0.4178
1.30	0.37	0.1594	0.3851
1.05	0.52	0.0990	0.3220
0.82	0.67	0.0	0.0
0.58	0.82	0.0	0.0

3.1. (b) Static film model

n.b. Remainder of data for the static film model is identical to the oscillating film model

Table 3.1. Data for a long bearing - Reynolds' boundary condition.

$$\varepsilon'' - \phi'^2 = \nu\left\{\cos\phi - S_s\left[-\frac{\varepsilon}{2}(1-2\phi')I4 + I6\varepsilon'\right]\right\} \tag{3.31}$$

$$\varepsilon\phi'' + 2\varepsilon'\phi' = -\nu\left\{\sin\phi - S_s\left[\frac{\varepsilon}{2}(1-2\phi')I5 - I4\varepsilon'\right]\right\}$$

with θ_1 determined from equation (3.29).

The relationship between the modified Sommerfeld number and the steady state eccentricity ratio is:

$$S_s = \frac{4(1-\varepsilon_s^2)^2}{\varepsilon_s\{\pi^2(1-\varepsilon_s^2)+16\varepsilon_s^2\}^{1/2}} \qquad \text{(see Figure 3.2)} \tag{3.32}$$

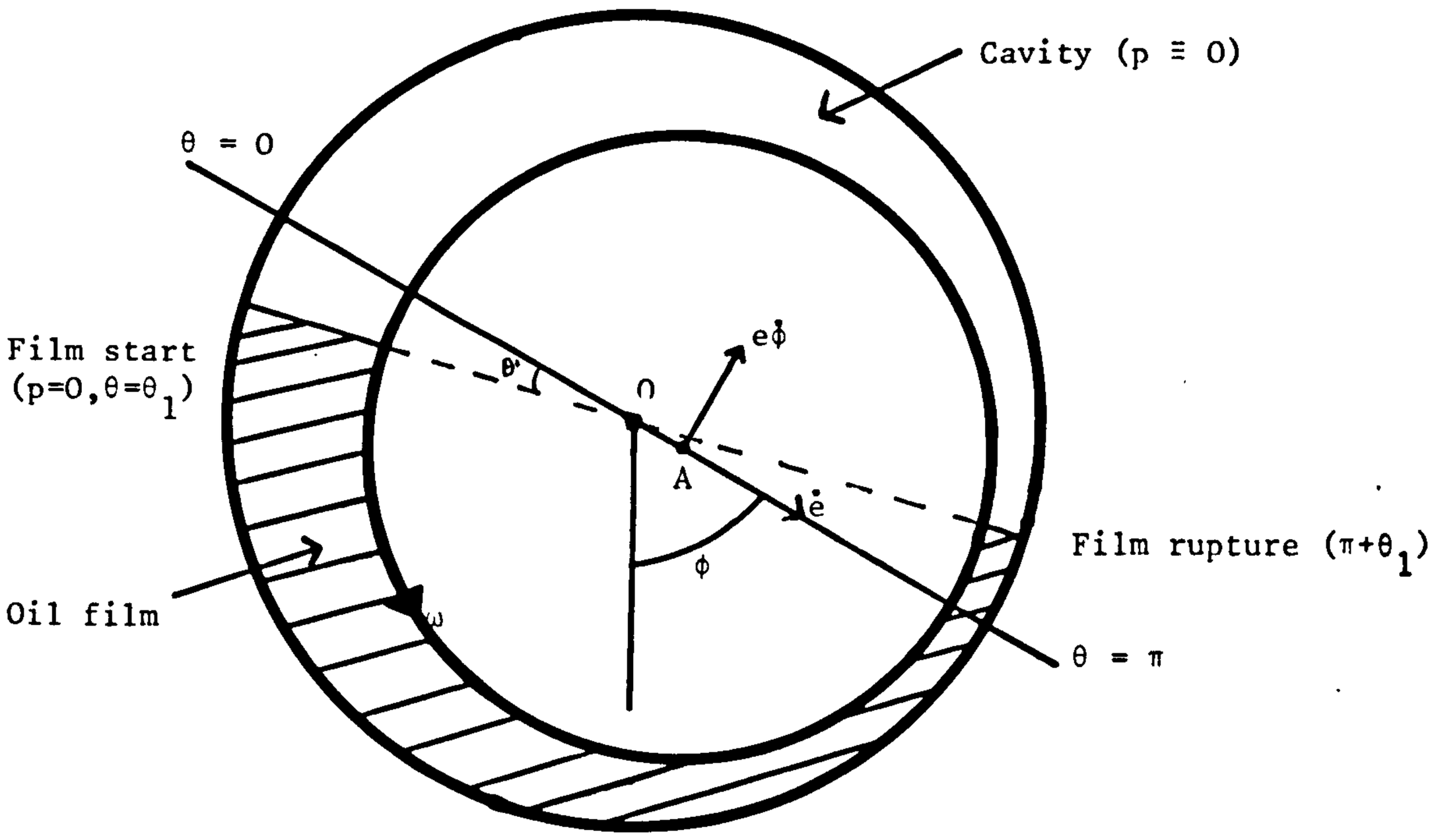

Figure 3.10 A short bearing operating with a half film.

The locus of the journal centre under steady state condition is described by:

$$\tan\phi_s = \frac{\pi(1-\varepsilon_s^2)^{1/2}}{4\varepsilon_s} \qquad \text{(see Figure 3.3)} \tag{3.33}$$

A typical steady state pressure profile is shown in Figure 3.4 for $\varepsilon_s = 0.6$, $z = L/2$.

Equations (3.31), together with equation (3.29) for θ_1, describe the complete motion of the journal. It follows from equation (3.29) that during a small amplitude vibration of the journal θ_1 will be a small quantity:

$$\text{ie.} \quad \theta_1 = \tan^{-1}\left(\frac{2\delta'}{\varepsilon_s}\right) \quad \text{to first order} \tag{3.34}$$

The equations of motion may then be linearised following a similar procedure to the one outlined in section 3.3 for the model with the half Sommerfeld film. In this case the "θ_1 terms" make no contribution to the linearised equations - the result is the same as taking the oil film from 0 to π. However this is not obvious and is peculiar to the short bearing. It would not be correct to neglect the "θ_1 terms" in a large amplitude motion of the journal since θ_1 would not then necessarily be a small angle.

The eight velocity and displacement coefficients are:

$$B_{xx} = -2K_{yx} = \frac{2\pi(1+2\varepsilon_s^2)}{\varepsilon_s(1-\varepsilon_s^2)^{1/2}(\pi^2(1-\varepsilon_s^2)+16\varepsilon_s^2)^{1/2}}$$

$$B_{xy} = B_{yx} = -2K_{yy} = \frac{-8}{(\pi^2(1-\varepsilon_s^2)+16\varepsilon_s^2)^{1/2}} \tag{3.35}$$

$$B_{yy} = 2K_{xy} = \frac{2\pi(1-\varepsilon_s^2)^{1/2}}{\varepsilon_s(\pi^2(1-\varepsilon_s^2)+16\varepsilon_s^2)^{1/2}} \qquad K_{xx} = \frac{8(1+\varepsilon_s^2)}{(1-\varepsilon_s^2)(\pi^2(1-\varepsilon_s^2)+16\varepsilon_s^2)^{1/2}}$$

from which the stability borderline (Figure 3.5) and the critical frequency (Figure 3.6) may be calculated.

3.6 RESULTS AND DISCUSSION.

Stability borderlines and critical frequency curves for all the models examined in this Chapter are shown in Figures 3.5 and 3.6 respectively. The velocity and displacement coefficients are illustrated

in Figures 3.11 and 3.12. The inclusion of cavitation has a stabilising effect on the journal which is now stable provided the parameter ν exceeds a critical value. However the critical value varies considerably for the range of different cavitation boundary conditions. These differences will now be examined in more detail.

i) A bearing operating with a static half film is much more stable than with a swinging film (ie. requires a lower value of ν for stability). Thus, the stability of the journal depends upon the behaviour of the oil film during vibration. An accurate model must therefore reflect the correct oil film behaviour. In the linear analysis only two of the eight coefficients are different for the two models (equations 3.8 and 3.13):- K_{xy} and K_{yy}. It is instructive to think about the situation more closely.

In the case of the oscillating, or swinging film model (Figure 3.1(a)), the oil film occupies the same section of the bearing during journal vibration as under steady state conditions (ie. the converging film section of the bearing). The hydrodynamic forces so generated are functions of ε, $\dot{\varepsilon}$, $\dot{\phi}$ (but not ϕ). Thus, the expressions for the two displacement coefficients K_{xy} and K_{yy} defined by equations (1.18) reduce to:

$$K_{xy} = \frac{S}{\varepsilon_s} \bar{F}_{ts} \qquad K_{yy} = -\frac{S}{\varepsilon_s} \bar{F}_{rs} \tag{3.36}$$

The situation is different for the static film model, where additional forces are generated during journal vibration because the oil film does not occupy the same section of the bearing as under steady state conditions (see Figure 3.1(b) and also equation II.4). It is these additional terms, being implicit functionsof ϕ, which alter the two displacement coefficients K_{xy} and K_{yy}.

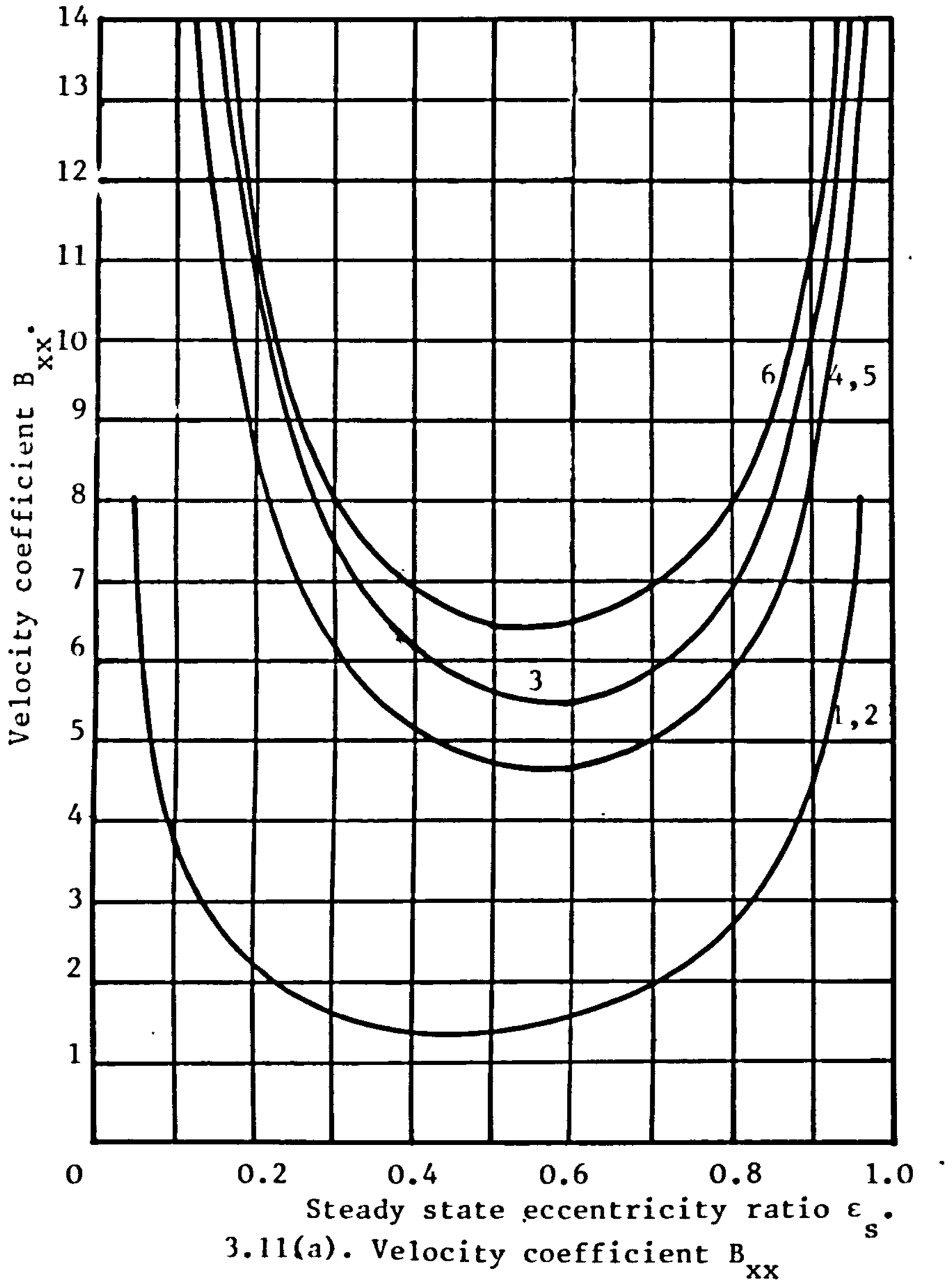

3.11(a). Velocity coefficient B_{xx}

Key to Figures 3.11 and 3.12.

1. Long bearing (Oscillating half film).
2. Long bearing (Static half film).
3. Long bearing (Half Sommerfeld film).
4. Long bearing (Reynolds' B.C. - Oscillating film).
5. Long bearing (Reynolds' B.C. - Static film).
6. Short bearing (Half film).

Figure 3.11. Velocity coefficients for models with different cavitation boundary conditions at film rupture.

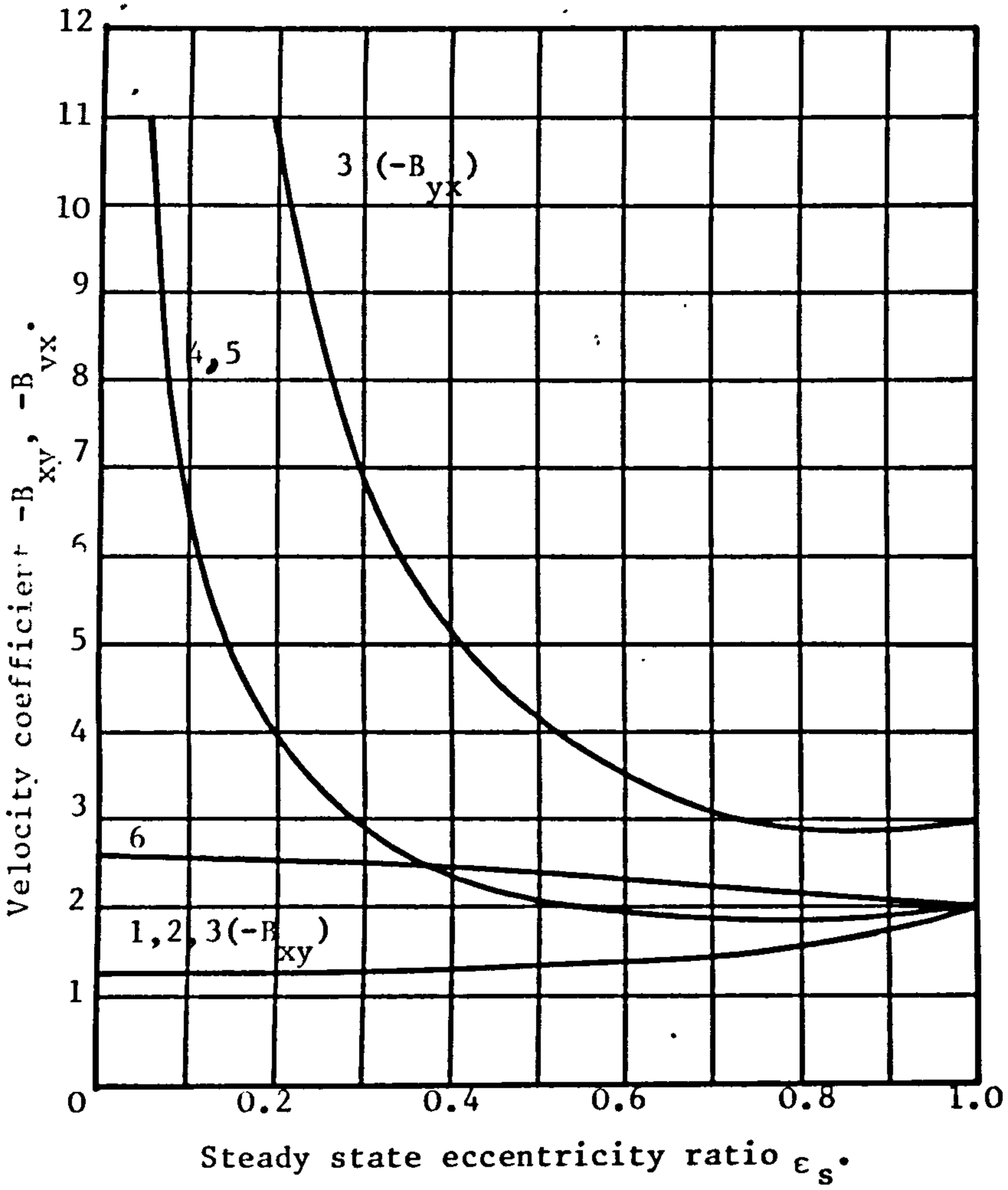

3.11(b). Velocity coefficients $-B_{xy}$, $-B_{yx}$.

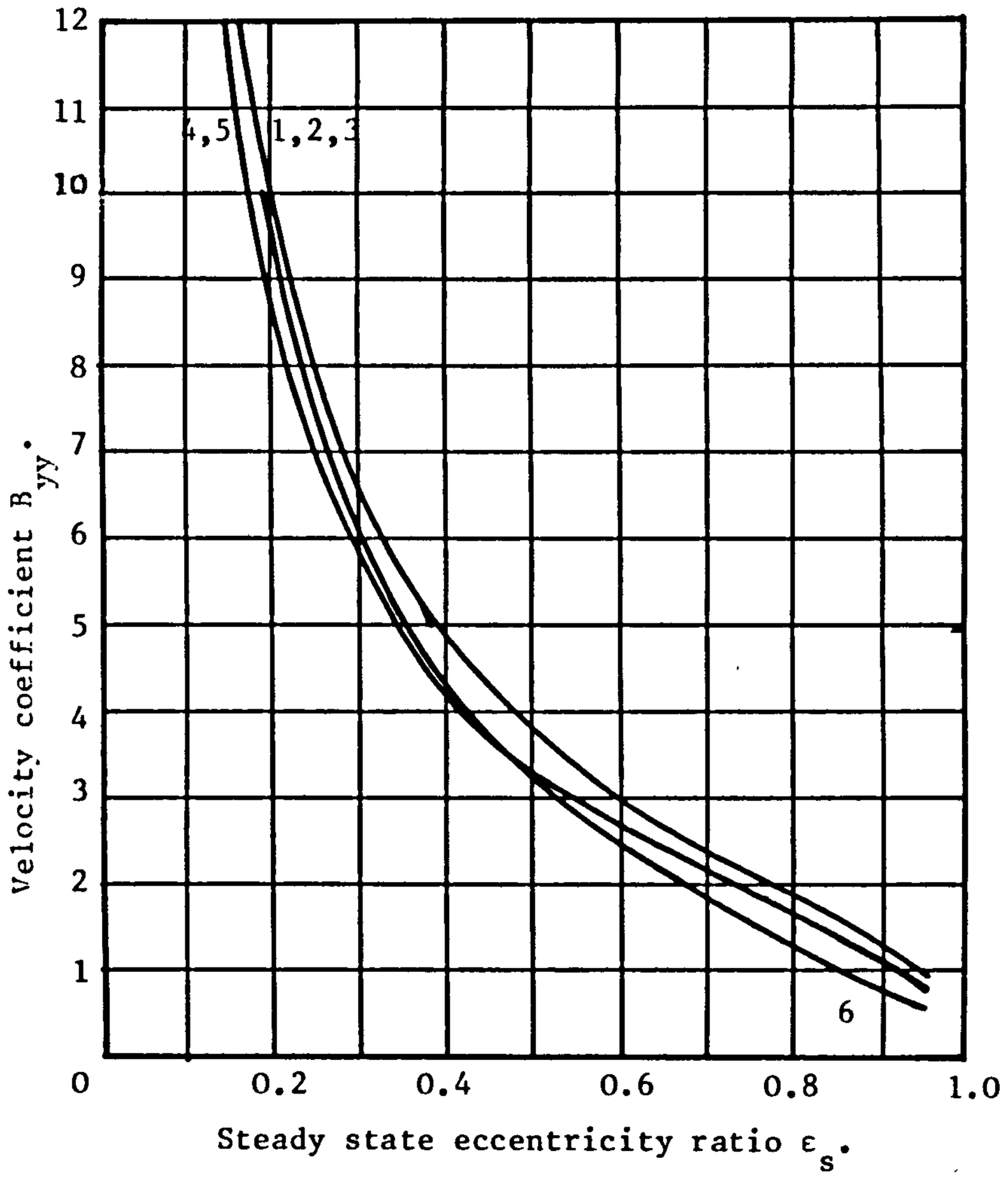

3.11(c). Velocity coefficient B_{yy}.

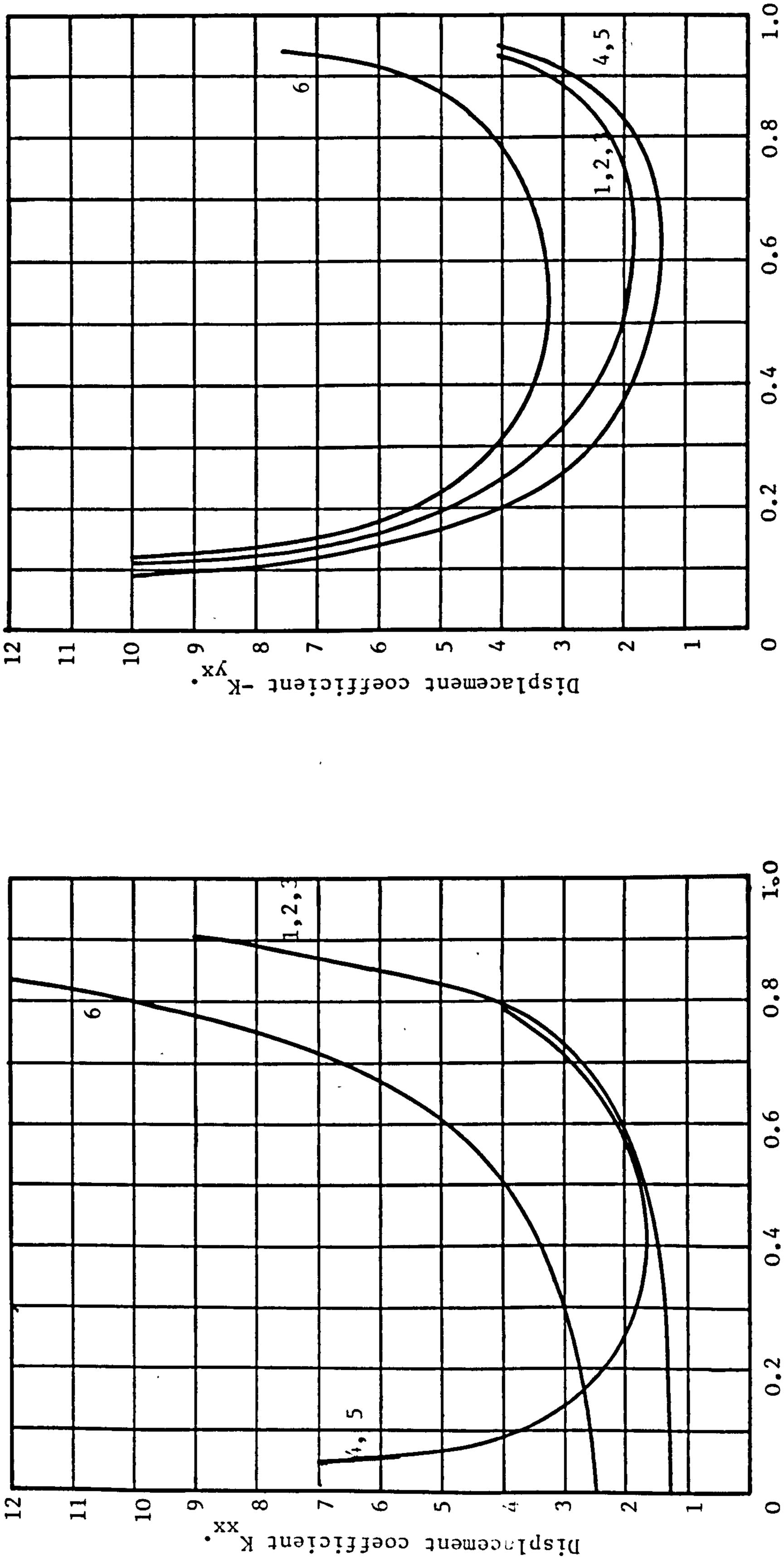

3.12(b). Displacement coefficient $-K_{yx}$ for models with different cavitation boundary conditions at film rupture.

3.12(a). Displacement coefficient K_{xx} for models with different cavitation boundary conditions at film rupture.

Figure 3.12. Displacement coefficients for models with different cavitation boundary conditions at film rupture.

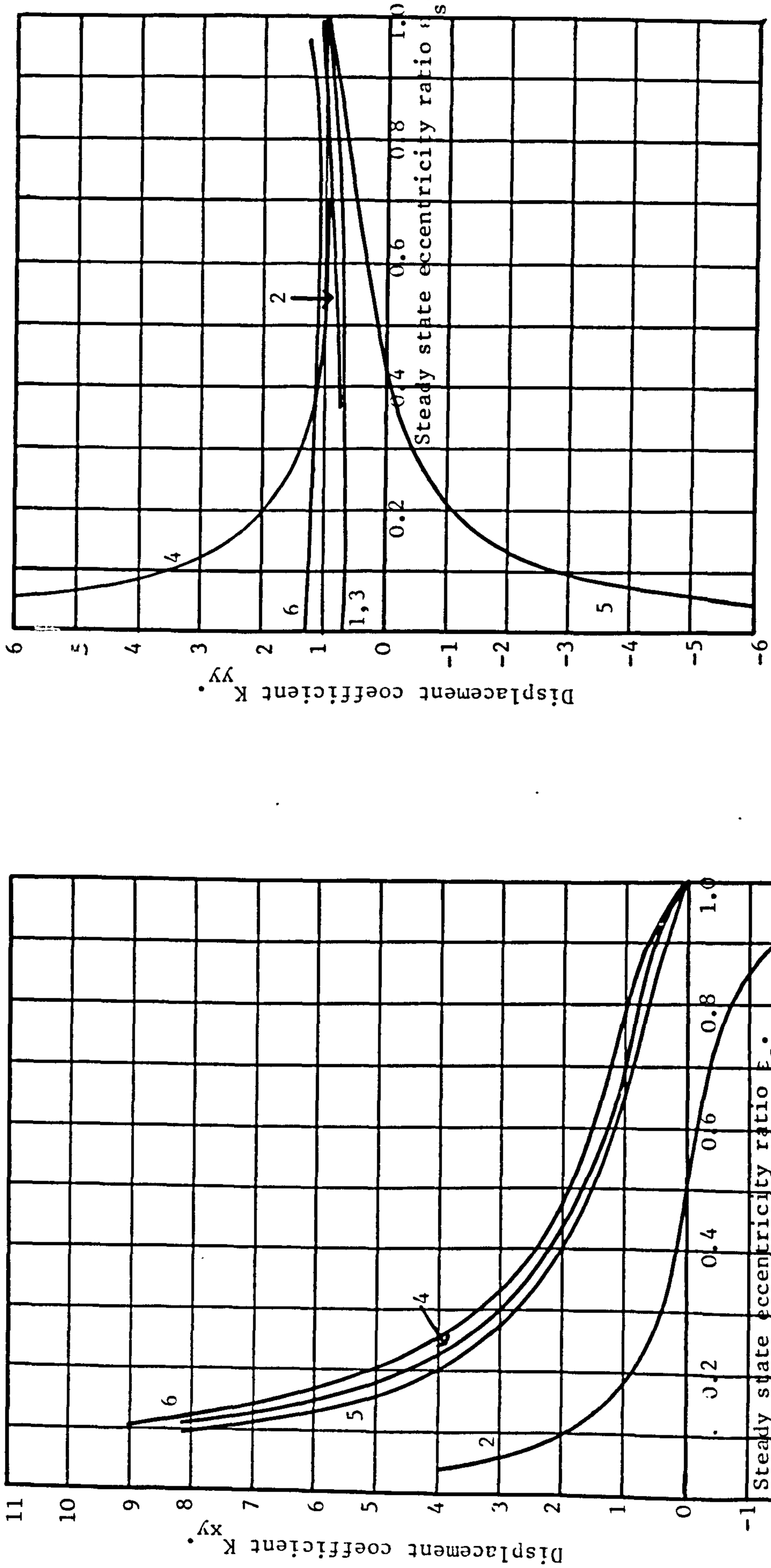

3.12(d). Displacement coefficient K_{yy}.

3.12(c). Displacement coefficient K_{xy}.

In this case the K_{yy} coefficient is not altered significantly (Figure 3.12(d)), but the K_{xy} coefficient is much lower and goes negative for $\varepsilon_s > 0.55$ (Figure 3.12(c)). This means the difference in the cross coupled displacement terms $(K_{xy} - K_{yx})$ is much lower than for the oscillating film. Holmes (1966) and Smith (1963) have both indicated that a low value of $(K_{xy} - K_{yx})$ favours stability. Thus the static film is more stable than the oscillating one.

ii) The model with a half Sommerfeld film is also much more stable than the oscillating half film. Basically the two models are different because the pressure distributions have different $\dot{\varepsilon}$ terms (see equations 2.2 and 3.2). This means the velocity coefficients B_{xx} and B_{yx} are different for the two models (Figure 3.11); the remaining six coefficients are identical. It is interesting to note that the half Sommerfeld model is the only model in which the cross coupled velocity coefficients B_{xy} and B_{yx} were found <u>not</u> to be equal.

iii) The stability curves all predict that above some values of ε_s, the journal will be stable for all values of ν (ie. $\nu_{crit.} = 0$). This value is close to 0.8 for all the models apart from the static half film model when it is 0.55. High eccentricity ratios therefore favour stability.

iv) With the exception of one model the critical frequency curves are similar and predict whirl frequency ratios below 0.6. For the model with the oscillating half film the ratio is much higher and has a maximum value of 1.15. It must be stressed that this is only the frequency of a small amplitude oscillation about the equilibrium position.

v) The two models with the Reynolds boundary condition have different stability borderlines. Surprisingly in this case it is the oscillating film model which is more stable (the reverse of the trend for the half film). The stability of the journal thus depends upon the cavitation boundary conditions as well as oil film behaviour. An accurate model

must therefore incorporate the correct boundary conditions and the correct behaviour of the oil film during vibration.

The two coefficients K_{xy} and K_{yy} are again the only two terms which are altered in the stability analysis (for the same reasons as discussed previously). In this case it is the K_{yy} coefficient which is altered significantly (Figure 3.12(c),(d)) and for the static film it is negative at low eccentricities. A negative value of K_{yy} may be associated with instability and is the reason why the static film model is less stable than the oscillating film model.

vi) The stability borderline for the short bearing is not vastly different to several of those for the long bearing when eccentricity ratio is used as an operating parameter. However, since a decrease in bearing length increases ε_s, short bearings are likely to give greater stability when other parameters remain constant.

The stability borderlines may be used to determine whether or not a rotor system is stable at a particular rotor speed. The critical value of the parameter ν corresponds to a maximum rotor speed below which the system will be stable (the threshold speed). The threshold speed clearly depends upon which model is used. To illustrate this consider a rotor mounted on two plain identical cylindrical journal bearings with the following parameters:

L = 0.05m	μ = 0.1 Pa s.
D = 0.05m	F = 3000N (the load on each bearing)
R = 0.025m	c = 0.00025m

Assuming a rotor speed of 5000rpm, and that long or short bearing theory is applicable, the Sommerfeld number may be calculated and the equilibrium position determined from Figures 3.2 and 3.3. Figure 3.5 may then be used to calculate the threshold speed and whether or not the system is stable. The results are summarised in Table 3.2.

Rotor speed 5000rpm.				
MODEL	ε_s	ν_{crit}	THRESHOLD SPEED RPM	STABILITY?
1	0.44	0.77	2150	Unstable
2	0.44	0.08	6700	Stable
3	0.44	0.15	5600	Stable
4	0.37	0.17	4600	Unstable
5	0.37	0.27	3650	Unstable
6	0.58	0.135	5150	Stable

For key to model numbers see Figure 3.11

Table 3.2 An example showing the variation in the threshold speed for the different models.

The table illustrates the wide discrepancies which occur in the estimate of the system's threshold speed by making different assumptions about the oil film in the bearings. Therefore to obtain an accurate value of the threshold speed the oil film must be modelled correctly.

Another factor not normally considered in the stability analysis is the degree of stability (or instability). A stability borderline can only be used to determine whether or not the journal is stable for given parameter values. The degree of stability may be determined by solving the frequency equation associated with the linearised equations, and calculating the logarithmic decrement of the roots. Consider, for example, the frequency equation for a short bearing (half film) derived from equations (3.35):

$$\bar{\lambda}^4 + \frac{2\nu\pi(2+\varepsilon_s^2)\bar{\lambda}^3}{\varepsilon_s(1-\varepsilon_s^2)^{1/2}(\pi^2(1-\varepsilon_s^2)+16\varepsilon_s^2)^{1/2}} + 4\nu\left\{\frac{(3+\varepsilon_s^2)}{(1-\varepsilon_s^2)(\pi^2(1-\varepsilon_s^2)+16\varepsilon_s^2)^{1/2}} + \frac{\nu(\pi^2(1+2\varepsilon_s^2)-16\varepsilon_s^2)}{\varepsilon_s^2(\pi^2(1-\varepsilon_s^2)+16\varepsilon_s^2)}\right\}\bar{\lambda}^2 \qquad (3.37)$$

$$+\frac{8\nu^2\pi(3+\varepsilon_s^2)\bar{\lambda}}{\varepsilon_s(1-\varepsilon_s^2)^{1/2}(\pi^2(1-\varepsilon_s^2)+16\varepsilon_s^2)}+\nu^2\left\{\frac{32\varepsilon_s^2(1+\varepsilon_s^2)+\pi^2(1-\varepsilon_s^2)(1+2\varepsilon_s^2)}{\varepsilon_s^2(1-\varepsilon_s^2)(\pi^2(1-\varepsilon_s^2)+16\varepsilon_s^2)}\right\}=0$$

The equation was solved numerically for a range of values of ν and ε_s ($0.01 \leq \nu \leq 1.0$, $0.01 \leq \varepsilon_s \leq 0.99$). Typical roots of the equation are:

$\bar{\lambda} = -0.02 \pm 0.57i, -0.94 \pm 0.58i$ for $\varepsilon_s = 0.50$, $\nu = 0.20$ (Stable)

$\bar{\lambda} = 0.03 \pm 0.39i, -0.42 \pm 0.48i$ for $\varepsilon_s = 0.50$, $\nu = 0.08$ (Unstable)

It was found that, for all cases in which the journal was unstable, only one pair of roots had a positive real part and thus the degree of instability could be measured by calculating the logarithmic decrement of the unstable root. When the journal was stable both pairs of roots had negative real parts with one pair having a much smaller modulus (by at least an order of magnitude). Thus the degree of stability could be measured by calculating the logarithmic decrement of this root. Curves of constant damping (ie. constant logarithmic decrement) are shown in Figure 3.13.

The curves are extremely interesting since they show that increasing the parameter ν does not necessarily increase the damping of the system. At low and high eccentricities the damping is always weak and even for low values of the logarithmic decrement the curves do not "follow" the stability borderline. The damping is "sharpest" for moderate eccentricities.

It is possible to derive analytic expressions for the curves of constant damping for small ε_s and to investigate why the damping is always weak. Letting $\varepsilon_s \to 0$ so that $O(\varepsilon_s^2)$ terms may be neglected the frequency equation (3.37) reduces to the cubic equation:

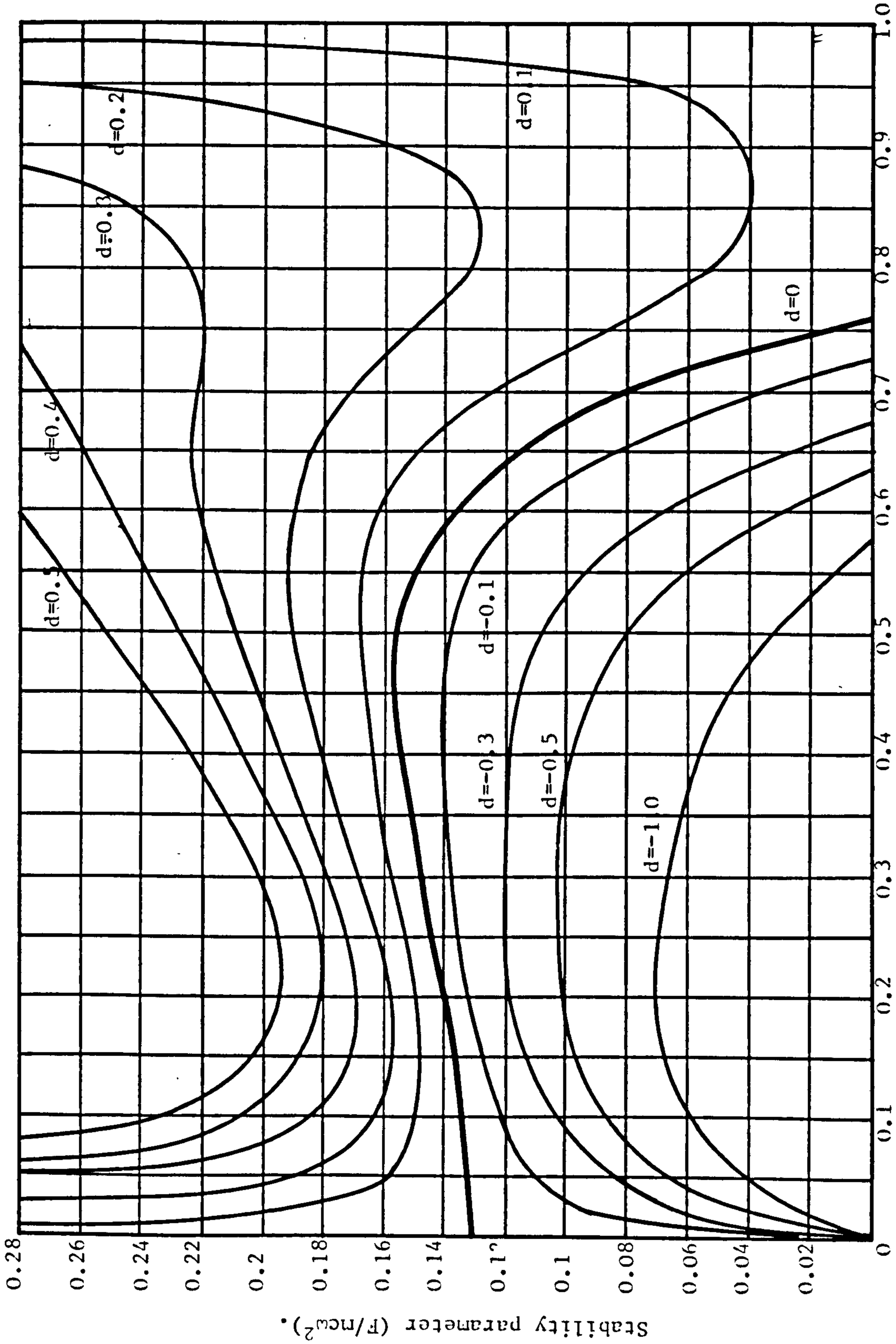

Figure 3.13. Curves of constant logarithmic decrement for a short bearing (Half film).

$$\bar{\lambda}^3 + \frac{\nu}{\varepsilon_s}\ \bar{\lambda}^2 + \frac{6}{\pi}\quad \nu\bar{\lambda} + \frac{\nu}{4\varepsilon_s} = 0 \tag{3.38}$$

Consider now the general cubic equation:

$$s^3 + A_2 s^2 + A_1 s + A_o = 0 \tag{3.39}$$

which has one real root and a pair of complex conjugate roots:

$-p_1, p_2 \pm iq_2$ say. Routh's criterion for a cubic equation is:

A_o, A_1, $A_2 > 0$ and $R = A_1A_2 - A_o > 0$ for stability.

At the point of neutral stability p_1 is positive and p_2 zero. It follows therefore that close to the point of neutral stability p_2 is small.

The cubic equation may be written:

$$(s+p_1)(s-p_2-iq_2)(s-p_2+iq_2) = 0 \tag{3.40}$$

Expanding the above equation, neglecting p_2^2 terms and equating powers of s with equation (3.39):

$$\Rightarrow A_2 = p_1 - 2p_2 \qquad A_1 = -2p_1p_2 + q_2^2 \qquad A_o = p_1q_2^2 \tag{3.41}$$

Eliminating p_1, q_2 from the equations:

$$\Rightarrow p_2 = \frac{-R}{2(A_1+A_2^2)} \qquad \text{(for small } p_2\text{)} \tag{3.42}$$

Returning to the cubic equation (3.38), substituting for A_2, A_1, A_o gives the following expression for the real part of the root close to the stability borderline:

$$\bar{p}_2 = \frac{-\varepsilon_s(24\nu-\pi)}{8\pi\nu} \tag{3.43}$$

It can be seen from this expression that:

i) $\bar{p}_2 \to 0$ as $\varepsilon_s \to 0 \forall \nu \neq 0$. Thus increasing ν for sufficiently small ε_s will not increase the damping (Figure 3.13).

ii) $\bar{p}_2$ is also zero when $\nu = \pi/24$ (0.1308).

Replacing $\bar{p}_2$ by the logarithmic decrement d ie. $d = -2\pi\frac{p_2}{\Omega} \approx -4\pi\bar{p}_2$

and rearranging equation (3.43):

$$\Rightarrow \nu = \frac{\pi\varepsilon_s}{2(12\varepsilon_s - d)} \qquad (3.44)$$

which is the equation of constant damping curves (for small ε_s,d). The equation represents a family of hyperbolae for different values of d (Figure 3.14). Comparing Figures 3.13 and 3.14 it can be seen that there is a reasonable agreement between the two sets of curves.

Smalley and Malanoski (1978) have stated that in practice the logarithmic decrement should not be below 1/2. Figure 3.13 shows that the curve for d = 0.5 is vastly different to the stability curve (d = 0). The curve can be used to calculate the maximum speed at which the damping will be greater than 0.5. This speed will be much lower than the threshold speed. Consider for example the rotor system described previously and assume that the rotor speed varies from 1000 to 6000 rpm. For each operating speed the modified Sommerfeld number may be calculated from which the steady state position is deduced (Figures 3.2 and 3.3). The threshold speed and the maximum speed at which the damping is greater than 0.5 is then calculated from Figure 3.13. The results are summarised in table 3.3.

The table shows the wide variation between the threshold speed when the system becomes unstable and the maximum speed for which d = 0.5. The system becomes unstable at a speed just in excess of 5000 rpm, but the damping falls below 0.5 above a speed of 3400 rpm.

Figure 3.14. Curves of constant logarithmic decrement for a short bearing (Half film) - small ε_s theory.

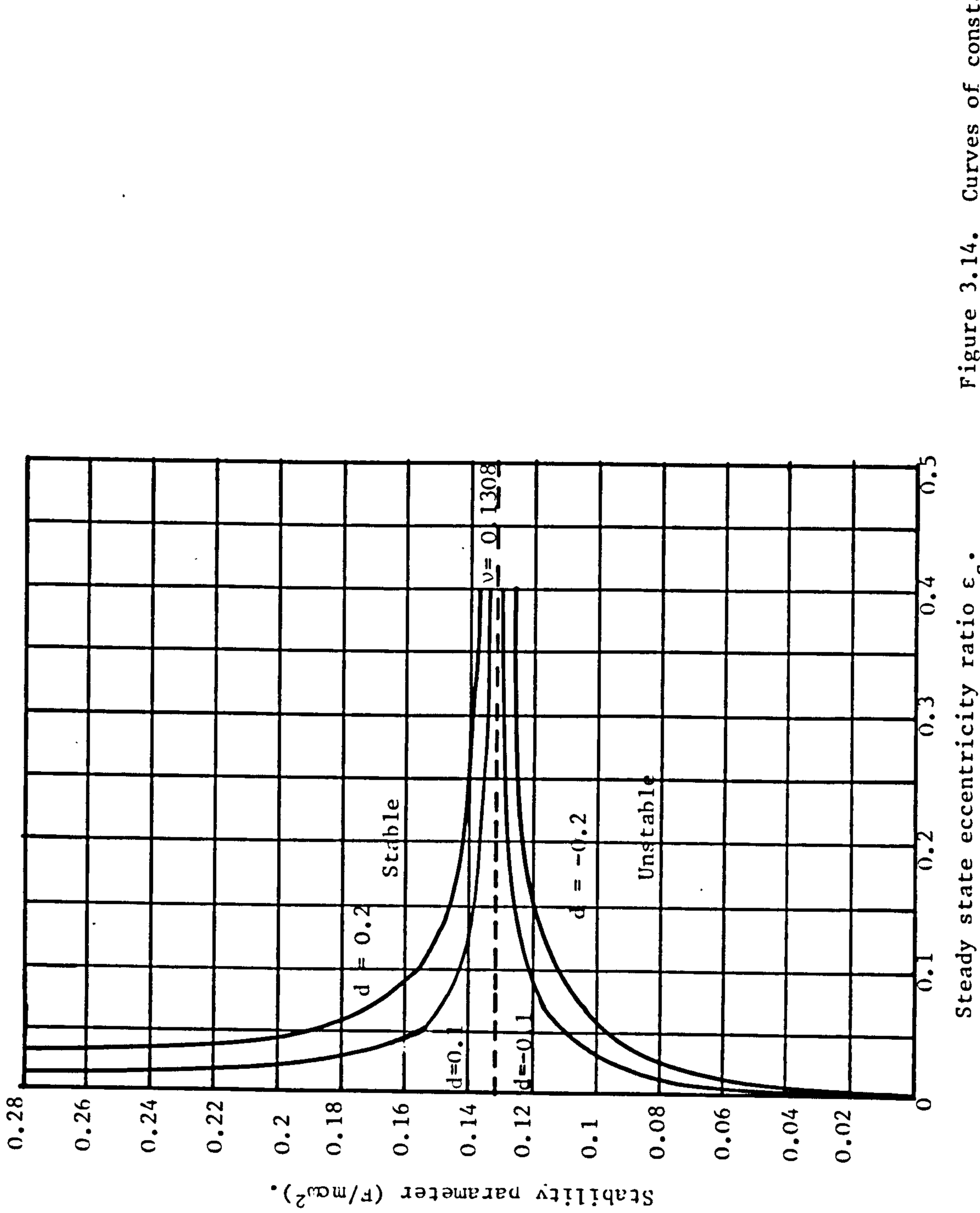

ω rpm	S_s	ε_s	THRESHOLD SPEED	UNSTABLE OR STABLE	SPEED AT WHICH d=0.5	d
1000	0.17	0.82	∞	STABLE	2900	2.20
2000	0.35	0.72	8450	STABLE	3200	1.30
3000	0.53	0.66	6000	STABLE	3350	0.70
4000	0.70	0.62	5250	STABLE	3500	0.30
5000	0.87	0.58	5150	STABLE	3600	0.08
6000	1.04	0.55	5050	UNSTABLE	3650	-0.25

Table 3.3 An example showing the degree of damping for a range of rotor speeds.

It is possible of course to solve the frequency equations for the other models discussed in this Chapter. It is found that a similar pattern emerges - the damping is weak at low and high eccentricities. The results are not shown because of this similarity.

Several of the models discussed in this Chapter have been investigated by other authors. Holmes (1960) examined the vibrational characteristics of a short bearing operating with a half film and the stability borderline shown in Figure 3.5 agrees with his. Hori (1959) used the oscillating half film model for a long bearing in his work on flexible rotors. The stability borderline shown in Figure 3.5 corresponds to Hori's curve for the case of infinite shaft stiffness. Holmes (1966) has also shown a stability curve for the long bearing with Reynolds' boundary condition using values for the eight coefficients derived by Smith (1963). Smith's model corresponds to an oscillating film and he calculated the coefficients from the steady state data and an interpolation method. The stability curve shown by Holmes is in rough agreement with the curve shown in Figure 3.5, which in based upon a more accurate calculation of the coefficients described in this Chapter. Hahn (1976) has reached similar conclusions about the degree of damping

in the system ie. at low and high eccentricities the journal may be stable theoretically, but be only weakly damped. The remainder of the work in this Chapter, particularly the sensitivity of the vibrational characteristics to different cavitation boundary conditions and oil film behaviour, does not appear to have been widely studied.

In general in this Chapter it is the boundary conditions at film rupture which have been investigated. Little attention has so far been given to the boundary conditions at the start of the oil film. The assumption that the film begins at the line of maximum film thickness is widely used. This is not as accurate boundary condition since it violates flow continuity at the boundary unless an oil groove is situated there through which oil is admitted to the bearing. However, this is not a satisfactory solution because a groove is fixed in space, whereas the line of maximum film thickness alters for each equilibrium position (and also during a vibration of the journal). The correct approach for the axial groove bearing is to carry out the analysis for a fixed position of the groove. An investigation of the axial groove bearing is made in Chapter 4, where many of the ideas developed is this Chapter regarding boundary conditions and oil film behaviour are used to produce an accurate model.

3.7 CONCLUSIONS.

i) Cavitation is a stabilising mechanism. The journal is stable provided the parameter ν exceeds a critical value. Thus from a vibrational point of view it is desirable to have cavitation in bearings.

ii) The vibrational characteristics of the journal are sensitive both to different cavitation boundary conditions at film rupture and to the behaviour of the oil film during vibration. An accurate model must adopt accurate boundary conditions and account correctly for the behaviour of the oil film.

iii) High eccentricity ratios favour stability and hence short bearings

are likely to be more stable than long ones (but also see iv below).

iv) The journal may be stable theoretically but be only weakly damped. Any vibrations will therefore persist and this could adversely affect the smooth running of the journal. The damping is particularly weak at low and high eccentricity ratios and in these regions the degree of damping is insensitve to the stability parameter ν.

CHAPTER 4

VIBRATIONAL CHARACTERISTICS OF THE AXIAL GROOVE JOURNAL BEARING.

In practice, oil is admitted to bearings through axial or circumferential grooves located in the bearing sleeve. In this Chapter an investigation of the axial groove journal bearing is made with particular emphasis on the effect of the groove position and oil supply pressure on the vibrational characteristics of the bearing. The actual grooving arrangement may be quite complicated with several grooves distributed around the bearing sleeve. This investigation is confined to a single axial groove.

The findings in Chapter 3 have highlighted the need for a model which utilises accurate boundary conditions at both film rupture and film reformation and which also accounts correctly for the behaviour of the oil film during vibration. As far as possible these features are incorporated into the model.

4.1 DESCRIPTION OF THE AXIAL GROOVE JOURNAL BEARING.

The axial groove journal bearing is illustrated in Figure 4.1. The axial groove is located in the bearing sleeve, fixed in space, at a given angle β to the loadline. The oil may be fed into the bearing under pressure which is usually small compared with the hydrodynamic pressures generated in the bearings.

Initially it was assumed that the oil film build up began at the groove and ended where both the pressure and the pressure gradient were zero (Figure 4.1(a)). The appropriate boundary conditions were then:

$$p = p_g \text{ at } \theta = \theta_1 \quad \text{Film formation} \tag{4.1}$$
$$p = \frac{dp}{d\theta} = 0 \text{ at } \theta = \theta_2 \quad \text{Film rupture}$$

where p_g = the oil supply pressure.

The cavity was assumed to exist over the remaining section of the bearing and to be at ambient pressure. Thus, the formation of the film upstream of the groove over which the oil film pressure will rise to the supply pressure was neglected (the limitations of the model are discussed

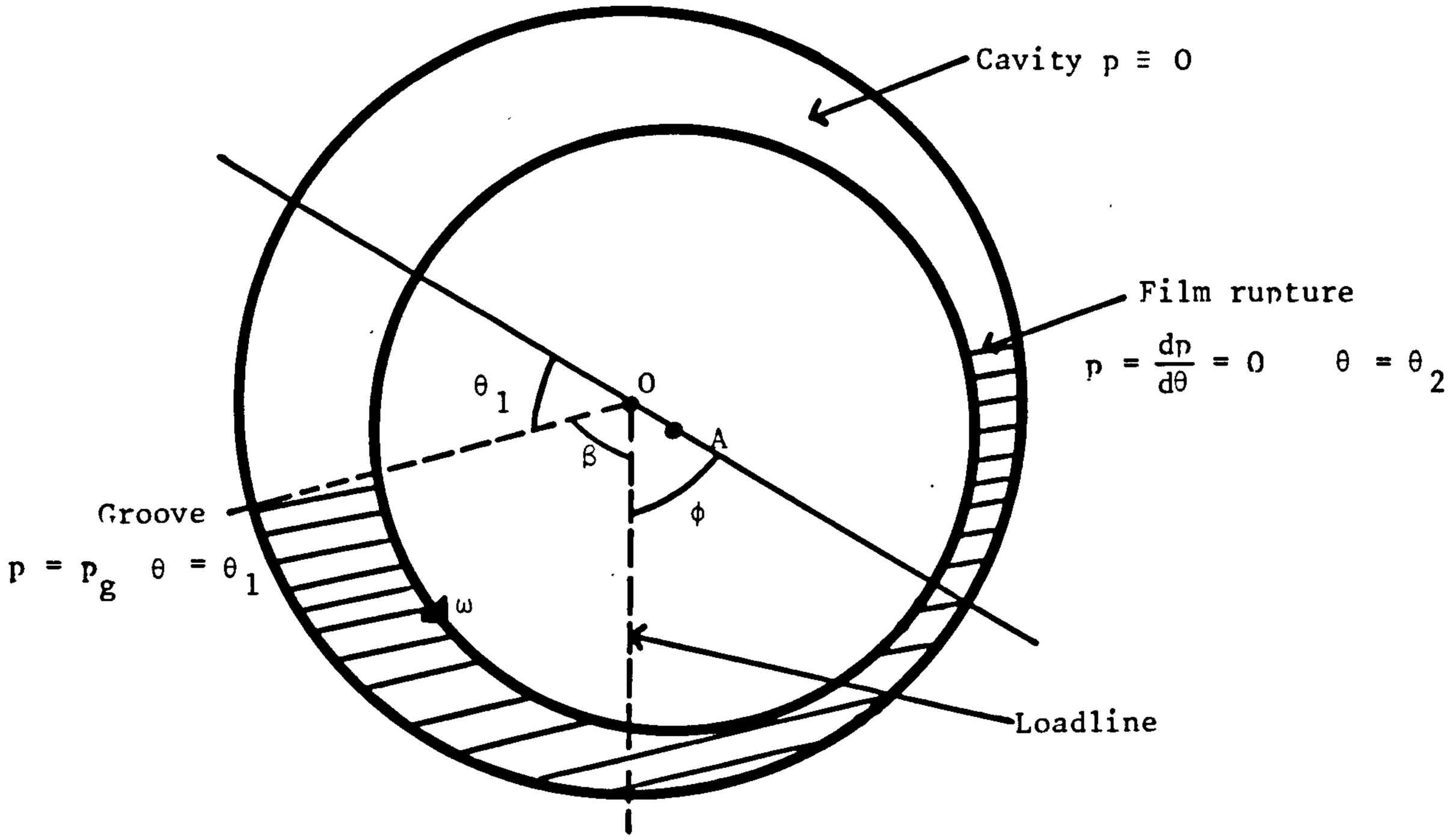

4.1(a). Start of film at the groove.

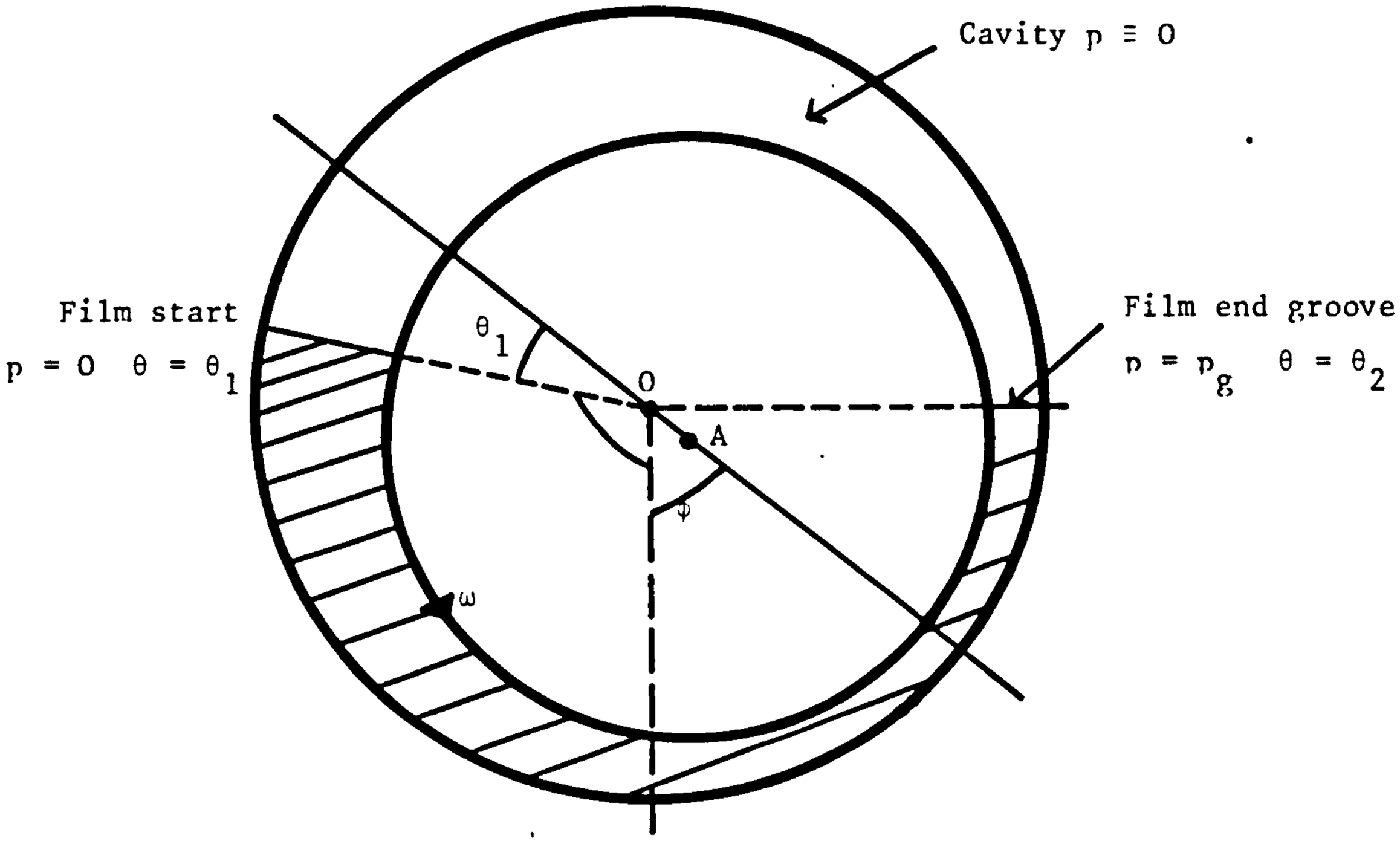

4.1(b). Film termination at the groove.

Figure 4.1. The axial groove journal bearing.

later in this Chapter).

The Reynolds equation for the long bearing (equation 2.1) was solved with the above boundary conditions to obtain the hydrodynamic pressure and forces. The equations of motion were then formulated and linearised to obtain the eight velocity and displacement coefficients. The details of this work, which follows very closely the work relating to the Reynolds boundary condition described in Chapter 3, are given in Appendix II.

During a vibration of the journal about its equilibrium position, the position of the line of centres varies in space and hence the groove position relative to the line of centres is altered (Figure 4.2(a)). Thus:

$$\theta_{ls} \rightarrow \theta_{l} = \theta_{ls} - \gamma \text{ during journal vibration}$$

In this model the oil film behaviour is determined through the assumption that the oil film build up begins at the groove and continues to do so during journal vibration. The variation of the groove position relative to the line of centres during journal vibration must be accounted for in the stability analysis, otherwise the model will be inaccurate (as shown in Chapter 3).

A computer program was written to calculate the steady state data and the eight velocity and displacement coefficients for given values of β (the groove position) and oil supply pressure. Since the groove position relative to the line of centres is different for each value of ε_s (Figure 4.2(b)), it was necessary to use an iteration procedure to locate the groove position relative to the line of centres. A flow-chart of the computer program is given in Figure 4.3. After calculating the steady state data it was possible to calculate the velocity and displacement coefficients. Routh's criterion was then used to calculate the critical values of the stability parameter and whirl frequency ratio.

The model described in the preceding pages was adequate for investigating groove positions less than 180^{o} before the loadline.

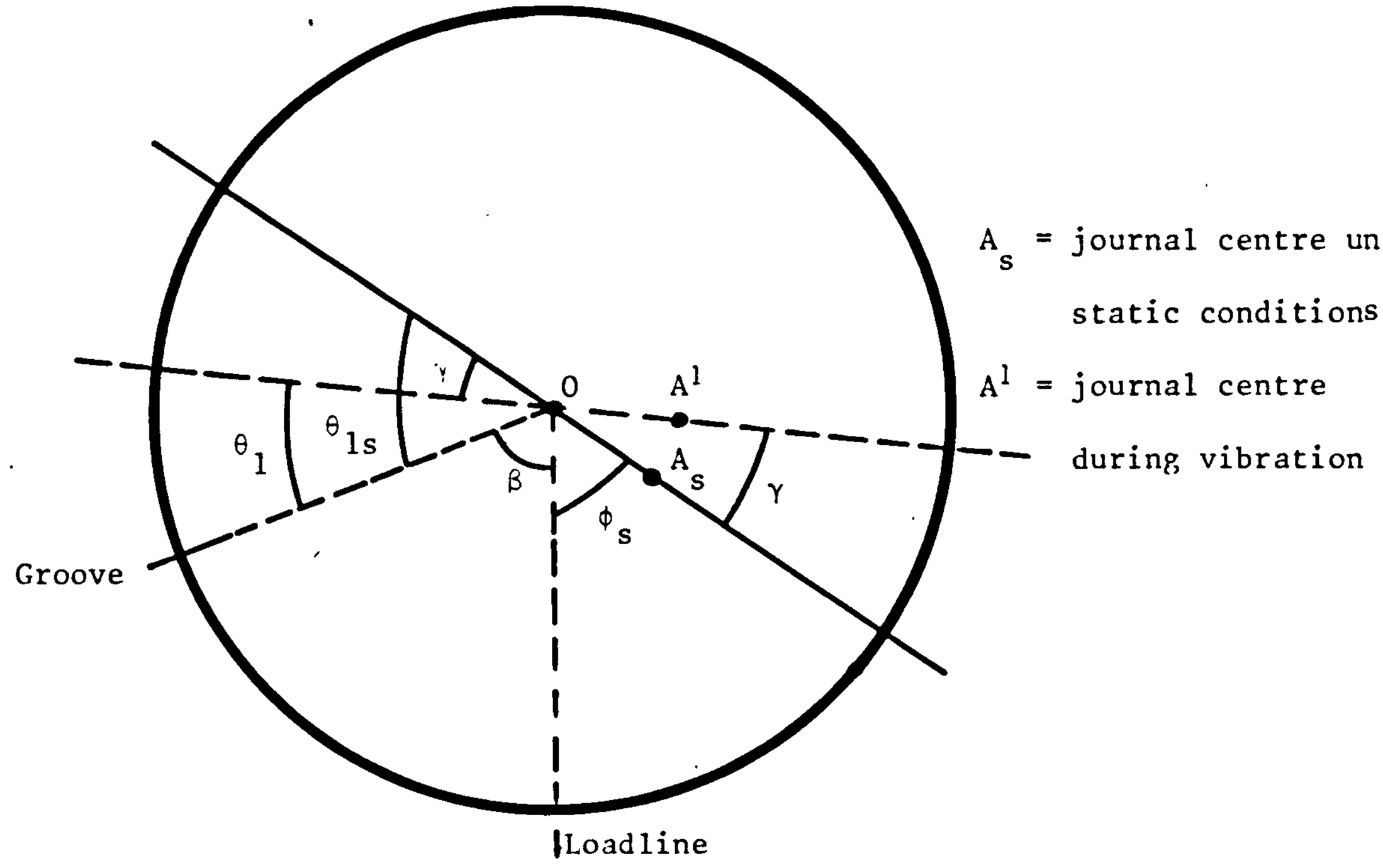

4.2(a). During journal vibration about its equilibrium position.

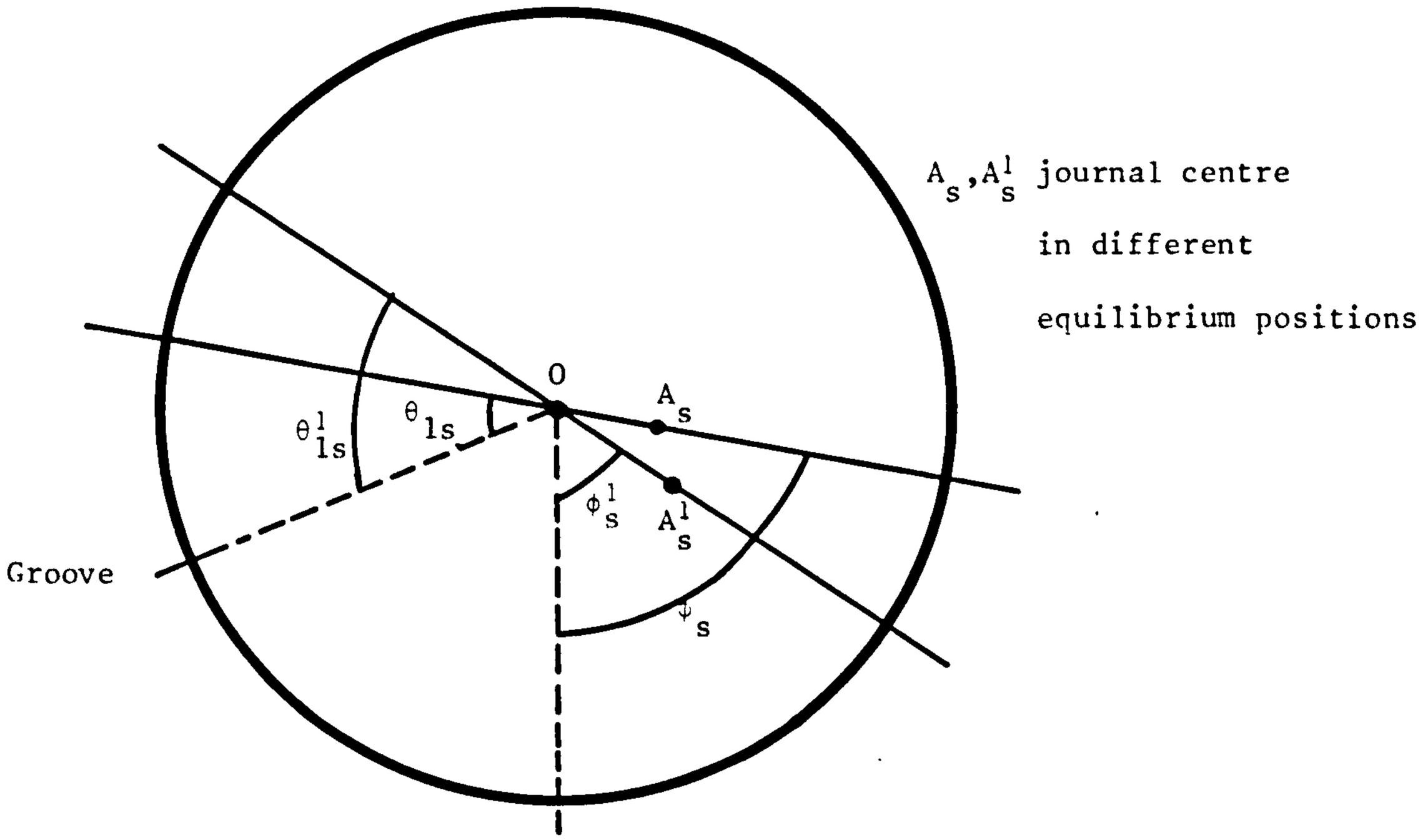

4.2(b). For different equilibrium positions.

Figure 4.2. Variation of the line of centres w.r.t. the groove position.

Figure 4.3. Flow chart of computer program to calculate data for the axial groove journal bearing.

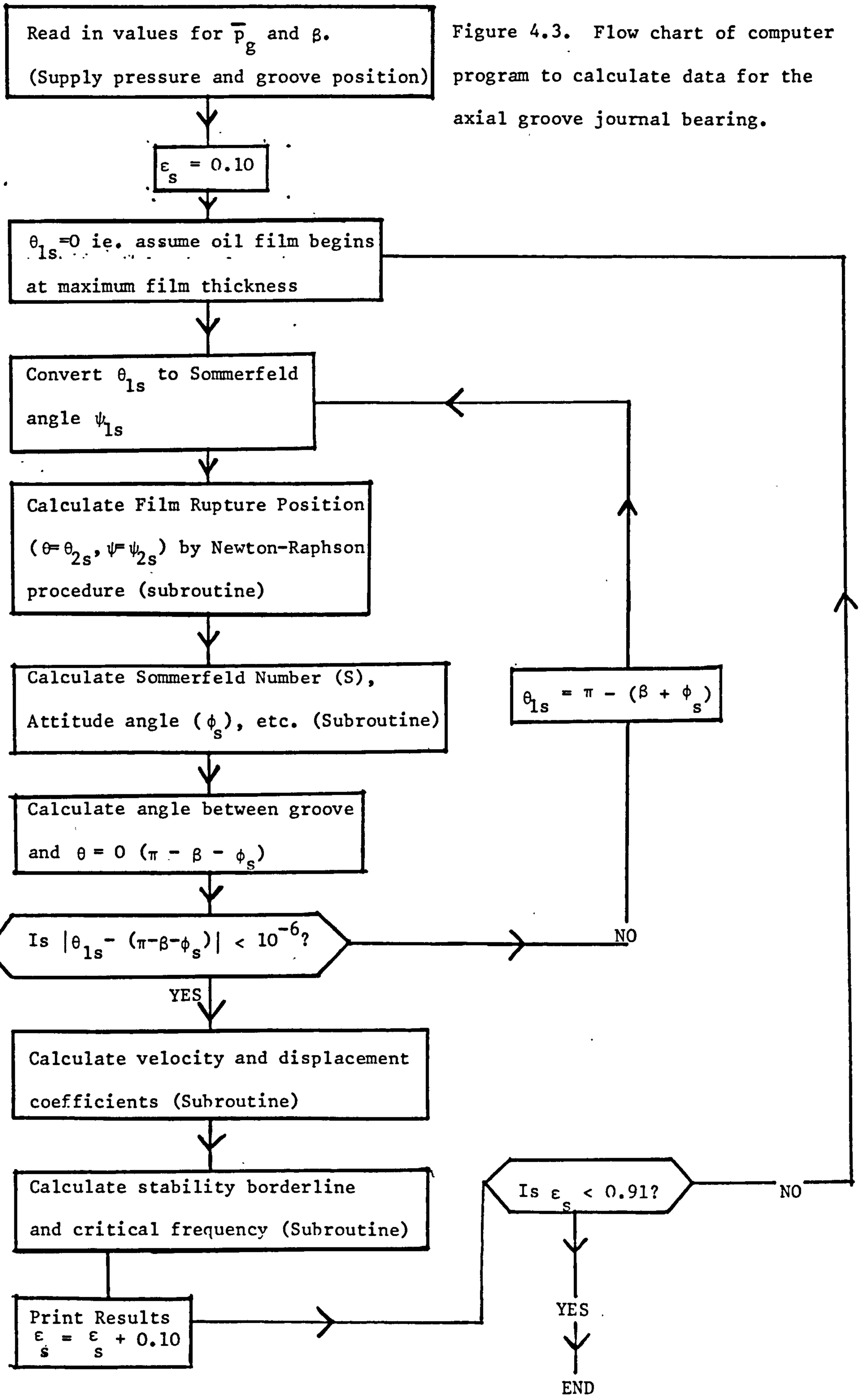

For β greater than 180^{o}, with the groove far into the diverging film section of the bearing (Figure 4.1(b)), the assumption that the oil film began at the groove was no longer valid (an attempt to use this assumption failed because the film rupture positions could not be determined). If the formation of the oil film is not at a groove, the appropriate boundary conditions are rather complicated (see section 4.3), although it is usually assumed that the film forms close to the position of maximum film thickness.

To examine values of β greater than 180^{o} a simple model was taken. It was assumed that the oil film was complete with the pressure specified at the groove:

$$p = p_g \text{ at } \theta = \theta_2, \theta_2 + 2\pi \qquad (4.2)$$

Any subambient pressures were neglected and the film was assumed to form at a position of ambient pressure.

$$\text{ie. at } \theta = \theta_1 \text{ where } p(\theta_1) = 0 \qquad (4.3)$$

The pressure distribution was then taken over the range $\theta_1 < \theta < \theta_2$ with the cavity occupying the remaining film section of the bearing (Figure 4.1(b)). Thus, the oil film was assumed to end at the groove and, for a non-zero supply pressure, the "tail-off" as the pressure falls to ambient downstream of the groove position, was neglected. This is a reasonable assumption only if the supply pressure is small compared with the hydrodynamic pressure generated in bearings.

The Reynolds equation was solved with the above boundary conditions (equations 4.2 and 4.3) and the velocity and displacement coefficients etc. were calculated (the details of the work, which is similar to that described in Chapter 3 for the half Sommerfeld film, are given in Appendix III). With a combination of the two models described in the preceding pages it was possible to analyse any groove position

$(0^{o} < \beta < 360^{o})$.

4.2 RESULTS AND DISCUSSION.

Results are presented for the following values of β and $\bar{p}_g$ (the non-dimensional supply pressure):

β =	30^{o}	60^{o}	90^{o}	135^{o}	180^{o}	270^{o}
$\bar{p}_g$ =	0	0	0	0	0	0
	1.0	1.0	1.0	1.0	1.0	1.0

where $\bar{p}_g = \left(\frac{c}{R}\right)^2 p_g \frac{1}{\mu\omega}$

The values above are representative of a more comprehensive study which was carried out. Five values of β less than 180^{o} were chosen and only one for β greater than 180^{o} because, in general, a bearing would not be designed with an axial groove at an angle greater than 180^{o} before the loadline (a typical groove position would range from 90^{o} to 180^{o} before the loadline). Also the model described in section 4.1 is more accurate when β is less than 180^{o}.

A non-dimensional supply pressure of 1.0 was chosen because it represents a compromise between the need to choose a value large enough to affect the bearing performance, but not be unrealistic. For a bearing with:

$\left(\frac{c}{R}\right) = 0.002$, $\mu = 0.004$ Pa.s. and $\omega = 250$ rad/sec ($\simeq$ 2,500rpm)

a non-dimensional supply pressure of 1.0 corresponds to an actual supply pressure of 2.5 atmospheres (approximately). In practice the supply pressure is usually small compared with the hydrodynamic pressure generated in the bearing. Figure 4.4 shows a pressure profile for $\beta = 90^{o}$, $\bar{p}_g = 0$, $\varepsilon_s = 0.6$. The profile shows a maximum value for the pressure of 5.0. Thus, in this case, supplying oil to the bearing at a pressure of 1.0 would represent roughly 20% of the maximum hydrodynamic pressure.

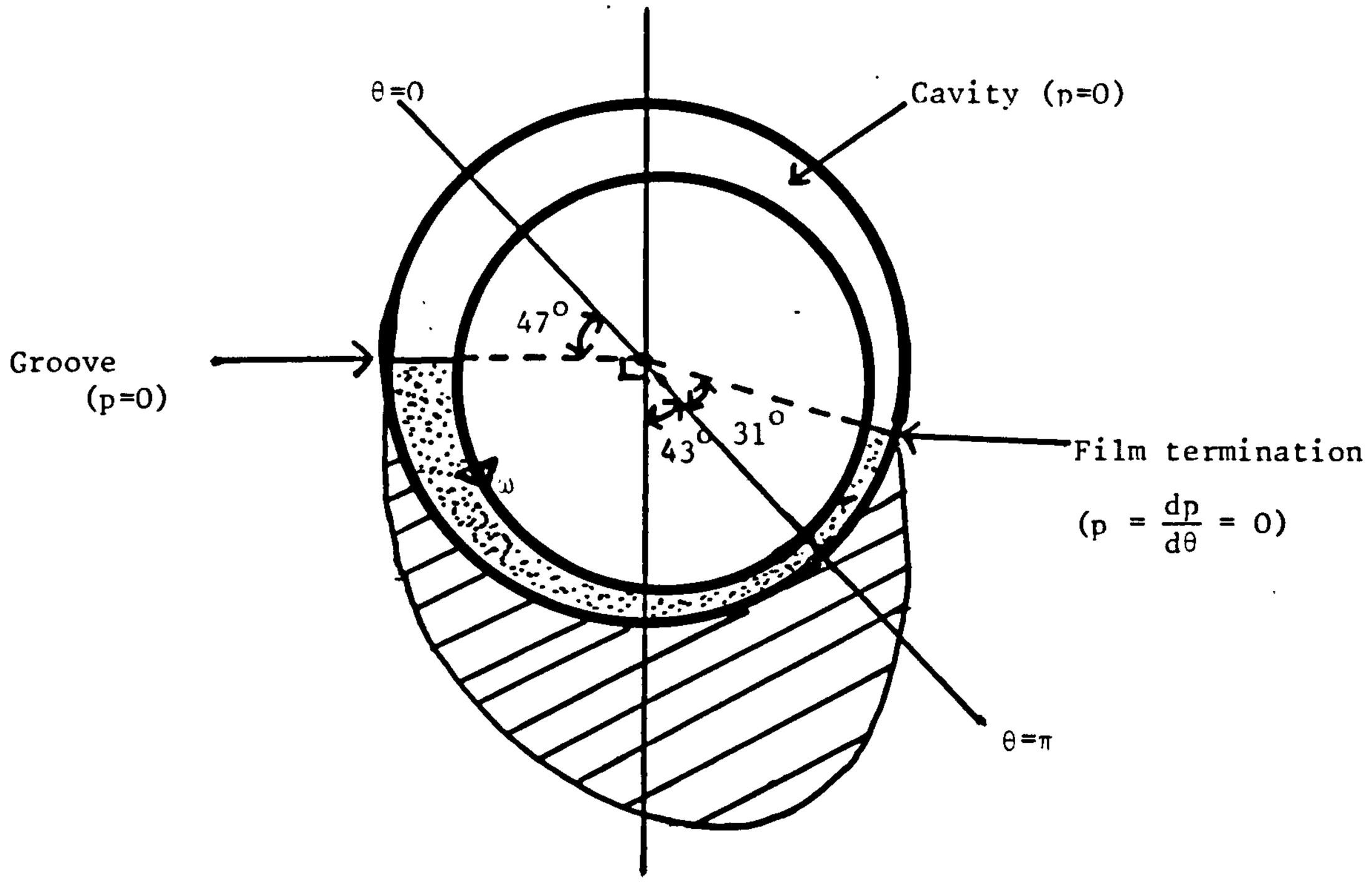

Steady state eccentricity ratio = 0.6

Attitude angle = 43.1°

Film extent = 164°

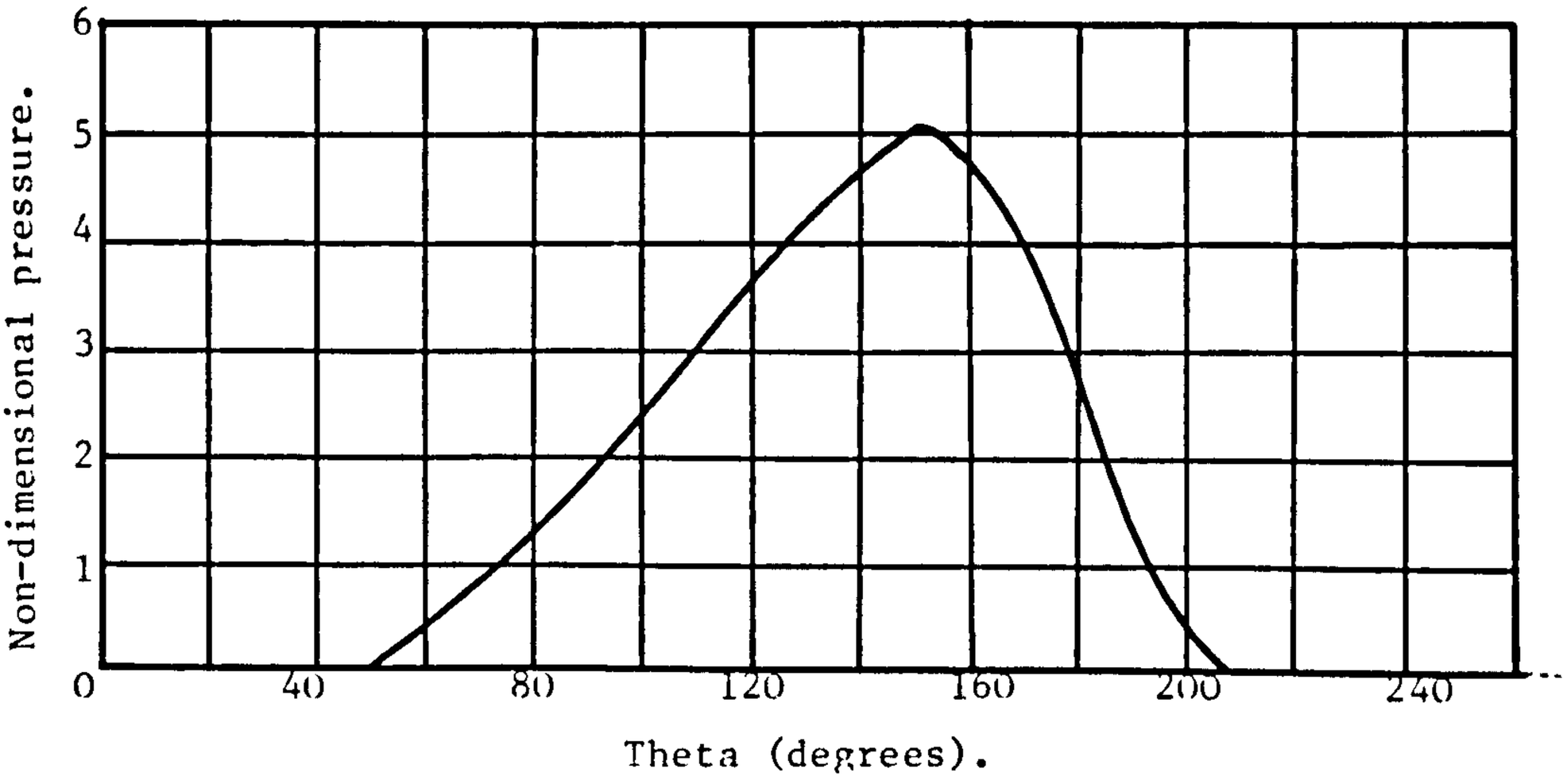

Figure 4.4. Theoretical steady state pressure distribution for the axial groove bearing. Groove position 90° before the loadline.

Curves are presented of:

i) the film extent ($\theta_{2s} - \theta_{1s}$) in Figure 4.5

ii) stability borderlines in Figure 4.6

iii) whirl frequency ratios in Figure 4.7

Tables of values for the steady state data and the eight velocity and displacement coefficients are given in Appendix II.

Discussion.

i) It is evident from Figure 4.6 that the groove position has an important effect on the stability of the journal, both charts showing the same trends. As β is increased from 30^{o} to 90^{o} the stability of the system increases for all eccentricity ratios. For β greater than 90^{o} (up to 180^{o}) there is a decrease in stability for low eccentricity ratios, whilst an increase for higher values. The reason for this decrease in stability is to be found in the film extent which increases as β varies from 30^{o} to 180^{o} (Figure 4.5). Thus the cavity extent is contracting over the range $30^{o} < \beta < 180^{o}$ and since no cavity means complete instability, it may be anticipated that this will adversely effect the stability of the journal. It is interesting to note in this respect, that a groove position of 30^{o} before the loadline is the least stable over a full range of eccentricity ratios and is also the position which has the largest cavity. It would appear, therefore, that too much cavitation can also adversely affect the stability of the system.

With the exception of the case $\beta = 270^{o}$ all the curves indicate that above a specific value of the eccentricity ratio the journal will operate in a stable manner for all values of ν (the value ranges from 0.76 for $\beta = 180^{o}$ to 0.94 for $\beta = 30^{o}$). The stability borderline for $\beta = 270^{o}$ does not follow the same pattern as the other curves. At low eccentricities it is, in fact, the most stable, but it becomes less stable as ε_s increases. Since most bearings operate at moderate to high eccentricity ratios this is one explanation of why bearings are not normally designed

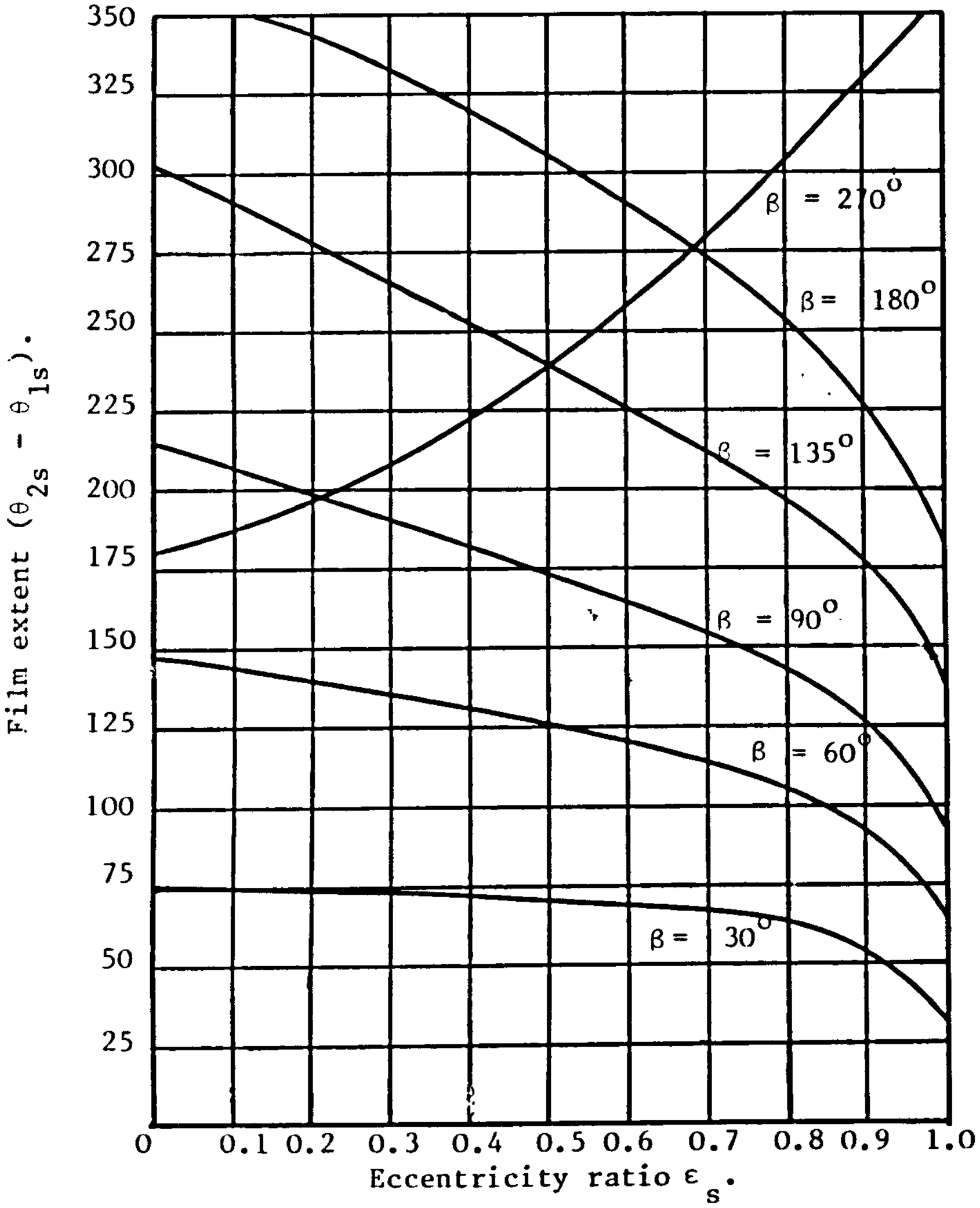

a). Supply pressure = 0.

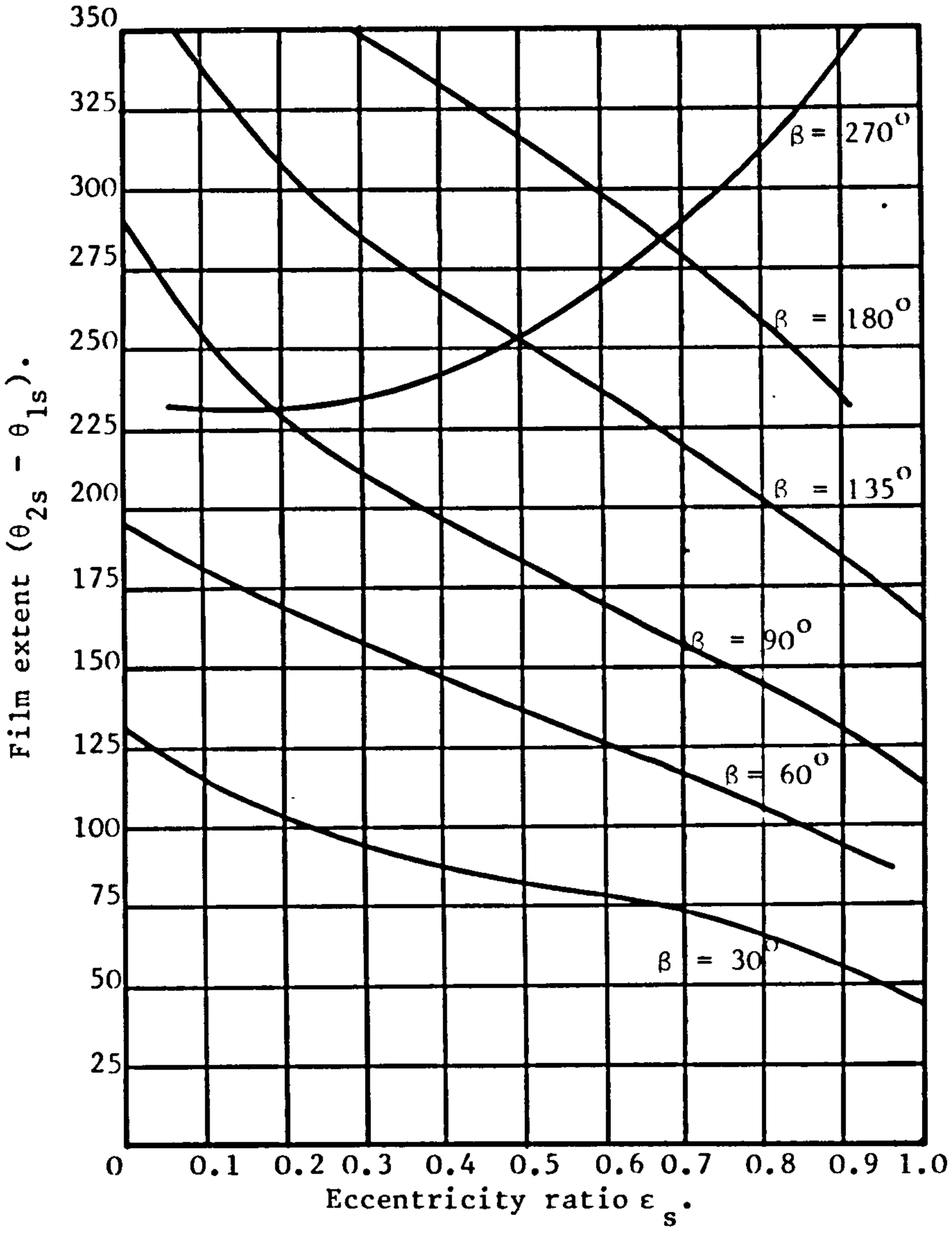

b).. Supply pressure = 1.0.

Figure 4.5. Film extent for the axial groove journal bearing.

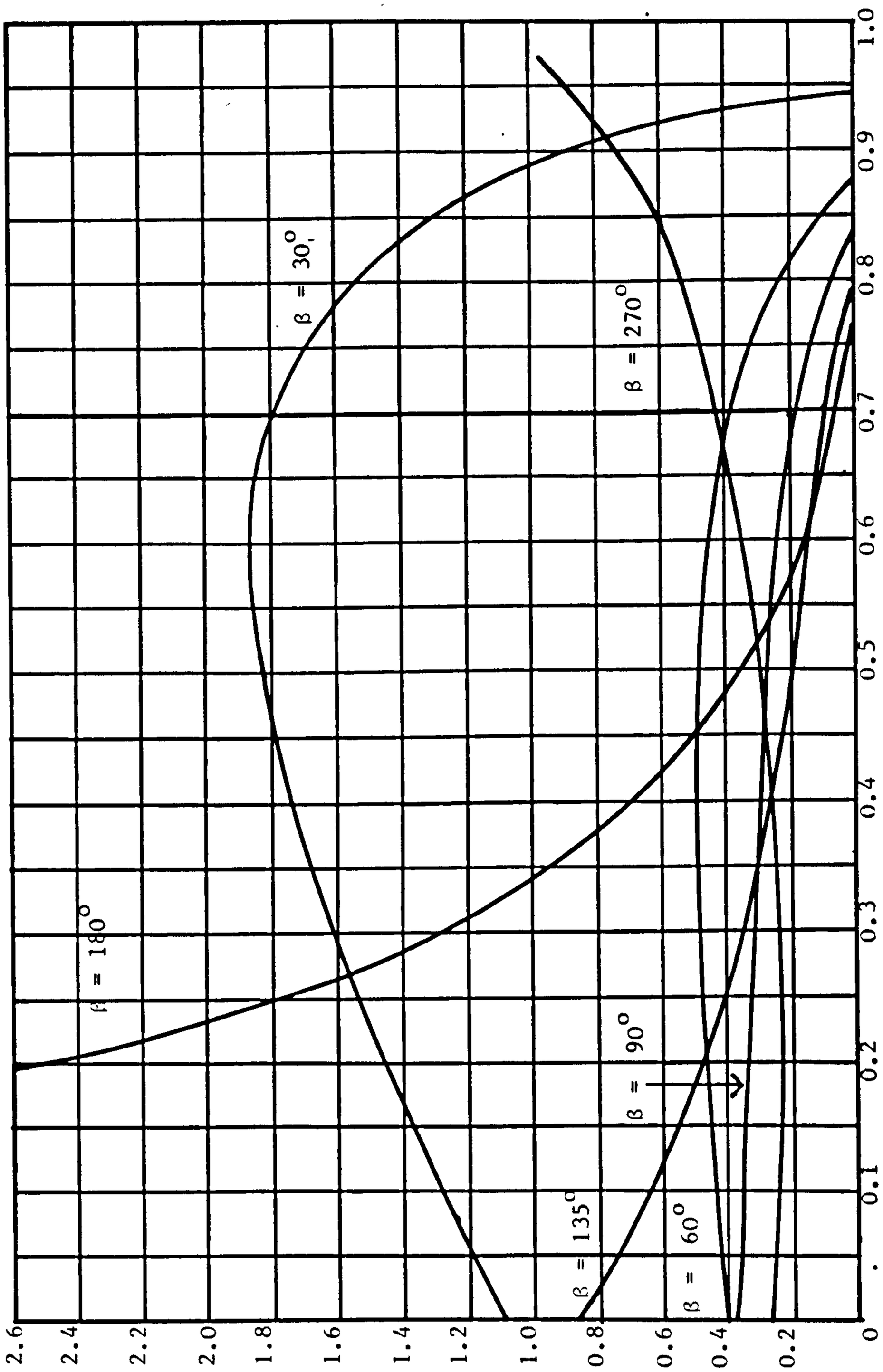

Figure 4.6. Stability curves for the axial groove journal bearing.
4.6(a). Supply pressure = 0.0.

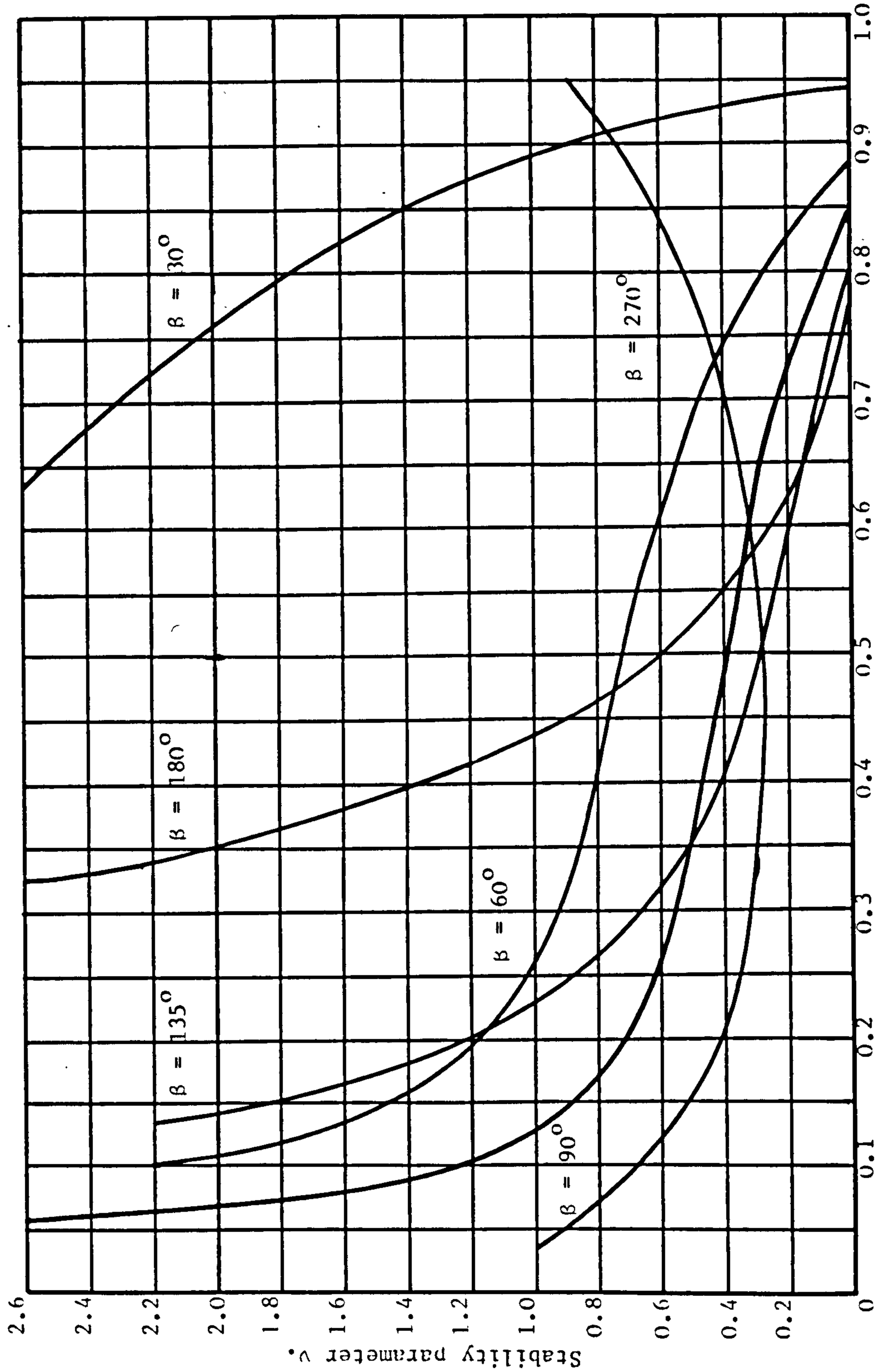

Figure 4.6. continued. Stability curves for the axial groove journal bearing.
4.6(b). Supply pressure = 1.0.

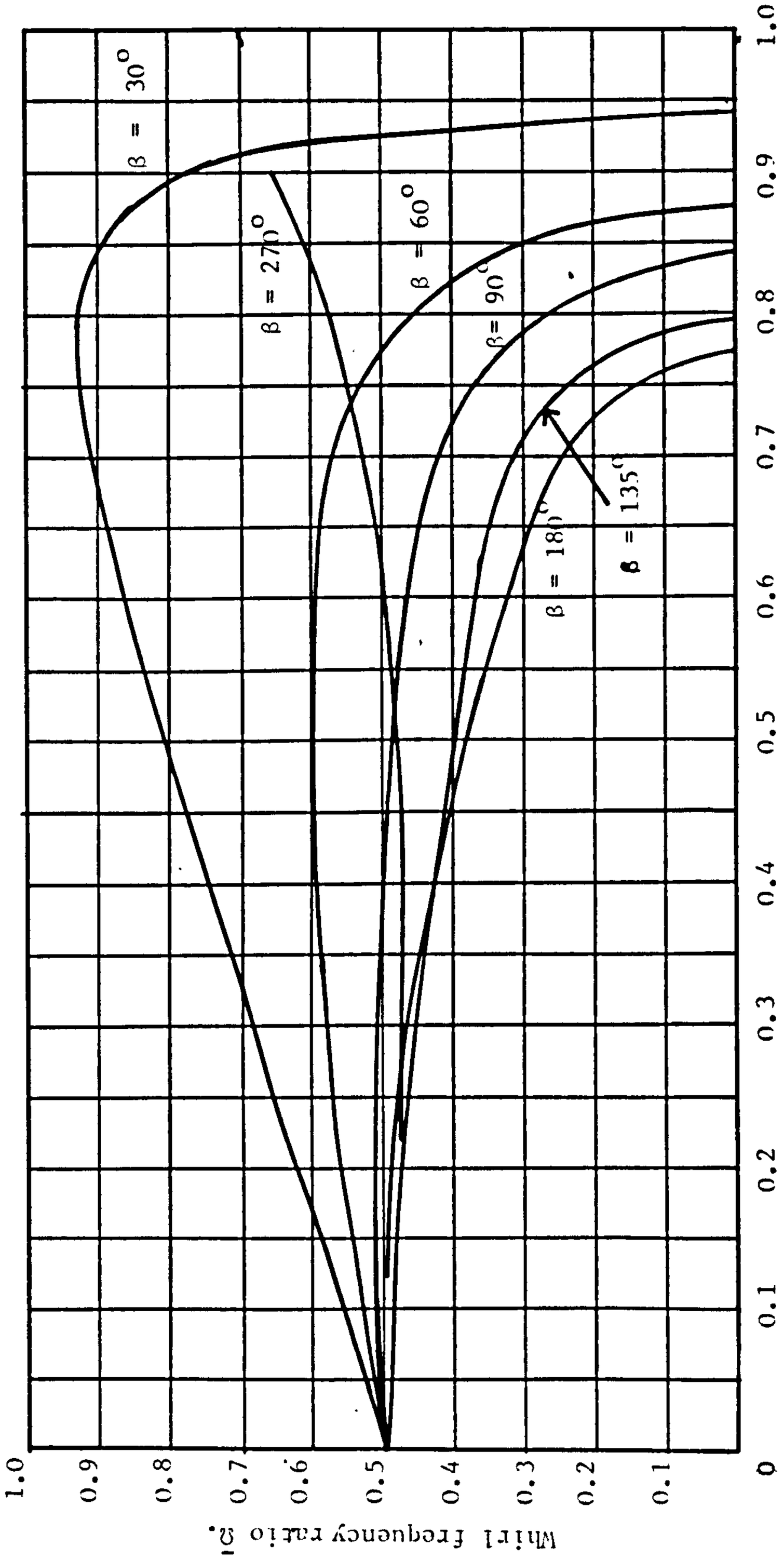

Figure 4.7. Critical frequency curves for the axial groove journal bearing.
4.7(a). Supply pressure = 0.0

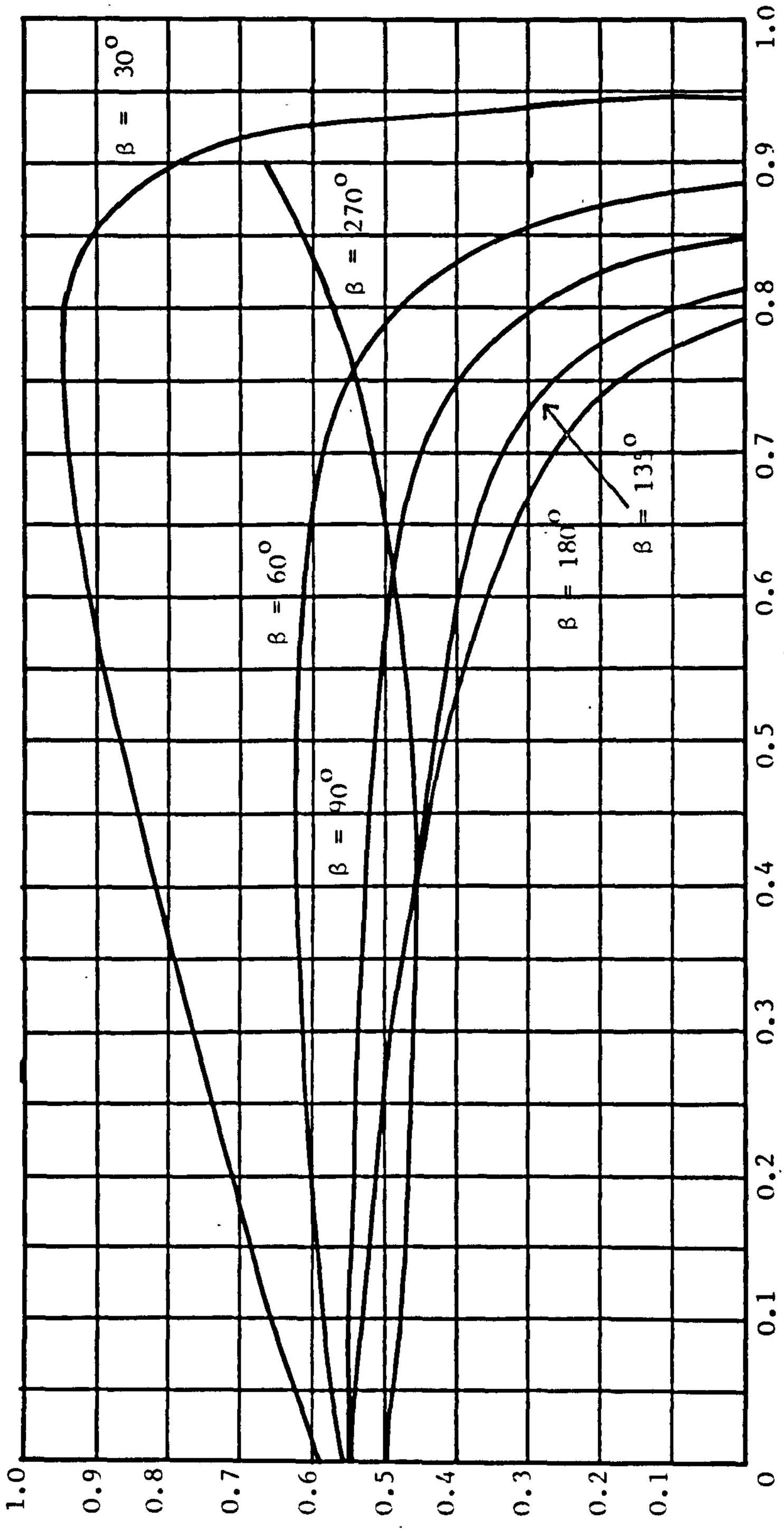

4.7(b). Supply pressure = 1.0.

. continued. Critical frequency curves for the axial groove journal bearing.

Figure 4.7.

with an axial groove in this region.

The stability charts may be used when designing the bearing to select the groove position which will optimise the stability of the journal (and hence minimise vibrational problems). The optimum groove position depends on both the supply pressure and the journal eccentricity (and thus on the operating speed range of the bearing). Over a range of eccentricities, a groove position of 90^{o} before the loadline would appear to be the most suitable, increasing to 180^{o} for higher eccentricities. From a vibrational viewpoint a groove position of around 30^{o} (or less) before the loadline is unsuitable.

ii) The oil supply pressure is also a factor which influences the vibrational behaviour of the journal (Figure 4.6(a) and 4.6(b)). Apart from one case it was always found that increasing the oil supply pressure was a destabilising factor, the exception being for $\beta = 270^{o}$, where the stability was slightly increased for $\varepsilon_s > 0.5$. Figure 4.5 shows that the film extent is increased by raising the supply pressure, implying a correspondence decrease in the cavity extent. Not surprisingly the effect of the supply pressure is most pronounced for small values of ε_s when the supply pressure is comparable to or greater than the hydrodynamic pressure.

The results regarding the effect of oil supply pressure are at variance with a number of experimental observations where it has been found that increasing the oil supply pressure reduced whirling (eg. Pinkus (1956), Holmes (1963)). The grooving arrangements in these experiments were more complicated than in the model described here. The argument that increasing the oil pressure reduces the cavitation region and hence makes the journal less stable does seem to be a reasonable one. The apparent discrepancy between theoretical prediction and experimental observation is worthy of further investigation.

iii) Curves of the critical whirl frequency ratio are shown in Figure

4.7. For $\beta = 30^{o}$ the ratio may be as high as 0.9, but for the remaining values of $\beta(> 60^{o})$ the ratio is less than 0.6. The ratio is increased slightly by raising the oil supply pressure.

iv) The steady state data and the eight velocity and displacement coefficients for the axial groove bearing may be found in Appendix II (Tables II.1 - II.12). The displacement coefficient K_{yy} is negative for low values of ε_s (apart from the case $\beta = 270^{o}$). This is due to a combination of oil film behaviour during journal vibration and use of Reynolds' condition at film rupture (as shown in Chapter 3). For all the cases studied with $\beta < 180^{o}$ the cross term velocity coefficients B_{xy} and B_{yx} were found to be identical. The boundary conditions used for $\beta = 270^{o}$ do not yield equal values for these coefficients (as discussed in Chapter 3).

4.3 DISCUSSION OF THE MODEL.

The model of the axial groove journal bearing presented in this Chapter is, like any mathematical model, based upon a number of assumptions. It is important, not only to be aware of these assumptions, but of their limitations when compared with the real situation. The main area for discussion centres around the boundary conditions which have been used to model the lubricating film in the bearing. Cavitation is a phenomenon which has been extensively studied with the result that numerous models have been proposed to explain the different features which have emerged (a thorough account of the history of modelling cavitation is given by Dowson and Taylor (1979)). The purpose of this section is to highlight the deficiences of the model presented in this Chapter and to discuss briefly some alternative models.

Film Rupture.

In this work the Reynolds condition was used to locate the film rupture position (provided the groove was not located there). The deficiency of the Reynolds condition lies in its inability to predict

the frequently observed subambient pressure loop immediately upstream of the cavitating region (Dowson (1957)).

Such observations led to the idea that flow separation may play a role in film rupture (Hopkins (1957), Birkhoff and Hays (1963)). In such a model the cavity is assumed to form where fluid separates from the stationary surface ie. where the velocity and tangential stress are both zero (Figure 4.8). Translating this into a condition on pressure gradient yields,

$$\frac{dp}{dx} = 2\mu \frac{U}{h_c^2} \quad \text{at rupture} \tag{4.4}$$

for the two dimensional situation (h_c is the gap thickness at rupture). Thus, the pressure gradient is positive at rupture, and this, together with the assumption of zero pressure, implies that subambient pressures exist immediately upstream of the separation position (Figure 4.9).

The separation model assumes that a considerable proportion of the lubricant will be carried away over the cavitating region by the moving surface (Figure 4.8). The reverse flow region that develops downstream of the separation point indicates a mechanism whereby gas bubbles may be directed to form a cavity. This simple explanation of cavitation relies on the questionable assumption that, the introduction of a cavity, which extends upstream to the separation point, does not effect where the fluid film separates from the stationary surface. The cavity is assumed to form at the separation point and thus if there is no separation there is no cavity (separation does not occur in journal bearings for eccentricity ratios below 0.3).

Coyne and Elrod (1970,1971) have developed the separation model in a detailed, two dimensional analysis of the cavity - fluid interface when a thin viscous film separates from a stationary surface and is swept away by the moving surface (Figure 4.10). Comparing flow rates in the x - direction just upstream of rupture and far downstream where

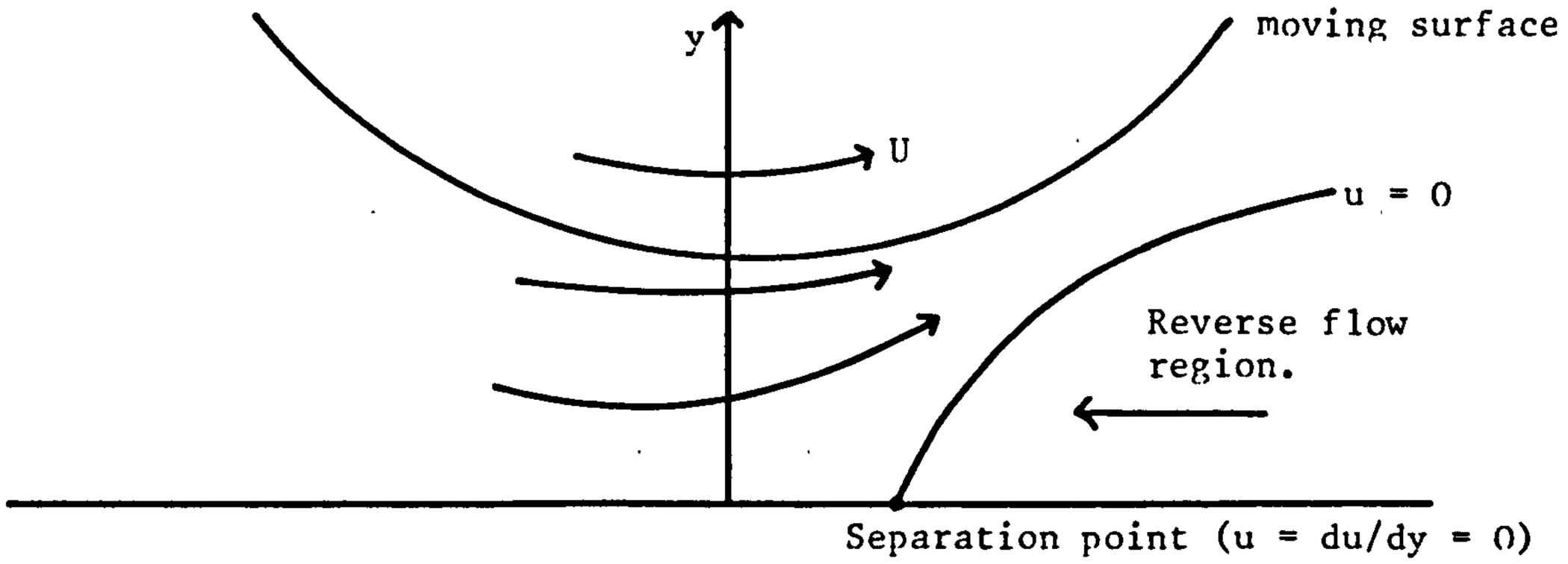

Figure 4.8. Separation from a stationary surface.

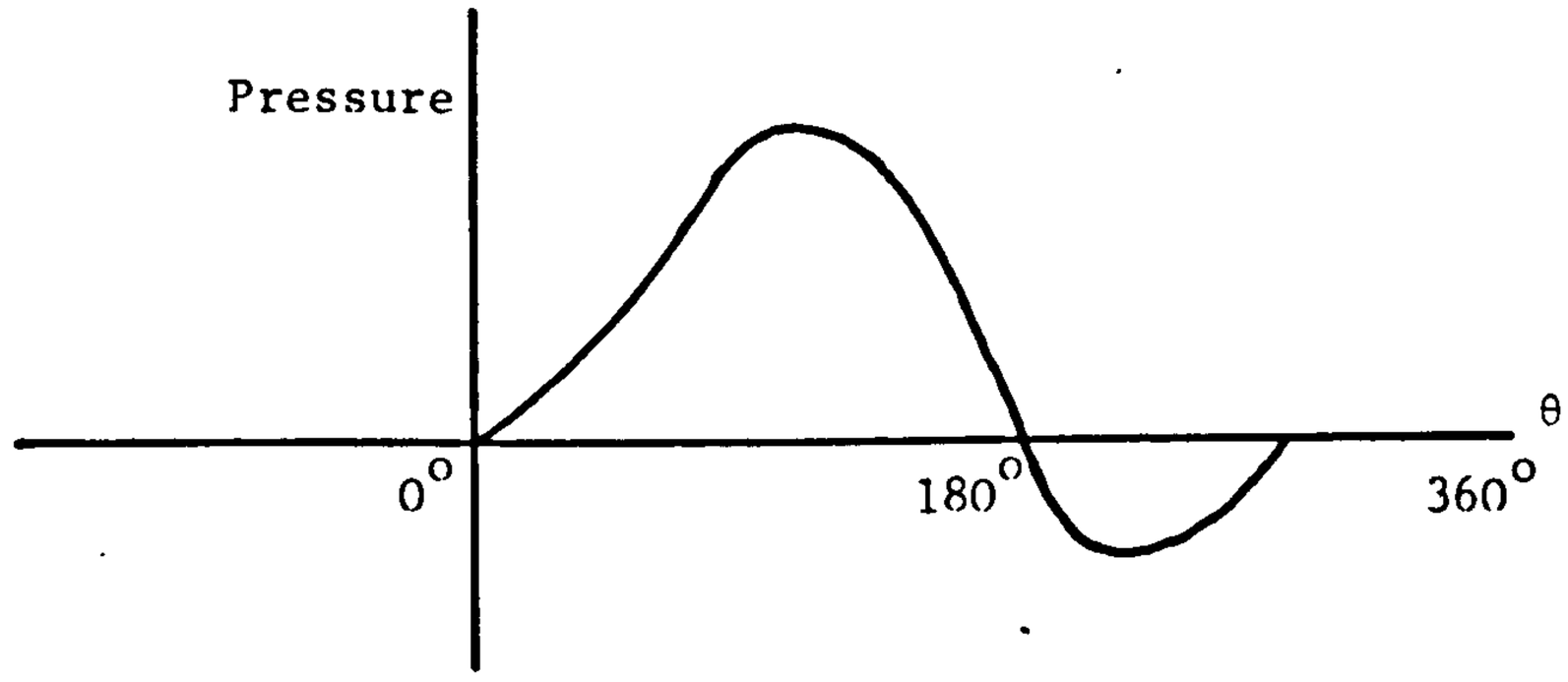

Figure 4.9. Pressure profile using a separation model.

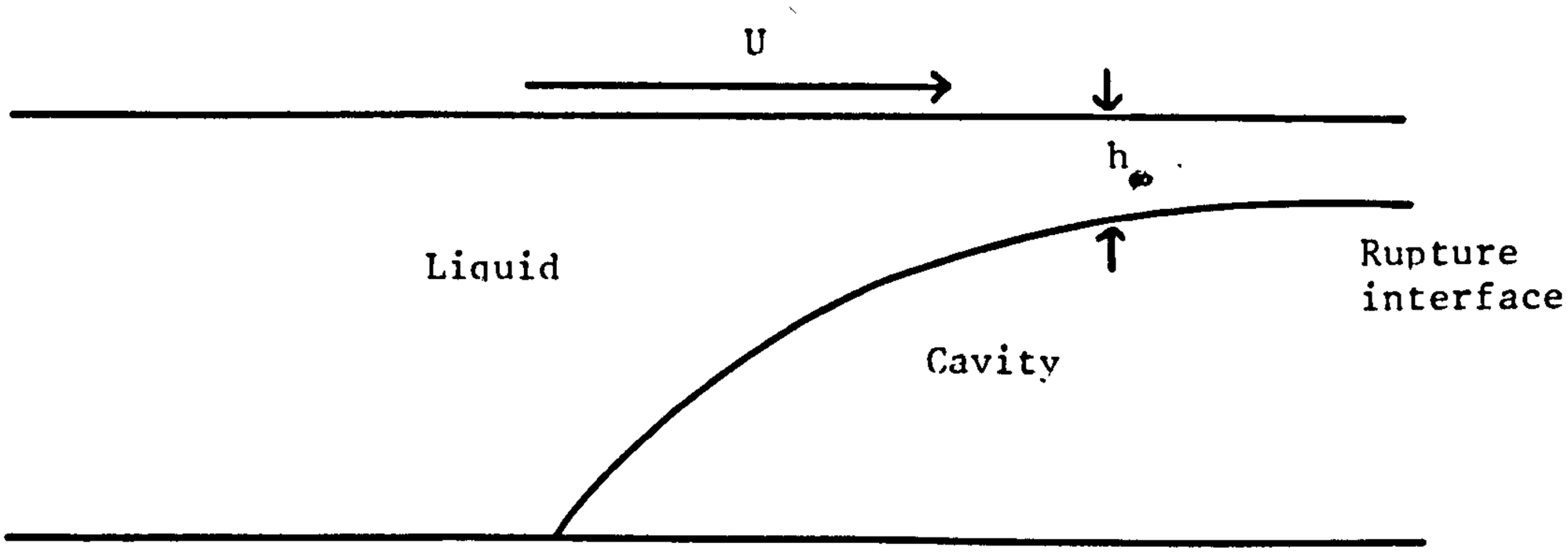

Figure 4.10. Separation with a liquid-gas interface.

a uniform fluid film of thickness h_∞ is formed leads to the following condition on pressure at rupture:

$$\frac{dp}{dx} = 6\mu \frac{U}{h_c^2} \left(1 - 2 \frac{h_\infty}{h_c}\right) \tag{4.5}$$

A condition on pressure gradient was also derived, namely that:

$$p = - \frac{T}{R_1} + \Delta p \tag{4.6}$$

where R_1 is the radius of curvature of the free film at the separation point, T is the surface tension between the lubricant and the air and Δp represents the pressure change across the transition region from the lubrication type flow just upstream of the cavity.

Coyne and Elrod were also able to determine the ratio h_∞/h_c and R_1/h_∞ as functions of the surface tension parameter $\mu U/T$, the importance of which had been demonstrated previously by Bretherton (1960) and Taylor (1963).

Smith (1975) obtained very good theoretical / experimental agreement using the Coyne and Elrod rupture boundary condition for the cylinder-plane geometry. However, Smith (1975) and Savage (1977) have both shown that the Coyne and Elrod model is not strictly applicable to loaded journal bearings. The reason for this lies in the nature of the cavity - fluid interface which has frequently been observed to consist of "sharp-pointed"fingers separated by fluid. Such an interface does not fullfil the requirements of Coyne and Elrod's theory which assumes the presence of a continuous cavity - fluid interface above which all the fluid flows to form a uniform layer.

The Reynolds condition, while failing to predict subambient pressures, does assume sharp-pointed finger-like cavities (see Figure 3.8). It provides a reasonably accurate description of film rupture for journal bearings sustaining moderate to high loads (the magnitude of the subambient pressure is then small compared with the superambient pressure), but not under conditions of light loading. Since most journal bearings operate with

moderate to high loads, use of the Reynolds condition is justified.

Film Reformation.

The assumption that the oil film build up began at the groove is less easy to justify. In practice and particularly where the supply pressure is superambient, the film will form upstream of the groove and over this region the lubricant pressure will rise to the supply pressure. However, the boundary condition used, namely $p = p_g$ at the groove, is simple to apply and does not violate flow continuity at the formation of the film (assuming the film to start upstream of the cavity would violate flow continuity). Also, it was found in Chapter 3 that the actual position of film formation did not significantly affect the bearing characteristics.

Film reformation in journal bearings has not been as widely studied as film rupture and remains an important area for future research. Floberg (1975), using a continuity of flow argument, has derived the following boundary condition to locate the film reformation position for the three dimensional situation:

$$\left[\frac{\partial p}{\partial x} - \frac{\partial p}{\partial z}\frac{\partial x}{\partial z}\right]_1 = \frac{6\mu U(h_2-h_1)}{h_2^3} \qquad (4.7)$$

where h_1 and h_2 are the oil film thickness at rupture and at reformation respectively at a particular axial location. The subscript 1 indicates the position of film start.

The model could therefore be improved by allowing for film reformation, eg. by use of the above boundary condition. This would have the most effect when the supply pressure is superambient. It would also give a more accurate model when the oil film terminates at the groove ($\beta = 270^o$). However, such an analysis would be rather complicated to undertake since both boundaries are then unknown. It would be best treated by numerical calculation using one of the methods described later in this Chapter.

Other Considerations.

The boundary conditions which were used in this model were derived under steady state conditions (as is nearly all the work on film rupture and reformation). The assumption that these boundary conditions remain valid during small amplitude vibrations is widely made. In this work the movement of the rupture boundary during journal vibration was included in the analysis. The model accounted correctly for the behaviour of the oil film during journal vibration by allowing for the movement of the line connecting the centres of the journal and the bearing with respect to the groove position.

Experimental Work.

To test the theoretical predictions of the influence of groove position and oil supply pressure on the vibrational characteristics of the axial groove journal bearing, a test rig, consisting of a rotor mounted on two plain journal bearings, was designed and built. The design of the rig, together with an account of some early testing and the problems which were encountered, is discussed in Appendix IV.

4.4 COMPARISON WITH OTHER WORK AND NUMERICAL METHODS.

Finally in this Chapter it is appropriate to compare the results obtained with those of other workers and to discuss briefly the numerical methods which are available to calculate the eight velocity and displacement coefficients for bearings with finite L/D ratios.

In reality, side leakage cannot be neglected and is an important factor influencing the bearing performance. The long bearing approximation to the Reynolds equation is no longer valid and a numerical solution of the full equation must be sought. However, analytic solutions are important since they can be used to check a numerical method and it is easier to assess the importance of such factors as oil film behaviour and movement of the rupture boundary with an analytic model.

Several numerical methods have been devised to calculate the eight bearing

coefficients. Three such methods are discussed briefly below, together with a comparison of the coefficients calculated using these methods with those obtained from the present work.

i) Woodcock and Holmes (1970).

The numerical method described by Woodcock and Holmes is based upon a finite difference solution of the Reynolds equation followed by numerical integration of the pressure field to calculate the hydrodynamic forces. The equation is first solved under steady state conditions at an eccentricity ratio ε_s. The eight coefficients are then calculated by numerical differentiation; for example, the journal centre is given a small displacement (δx) in the x-direction from equilibrium and the equation re-solved. The procedure is repeated for a displacement ($-\delta x$) and the displacement coefficient K_{xx} may then be calculated via:

$$K_{xx} = -\left(\frac{f_x(x_s + \delta x) - f_x(x_s - \delta x)}{2\delta x}\right)$$

where $f_x(x_s + \delta x)$ is the x- component of the force at $x = x_s + \delta x$, etc.

Programs based upon this method have been developed by Craighead (1976) and Ruddy (1980) to study a wide variety of bearing types. Results obtained for the long axial groove bearing indicate reasonable agreement with the results presented in the Chapter (private communication with A.V. Ruddy).

The method calculates any movement of the rupture boundary which may occur when the journal is displaced from equilibrium (the Reynolds condition is normally used). Any variation of the line of centres with respect to the groove position is automatically considered (and hence its importance remains unnoticed). The method always gives $B_{xy} \neq B_{yx}$, the difference being most pronounced at low eccentricities. It is generally felt that the reason for this is the movement of the rupture boundary which is included in the method. This is incorrect however, since the analysis described in this Chapter perturbs the rupture boundary ($\theta_2 \rightarrow \theta_{2s} + \delta\theta_2$), but still yields

$B_{xy} = B_{yx}$. It is interesting to note that experimental work does not give equal values for these coefficients (private communication with G.E.C.).

The method is fairly lengthy in computing time in comparison with method 3 and suffers from the inherent inaccuracies of numerical differentiation (which is one possible explanation of why $B_{xy} \neq B_{yx}$).

ii) Lundholm (1969, 1971, 1973).

Lundholm (1969, 1971, 1973) has made a complete study of both the axial groove journal bearing and the circumferential groove bearing for a range of L/D ratios. For the axial groove bearing, the boundary conditions used by Lundholm were:

$$p = 0 \quad \text{and} \quad \frac{\partial p}{\partial \theta} = \frac{\partial p}{\partial z} = 0 \tag{4.8}$$

at film fupture (provided the groove is not located there). Equation (4.8) represents the generalisation of the Reynolds condition to the three dimensional situation. The start of the oil film was assumed to be at the groove or downstream of it. Lundholm found that if the angle between the groove and the loadline was less than 90^{o} the film start was always at the groove. However, if it was greater than 90^{o} the same assumption caused negative pressures to be generated in a limited region after the groove. The formation of the film was then located from a continuity condition similar to Floberg's condition for film reformation (equation 4.7), which gives at a particular z location:

$$\frac{Uh_3}{2} = \frac{Uh_1}{2} - \frac{h_1^3}{12\mu} \left(\frac{1}{R} \frac{\partial p}{\partial \theta} - R \frac{\partial p}{\partial z} \frac{\partial \theta}{\partial z} \right)_{\theta = \theta_1} \tag{4.9}$$

where subscript 1 indicates the position of film start and 3 the groove.

The above conditions apply to finite bearings. For the long bearing Lundholm found that this problem did not arise. The film was assumed to start at the groove (or end at it). Lundholm did not discuss clearly the boundary conditions for the situation in which the film ended at the groove

(eg. $\beta = 270^{o}$). Apart from this case, the boundary conditions used by Lund-holm are identical to those described in this Chapter and thus a direct comparison of the results can be made.

The technique used by Lundholm to calculate the velocity and displacement coefficients is a mixed method which utilises both finite difference solutions to the Reynolds equation and information deduced from the steady state characteristics. The equation is first solved under steady state conditions from which the attitude - eccentricity curve is deduced. The four displacement coefficients are then expressed as functions of the load capacity and attitude characteristics. Two of the velocity coefficients B_{xy} and B_{yy} are calculated similarly, with the remaining two coefficients calculated by solving the Reynolds equation with the squeeze film terms included.

Table 4.2 compares results obtained from this Chapter with Lundholm's results for a long bearing with $\beta = 90^{o}$, $\bar{p}_g = 0$ (Lundholm did not consider the effect of oil supply pressure). The first column is taken from Lund-holm's work in 1971. It can be seen that the steady state data (S, ϕ_s) and the four velocity coefficients are in good agreement for the two methods. The four displacement coefficients, however, do not agree. Part of the reason for this is that Lundholm's original work (1971) did not include the variation of the line of centres with respect to the groove position during journal vibration. Lundholm (1973) has subsequently corrected for this error and the results obtained with the more accurate theory are shown in column 2 of Table 4.2. There is then good agreement with the results of the Chapter, although it is unclear why, in Lundholm's corrected work, all four displace-ment coefficients are altered instead of just the two coefficients K_{xy} and K_{yy} (as discussed in Chapter 3). Comparing Lundholm's work in 1971 and 1973 shows that there are considerable differences in the stability charact-eristics for the same values of β and ε_s - the more accurate theory predicting the bearing to be less stable. Surprisingly Lundholm does not comment on this difference.

	Lundholm (1971)	Lundholm (1973)	Myers (1981)	Lundholm (1971)	Lundholm (1973)	Myers (1981)	Lundholm (1971)	Lundholm (1973)	Myers (1981)
ε_s	0.4	0.4	0.4	0.6	0.6	0.6	0.8	0.8	0.8
S	0.28	0.28	0.28	0.16	0.16	0.16	0.08	0.08	0.08
ϕ_s^o	49.9	49.9	49.9	43.1	43.1	43.1	33.3	33.3	33.3
B_{xx}	6.80	6.80	6.80	5.94	5.94	5.94	6.83	6.83	6.83
$B_{xy}=B_{yx}$	-3.22	-3.22	-3.22	-2.43	-2.43	-2.43	-2.09	-2.09	-2.09
B_{yy}	3.83	3.83	3.83	2.28	2.28	2.28	1.37	1.37	1.37
K_{xx}	2.21	2.33	2.31	2.56	2.72	2.68	4.77	4.95	4.92
K_{xy}	1.91	2.44	2.39	1.14	1.53	1.44	0.69	0.90	0.86
K_{yx}	-1.82	-2.20	-2.18	-1.45	-1.82	-1.80	-1.82	-2.14	-2.13
K_{yy}	1.61	-0.20	-0.12	1.22	0.32	0.38	1.04	0.68	0.69
ν_{crit}	0.11	0.31	0.30	0.12	0.25	0.24	0.02	0.07	0.07

Groove position 90^o before the loadline

Table 4.1. Comparison of Lundholm's work with the present work.

iii) Lund and Thomsen (1978).

Lund and Thomsen (1978) have devised a numerical method for calculating the velocity and displacement coefficients based upon a first order expansion of the full Reynolds equation.

$$\frac{\partial}{\partial\theta}\left\{\bar{h}^3\frac{\partial p}{\partial\theta}\right\} + R^2\frac{\partial}{\partial z}\left\{\bar{h}^3\frac{\partial p}{\partial z}\right\} = 6\mu\left(\frac{R}{c}\right)^2\left\{-\varepsilon(1-2\phi')\sin\theta + 2\varepsilon'\cos\theta\right\} \qquad (4.10)$$

The linearisation is carried out before integrating (instead of after). During a small amplitude vibration of the journal about its equilibrium position, the journal centre has co-ordinates (x,y) or $(\delta, \varepsilon_s\gamma)$ - see Figure 4.11. The film thickness h may be written:

$$\bar{h} = 1 + \varepsilon\cos\theta = (1+\varepsilon_s\cos\theta^1) + \cos\theta^1\delta x + \sin\theta^1\delta y \qquad (4.11)$$
$$= \bar{h}_s + \cos\theta^1\delta x + \sin\theta^1\delta y$$

In the above expression θ, the angular co-ordinate, is replaced by $\theta^1 - \gamma$ ie. the analysis is based upon the angular co-ordinate measured from the equilibrium position of the line of centres (Figure 4.11). This is done to introduce a y term into the equations. Its importance in relation to boundary conditions is discussed later.

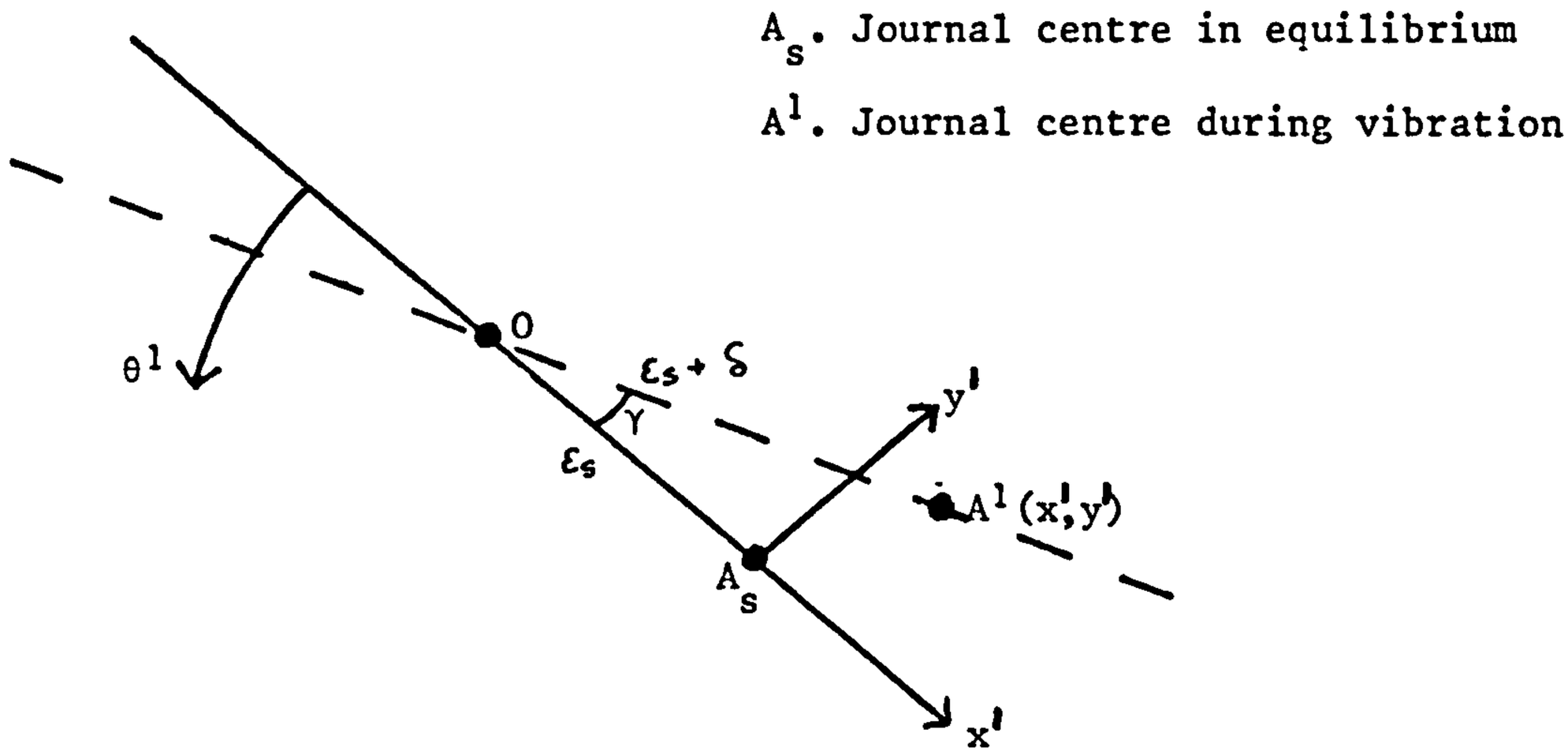

Figure 4.11. Co-ordinate system used in perturbing the Reynolds equation.

A first order expansion of the pressure may be written as:

$$p = p_s + p_x x + p_y y + p_{\dot{x}} \dot{x} + p_{\dot{y}} \dot{y} \tag{4.12}$$

Substituting equations (4.11) and (4.12) into (4.10) and retaining only first order terms yields five equations:

$$\left[\frac{\partial}{\partial \theta^1} \left(\bar{h}_s^3 \frac{\partial}{\partial \theta^1} \right) + R^2 \frac{\partial}{\partial z} \left(\bar{h}_s^3 \frac{\partial}{\partial z} \right) \right] \left\{ \begin{matrix} p_s \\ p_x \\ p_y \\ p_{\dot{x}} \\ p_{\dot{y}} \end{matrix} \right\} \tag{4.13}$$

$$= \left\{ \begin{matrix} -6\mu \left(\frac{R}{c}\right)^2 \varepsilon_s \sin\theta^1 \\ -6\mu \left(\frac{R}{c}\right)^2 \sin\theta^1 - 3 \frac{\partial}{\partial \theta^1} \left(h_s^2 \cos\theta^1 \frac{\partial p_s}{\partial \theta^1} \right) \\ 6\mu \left(\frac{R}{c}\right)^2 \cos\theta^1 - 3 \frac{\partial}{\partial \theta^1} \left(h_s^2 \sin\theta^1 \frac{\partial p_s}{\partial \theta^1} \right) \\ 12\mu \left(\frac{R}{c}\right)^2 \cos\theta^1 \\ 12\mu \left(\frac{R}{c}\right)^2 \sin\theta^1 \end{matrix} \right.$$

The boundary conditions are:

$$\left. \begin{matrix} \text{at } z = 0, L \\ \theta^1 = \theta^1 \\ \theta^1 = \theta_2^1 \end{matrix} \right\} \quad p = 0 \Rightarrow p_s = p_x = p_y = p_{\dot{x}} = p_{\dot{y}} = 0 \tag{4.14}$$

where $z = 0, L$ are the bearing edges, $\theta^1 = \theta_1^1$ the film start (assumed to be at a groove, or the line of maximum film thickness), and $\theta^1 = \theta_2^1$ the film rupture position. In the three dimensional case the film rupture position at $\theta^1 = \theta^1{}_2$ is a function of z and the boundary curve is located by the condition that, in addition to the pressure being zero along the curve, the pressure gradient normal to the curve is also zero:

$$\text{at } \theta^1 = \theta_2^1 \ (z): \quad p = \frac{\partial p}{\partial n} = 0 \Rightarrow p = \frac{\partial p}{\partial \theta} = \frac{\partial p}{\partial z} = 0 \tag{4.15}$$

The boundary curve is determined by an iterative procedure when solving for the static pressure p_s. Under dynamic conditions a point on the curve (θ_s^1, z_s) moves to a new position $(\theta_s^1 + \Delta\theta^1, z_s + \Delta z)$ and requiring the pressure to be zero on the new boundary yields:

$$p(\theta_2^1, z_2) = 0 = p(\theta_{2s}^1, z_{2s}) + \left(\frac{\partial p}{\partial \theta_2^1}\right)\Delta\theta^1 + \left(\frac{\partial p}{\partial z}\right)\Delta z \tag{4.16}$$

Writing equation (4.12) as $p = p_s + \Delta p$ and substituting into equation (4.16) yields:

$$p(\theta_2^1, z_s) = 0 = p_s(\theta_{2s}^1, z_{2s}) + \Delta p(\theta_{2s}^1, z_{2s}) + \left(\frac{\partial p_s}{\partial \theta}\right)_s \Delta\theta' + \left(\frac{\partial p_s}{\partial z}\right)_s \Delta z \tag{4.17}$$

from which it follows that $\Delta p(\theta_s^1, z_s) = 0$ because p_s and its gradients are zero on the original boundary curve. Hence, the boundary conditions at the film rupture are:

$$\text{at } \theta^1 = \theta_2^1 \ (z) \qquad p_s = \frac{\partial p_s}{\partial \theta} = \frac{\partial p_s}{\partial z} = 0 \tag{4.18}$$

$$p_x = p_y = p_{\dot{x}} = p_{\dot{y}} = 0$$

With the given boundary conditions, the five equations (4.13) may be solved numerically by the finite difference method. The pressures are then integrated numerically over the film domain to obtain the static forces and the eight linear coefficients.

$$\text{eg. } K_{xx} = -\int_0^L \int_{\theta^1}^{\theta_2^1} p_x \cos\theta^1 d\theta^1 dz \tag{4.19}$$

This method has several advantages over the one devised by Woodcock and Holmes (1969-70). Less computing time is involved since equations (4.13) are basically similar, differing only in their right hand sides. It is also a more accurate method since it does not relv on numerical differentiation. Results published by Lund and Thomsen (1978) for a variety of bearing types and grooving arrangements always show that $B_{xy} = B_{yx}$. Unfortunately they did

not publish results for the axial groove bearing. However, by making the long bearing approximation to equations (4.13) they may be integrated analytically to determine the eight coefficients. Results obtained using this alternative method were found to be identical with the results given in this Chapter.

As a means of simply obtaining the linear coefficients this method has much to recommend it. The boundary conditions are easier to apply since the pressure field is written as a first order expansion, with the static pressure chosen to satisfy:

$$p_s = 0 \text{ at } \theta^1 = \theta^1_{1s}. \quad p_s = \frac{dp_s}{d\theta^1} = 0 \text{ at } \theta^1 = \theta^1_{2s} \tag{4.20}$$

The perturbed pressures are then superimposed on the static boundary

$$\text{eg. } p_x = 0 \text{ at } \theta^1 = \theta^1_{1s} \text{ and at } \theta^1 = \theta^1_{2s} \tag{4.21}$$

In the scheme described in this Chapter and the previous one, the full boundary conditions were applied to the pressure "en bloc" which then required movement of the rupture boundary during vibration ($\theta_2 \rightarrow \theta_{2s} + \delta\theta_2$). The intention in this work was to derive the full nonlinear equations and then linearise. In the end the two methods are equivalent since they give identical results.

In Lund and Thomsen's method the angular co-ordinate θ^1 is measured from the equilibrium position of the line of centres. Thus, there is no variation of the angular co-ordinate with respect to the groove position to account for during vibration. To elucidate this point note that if the equations are solved for a half film model with:

$$p = 0 \text{ at } \theta^1 = 0, \pi \tag{4.22}$$

the results obtained are identical with those of the static half film model discussed in Chapter 3. The method is therefore well suited to examine bearings with grooves and static films. To model an oscillating film the boundary conditions would have to include a γ variation eg. the appropriate boundary

conditions for the oscillating half film are:

$$p = 0 \text{ at } \theta^1 = \gamma, \pi + \gamma \qquad (4.23)$$

4.5 CONCLUSIONS.

i) A detailed analysis of the axial groove bearing (neglecting side leakage) has been made in which careful consideration has been given to the appropriate boundary conditions which are applicable at both film reformation and rupture. The analysis accounts correctly for the behaviour of the oil film during vibration.

ii) The location of the axial groove is an important factor influencing the vibrational characteristics of the bearing. By selecting the optimum groove position it is possible to raise the threshold speed, thus minimising the threat of vibrational problems.

iii) Increasing the oil supply pressure contracts the cavitation region and has a destabilising effect by lowering the threshold speed.

iv) The numerical methods used to calculate the velocity and displacement coefficients for finite bearings give reasonable results for the long bearing when compared with the results given in this Chapter. There appears to be, however, a lack of clarity in the assumptions made about boundary conditions and oil film behaviour during vibration. This arises because the importance of these assumptions is not fully appreciated.

PART 2.

THE APPLICATION OF NONLINEAR TECHNIQUES TO EXAMINE THE PHENOMENON OF OIL WHIRL IN FLUID FILM JOURNAL BEARINGS.

INTRODUCTION TO PART 2.

Linear stability theory provides information about the instability threshold which is conveniently displayed on a stability chart. It is easily deduced from the stability chart whether the bearing will operate stably, or unstably, at a particular rotor speed. However, it is important to remember that linear stability theory is valid only when the journal is close to its equilibrium position. Above the threshold speed the journal is unstable and will spiral away from its equilibrium position. Under these conditions, linear analysis cannot describe the motion of the journal for very long, since nonlinear effects must, at some stage, become important. Therefore, an investigation of the full nonlinear equations of motion is necessary to determine the complete motion of the journal. This is carried out in Part 2, where the following nonlinear techniques are employed to solve the equations of motion:

i) bifurcation theory

ii) multiple scaling

iii) the method of averaging

iv) numerical integration.

These techniques are used to establish various features of the equations and, in particular, to examine the structure of periodic solutions for rotor speeds close to the threshold speed. Results obtained from the different techniques are contrasted and an assessment is made of how suitable these methods are for examining the phenomenon of oil whirl in fluid film journal bearings.

CHAPTER 5

HOPF BIFURCATION THEORY APPLIED TO THE EQUATIONS GOVERNING OIL WHIRL IN FLUID FILM JOURNAL BEARINGS.

In this Chapter, Hopf bifurcation theory is used to establish rigorously the existence of small amplitude periodic solutions of the equations governing the motion of a rotor supported in fluid film journal bearings. It is shown that two different types of bifurcation may occur:- supercritical bifurcation in which a stable periodic orbit bifurcates from the steady state equilibrium position for rotor speeds just in excess of the threshold speed, or subcritical bifurcation in which an unstable periodic orbit bifurcates from the equilibrium position for rotor speeds just below the threshold speed. The type of bifurcation which occurs depends upon the region of parameter space in which the rotor is operating - both types cannot occur simultaneously.

A numerical investigation supports the findings of the analytic results and in addition makes it possible to pursue the development of the whirl orbit as the rotor speed is altered. This combined analytic and numerical approach establishes that the onset of oil whirl is a bifurcation phenomenon and identifies several features of oil whirl which have not been previously observed.

5.1 HOPF BIFURCATION THEORY.

Hopf bifurcation theory is concerned with the bifurcation of periodic orbits from the equilibrium points of a real n-dimensional first order system of ordinary differential equations (O.D.E.) as a parameter crosses a critical value. Consider the differential equation:

$$\frac{d}{dt}\underline{x} = \underline{F}(\underline{x},\nu) \qquad (5.1)$$

which is a real n-dimensional autonomous first order system of O.D.E. ($n \geq 2$). ν is a real parameter. Assume that:

i) $\underline{x} = \underline{a}^{\nu}$ is an equilibrium point of equation (5.1) ($\Leftrightarrow \underline{F}(\underline{a}^{\nu},\nu) = 0$).

ii) the Jacobean matrix $\underline{F}_{\underline{x}}(\underline{a}^{o},0)$ has exactly two non-zero, purely imaginary

eigenvalues $\pm i\Omega_o$ ($\Omega_o > 0$) and (n-2) eigenvalues with non-zero real parts.

iii) $\underline{F}$ is analytic in a neighbourhood of $(\underline{x},\nu) = (\underline{a}^o,0)$.

iv) $(d\alpha/d\nu)_{(\underline{a}^o,0)} \neq 0$, where $\alpha(\nu)+i\Omega(\nu)$ denotes that eigenvalue of $\underline{F}_{\underline{x}}(\underline{a}^\nu,\nu)$ which is a continuous extension of $+i\Omega_o$.

Under these conditions Hopf (1942) proved that a nonconstant periodic orbit bifurcates from $(\underline{x},\nu) = (\underline{a}^o,0)$. Hopf also supplied a uniqueness theorem and information regarding stability. Besides the smoothness assumptions on $\underline{F}(\underline{x},\nu)$ the essential requirements in this theorem are those on the eigenvalues of the matrix $\underline{F}_{\underline{x}}(\underline{a}^o,0)$ and the non-zero derivative of the real part of the eigenvalue $\alpha(\nu)+i\Omega(\nu)$ at $\nu = 0$. In applications, these requirements are often satisfied when there is an exchange in the stability of an equilibrium point as two complex conjugate eigenvalues cross the imaginary axes.

Although it is fairly straightforward to establish the <u>existence</u> of a Hopf bifurcation in concrete examples, (which essentially requires an analysis of the eigenvalues of the linearised system of equations), a major difficulty with the theory lies in determining the <u>direction of bifurcation</u> (ie. $\nu < 0$, or $\nu > 0$) and the stability of the periodic orbit.

In Hopf's original approach the determination of the direction of bifurcation and the stability of the orbit for concrete examples is possible, but difficult. Subsequently several authors have sought to simplify the calculation (Friedrichs (1965), Hsü and Kazarinoff (1976), Marsden and McCracken (1976)). Most of the available methods require a transformation of the equations by introducing new variables. For equations in which $n > 3$ and with several nonlinear terms these transformations become extremely complicated. Poore (1976) has removed many of these difficulties by deriving algebraic criteria which are sufficient to determine the direction of bifurcation and the stability of the periodic orbit. It is this aspect of Poore's work which is of

primary importance here and therefore it is valuable to present the essential features of his work.

Consider again the differential equation (5.1). Poore makes the following change of variables:

$$\underline{x} = \underline{a}^{\nu} + \mu\underline{y} \qquad t = (1+\mu\eta)s \qquad \underline{A}^{\nu} = \underline{F}_{\underline{x}}(\underline{a}^{\nu},\nu)$$
$$\nu = \mu\delta(\mu) \qquad \nu\underline{B}^{\nu} = \underline{A}^{\nu} - \underline{A}^{o} \qquad \underline{B}^{o} = \left.\frac{d\underline{A}}{d\nu}\right|_{\nu = 0} \tag{5.2}$$

$$\underline{F}(\underline{a}^{\nu}+\mu\underline{y},\nu)=\mu\underline{A}^{\nu}\underline{y}+\mu^{2}\underline{Q}(\underline{y},\mu,\nu) \qquad \underline{G}(\underline{y},\mu,\delta,\eta)=\delta\underline{B}^{\mu\delta}\underline{y}+\eta\underline{A}^{\mu\delta}\underline{y}+(1+\mu\eta(\mu))\underline{Q}$$

which transforms equation (5.1) to:

$$\frac{d}{ds}\underline{y} = \underline{A}^{o}\underline{y} + \mu\underline{G}(\underline{y},\mu,\delta,\eta) \tag{5.3}$$

The purpose of the change in variables is to reduce the problem of periodic solutions of equation (5.1) to a perturbation problem in μ in equation (5.3). At $\mu = 0$ equation (5.3) has two linearly independent $2\pi/\Omega_o$ periodic solutions corresponding to the eigenvalues $\pm i\Omega_o$ of the matrix $\underline{A}^{o}$. The various parameters are introduced for the following reasons:

i) μ is a measure of the amplitude of the periodic orbit ($\underline{x}=\underline{a}^{\nu}+\mu\underline{y}$). In general the bifurcated periodic orbit will not be differentiable in ν at $\nu = 0$, but will be differentiable in μ at $\mu = 0$.

ii) δ in $\nu = \mu\delta(\mu)$ is used to determine the relationship between ν and μ.

iii) η in the time scale is introduced to account for the change in the period of oscillation in t as μ varies.

μ is the independent small parameter thoughout with η and δ to be determined. The statement of the existence theorem proved by Poore is contained in theorem 1.

Theorem 1

Referring to the differential equation (5.1) assume that:

i) $\underline{x} = \underline{a}^{\nu}$ is an equilibrium point of the equation.

ii) the Jacobean matrix $\underline{F}_{\underline{x}}(\underline{a}^{o},0)$ has exactly two non-zero, purely imaginary eigenvalues $\pm i\Omega_{o}$ ($\Omega_{o}>0$) and (n-2) eigenvalues with non-zero real parts.

iii) $\underline{F}(\underline{x},\nu) \in C^{k}\ (Dx(-\nu_{o},\nu_{o}))$, $k \geq 3$. D is a domain in R^{n} containing $\underline{a}^{o}$; and $\nu_{o} > 0$.

iv) the derivative $\alpha^{1}(0) = (d\alpha/d\nu)_{\nu=0} \neq 0$, where $\alpha(\nu)+i\Omega(\nu)$ denotes the eigenvalue of $\underline{A}$ which is a continuous extension of the eigenvalue $+i\Omega_{o}$.

For any fixed integer p, define $T = 2\pi p/\Omega_{o}$ and R_{T} to be the Banach space of all T - periodic continuous vector functions which map R^{1} to R^{n} with the norm $||\underline{y}|| = \sup\{|\underline{y}(s)| : 0 \leq s \leq T\}$.

Then, for some sufficiently small $\mu_{1} > 0$, $\exists$ real-valued functions $\delta(\mu),\eta(\mu) \in C^{k-2}\ (-\mu_{1},\mu_{1})$ and $\underline{y}(s,\mu) \in R_{T}$ such that:

$\delta(0) = \eta(0) = 0$ and

$\underline{x}(t,\mu) = \underline{a}^{\nu(\mu)}+\mu\underline{y}(s,\mu)$ is a $(1+\mu\eta(\mu))T$ - periodic solution of equation (5.1) for $\nu(\mu) = \mu\delta(\mu)$.

If $\delta = \delta(\mu)$ and $\eta = \eta(\mu)$ in equation (5.3), then $\underline{y}(s,\mu)$ is a T - periodic solution of equation (5.3) with $\underline{y}(s,\mu) \in C^{k-2}\ (-\mu_{1},\mu_{1})$, uniformly in s.

It is now possible to discuss the significance of the functions $\eta(\mu)$ and $\delta(\mu)$:

i) Since $\nu = \mu\delta(\mu) = \mu^{2}\delta^{1}(0) + O(\mu^{3})$ as $\mu \to 0$ the bifurcated periodic orbit exists for $(\underline{x},\mu)$ in a sufficiently small neighbourhood of $(\underline{a}^{o},0)$

only for $\underline{\nu > 0}$ if $\underline{\delta^{1}(0) > 0}$; or only for $\underline{\nu < 0}$ if $\underline{\delta^{1}(0) < 0}$.

Therefore the sign of $\delta^{1}(0)$ determines the direction of bifurcation (provided $\delta^{1}(0) \neq 0$).

ii) The period of oscillation of the periodic solution $\underline{x}(t,\mu)$ is:

$$T(1+\mu\eta(\mu)) = p\frac{2\pi}{\Omega_o}\ (1+\mu^2\eta^1(0)+O(\mu^3))\ \text{as}\ \mu \to 0.$$

Hence the period increases, or decreases from $T = 2\pi p/\Omega_o$ according to the sign of $\eta^1(0)$.

Poore discusses the stability of the bifurcated periodic orbit and shows that this depends upon the sign of the quantity $\alpha^1(0)\delta^1(0)$ and the remaining (n-2) eigenvalues of the matrix $\underline{A}^o$. The result is contained in theorem 2.

Theorem 2

If $\alpha^1(0)\delta^1(0) > 0$ and the remaining (n-2) eigenvalues of the matrix $\underline{A}^o$ have negative real parts the bifurcated periodic orbit will be asymptotically orbitally stable. However, if $\alpha^1(0)\delta^1(0) < 0$, or any of the remaining eigenvalues has a positive real part, the orbit will be unstable.

Having established the importance of the quantities $\delta^1(0)$, $\alpha^1(0)\delta^1(0)$ and $\eta^1(0)$ Poore derives algebraic expressions for these quantities. The result is contained in theorem 3.

Theorem 3

Let $\underline{F}(\underline{x},\nu)$ satisfy all the conditions of theorem 1 and let $\underline{u}$ and $\underline{v}$ denote left and right eigenvectors respectively for the eigenvalue $+i\Omega_o$ of the matrix $\underline{A}^o$. If $\underline{u}$ and $\underline{v}$ are normalised by the requirement $\underline{u}\,\underline{v} = 1$ then:

$$\alpha^1(0)\delta^1(0)+i\,(\Omega^1(0)\delta^1(0)+\Omega_o\eta^1(0)) \tag{5.4}$$

$$= k^2\left\{-u_\ell \frac{\partial^3 F^\ell}{\partial x_j \partial x_k \partial x_p}\ v_j v_k \bar{v}_n + 2u_\ell \frac{\partial^2 F^\ell}{\partial x_j \partial x_k}\ v_j (\underline{A}^{o-1})_{kr} \frac{\partial^2 F^r}{\partial x_p \partial x_q}\ v_p \bar{v}_q\right.$$

$$\left. + u_\ell \frac{\partial^2 F^\ell}{\partial x_j \partial x_k}\ \bar{v}_j\ ((\underline{A}^o - 2i\Omega_o \underline{I})^{-1})_{kr} \frac{\partial^2 F^r}{\partial x_p \partial x_q}\ v_p v_q\right\}.$$

where $\alpha^1(0)+i\Omega^1(0)$ denotes the derivative of the complex eigenvalue $\alpha(\nu)+i\Omega(\nu)$ at $\nu = 0$, the partial derivatives $\partial^2 F^{\ell}/\partial x_j \partial x_k$ etc. $(\ell,j,k = 1,2,....n)$ are evaluated at $\underline{x} = \underline{a}^o, \nu = 0$, $(\underline{A}^{o-1})_{kr}$ denotes the element in the k^{th} row and the r^{th} column of $\underline{A}^{o-1}$, $\bar{v}_j$ denotes the complex conjugate of v_j, k^2 is a positive constant and repeated indices within each term imply a sum from 1 to n. Equation (5.4) represents two real equations for $\delta^1(0)$ and $\eta^1(0)$. Since k^2 is a positive constant the sign of the real and imaginary parts of the right hand side of equation (5.4) are independent of the value of k^2.

Note

i) Provided $\underline{F}$ is analytic in a neighbourhood of $(\underline{x},\nu) = (\underline{a}^o,0)$ the periodic solutions of equation (5.1) occur in a sufficiently small neighbourhood of $(\underline{a}^o,0)$ for one, and only one of three cases:

$$\nu < 0,\ \nu \equiv 0 \text{ or } \nu > 0$$

This result is stated by Poore and contained in a uniqueness theorem proved by Hopf. Thus only one-sided bifurcation can occur. The situation in which the periodic solutions exist only for ν identically equal to zero is a rather special case characterised by the function $\delta(\mu)$ being identically equal to zero.

ii) If $\delta'(0) \neq 0$ the relationship between ν and μ is given by:

$$\nu = \mu^2\delta^1(0) \text{ as } \mu \to 0$$

Hence the amplitude of the periodic solution is proportional to:

$$|\nu|^{1/2} \text{ as } \nu \to 0.$$

iii) Poore has reduced the calculation of the existence, the stability and the direction of bifurcation to an algebraic problem (provided $\delta^1(0) \neq 0$). The algebraic criteria derived by Poore do not require $\underline{F}(\underline{x},\nu)$ to be in any special form, nor is it necessary to transform the

equations to new variables. In applications to concrete examples this is a considerable advantage.

The situation may be summarised by assuming that at $\nu = 0$ the remaining (n-2) eigenvalues of the matrix $\underline{F}_{\underline{x}}$ have negative real parts and the derivative $(d\alpha/d\nu)_{\nu=0} > 0$. Discounting the special case in which the bifurcated periodic orbit exists only for $\nu \equiv 0$, the two possibilities which can occur are illustrated in Figure 5.1. If $\delta^1(0) < 0$ bifurcation occurs for $\nu < 0$ (subcritical bifurcation), whereas if $\delta^1(0) > 0$ bifurcation occurs for $\nu > 0$ (supercritical bifurcation). In each case the stability of the bifurcated periodic orbit is deduced from theorem 2, which shows subcritical bifurcation to be unstable (Figure 5.1(i)), and supercritical bifurcation to be stable (Figure 5.1(ii)).

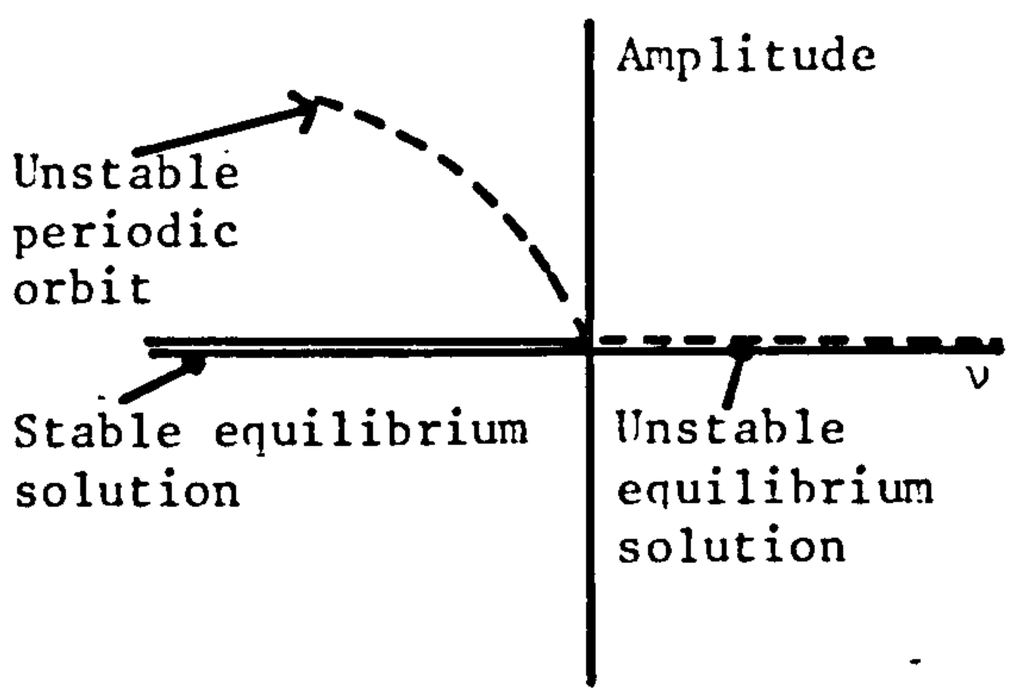

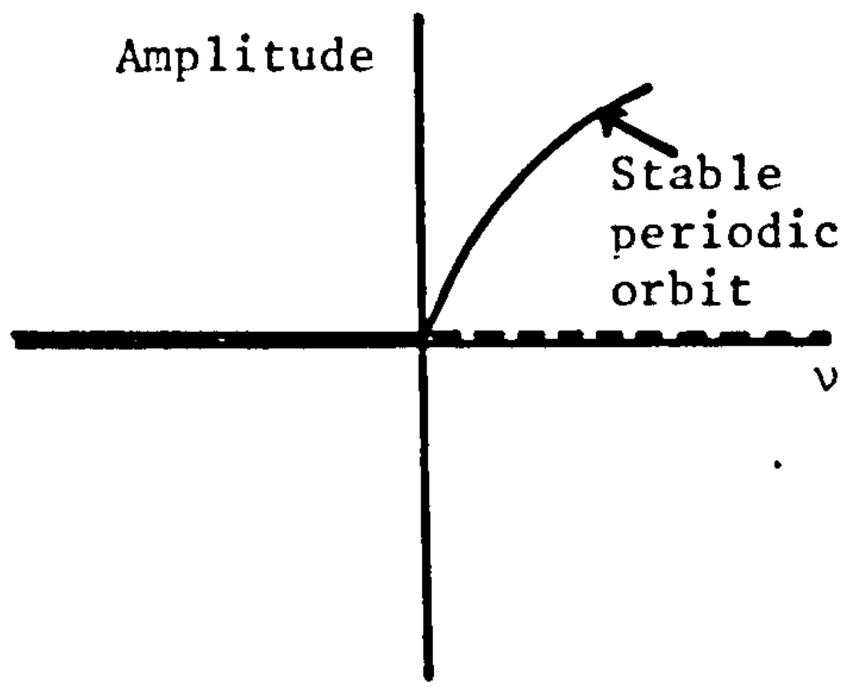

5.1(i) Subcritical ($\delta^1(0)<0, \nu<0$) ii) Supercritical ($\delta^1(0)>0, \nu>0$)

Figure 5.1. Bifurcation diagrams (for the case $\alpha^1(0)>0$)

5.2 THE APPLICATION OF BIFURCATION THEORY TO THE EQUATIONS GOVERNING OIL WHIRL.

The purpose of this section is to:

i) establish the existence of a Hopf bifurcation to equations which model oil whirl in a simple rotor–bearing system and hence to prove the existence of small amplitude periodic solutions to the equations.

ii) determine the direction of bifurcation and the stability of the bifurcated periodic orbit.

iii) determine whether or not the period increases, or decreases from its value at $\mu = 0$ $(2\pi p/\Omega_o)$.

The model used for this investigation is the same as that used throughout this thesis - a rigid, symmetric rotor mounted in two identical plain, cylindrical, journal bearings. The type of whirling considered is cylindrical whirling in which the two ends of the rotor remain in phase. It is sufficient, therefore, to consider only one bearing, which then carries a load equal to half the weight of the rotor. With the rotor mass equal to 2m and the journal centre having displacements (X^1,Y^1) (Figure 5.2), the equations of motion of the journal centre are:

$$m\frac{d^2X^1}{dt^2} = F_X(X^1,Y^1,\frac{dX^1}{dt},\frac{dY^1}{dt},S) \qquad m\frac{d^2Y^1}{dt^2} = F_Y(X^1,Y^1,\frac{dX^1}{dt},\frac{dY^1}{dt},S) \tag{5.5}$$

where $S = \frac{LR^3\omega\mu}{Fc^2}$, the Sommerfeld number.

The forces F_X and F_Y consist of the hydrodynamic forces generated in the bearing together with the applied load F (Figure 5.2). In general these forces are nonlinear in the four arguments $X^1,Y^1,\dot{X}^1,\dot{Y}^1$. The equations may be non-dimensionalised by writing:

$$\tau = \omega t \quad X = \frac{X^1}{c} \quad Y = \frac{Y^1}{c} \quad \bar{\omega} = \left(\frac{mc}{F}\right)^{1/2}\omega \quad \bar{F}_X = \frac{F_X}{SF} \quad \bar{F}_Y = \frac{F_Y}{SF} \tag{5.6}$$

which yields the non-dimensional form of the equations of motion:

$$X'' = \frac{S}{\bar{\omega}^2}\bar{F}_X(X,Y,X',Y',S) \qquad Y'' = \frac{S}{\bar{\omega}^2}\bar{F}_Y(X,Y,X',Y',S) \tag{5.7}$$

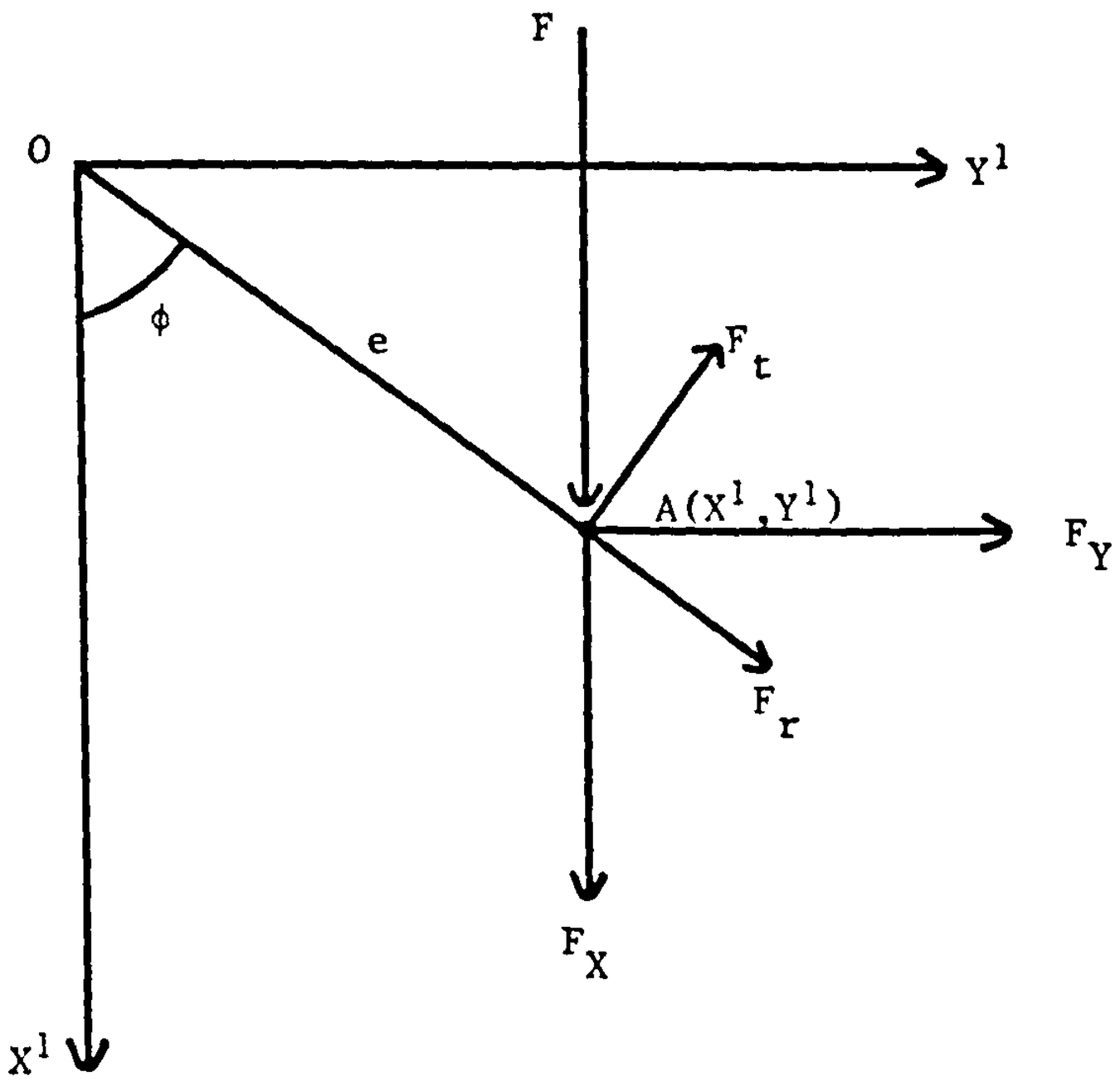

O = Bearing centre

A = Journal centre

Figure 5.2. The Cartesian co-ordinate system.

Note

i) The equations of motion have been written in terms of a fixed Cartesian co-ordinate system (Figure 5.2), rather than in polar co-ordinates (ε,ϕ), which were used extensively in Part 1. There are a number of reasons for switching to a Cartesian system, the main one being that both equations now have a similar form. This symmetry in the equations makes the theory easier to apply.

ii) The stability parameter $\nu = F/mc\omega^2$ used throughout part 1 is replaced by $\bar{\omega}$ the normalised rotor speed $(\bar{\omega} = 1/\nu^{1/2})$. The reasons for doing this will become apparent later in this Chapter.

In solving the Reynolds equation, polar co-ordinates (ε,ϕ) are used and the hydrodynamic forces are calculated as a radial and a tangential component as functions of $\varepsilon,\dot{\varepsilon},\phi,\dot{\phi}$. Therefore, it is necessary to transform these expressions to Cartesian components and to express $\varepsilon,\dot{\varepsilon},\phi,\dot{\phi}$ in terms of $X,Y,\dot{X},\dot{Y}$. Referring to Figure 5.2:

$$\bar{F}_X = \frac{1}{S} + \bar{F}_r\cos\phi - \bar{F}_t\sin\phi \qquad \bar{F}_Y = \bar{F}_r\sin\phi + \bar{F}_t\cos\phi \tag{5.8}$$

With the origin of the X-Y co-ordinate system located at the bearing centre O, the relationship between the polar and the Cartesian co-ordinates are:

$$X = \varepsilon\cos\phi \qquad Y = \varepsilon\sin\phi \tag{5.9}$$

The transformation is discussed more fully in Appendix III, where, for example, it is shown how to calculate the force derivatives $\partial F_X/\partial X$ etc. The transformation, together with equation (5.8) define the force com-onents $\bar{F}_X$ and $\bar{F}_Y$ as functions of $X,Y,\dot{X},\dot{Y}$. Since $\bar{F}_r$ and $\bar{F}_t$ are analytic functions of $\varepsilon,\dot{\varepsilon},\phi,\dot{\phi}$ (for $0 \leqslant \varepsilon < 1$) it follows that $\bar{F}_X$ and $\bar{F}_Y$ are analytic functions of $X,Y,\dot{X},\dot{Y}$ (for $0 \leqslant X^2+Y^2 < 1$).

So far in this Chapter no attention has been given to the assumptions which have been made about the oil film in the bearing. It is

possible to discuss some general properties of the equations of motion (equations (5.7)) without referring explicitly to a particular model. At this stage it is necessary only to assume that film rupture is included (by using one of the models discussed in Part 1). Towards the end of the Chapter a simple model will be chosen to extend the theory.

In order to apply the Hopf bifurcation theorem (theorem 1) it is necessary to convert equations (5.7) to a first order system of ordinary differential equations. Writing:

$$X_1 = X \qquad X_2 = \dot{X} \qquad X_3 = Y \qquad X_4 = \dot{Y} \tag{5.10}$$

equations (5.7) become:

$$\begin{aligned}
\dot{X}_1 &= X_2 \\
\dot{X}_2 &= \frac{S}{\bar{\omega}^2}\ \bar{F}_X(X_1,X_2,X_3,X_4,S) \\
\dot{X}_3 &= X_4 \\
\dot{X}_4 &= \frac{S}{\bar{\omega}^2}\ \bar{F}_Y(X_1,X_2,X_3,X_4,S)
\end{aligned} \qquad \Rightarrow \qquad \frac{d\underline{X}}{d\tau} = \underline{F}(\underline{X},\bar{\omega},S) \tag{5.11}$$

The system of equations (5.11), which describe the motion of a journal supported in fluid film journal bearings, is now in a suitable form for the application of the Hopf bifurcation theorem, with $\bar{\omega}$, the normalised rotor speed, taking on the role of the bifurcation parameter ν in the general theory.

Equilibrium Solutions. The steady state solution of equations (5.11) is governed by the value of the Sommerfeld number S.

$$\underline{F}(\underline{X}_s,\bar{\omega},S) = 0 \iff S = S(\varepsilon_s) = \frac{1}{(\bar{F}_{rs}^2+\bar{F}_{ts}^2)^{1/2}} \tag{5.12}$$

$$\text{and } \tan\phi_s = \frac{\bar{F}_{ts}}{-\bar{F}_{rs}} \tag{5.13}$$

with $X_{1s} = \varepsilon_s \cos\phi_s \qquad X_{3s} = \varepsilon_s \sin\phi_s \qquad X_{2s} = X_{4s} = 0$

Equation (5.12) describes the relationship between the Sommerfeld number and the steady state eccentricity ratio (the relationship is illustrated for various models in Part 1 - Figure 3.2). The important point here is that for each value of the Sommerfeld number there is a unique equilibrium position. Equation (5.13) describes the locus of the journal centre under steady state conditions (Figure 3.3).

Stability of the Equilibrium Position. The stability of the equilibrium position is examined by calculating the Jacobean matrix of $\underline{F}$ with respect to $\underline{X}$:

$$A(\bar{\omega}) = \left(\nabla_{\underline{X}} \underline{F}\ (\underline{X}, \bar{\omega}, S)\right)_{\underline{X}=\underline{X}_s} = \begin{pmatrix} 0 & 1 & 0 & 0 \\ -\frac{K_{XX}}{\bar{\omega}^2} & -\frac{B_{XX}}{\bar{\omega}^2} & -\frac{K_{XY}}{\bar{\omega}^2} & -\frac{B_{XY}}{\bar{\omega}^2} \\ 0 & 0 & 0 & 1 \\ -\frac{K_{YX}}{\bar{\omega}^2} & -\frac{B_{YX}}{\bar{\omega}^2} & -\frac{K_{YY}}{\bar{\omega}^2} & -\frac{B_{YY}}{\bar{\omega}^2} \end{pmatrix}_{\varepsilon=\varepsilon_s, \underline{X}=\underline{X}_s} \quad (5.14)$$

where $K_{XY} = -S\frac{\partial \bar{F}_X}{\partial Y}\left(= -S\frac{\partial \bar{F}_X}{\partial X_3}\right) \qquad B_{XY} = -S\frac{\partial \bar{F}_X}{\partial \dot{Y}}\left(= -S\frac{\partial \bar{F}_X}{\partial X_4}\right)$ etc.

The eigenvalues of the matrix $A(\bar{\omega})$ satisfy the familiar characteristic equation:

$$\bar{\lambda}^4 + \frac{1}{\bar{\omega}^2}(B_{XX}+B_{YY})\bar{\lambda}^3 + \frac{1}{\bar{\omega}^2}\left\{(K_{XX}+K_{YY}) + \frac{1}{\bar{\omega}^2}(B_{XX}B_{YY}-B_{XY}B_{YX})\right\}\bar{\lambda}^2$$

$$+ \frac{1}{\bar{\omega}^4}\{B_{XX}K_{YY}+B_{YY}K_{XX}-B_{XY}K_{YX}-B_{YX}K_{XY}\}\bar{\lambda} + \frac{1}{\bar{\omega}^4}\{K_{XX}K_{YY}-K_{XY}K_{YX}\} = 0 \quad (5.15)$$

As discussed at some length in Part 1 the roots of this equation are examined by using Routh's criterion which leads to the condition:

$$\bar{\omega} < \bar{\omega}_{th}(\varepsilon_s) \quad \text{for stability}$$

The normalised threshold speed $\bar{\omega}_{th}$ is a function only of the steady state eccentricity ratio. Below the threshold speed the equilibrium position is stable (all four eigenvalues have negative real parts). At the threshold speed two of the eigenvalues are purely imaginary and the equilibrium position is neutrally stable (Figure 5.3). Above the threshold speed two eigenvalues cross the imaginary axes into the right half plane and the equilibrium position becomes unstable.

A large number of stability borderlines ($\nu_{crit}/\varepsilon_s \equiv \bar{\omega}_{th}^{-1/2}/\varepsilon_s$) have been presented in Part 1 (Figures 3.5 and 4.6). In general, the equilibrium position is always stable above an eccentricity ratio of approximately 0.8 (ie. $\bar{\omega}_{th} = \infty$ for $\varepsilon_s > 0.8$). Therefore, there is a bifurcation point in parameter space at $(\varepsilon_s, \bar{\omega}_{th})$ for every ε_s less than approximately 0.8.

The critical, or threshold value of the whirl frequency ratio is easily calculated from the characteristic equation (see Chapter 1, equation (1.27)). Since the frequency is never zero for any $\varepsilon_s < 0.8$ (Figures 3.6 and 4.7), it follows that the eigenvalues which cross the imaginary axes at $(\varepsilon_s, \bar{\omega}_{th})$ do not pass through the origin.

The derivative $(d\bar{\alpha}/d\bar{\omega})_{\omega_{th}}$ is also required. In this calculation it is nesessary to consider the relationship between the parameters $\bar{\omega}$, S and ε_s. A change in the rotor speed ω alters the Sommerfeld number and hence the corresponding equilibrium position. It is necessary, therefore, to introduce a system parameter σ, independent of the rotor speed, which is constant for any rotor system (assuming the lubricant viscosity μ remains constant).

$$\text{Define } S = \frac{LR^3\omega\mu}{Fc^2} = \sigma\bar{\omega} \Rightarrow \sigma = \frac{LR^3\mu}{(Fmc)^{1/2}c^2}$$

The introduction of a system parameter, independent of the rotor speed, follows the approach of Lund and Saibel (1967). Their work, which

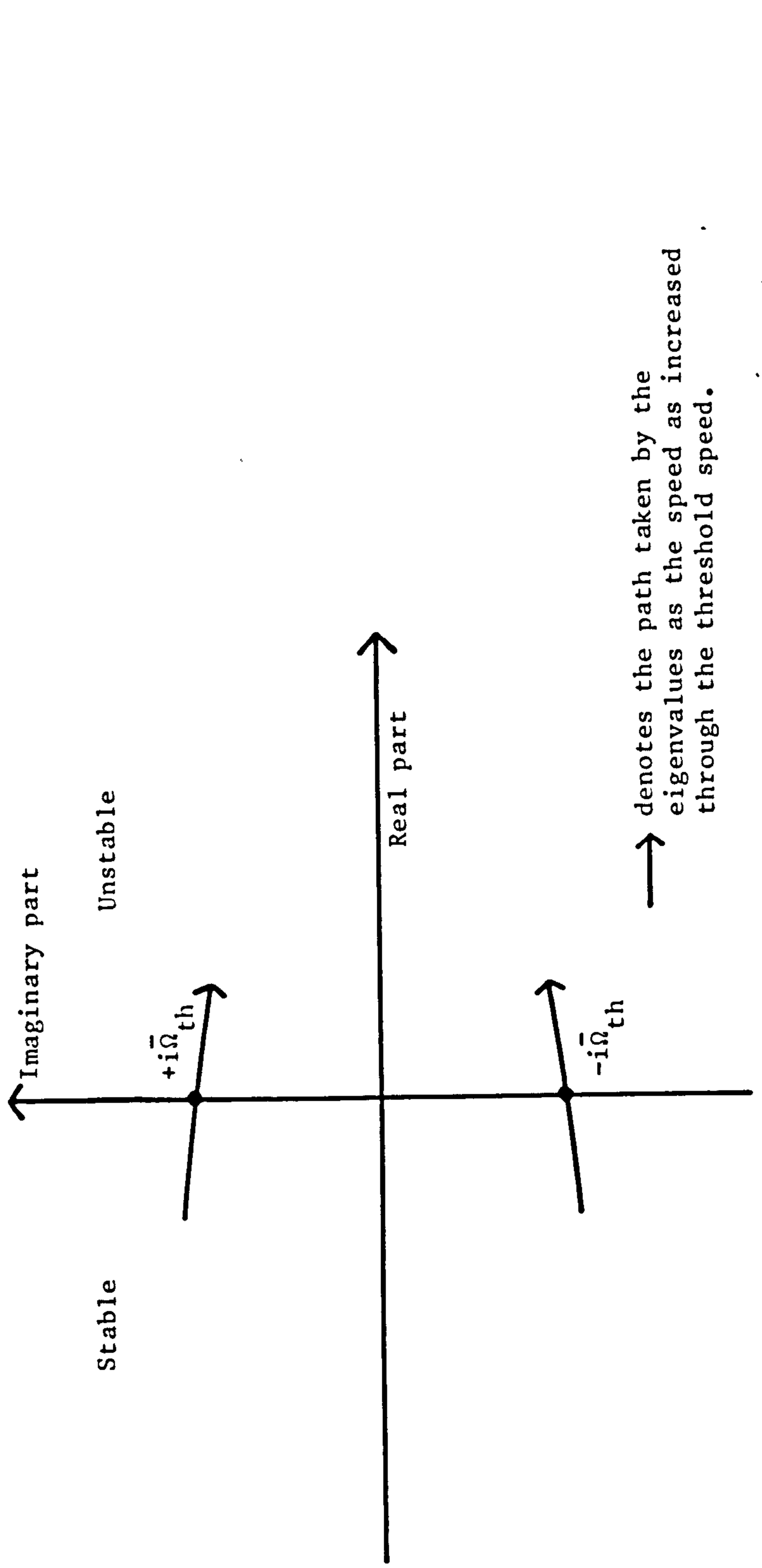

→ denotes the path taken by the eigenvalues as the speed as increased through the threshold speed.

Figure 5.3. Eigenvalues at the threshold speed.

concentrated exclusively on the short bearing, is discussed in Chapter 7. The derivatives $(d\bar{\alpha}/d\bar{\omega})_{\bar{\omega}_{th}}$ and $(d\bar{\Omega}/d\bar{\omega})_{\bar{\omega}_{th}}$ may be calculated from the characteristic equation for constant values of σ (see Appendix III). It follows that $(d\bar{\alpha}/d\bar{\omega})_{\bar{\omega}_{th}} > 0$ since the equilibrium position loses its stability as the rotor speed is increased through its threshold value. (This is the main reason for using $\bar{\omega}$ instead of ν as the bifurcation parameter). To summarise, it has been shown that the system of equations (5.11) possess the following properties:

i) $\underline{F}(\underline{X},\bar{\omega})$ is analytic in a suitable neighbourhood of $(\underline{X},\bar{\omega})$ $(\underline{X}_s,\bar{\omega}_{th})$.

ii) a locus of equilibrium points determined by the Sommerfeld number. For each value of the Sommerfeld number there is a unique equilibrium position.

iii) the matrix $\underline{A}^{\bar{\omega}}th$ has a single pair of complex conjugate, purely imaginary eigenvalues $\pm i\bar{\Omega}_{th}$ $(\bar{\Omega}_{th}>0)$ for each ε_s less than approximately 0.8. The remaining two eigenvalues have negative real parts.

iv) $(d\bar{\alpha}/d\bar{\omega})_{\bar{\omega}_{th}} > 0$ for each $\varepsilon_s < 0.8$.

Therefore all the conditions of theorem 1 are satisfied. The existence of small amplitude periodic solutions of the system at speeds close to the threshold speed has been proved.

Since $(d\bar{\alpha}/d\bar{\omega})_{\bar{\omega}_{th}} > 0$ and the remaining two eigenvalues of $\underline{A}^{\bar{\omega}}th$ have negative real parts, theorem 2 implies that stable whirl orbits may exist only at speeds above the threshold speed (supercritical bifurcation), whereas whirl orbits below the threshold speed will be unstable (subcritical bifurcation).

It remains to determine:

i) the direction of bifurcation (ie. for $\bar{\omega} < \bar{\omega}_{th}$, or $\bar{\omega} > \bar{\omega}_{th}$). The stability of the bifurcated orbit will then follow from the comment made above.

ii) whether the period increases or decreases from its value at $\mu = 0$.

This information may be deduced by calculating the sign of the quantities $\delta^1(0), \eta^1(0)$ as discussed in section 5.1. This was achieved by using the algebraic formula derived by Poore (equation 5.4), which required the calculation of the following:

i) the left and right eigenvectors $\underline{u}$ and $\underline{v}$ for the eigenvalue $+i\bar{\Omega}_{th}$ of $A^{\bar{\omega}}_{th}$.

ii) the second and third order partial derivatives of $\underline{F}$ (ie. $\frac{\partial^2 F^{\ell}}{\partial x_j \partial x_k}$, $\frac{\partial^3 F^{\ell}}{\partial x_i \partial x_j \partial x_k}$, $i,j,k,\ell = 1,2,3,4$).

iii) the inverse of the matrices $\underline{A}^{\bar{\omega}}th$ and $(\underline{A}^{\bar{\omega}}th - 2i\bar{\Omega}_{th}\underline{I})$.

In order to carry out the calculation it was necessary to take a specific model. In theory any of the models discussed in Part 1 could have been used. However, the calculation is a lengthy and unpleasant one even for the simplest of models, the two major difficulties being the length of the calculation and the determination of the second and third order partial derivatives of $\underline{F}$. For this reason the calculation was performed only for a simple model - a long bearing operating with an oscillating half film (as discussed in Chapter 3, section 3.1).

The hydrodynamic forces for this model are:

$$-\bar{F}_r = \frac{12\varepsilon^2(1-2\dot{\phi})}{(2+\varepsilon^2)(1-\varepsilon^2)} + \frac{6(\pi^2(2+\varepsilon^2)-16)\dot{\varepsilon}}{\pi(2+\varepsilon^2)(1-\varepsilon^2)^{3/2}} \qquad (5.16)$$

$$\bar{F}_t = \frac{6\pi\varepsilon(1-2\dot{\phi})}{(2+\varepsilon^2)(1-\varepsilon^2)^{1/2}} + \frac{24\varepsilon\dot{\varepsilon}}{(2+\varepsilon^2)(1-\varepsilon^2)}$$

The relationship between the Sommerfeld number and ε_s is given by:

$$S(\varepsilon_s) = \sigma\bar{\omega} = \frac{(2+\varepsilon_s^2)(1-\varepsilon_s^2)}{6\varepsilon_s\{\pi^2(1-\varepsilon_s^2)+4\varepsilon_s^2\}^{1/2}} \qquad (5.17)$$

and the locus of the journal centre under steady state conditions is:

$$\tan\phi_s = \frac{\pi(1-\varepsilon_s^2)^{1/2}}{2\varepsilon_s} \qquad (5.18)$$

The stability borderline $(\bar{\omega}_{th}/\varepsilon_s)$ for this model is shown in Figure 5.4, together with a series of operating curves for different values of the system parameter σ. Each curve illustrates the relationship between the rotor speed and the corresponding unique equilibrium position. The derivatives $(d\alpha/d\omega)_{\bar{\omega}_{th}}$ and $(d\Omega/d\omega)_{\bar{\omega}_{th}}$ were calculated for constant values of σ and are given in Table 5.1 (details of the calculation may be found in Appendix III).

Having specified the model, it was possible to calculate all the quantities required to use Poore's formula (equation 5.4) and hence determine the sign of the quantities $\delta^1(0)$ and $\eta^1(0)$. Even for this simple model the calculation was extremely tedious and took several weeks to perform. An outline of the calculation is given in Appendix III.

5.3 RESULTS.

The results of the calculation are summarised in Table 5.1. They are extremely interesting since they indicate that there are three distinct regions of parameter space to be considered (Figure 5.4).

Region I $(0 < \varepsilon_s \leq 0.14)$. In this region $\delta^1(0) < 0$ and therefore subcritical bifurcation takes place (ie. for $\bar{\omega} < \bar{\omega}_{th}$). The periodic orbit is unstable (theorem 2). From the uniqueness theorem proved by Hopf (1942), no small amplitude orbits may exist for $\bar{\omega} > \bar{\omega}_{th}$ (but there may be large amplitude ones). Also in this region $\eta^1(0) > 0$, hence the period of the unstable orbit increases from its threshold value $(2\pi p/\bar{\Omega}_{th})$.

Region II $(0.15 \leq \varepsilon_s \leq 0.74)$. The largest of the three regions; $\delta^1(0) > 0$ and therefore supercritical bifurcation occurs (ie. for $\bar{\omega} > \bar{\omega}_{th}$). The periodic orbit is stable with the period increasing from its threshold value $(\eta^1(0) > 0)$.

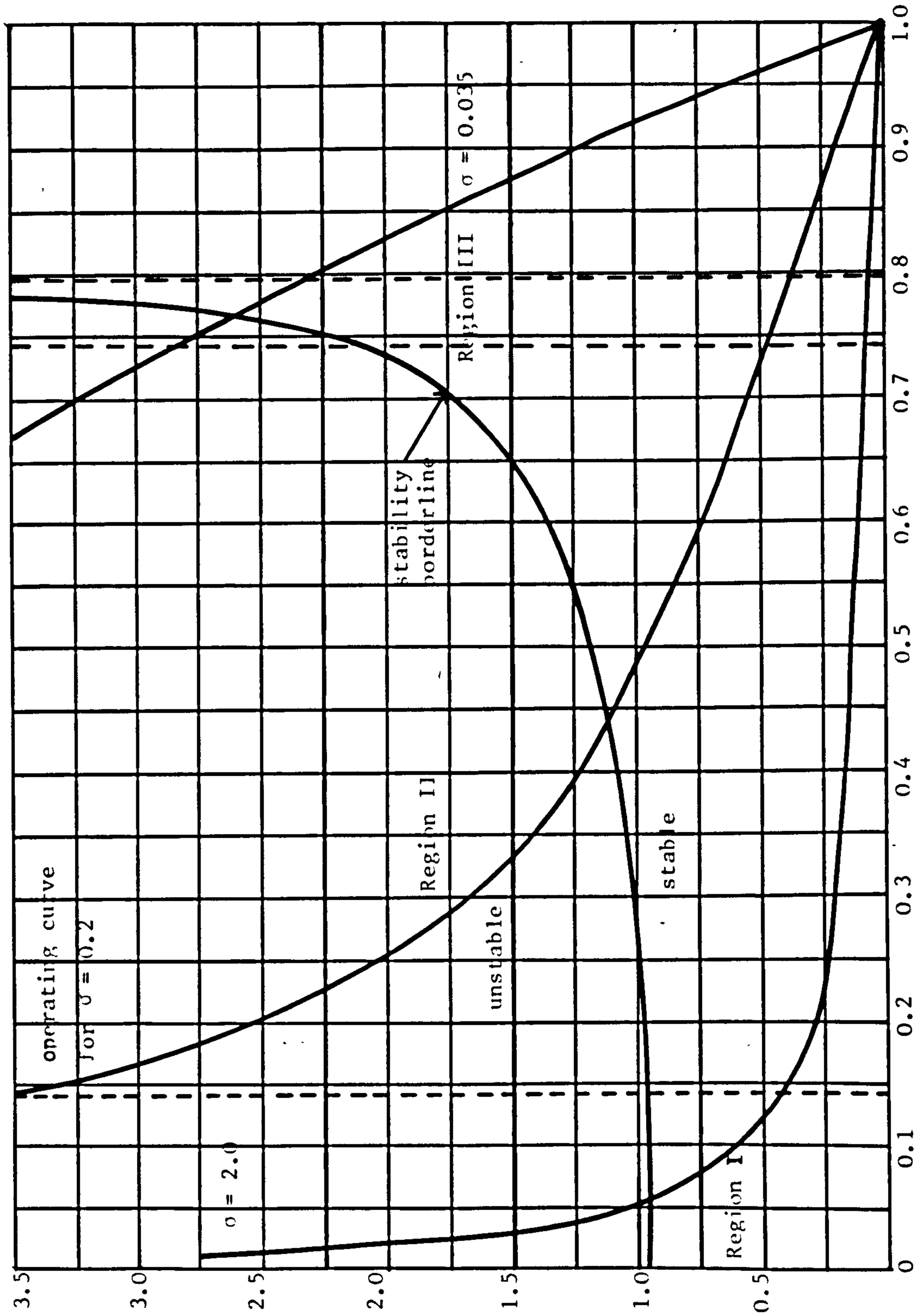

Figure 5.4. Stabil

ε_s	S	$\bar{\omega}_{th}$	σ_{th}	$\bar{\alpha}^1(\bar{\omega}_{th})$	$\bar{\Omega}_{th}$	$\bar{\Omega}^1(\bar{\omega}_{th})$	$\delta^1(0)$	$\eta^1(0)$	$\alpha^1(0)\delta^1(0)$
0.01	10.61	0.94	11.26	0.04	1.15	-0.0	<0	>0	<0
0.05	2.12	0.95	2.24	0.19	1.15	-0.03	<0	>0	<0
0.10	1.06	0.95	1.11	0.35	1.14	-0.11	<0	>0	<0
0.14	0.76	0.96	0.79	0.45	1.13	-0.19	<0	>0	<0
0.15	0.70	0.96	0.73	0.47	1.13	-0.22	>0	>0	>0
0.20	0.53	0.98	0.54	0.54	1.11	-0.33	>0	>0	>0
0.30	0.35	1.03	0.34	0.55	1.07	-0.53	>0	>0	>0
0.40	0.25	1.10	0.23	0.46	1.02	-0.62	>0	>0	>0
0.50	0.19	1.21	0.16	0.35	0.96	-0.63	>0	>0	>0
0.60	0.15	1.37	0.11	0.23	0.88	-0.55	>0	>0	>0
0.70	0.11	1.73	0.07	0.10	0.72	-0.38	>0	>0	>0
0.74	0.10	2.13	0.05	0.05	0.60	-0.26	>0	>0	>0
0.75	0.10	2.31	0.04	0.04	0.55	-0.22	<0	<0	<0
0.76	0.09	2.57	0.04	0.03	0.50	-0.18	<0	<0	<0
0.77	0.09	2.98	0.03	0.02	0.43	-0.14	<0	<0	<0
0.78	0.09	3.77	0.02	0.01	0.35	-0.09	<0	<0	<0
0.79	0.08	6.43	0.01	0.00	0.20	-0.03	<0	<0	<0

$$\bar{\alpha}^1(\bar{\omega}_{th}) = (d\bar{\alpha}/d\bar{\omega})_{\bar{\omega}_{th}} \qquad \bar{\Omega}^1(\bar{\omega}_{th}) = (d\bar{\Omega}/d\bar{\omega})_{\bar{\omega}_{th}} \qquad \sigma_{th} = S/\bar{\omega}_{th}$$

Table 5.1. Results obtained from bifurcation theory.

Region III ($0.75 \leqslant \varepsilon_s \leqslant 0.795$). Similar to region I. Subcritical bifurcation takes place and the resulting periodic orbits are unstable ($\delta^1(0) < 0$). The period decreases from its threshold value since $\eta^1(0) < 0$.

Thus, for the particular model investigated, the direction of bifurcation depends upon the region of parameter space $(\varepsilon_s, \omega_{th})$ in which the bearing is operating.

5.4 NUMERICAL INVESTIGATION.

A numerical investigation was also carried out to verify the results of the theory and to investigate how the whirl orbits evolve as the rotor speed is increased (or decreased) from the threshold speed. The equations of motion (equations 5.11) were integrated using a standard Nottingham Algorithms Group library routine which integrates a system of first order ordinary differential equations over a suitable step length using a variable order Adams method (Hall and Watt (1976)). It was necessary to specify:

i) the system parameter σ and rotor speed $\bar{\omega}$.

ii) initial conditions for $X, \dot{X}, Y, \dot{Y}$.

The results of the investigation are summarised here by selecting three different values of the system parameter: $\sigma = 0.035$, 0.2 and 2.0. The operating curves for these three rotor systems are shown in Figure 5.4. These particular values were chosen because the curves cross the stability borderline in separate regions of parameter space ($\sigma = 0.035$ in region III, $\sigma = 0.2$ in region II, $\sigma = 2.0$ in region I). For each value of σ the equations were integrated for a range of values of the rotor speed and suitable initial conditions. Particular emphasis was placed on how the initialconditions affected the final motion of the journal (if at all).

The results are shown in graphic form obtained by using a Calcomp

plotter (Figure 5.5, 5.6, 5.7). Each plot represents the motion of the journal centre. The outer circle is known as the clearance circle and is of a radius equal to the radial clearance of the bearing - the location of the journal centre must be contained within this circle if no distortion of the bearing components occurs.

Figure 5.5 illustrates the behaviour of a rotor system with a system parameter equal to 0.035. Well below its normalised threshold speed of 2.655, the journal is stable and spirals into its equilibrium position (Figures 5.5(i), 5.5(ii)). However, at a rotor speed of 2.5 ($< \bar{\omega}_{th}$) there are two different solutions, depending on the initial conditions (Figures 5.5(iii), 5.5(iv)). Close to its equilibrium position the journal is stable (Figure 5.5(iii)), but if the journal is started a long way from its equilibrium position, the final motion is a large amplitude whirl orbit (Figure 5.5(iv)). This is evidence for the existence of a stable limit cycle surrounding the unstable periodic orbit established by bifurcation theory. The same features are observed at a rotor speed of 2.6, which is still below the threshold speed - the limit cycle is slightly larger (Figures 5.5(v), 5.5 (vi)). At speeds above the threshold speed the journal is completely unstable for all initial conditions (Figures 5.5(vii), 5.5(viii)). The term "completely unstable" is used here to imply that there are no closed orbit solutions for $\varepsilon < 1$ - the journal approaches the bearing surface ($\varepsilon \to 1$).

The behaviour of a rotor with a system parameter equal to 0.2 is shown in Figure 5.6. At rotor speeds below the threshold value of 1.138 only the equilibrium solution is observed (Figures 5.6(i), 5.6 (ii)). However, immediately above the threshold speed, a stable small amplitude whirl orbit appears, which is independent of the initial conditions (Figures 5.6(iii), 5.6(iv)). This is the stable periodic orbit established by bifurcation theory. The amplitude of the whirl

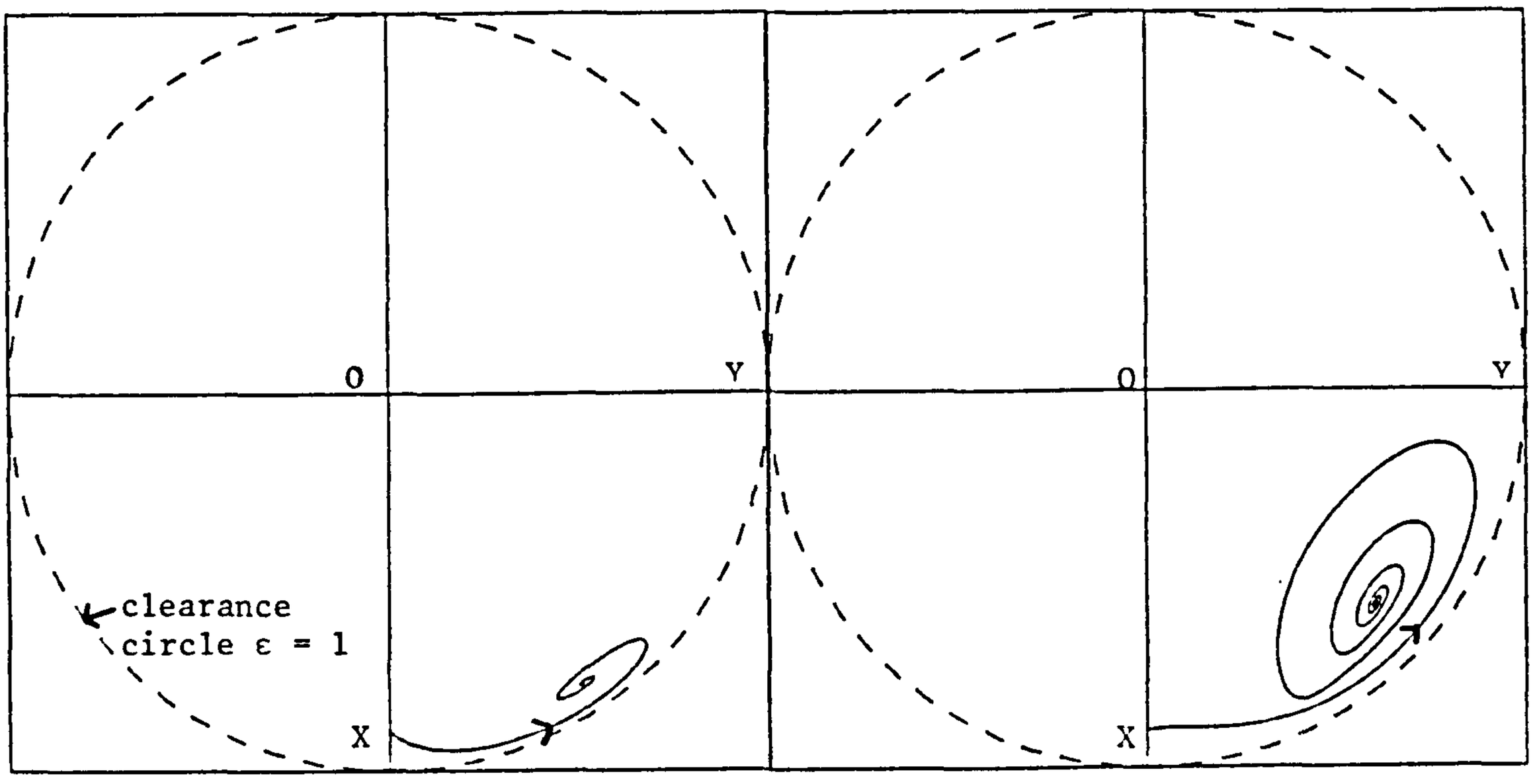

5.5(i) $\bar{\omega}$ = 1.0 X_i = 0.9 Y_i = 0.0

5.5(ii) $\bar{\omega}$ = 2.0 X_i = 0.9 Y_i = 0.0

(arrow indicates direction of whirling)

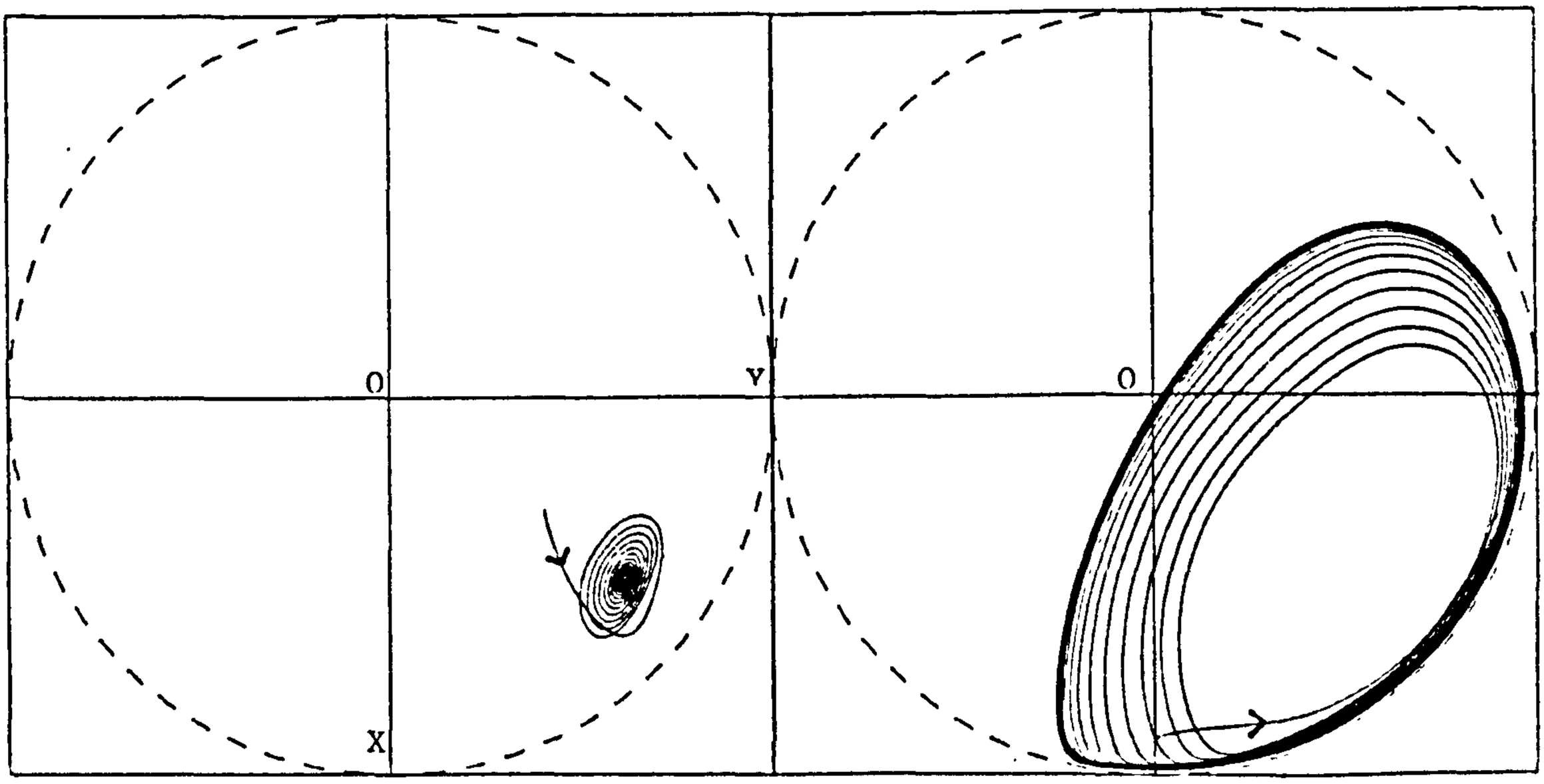

5.5(iii) $\bar{\omega}$ = 2.5 X_i = 0.3 Y_i = 0.4

5.5(iv) $\bar{\omega}$ = 2.5 X_i = 0.9 Y_i = 0.0

Figure 5.5. Whirl orbits of a rotor with a system parameter = 0.035.

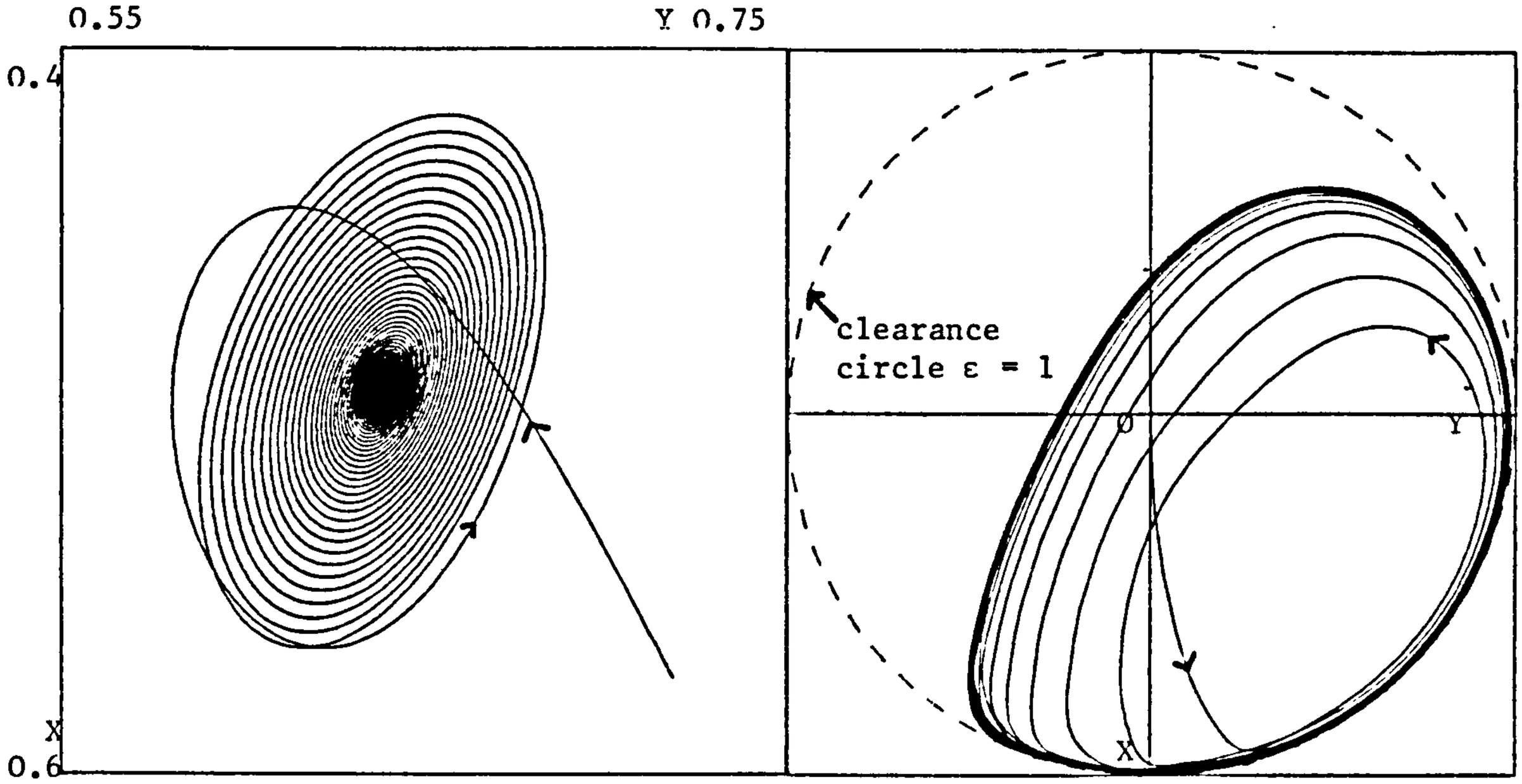

5.5(v) $\bar{\omega}$ = 2.6 X_i = 0.5665 Y_i = 0.7105 5.5(vi) $\bar{\omega}$ = 2.6 X_i = 0.0 Y_i = 0.0

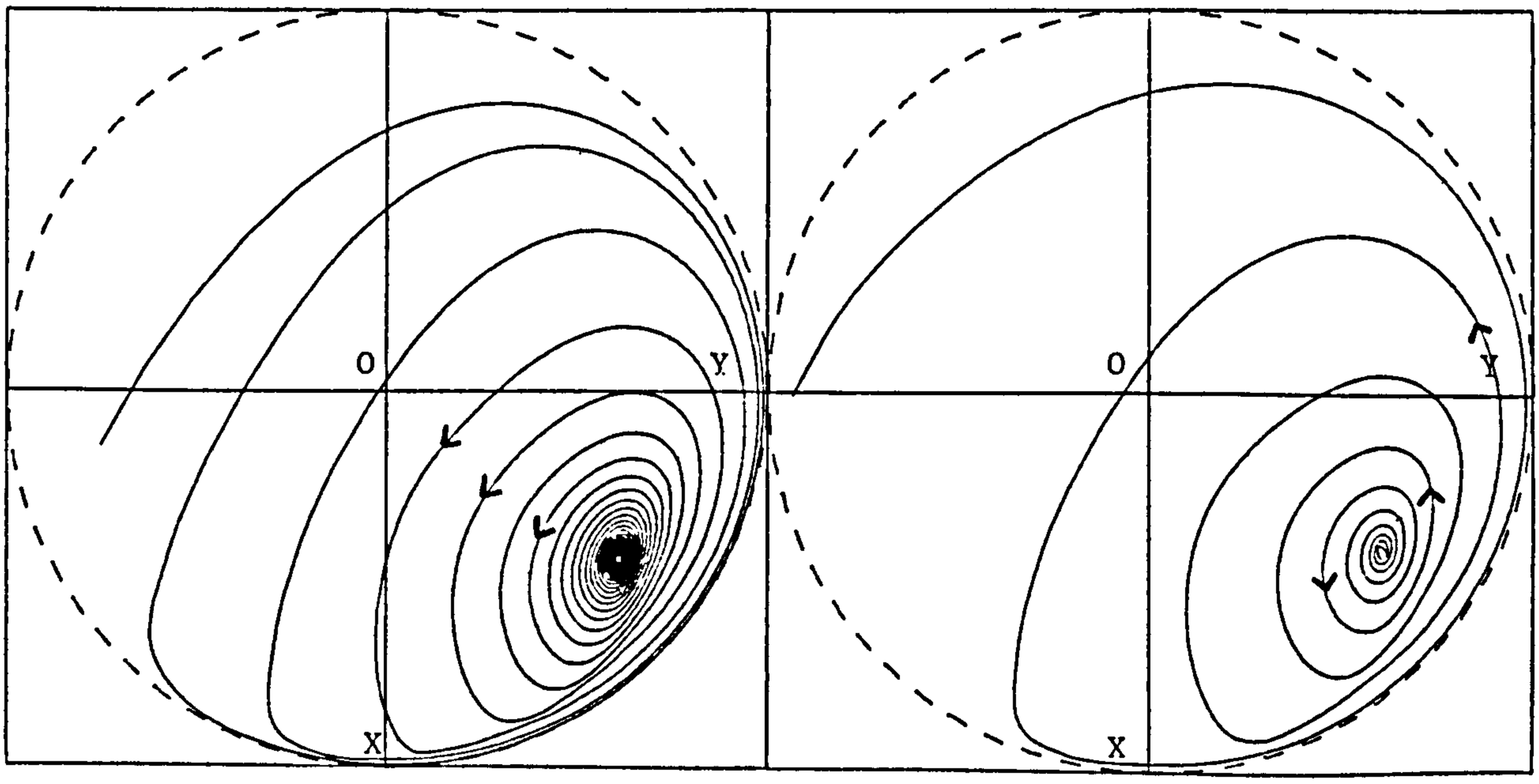

5.5(vii) $\bar{\omega}$ = 2.75 X_i = 0.46 Y_i = 0.62 5.5(viii) $\bar{\omega}$ = 3.0 X_i = 0.42 Y_i = 0.62

Figure 5.5. continued. Whirl orbits of a rotor with a system parameter = 0.035.

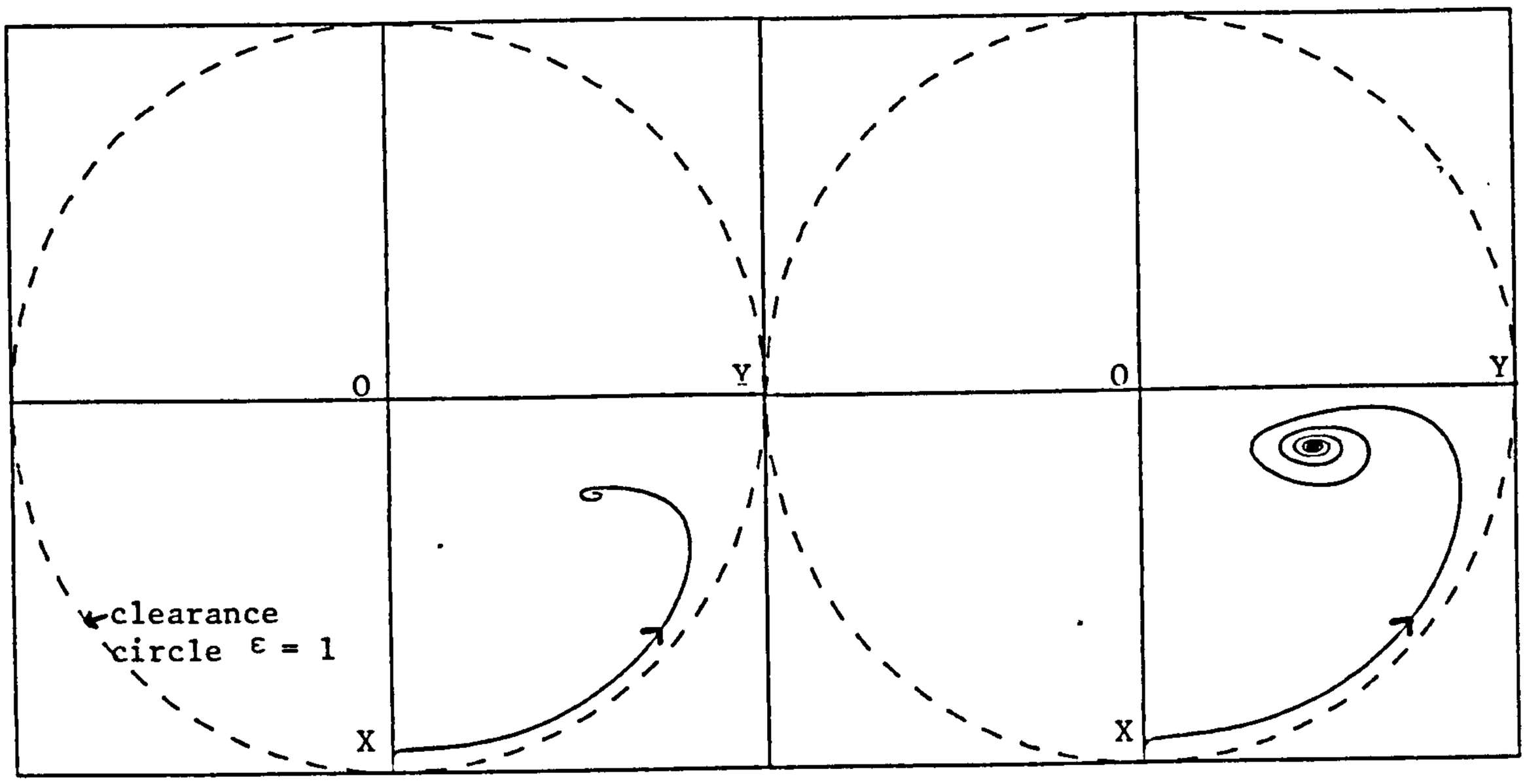

5.6(i) $\bar{\omega}$ = 0.75 X_i = 0.95 Y_i = 0.0

5.6(ii) $\bar{\omega}$ = 1.0 X_i = 0.95 Y_i = 0.0

(arrow indicates direction of whirling)

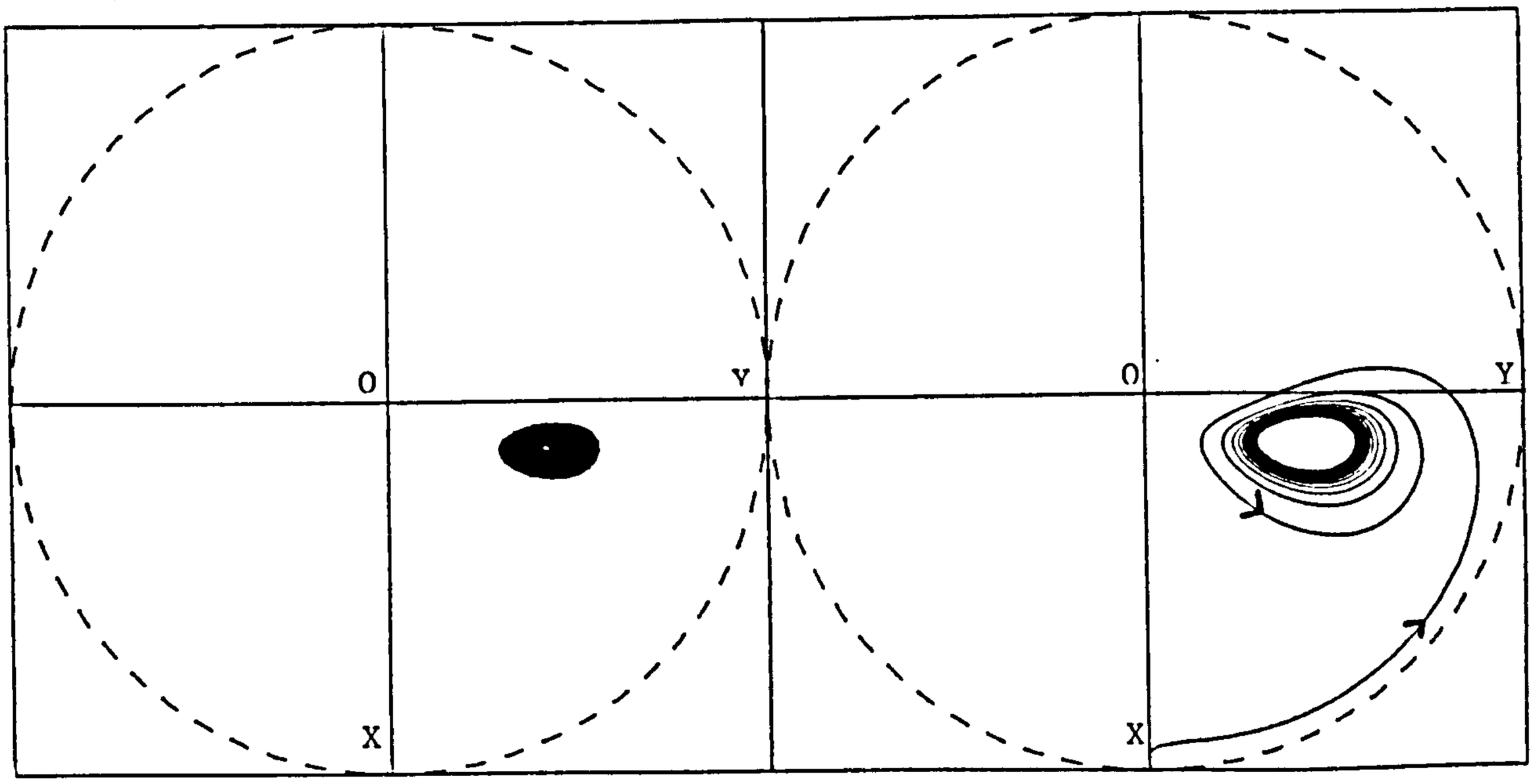

5.6(iii) $\bar{\omega}$ = 1.16 X_i = 0.13 Y_i = 0.43

5.6(iv) $\bar{\omega}$ = 1.16 X_i = 0.95 Y_i = 0.0

Figure 5.6. Whirl orbits of a rotor with a system parameter = 0.2.

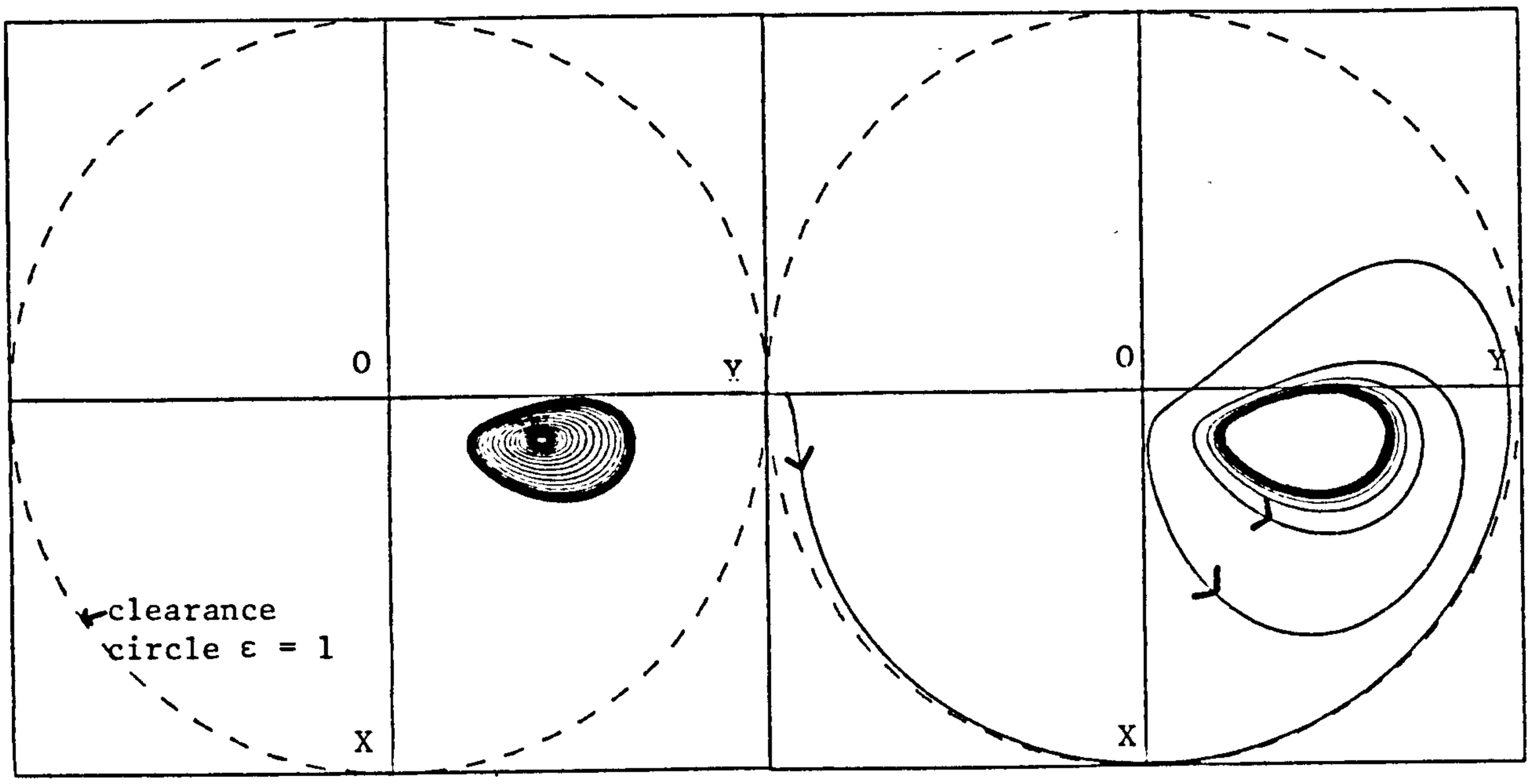

5.6(v) $\bar{\omega}$ = 1.2 X_i = 0.12 Y_i = 0.42

5.6(vi) $\bar{\omega}$ = 1.2 X_i = 0.0 Y_i = 0.95

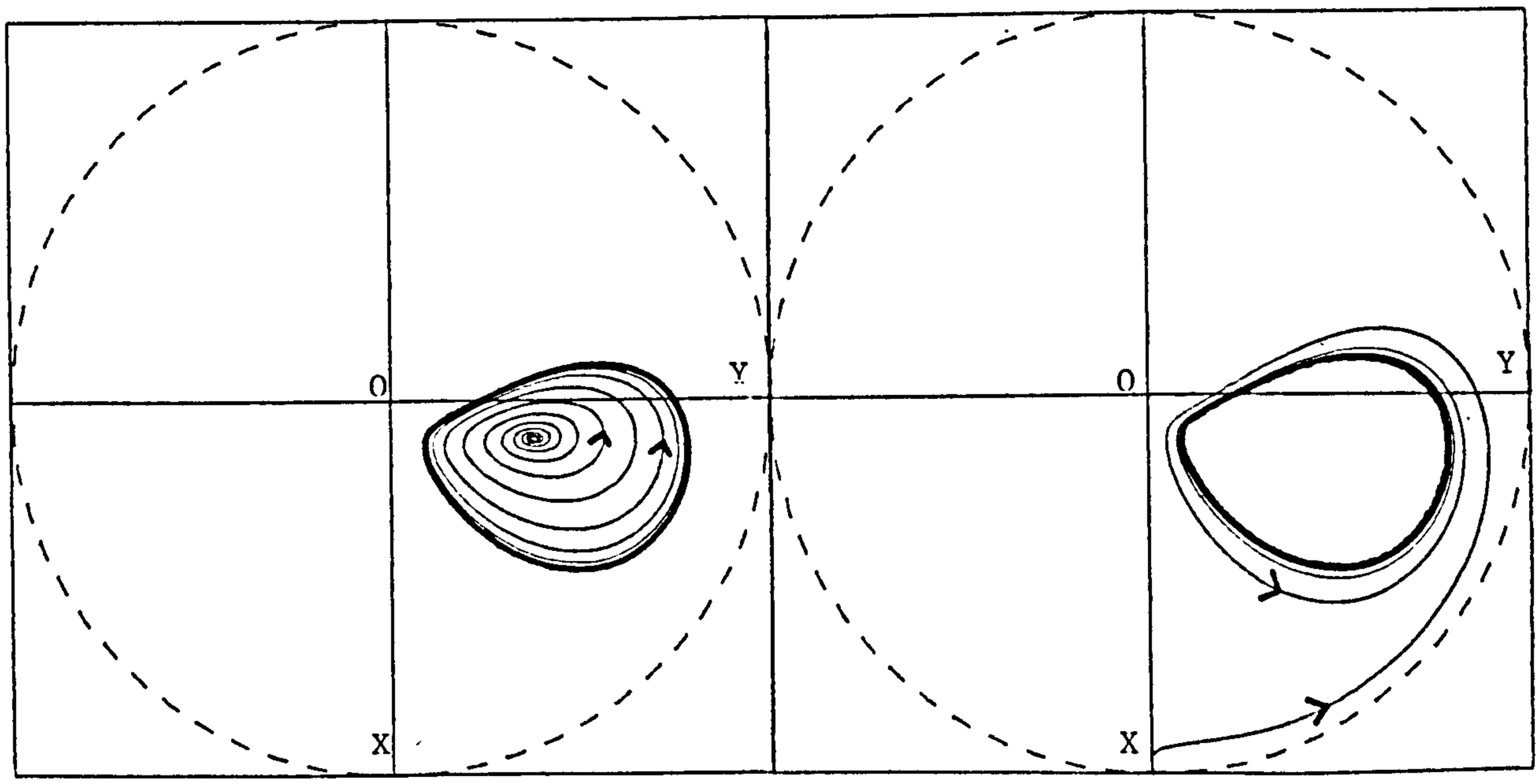

5.6(vii) $\bar{\omega}$ = 1.3 X_i = 0.11 Y_i = 0.39

5.6(viii) $\bar{\omega}$ = 1.3 X_i = 0.95 Y_i = 0.0

Figure 5.6. continued. Whirl orbits of a rotor with a system parameter = 0.2

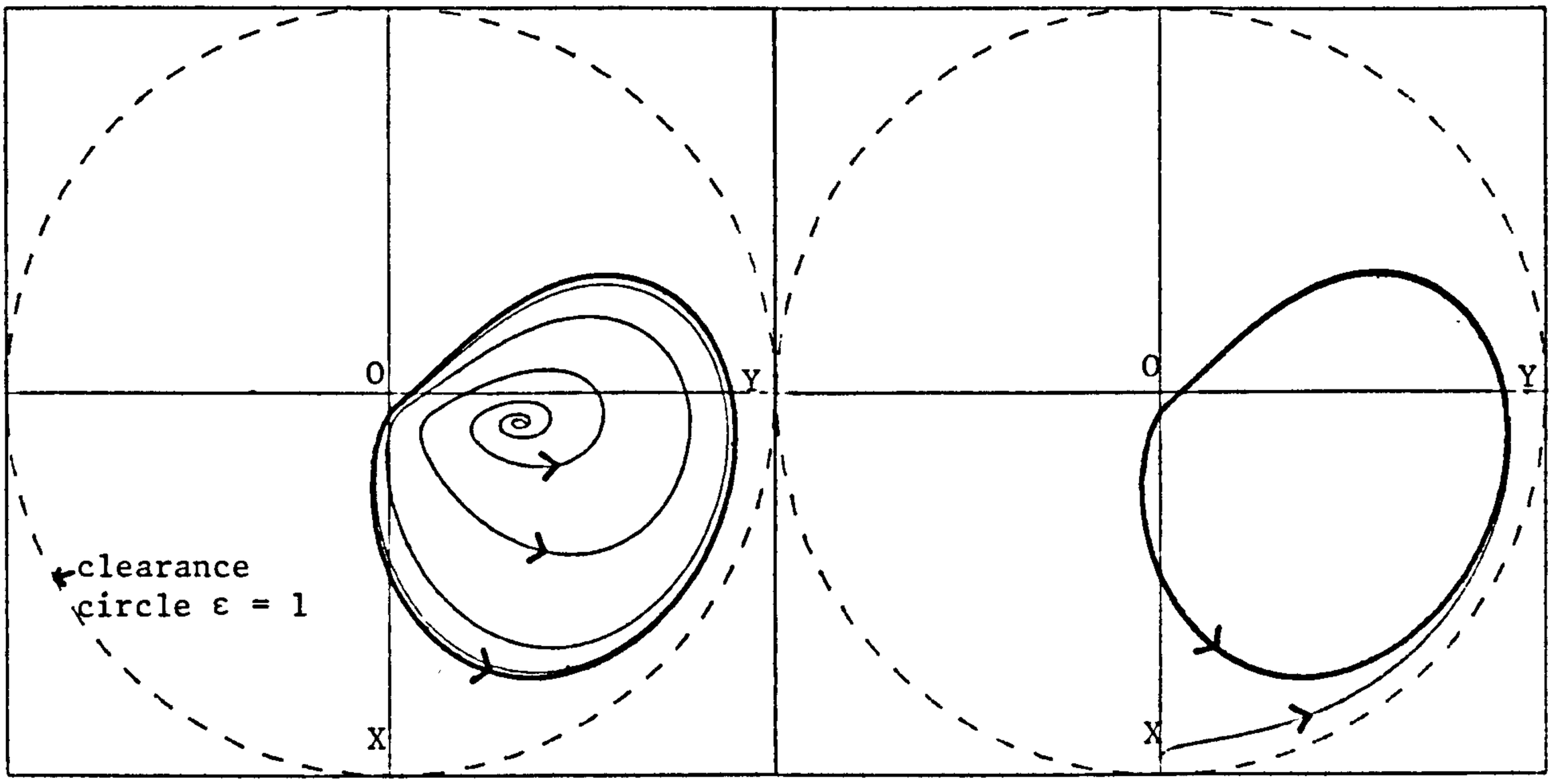

5.6(ix) $\bar{\omega}$ = 1.5 X_i = 0.08 Y_i = 0.35 5.6(x) $\bar{\omega}$ = 1.5 X_i = 0.95 Y_i = 0.0

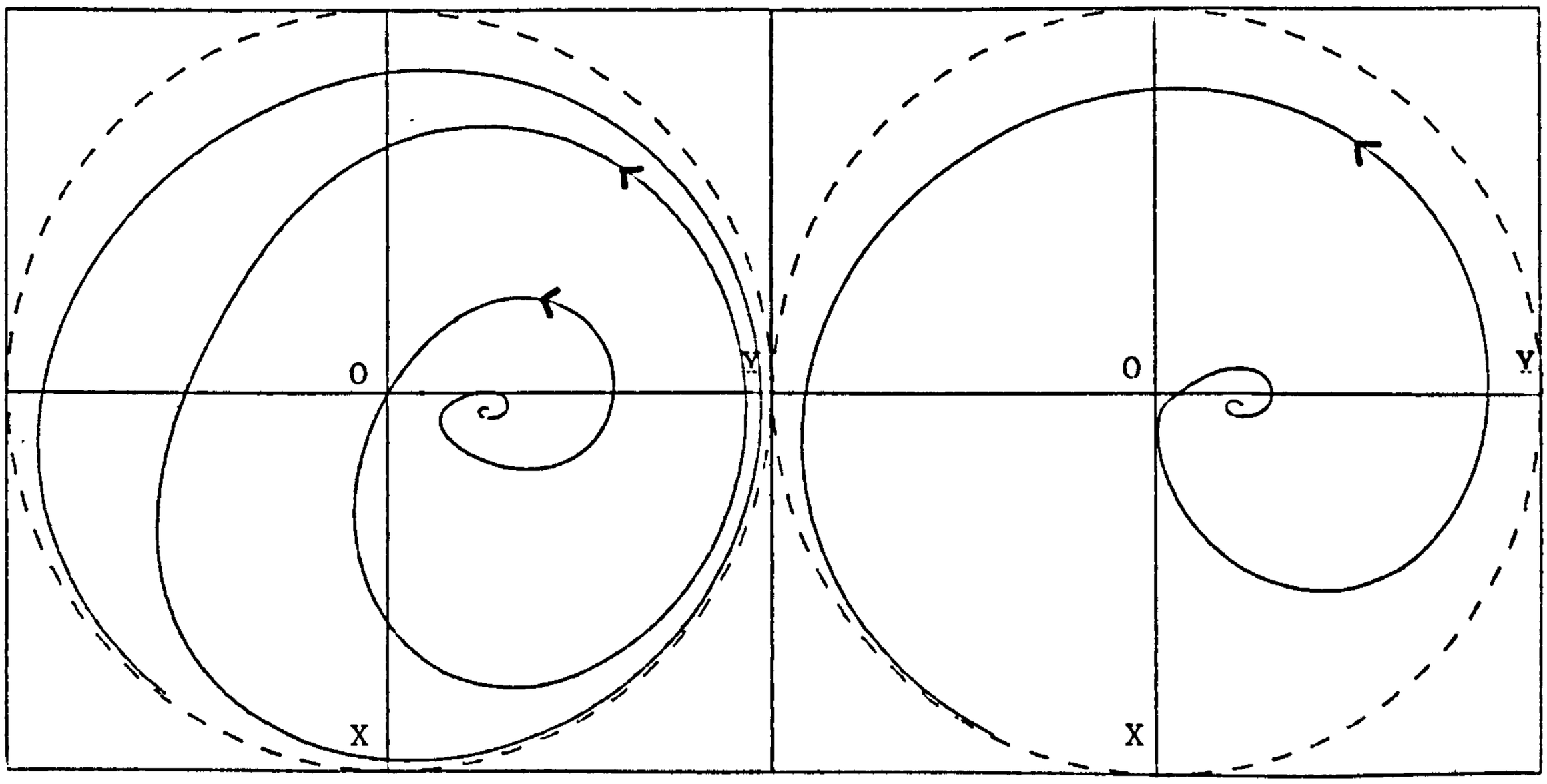

5.6(xi) $\bar{\omega}$ = 2.0 X_i = 0.05 Y_i = 0.26 5.6(xii) $\bar{\omega}$ = 2.5 X_i = 0.03 Y_i = 0.22

Figure 5.6. continued. Whirl orbits of a rotor with a system parameter = 0.2.

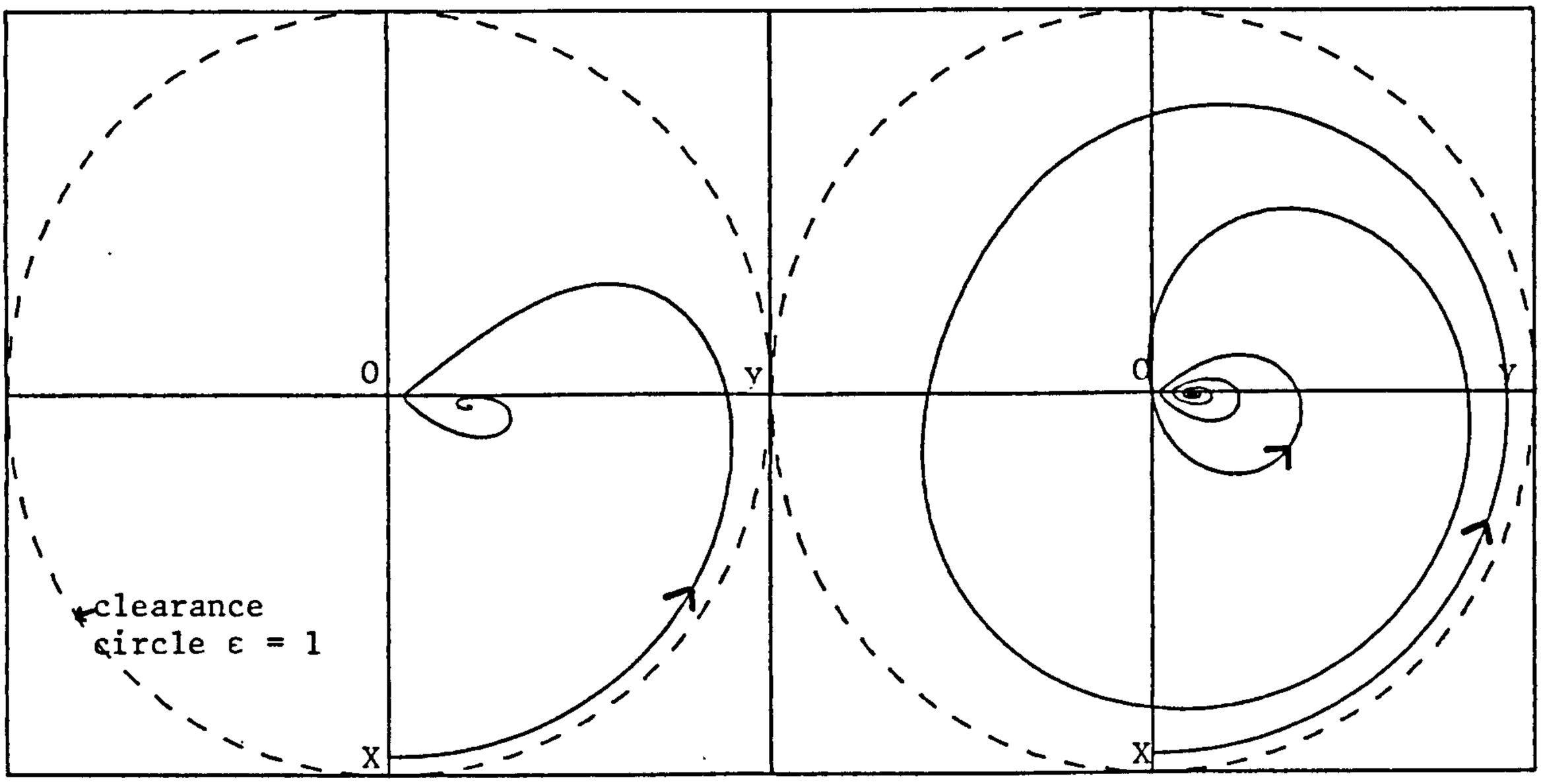

5.7(i) $\bar{\omega} = 0.25$ $X_i = 0.95$ $Y_i = 0.0$ 5.7(ii) $\bar{\omega} = 0.5$ $X_i = 0.95$ $Y_i = 0.0$

(arrow indicates direction of whirling)

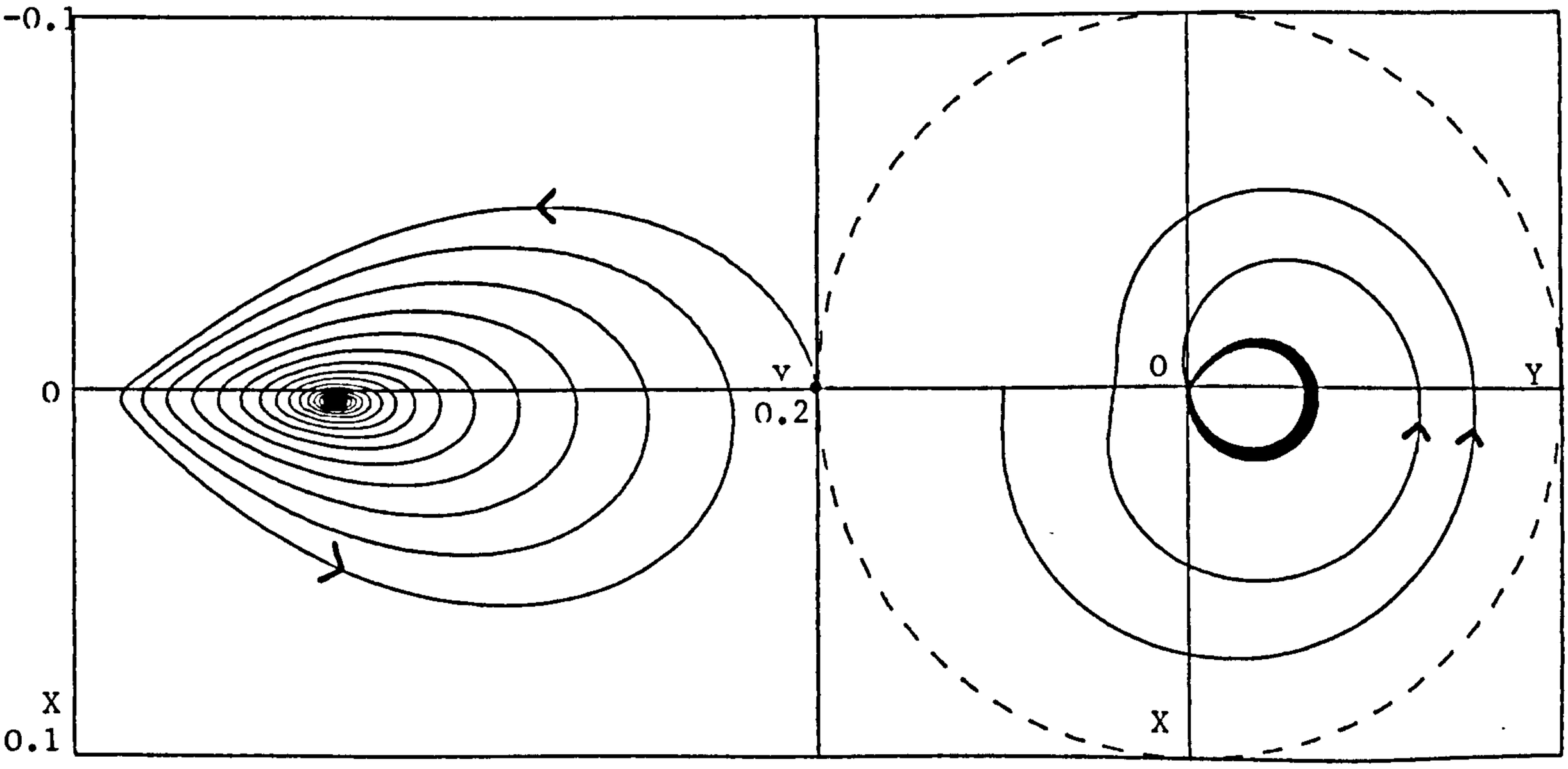

5.7(iii) $\bar{\omega} = 0.75$ $X_i = 0.0$ $Y_i = 0.2$ 5.7 (iv) $\bar{\omega} = 0.75$ $X_i = 0.0$ $Y_i = -0.50$

Figure 5.7. Whirl orbits of a rotor with a system parameter = 2.0.

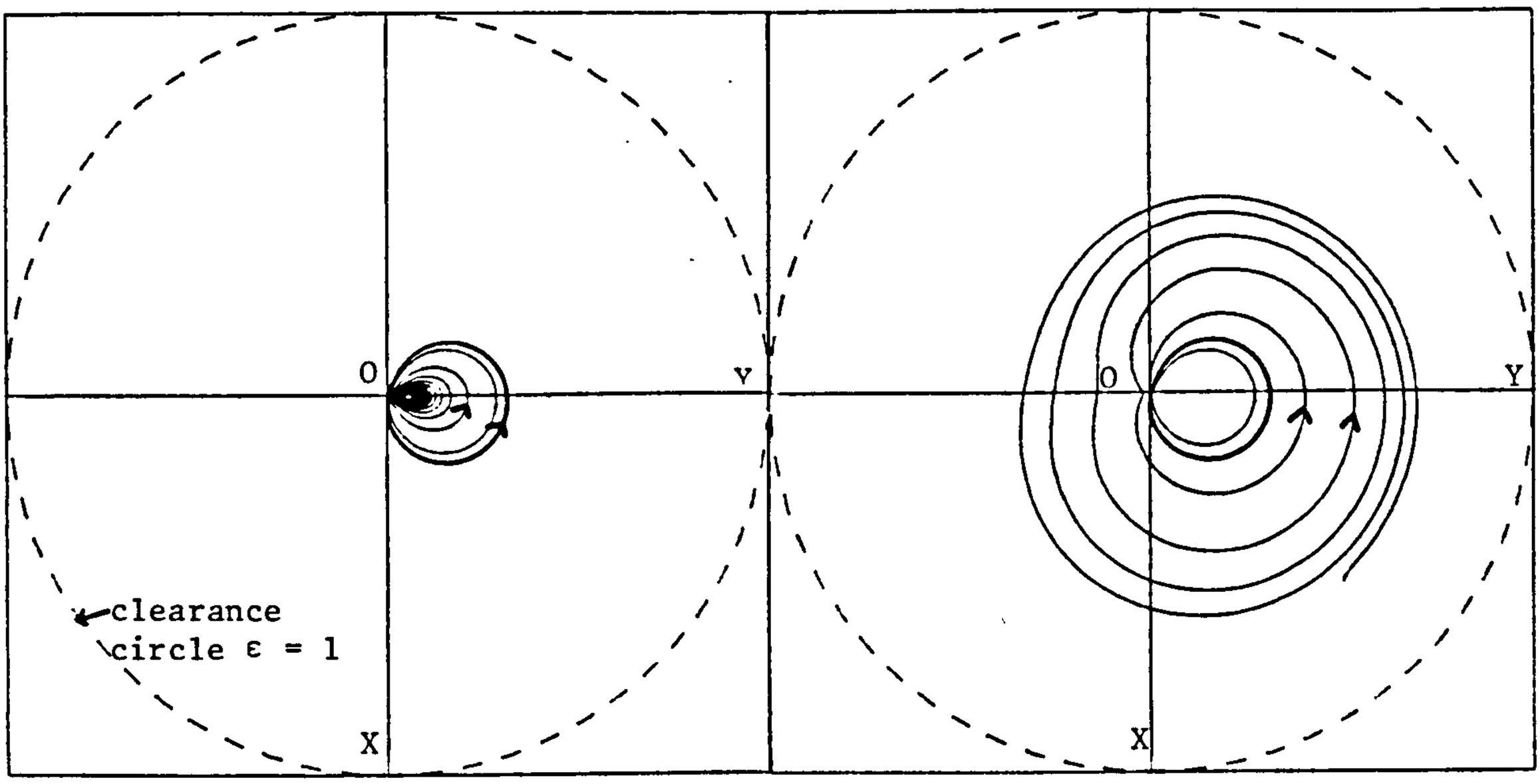

5.7 (v) $\bar{\omega}$ = 1.0 X_i = 0.01 Y_i = 0.06 5.7(vi) $\bar{\omega}$ = 1.0 X_i = 0.5 Y_i = 0.5

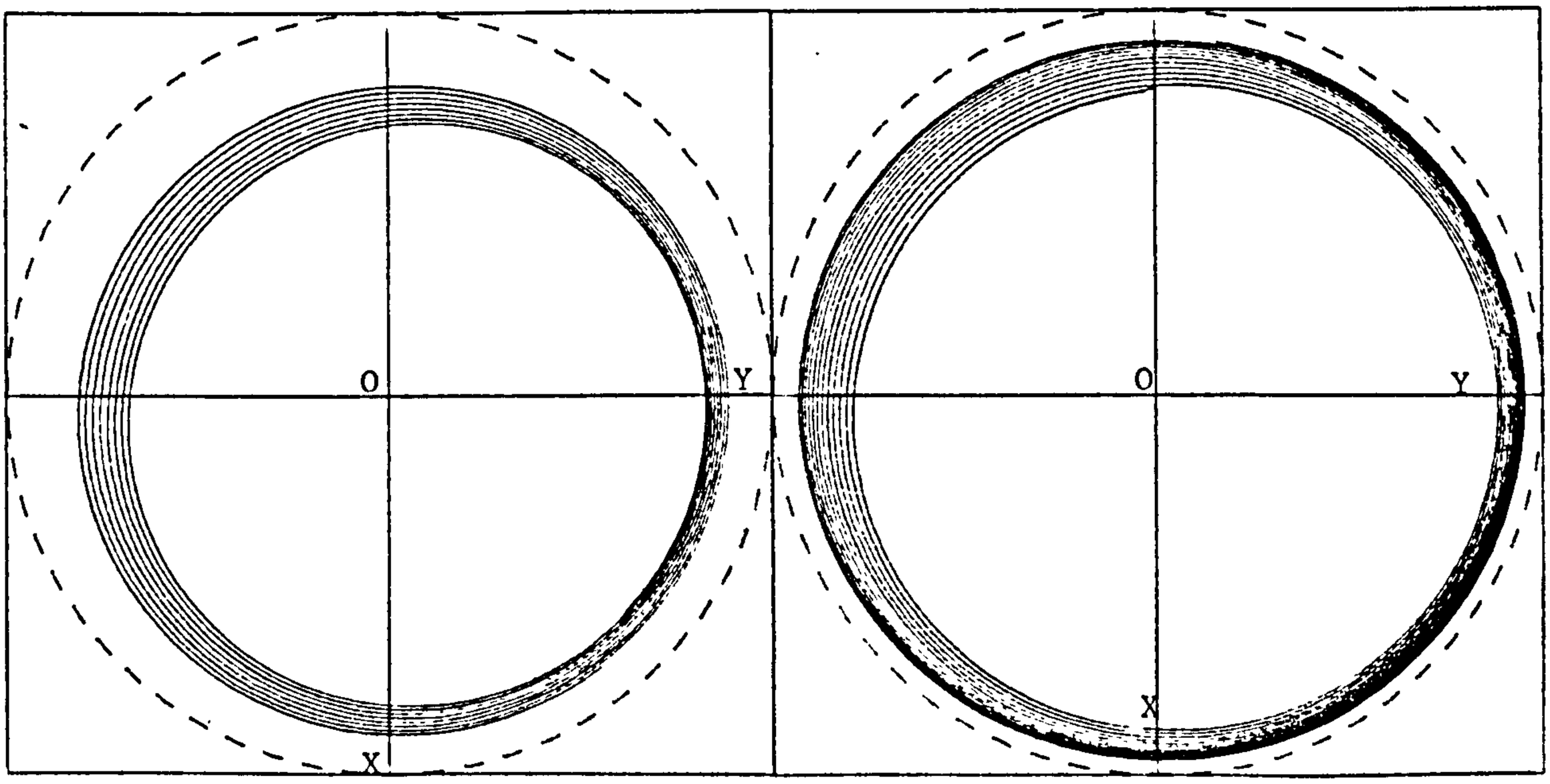

5.7(vii) $\bar{\omega}$ = 1.0 X_i = 0.6 Y_i = 0.6 5.7(viii) $\bar{\omega}$ = 1.0 X_i = -0.8 Y_i 0.0

Figure 5.7. continued. Whirl orbits of a rotor with a system parameter = 2.0

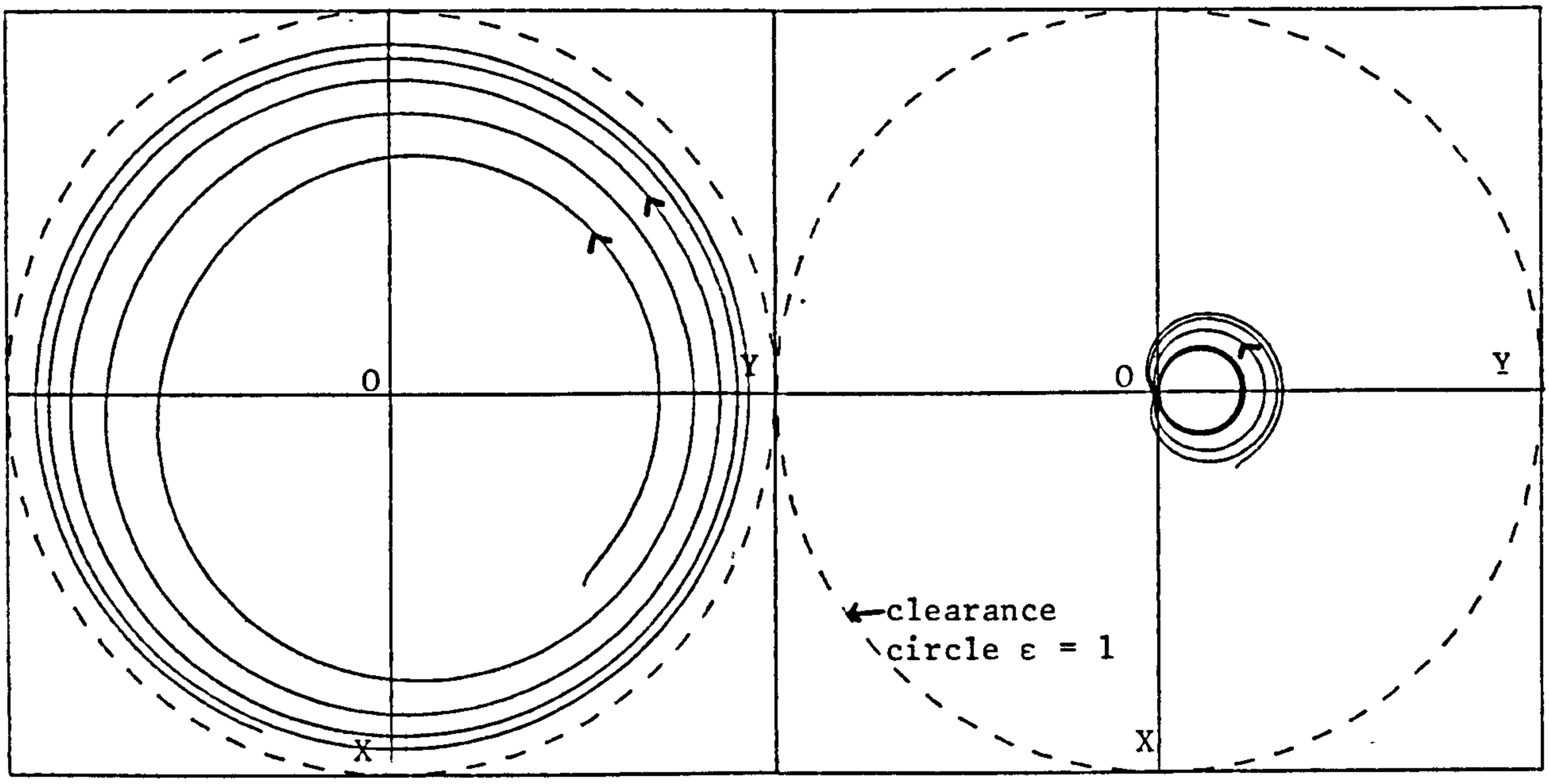

5.7(ix) $\bar{\omega}$ = 1.5 X_i = 0.5 Y_i = 0.5

5.7(x) $\bar{\omega}$ = 1.5 X_i = 0.2 Y_i = 0.2

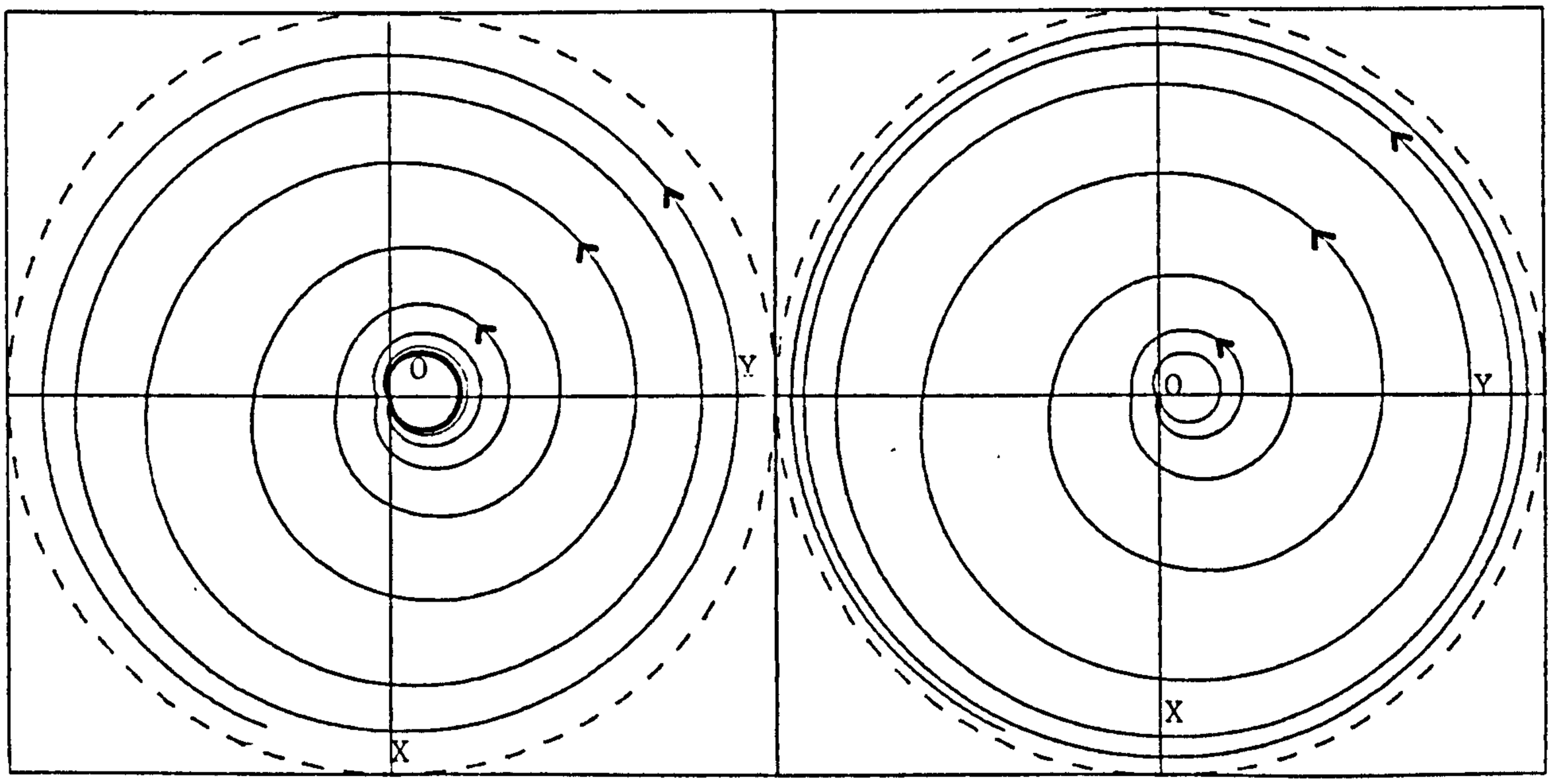

5.7(xi) $\bar{\omega}$ = 2.1 X_i = 0.0 Y_i = 0.0

5.7(xii) $\bar{\omega}$ = 2.5 X_i = 0.0 Y_i = 0.0

Figure 5.7. continued. Whirl orbits of a rotor with a system parameter = 2.0

orbit increases steadily as the rotor speed is increased, but the orbit remains independent of the initial conditions (Figures 5.6(v), 5.6(vi), 5.6(vii), 5.6(viii), 5.6 (ix), 5.6(x)), before becoming unstable at a rotor speed of approximately 2.0 (Figures 5.6(xi), 5.6(xii)).

It is evident from Figure 5.7 that the behaviour of a rotor with a system parameter equal to 2.0 may be quite complex. Well below its threshold speed of 0.945 the journal is stable and spirals into its equilibrium position (Figures 5.7(i), 5.7(ii)). At a rotor speed of 0.75 there are two possible solutions depending on the initial conditions:- stable if started close to the equilibrium position (Figure 5.7(iii)), or a limit cycle if started well away from the equilibrium position (Figure 5.7(iv)). This is again evidence of a stable limit cycle surrounding the unstable periodic orbit established by bifurcation theory. Above the threshold speed two solutions are still possible depending on the initial conditions:- a limit cycle (Figures 5.7(v), 5.7(vi)), or the journal may be completely unstable (Figures 5.7(vii), 5.7(viii)). These features remain as the rotor speed is increased (Figures 5.7(ix), 5.7(x)), with the limit cycle decreasing slightly in amplitude (compare Figures 5.7(x) and 5.7(vi)), but with the journal more prone to become completely unstable (compare Figures 5.7(vi) and 5.7 (ix)). Around a rotor speed of 2.1, the journal becomes completely unstable for all initial conditions (Figures 5.7(xi), 5.7(xii)).

A detailed numerical investigation suggests that the complete bifurcation diagrams for the three rotor systems are as shown in Figure 5.8.

5.5 DISCUSSION.

A combination of two alternative techniques - bifurcation theory and numerical integration provides a comprehensive investigation of the equations governing oil whirl in a long bearing operating with a

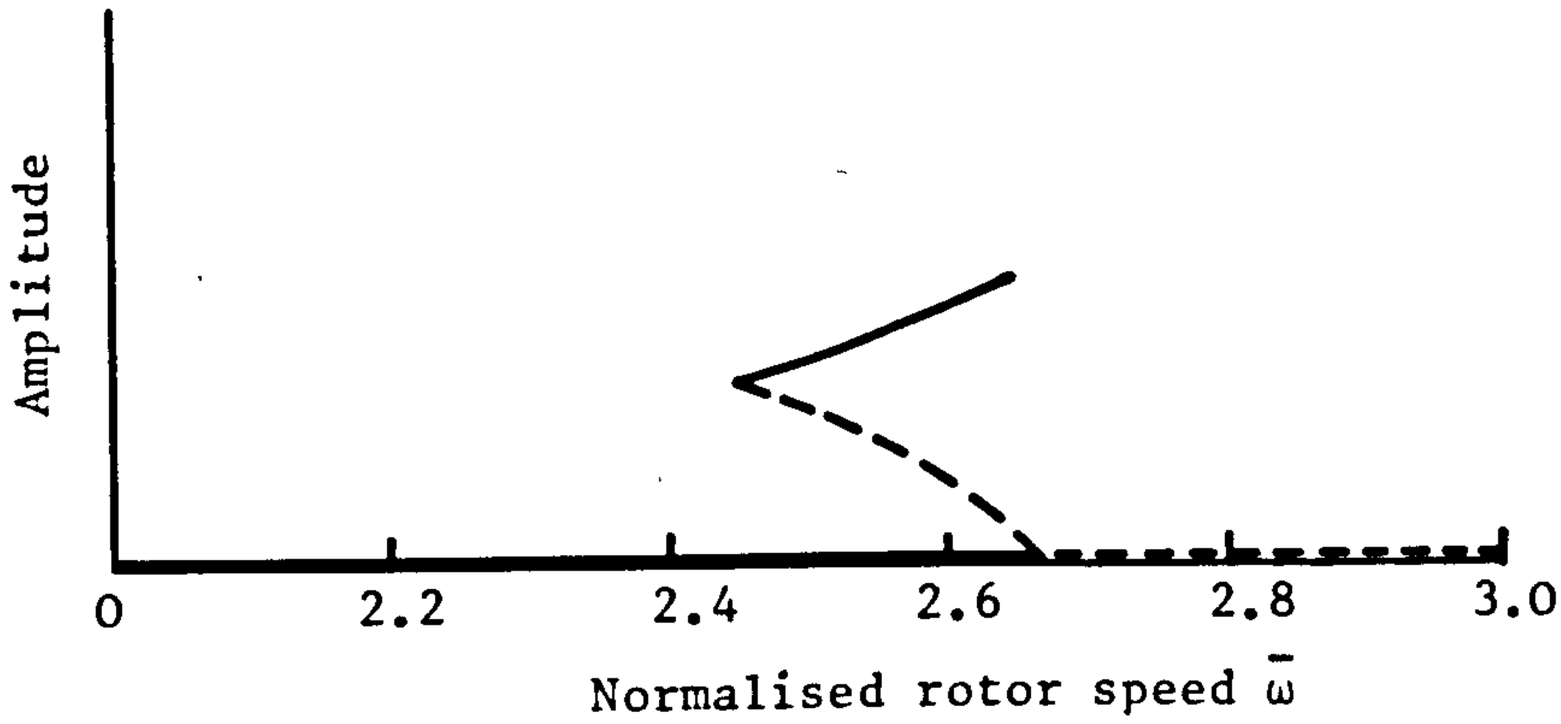

i) System parameter = 0.035

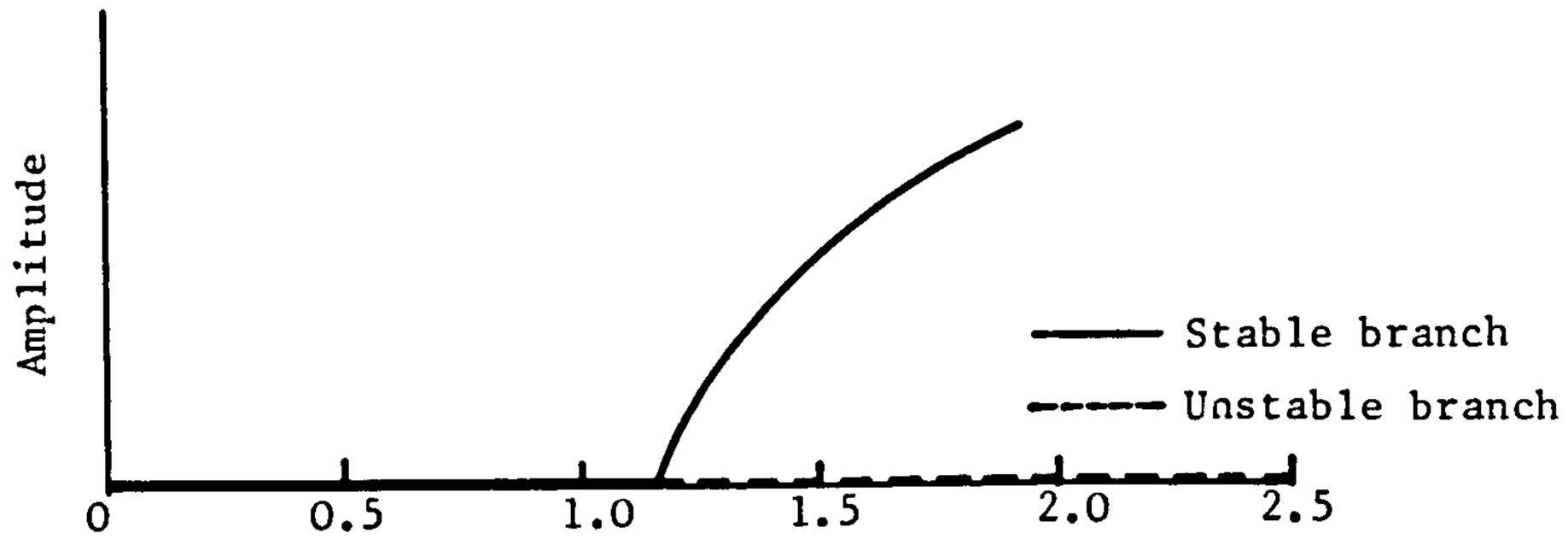

ii) System parameter = 0.2

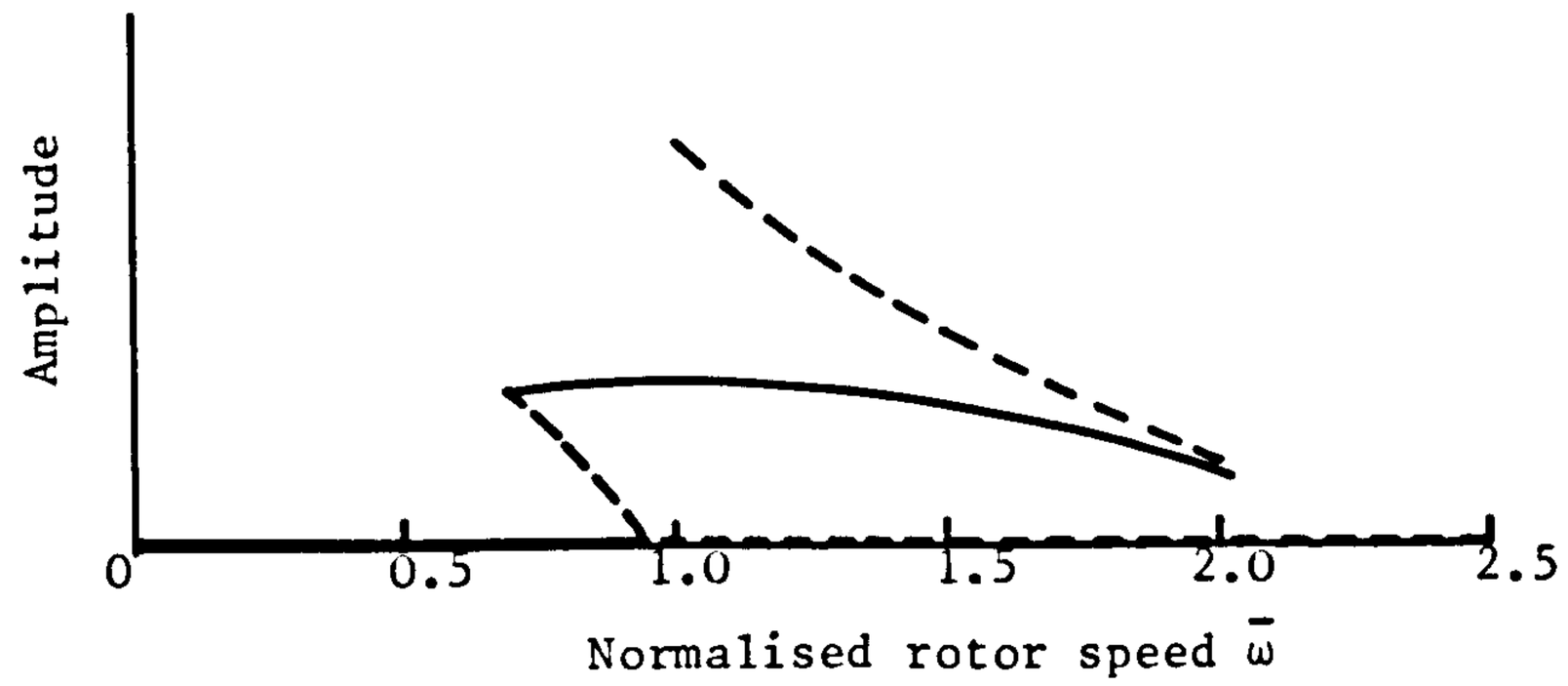

iii) System parameter = 2.0

Figure 5.8. Bifurcation diagrams for different rotor systems

half film. Bifurcation theory has been used to examine in some detail the structure of periodic solutions of the equations at speeds close to the threshold speed and to identify regions of parameter space where different behaviour occurs. Once these regions have been identified they may be investigated numerically. It is also possible to pursue the development of the whirl orbits as the rotor speed is increased, or decreased away from the threshold speed.

In theory it is possible to carry out similar investigations for all the models described in Part 1. In practice, however, it would be extremely difficult to use Poore's formula to determine the direction of bifurcation for the more complicated models, the major difficulty being in calculating the second and third order force derivatives. The model used for the present investigation was chosen for its simplicity and not because it is the most accurate model (see Chapters 3,4). It has, for example, already been mentioned that the model has a rather high value for the critical frequency ratio when compared with the other models (Figure 3.6). The purpose here and in the remaining Chapters, is to carry out a detailed examination of the full equations for one model using different techniques. In this way many different features of the equations may be observed and the validity of the various techniques may be assessed.

Note

During the preparation of this thesis the author learnt of a book which has recently been published in which the Hopf bifurcation is discussed comprehensively (Hassard, Kazarinoff and Wan (1981)). A major objective of this work is the determination of the direction of bifurcation, stability etc. for systems of equations which are too large, or too complicated for the calculation to be performed by hand. To this end the authors have developed a computer program to perform the

the complete Hopf bifurcation calculation numerically. (This program will shortly be available on the Amdahl computer at Leeds University). Such work may make it possible, in the near future, to perform the Hopf bifurcation calculation for a more accurate model.

5.6 CONCLUSIONS.

i) The onset of oil whirl in a simple rotor system supported in fluid film journal bearings is a bifurcation phenomenon which may be examined using Hopf bifurcation theory. The existence of small amplitude periodic solutions of the equations which govern oil whirl has been established for rotor speeds close to the threshold value.

ii) For the particular case studied (ie. a long bearing operating with a half film), it was found that the bifurcation may be subcritical, or supercritical depending on the value of the steady state eccentricity ratio.

iii) A numerical investigation supports the findings of the analytic work and the combination of the two methods provides a comprehensive examination of the features of the equations governing oil whirl.

iv) When supercritical bifurcation occurs there is a gradual transition from stability to complete instability. A stable, small amplitude whirl orbit appears as soon as the rotor speed exceeds its threshold value. The amplitude of the orbit increases gradually as the rotor speed is increased and the journal does not become completely unstable until well above the threshold speed.

v) When subcritical bifurcation occurs the behaviour of the rotor is more complicated and, in general, dependent on the initial conditions. Stable whirl orbits may exist both above and below the threshold speed. There is no gradual transition from stability to instability.

vi) Since the features described in this Chapter are due to the non-linearity of the equations, the limitations of a purely linearised

approach are exposed. This is not to say that nonlinear effects should always be included in bearing calculations, but there should certainly be a greater awareness of the role which the nonlinear terms may play in the phenomenon of oil whirl.

CHAPTER 6

THE METHOD OF MULTIPLE SCALING APPLIED TO THE EQUATIONS GOVERNING OIL WHIRL IN FLUID FILM JOURNAL BEARINGS.

6.1 INTRODUCTION.

Consider the ordinary differential equation:

$$\frac{d^2x}{dt^2} + \omega_o^2 x = \bar{\mu}\, f(x, \frac{dx}{dt}) \qquad (6.1)$$

in which $\bar{\mu}$ is a small parameter and ω_o is a constant. The solution of the equation for $\bar{\mu} = 0$ is:

$$x_o = a \cos(\omega_o t + \theta) \quad (a, \theta \text{ are constants}) \qquad (6.2)$$

The simplest method of obtaining a solution for $\bar{\mu}$ small, but non-zero, is to seek a perturbation expansion of the form:

$$x(t, \mu) = x_o(t) + \bar{\mu}\, x_1(t) + \bar{\mu}^2 x_2(t) + ... \qquad (6.3)$$

Unfortunately, this straightforward approach is often not very useful since it leads to secular terms (ie. terms of the form $x_1 = bt \cos(\omega_o t + \psi_1)$). Such terms "blow up" as $t \to \infty$ and the expansion is valid only for $t < 1/\bar{\mu}$. Several mathematical techniques, referred to as singular perturbation methods, have been developed to overcome this problem (Nayfeh (1972)). Two such methods are described in Chapters 6 and 7 and applied to the equations governing oil whirl in plain, cylindrical journal bearings. They are the method of multiple scaling and the method of averaging. Results obtained using these methods are compared with those derived in the previous Chapter.

6.2 THE METHOD OF MULTIPLE SCALING.

The method is most easily illustrated through the following example. Consider the differential equation:

$$\ddot{x} + (x^2 - \nu)\dot{x} + x = 0 \qquad (6.4)$$

in which ν is a real parameter ($|\nu| < 2$). Linearising the equation about the equilibrium position at $x = 0$ yields the characteristic equation:

$$\lambda^2 - \nu\lambda + 1 = 0 \quad \Rightarrow \lambda = \frac{\nu}{2} \pm i\,\frac{(4-\nu^2)^{1/2}}{2} \tag{6.5}$$

$$\Rightarrow \alpha(\nu) = \frac{\nu}{2}, \Omega(\nu) = \frac{(4-\nu^2)^{1/2}}{2}\,,\ \frac{d\alpha}{d\nu} = \frac{1}{2} \tag{6.6}$$

using the notation of the previous Chapter. Hence, by the Hopf bifurcation theorem discussed in the previous Chapter, a periodic orbit bifurcates from $(x,\nu) = (0,0)$. Using bifurcation theory, Murray (1976) has shown that a stable periodic orbit exists for $\nu > 0$. The existence of periodic solutions may also be investigated by using the method of multiple scaling.

The motivation for this approach comes from the following reasoning; consider equation (6.4) for ν just greater than zero. In this region the equilibrium point at $x = 0$ is unstable (based upon a linearised analysis), which implies that perturbations from $x = 0$ will initially grow exponentially with time. This (linearised) exponentially growing function cannot represent the solution for very long because the non-linear terms must, at some stage, become important. Suppose, now, this exponentially growing function tends to a stable oscillatory solution (limit cycle) then growth on another time scale must come into play. Thus, the perturbation from the unstable equilibrium point should exhibit a multi-time scale representation of the form $x(\tau) = A(\tau^*)P(s)$ where $P(s)$ represents a periodic oscillation on a "fast time" and $A(\tau^*)$ represents "slow time" modulation, which perhaps approaches a constant value as time $\tau \to \infty$.

To investigate periodic solutions in the region $\nu > 0$:

put $\nu = \delta^2$ (6.7)

introduce two time scales:

$\tau^* = \delta^2\tau$ "slow time" (6.8)

$s = (1+\delta\omega_1+\delta^2\omega_2+\ldots)\tau$ "fast time" (6.9)

and seek a solution of the form:

$$x(s,\tau^*) = \delta x_1(s,\tau^*) + \delta^2 x_2(s,\tau^*) + \delta^3 x_3(s,\tau^*) + ... \qquad (6.10)$$

The success of the method depends upon the correct choice of the forms (6.7 - 6.10). The correct scaling for the slow time scale τ^* is governed by the growth rate of the linearised exponential function as $\nu \to 0$:

$$\text{ie.} \quad e^{\alpha(\nu)\tau} \to e^{\alpha^1(0)\nu\tau} \text{ as } \nu \to 0 \qquad (\alpha(0) = 0)$$

Thus, from the remarks made earlier, the slow time scale must be of $O(\nu\tau)$. The quantities ω_i and the other unknowns which will occur are chosen according to the principle that secular terms are suppressed in such a way that a self-consistent procedure for determining bounded functions $x_i(s,\tau^*)$ with modulation only on the slow time scale τ^* is generated. The reason for seeking a solution in powers of δ and not, for example $\delta^{1/2}$ will be explained later.

The two time scales defined by equations (6.8) and (6.9) imply that:

$$\frac{d}{d\tau} = (1+\delta\omega_1+\delta^2\omega_2+ \ldots)\frac{\partial}{\partial s} + \delta^2 \frac{\partial}{\partial \tau^*} \qquad (6.11)$$

$$\Rightarrow \quad \frac{dx}{d\tau} = \delta\frac{\partial x_1}{\partial s} + \delta^2\left\{\frac{\partial x_2}{\partial s} + \omega_1 \frac{\partial x_1}{\partial s}\right\} + \delta^3 \left\{\frac{\partial x_3}{\partial s} + \omega_1 \frac{\partial x_2}{\partial s} + \omega_2 \frac{\partial x_1}{\partial s} + \frac{\partial x_1}{\partial \tau^*}\right\} \qquad (6.12)$$

$$\frac{d^2x}{d\tau^2} = \delta \frac{\partial^2 x_1}{\partial s^2} + \delta^2 \left\{\frac{\partial^2 x_2}{\partial s^2} + 2\omega_1 \frac{\partial^2 x_1}{\partial s^2}\right\} + \delta^3 \left\{\frac{\partial^2 x_3}{\partial s^2} + 2\omega_1 \frac{\partial^2 x_2}{\partial s^2} + 2\omega_2 \frac{\partial^2 x_1}{\partial s^2} + \omega_1^2 \frac{\partial^2 x_1}{\partial s^2} + 2 \frac{\partial^2 x_1}{\partial s \partial \tau^*}\right\} \qquad (6.13)$$

Substituting equations (6.10), (6.12) and (6.13) into equation (6.4) and equating the coefficient of like powers of δ yields:

$$\text{Order } (\delta) \quad \frac{\partial^2 x_1}{\partial s^2} + x_1 = 0 \qquad (6.14)$$

$$\text{Order } (\delta^2) \quad \frac{\partial^2 x_2}{\partial s^2} + x_2 = -2\omega_1 \frac{\partial^2 x_1}{\partial s^2} \tag{6.15}$$

$$\text{Order } (\delta^3) \quad \frac{\partial^2 x_3}{\partial s^2} + x_3 = (1-x_1^2)\frac{\partial x_1}{\partial s} - 2\omega_1 \frac{\partial^2 x_2}{\partial s^2} - 2\omega_2 \frac{\partial^2 x_1}{\partial s^2} - \omega_1^2 \frac{\partial^2 x_1}{\partial s^2}$$

$$- 2 \frac{\partial^2 x_1}{\partial s \partial \tau^*} \tag{6.16}$$

The solution to equation (6.14) is:

$$x_1(s,\tau^*) = A_1(\tau^*)e^{is} + \overline{A_1(\tau^*)}e^{-is} \tag{6.17}$$

where the unknown function $A_1(\tau^*)$ will be determined at a later stage of the perturbation procedure. $\overline{A_1(\tau^*)}$ denotes the complex conjugate of A_1. Substituting equation (6.17) into the right hand side of equation (6.15) yields:

$$\frac{\partial^2 x_2}{\partial s^2} + x_2 = 2\omega_1 \left\{ A_1(\tau^*)e^{is} + \bar{A}_1(\tau^*)e^{-is} \right\} \tag{6.18}$$

from which it can be seen that the suppression of secular terms requires that $\omega_1 = 0$ and thus the solution to equation (6.18) is:

$$x_2(s,\tau^*) = A_2(\tau^*)e^{is} + \overline{A_2(\tau^*)}e^{-is} \tag{6.19}$$

where $A_2(\tau^*)$ may also be determined at a later stage of the perturbation procedure. Equation (6.16) now becomes:

$$\frac{\partial^2 x_3}{\partial s^2} + x_3 = \left\{ iA_1 + 2\omega_2 A_1 - iA_1|A_1|^2 - 2i \frac{dA_1}{d\tau^*} \right\} e^{is} - iA_1 e^{3is} + \text{c.c.} \tag{6.20}$$

(c.c. denotes the complex conjugate of the preceeding expressions).

The suppression of secular terms requires that:

$$i \frac{dA_1}{d\tau^*} = A_1 \left\{ \omega_2 + \frac{i}{2} (1-|A_1|^2) \right\} \tag{6.21}$$

Equation (6.21) represents a complex amplitude equation for A_1. The real and imaginary parts may be separated out by writing $A_1(\tau^*) = R(\tau^*)e^{i\theta(\tau^*)}$

which yields:

$$\frac{dR}{d\tau^*} = \frac{R}{2}(1-R^2) \qquad \text{amplitude equation} \qquad (6.22a)$$

$$\text{and} \quad \frac{d\theta}{d\tau^*} = -\omega_2 \qquad \text{phase shift equation} \qquad (6.22b)$$

The important equation is the amplitude equation for R (equation 6.22a), the solution to which is:

$$R^2 = \frac{1}{1+Ce^{-\tau^*}} \Rightarrow R \to 1 \text{ as } \tau^* \to \infty \text{ (C constant)} \qquad (6.23)$$

Thus, equations (6.10) and (6.23) show an approach to a limit cycle of the form:

$$x(\tau) = 2\sqrt{\nu}\cos\{(1+O(\nu))\tau\} + O(\nu) \text{ as } \nu \to 0 \qquad (6.24)$$

(to within a phase shift)

Therefore, it has been established that a periodic solution of the form (6.24) bifurcates from $(x,\nu) = (0,0)$ for $\nu > 0$.

The stability of the orbit immediately follows from equation (6.22a) since:

$$\text{for } 0 < R < 1 \ \frac{dR}{d\tau^*} > 0, \text{ whereas for } R > 1 \ \frac{dR}{d\tau^*} < 1$$

which implies that, for $R(\tau^*)$ less (greater) than $\dot{R} = 1$, $dR/d\tau^*$ is greater (less) than zero implying motion towards the periodic orbit (ie. stability).

The existence of periodic solutions for $\nu < 0$ may be investigated similarly by substituting $\nu = -\delta^2$ into equation (6.4). This approach yields an amplitude equation:

$$\frac{dR}{d\tau^*} = \frac{R}{2}(-1-R^2) \Rightarrow R^2 = \frac{1}{Ce^{\tau^*}-1} \qquad (6.25)$$

Thus, as $\tau^* \to \infty$, $R \to 0$, which implies that there are no periodic solutions of equation (6.4) for $\nu < 0$. All states approach the equilibrium solution.

Note

i) In solving equations (6.14-6.16) it is simpler to write the solution in terms of complex exponentials rather than cos and sin terms.

ii) The complex amplitude equation (6.21) includes ω_2, which is indeterminate as far as the perturbation procedure is taken. It does not, however, appear in the equation for R (equation (6.22a)).

iii) The coefficient of R in equation (6.22a) represents the linear growth rate ($\alpha^1(o) = 1/2$).

iv) The amplitude equation contains both linear and cubic terms on the right hand side (equation 6.22a). The periodic solution exists when these terms are in balance and this is achieved by seeking a solution in powers of δ (equation 6.10). The form of equation (6.10) also agrees with the scaling obtained from the Hopf bifurcation theorem (see Chapter 5).

The method of multiple scaling as described here is a fairly straightforward approach and is successful here in establishing the existence of periodic solutions of equations (6.4). There are various other forms which the method of multiple scaling may take (Nayfeh (1972)). A very similar approach to the one described here is used by Cohen (1972) to investigate periodic solutions of equations in chemical reactor theory. The technique has also been successfully adopted to investigate the non-linear development of the Kelvin-Helmholtz instability by Weissman (1979).

6.3 THE APPLICATION OF THE METHOD OF MULTIPLE SCALING TO THE EQUATIONS GOVERNING OIL WHIRL.

The technique described in the previous section is now applied to the equations governing oil whirl in plain cylindrical journal bearings. In principle the technique is precisely the same, the only difference being the amount of algebra involved. The equations of motion may be written in the form:

$$\ddot{X} = \frac{S}{\bar{\omega}^2}\,\bar{F}_X(X,Y,\dot{X},\dot{Y},S) \qquad \ddot{Y} = \frac{S}{\bar{\omega}^2}\,\bar{F}_Y(X,Y,\dot{X},\dot{Y},S) \tag{6.26}$$

with $S = \sigma\bar{\omega} = S(\varepsilon_s)$

The derivation of these equations may be found in Chapter 5. The Cartesian co-ordinate system used is as shown in Figure 6.1.

The right hand side of equation (6.26) may be expanded as a Taylor series about the equilibrium position:

$$\begin{aligned}\ddot{X} = \frac{1}{\bar{\omega}^2} \Big\{ & a_1\Delta\dot{X} + a_2\Delta\dot{Y} + a_3\Delta X + a_4\Delta Y + \frac{1}{2}a_5\Delta X^2 + \frac{1}{2}a_6\Delta Y^2 \\ & + a_7\Delta X\Delta Y + a_8\Delta X\Delta\dot{X} + a_9\Delta Y\Delta\dot{Y} + a_{10}\Delta X\Delta\dot{Y} + a_{11}\Delta\dot{X}\Delta Y \\ & + \frac{1}{6}a_{15}\Delta X^3 + \frac{1}{6}a_{16}\Delta Y^3 + \frac{1}{2}a_{17}\Delta X^2\Delta Y + \frac{1}{2}a_{18}\Delta X^2\Delta\dot{X} + \frac{1}{2}a_{19}\Delta X^2\Delta\dot{Y} \\ & + \frac{1}{2}a_{20}\Delta Y^2\Delta X + \frac{1}{2}a_{21}\Delta Y^2\Delta\dot{X} + \frac{1}{2}a_{22}\Delta Y^2\Delta\dot{Y} + a_{23}\Delta X\Delta Y\Delta\dot{X} + a_{24}\Delta X\Delta Y\Delta\dot{Y} \Big\}. \end{aligned} \tag{6.27}$$

where: $a_1 = S\left(\frac{\partial \bar{F}_X}{\partial \dot{X}}\right)_s \quad a_2 = S\left(\frac{\partial \bar{F}_X}{\partial \dot{Y}}\right)_s \quad a_3 = S\left(\frac{\partial \bar{F}_X}{\partial X}\right)_s \quad a_4 = S\left(\frac{\partial \bar{F}_X}{\partial Y}\right)_s$ (6.28)

$$a_5 = S\left(\frac{\partial^2 \bar{F}_X}{\partial X^2}\right)_s \qquad a_{15} = S\left(\frac{\partial^3 \bar{F}_X}{\partial X^3}\right)_s \quad \text{etc.}$$

$$\Delta X = X - X_s \qquad \Delta Y = Y - Y_s \tag{6.29}$$

and similarly for the Y - equation (replacing a_i with b_i).

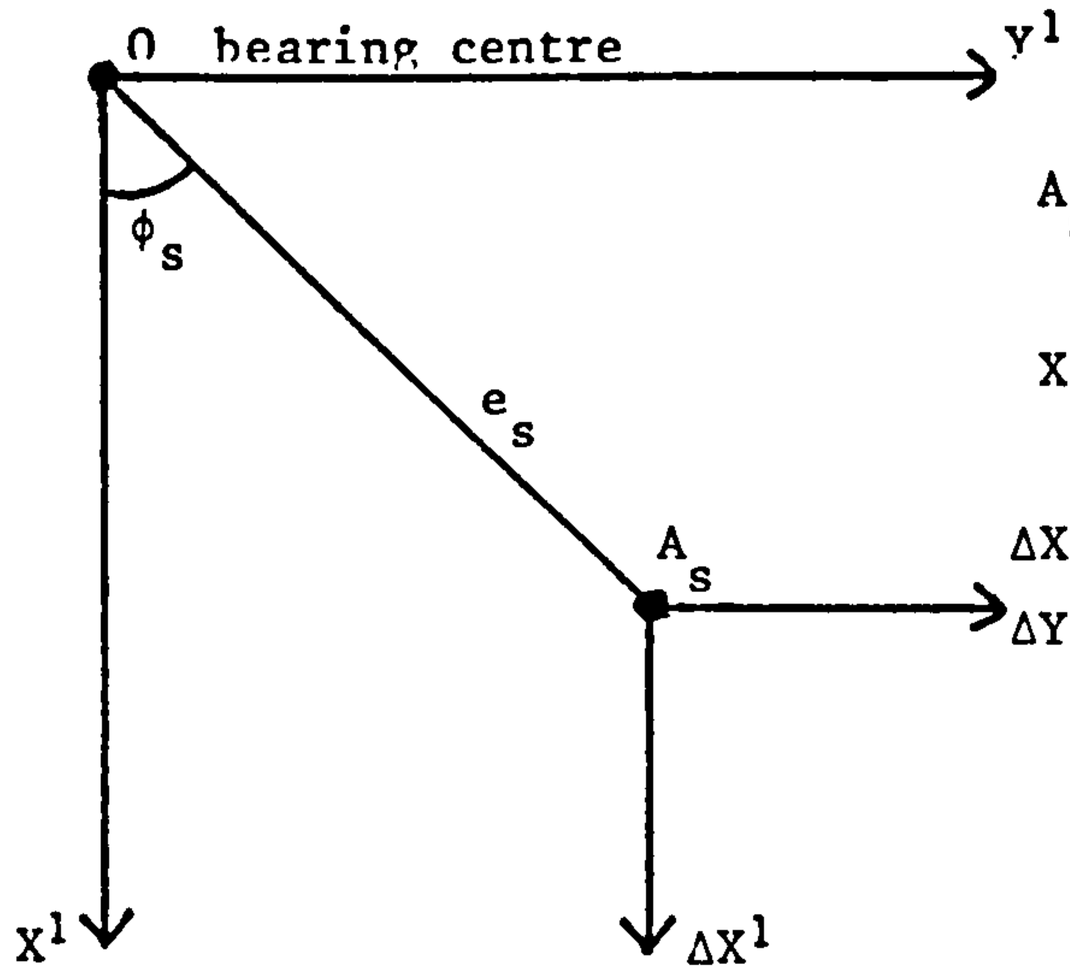

A_s. Steady state position of journal centre.

$$X = \frac{X^1}{c} \qquad Y = \frac{Y^1}{c}$$

$$\Delta X = \frac{\Delta X^1}{c} \qquad \Delta Y = \frac{\Delta Y^1}{c}$$

Figure 6.1. Cartesian co-ordinate system.

The missing terms in the Taylor expansion above are identically zero for the model of a long bearing operating with an oscillating half film which is used here to illustrate the technique. The coefficients $a_1 \to a_{34}$, $b_1 \to b_{34}$ for this model are given in Appendix III.

Before proceeding with the two timing approach it is useful to consider the following system of two ordinary differential equations:

$$\frac{d^2\Delta X}{d\tau^2} - \frac{a_1}{\bar{\omega}_{th}^2}\frac{d\Delta X}{d\tau} - \frac{a_2}{\bar{\omega}_{th}^2}\frac{d\Delta Y}{d\tau} - \frac{a_3}{\bar{\omega}_{th}^2}\Delta X - \frac{a_4}{\bar{\omega}_{th}^2}\Delta Y$$

$$= q_1 e^{i\bar{\Omega}_{th}\tau} + \bar{q}_1 e^{-i\bar{\Omega}_{th}\tau} + m_1 e^{2i\bar{\Omega}_{th}\tau} + \bar{m}_1 e^{-2\bar{\Omega}_{th}\tau} + n_1 \qquad (6.30)$$

$$\frac{d^2\Delta Y}{d\tau^2} - \frac{b_1}{\bar{\omega}_{th}^2}\frac{d\Delta X}{d\tau} - \frac{b_2}{\bar{\omega}_{th}^2}\frac{d\Delta Y}{d\tau} - \frac{b_3}{\bar{\omega}_{th}^2}\Delta X - \frac{b_4}{\bar{\omega}_{th}^2}\Delta Y$$

$$= q_2 e^{i\bar{\Omega}_{th}\tau} + \bar{q}_2 e^{-i\bar{\Omega}_{th}\tau} + m_2 e^{2i\bar{\Omega}_{th}\tau} + \bar{m}_2 e^{-2i\bar{\Omega}_{th}\tau} + n_2$$

The left hand sides of these equations correspond to the linearised form of equation (6.26) at the point of neutral stability. Neglecting transients, the solution to equations (6.30) may be written in the form:

$$\Delta X(\tau) = Ae^{i\bar{\Omega}_{th}\tau} + r_1\tau e^{i\bar{\Omega}_{th}\tau} + r_2 e^{i\bar{\Omega}_{th}\tau} + u_1 e^{2i\bar{\Omega}_{th}\tau} + \frac{v_1}{2} + \text{c.c.}$$

$$\Delta Y(\tau) = \lambda Ae^{i\bar{\Omega}_{th}\tau} + \lambda r_1\tau e^{i\bar{\Omega}_{th}\tau} + s_2 e^{i\bar{\Omega}_{th}\tau} + u_2 e^{2i\bar{\Omega}_{th}\tau} + \frac{v_2}{2} + \text{c.c.} \qquad (6.31)$$

where A is a constant and $A\begin{pmatrix}1\\ \lambda\end{pmatrix}$ represents the eigenvector corresponding to the eigenvalue $+i\bar{\Omega}_{th}$ of the homogeneous form of equation (6.30). The remaining quantities $r_1, r_2, u_1, v_1, s_2, u_2, v_2$ are determined by seeking the appropriate particular integral. In fact, it follows from the linearity of the equations that:

$$\begin{pmatrix} r_1 \\ r_2 \end{pmatrix} = \begin{pmatrix} B_1 & B_2 \\ B_3 & B_4 \end{pmatrix}\begin{pmatrix} q_1 \\ q_2 \end{pmatrix} \qquad \begin{pmatrix} u_1 \\ u_2 \end{pmatrix} = \begin{pmatrix} B_5 & B_6 \\ B_7 & B_8 \end{pmatrix}\begin{pmatrix} m_1 \\ m_2 \end{pmatrix} \qquad (6.32)$$

$$\begin{pmatrix} v_1 \\ v_2 \end{pmatrix} = \begin{pmatrix} B_9 & B_{10} \\ B_{11} & B_{12} \end{pmatrix} \begin{pmatrix} n_1 \\ n_2 \end{pmatrix}$$

where the B's may be complex. They may be determined by substituting equations (6.31) back into equations (6.30) etc. - the process is straightforward, but tedious. It follows from equation (6.31) that the elimination of secular terms requires:

$$r_1 = 0 \Rightarrow B_1 q_1 + B_2 q_2 = 0 \qquad (6.33)$$

This is the only piece of theory needed to carry out the two timing approach for equations (6.26).

To investigate the existence (or otherwise) of small amplitude periodic solutions of equations (6.26) for rotor speeds close to the threshold speed

$$\text{substitute } \bar{\omega} = \bar{\omega}_{th} + \delta^2 \quad (\text{ie. } \bar{\omega} > \bar{\omega}_{th}) \qquad (6.34)$$

introduce two time scales;

$$\tau^* = \delta^2 \tau \qquad \text{"slow time"} \qquad (6.35)$$

$$s = (1+\delta\omega_1+\delta^2\omega_2+\ldots)t \qquad \text{"fast time"} \qquad (6.36)$$

and seek a solution of the form:

$$\Delta X(s,\tau^*) = \delta X_1(s,\tau^*) + \delta^2 X_2(s,\tau^*) + \delta^3 X_3(s,\tau^*) + \ldots \qquad (6.37)$$

$$\Delta Y(s,\tau^*) = \delta Y_1(s,\tau^*) + \delta^2 Y_2(s,\tau^*) + \delta^3 Y_3(s,\tau^*) + \ldots$$

The appropriate scaling for the slow time variable τ^* is again governed by the non-zero value of the derivative $(d\bar{\omega}/d\bar{\omega})_{\bar{\omega} = \bar{\omega}_{th}}$ for the reasons discussed previously. The ω_i's in equation (6.36) are unknowns which are chosen according to the principle that secular terms will be suppressed.

Substituting equations (6.34), (6.37) into equations (6.27), making use of equations (6.11), (6.12) and (6.13) and equating like powers of δ, yields:

Order (δ)

$$\frac{\partial^2 X_1}{\partial s^2} - \bar{a}_1 \frac{\partial X_1}{\partial s} - \bar{a}_2 \frac{\partial Y_1}{\partial s} - \bar{a}_3 X_1 - \bar{a}_4 Y_1 = 0 \qquad (6.38a)$$

$$\frac{\partial^2 Y_1}{\partial s^2} - \bar{b}_1 \frac{\partial X_1}{\partial s} - \bar{b}_2 \frac{\partial Y_1}{\partial s} - \bar{b}_3 X_1 - \bar{b}_4 Y_1 = 0 \qquad (6.38b)$$

Order (δ^2)

$$\frac{\partial^2 X_2}{\partial s^2} - \bar{a}_1 \frac{\partial X_2}{\partial s} - \bar{a}_2 \frac{\partial Y_2}{\partial s} - \bar{a}_3 X_2 - \bar{a}_4 Y_2$$

$$= -2\omega_1 \frac{\partial^2 X_1}{\partial s^2} + \bar{a}_1 \omega_1 \frac{\partial X_1}{\partial s} + \bar{a}_2 \omega_1 \frac{\partial Y_1}{\partial s} + \frac{1}{2} \bar{a}_5 X_1^2 + \frac{1}{2} \bar{a}_6 Y_1^2$$

$$+ \bar{a}_7 X_1 Y_1 + \bar{a}_8 X_1 \frac{\partial X_1}{\partial s} + \bar{a}_9 Y_1 \frac{\partial Y_1}{\partial s} + \bar{a}_{10} X_1 \frac{\partial Y_1}{\partial s} + \bar{a}_{11} Y_1 \frac{\partial X_1}{\partial s} \qquad (6.39a)$$

$$\frac{\partial^2 Y_2}{\partial s^2} - \bar{b}_1 \frac{\partial X_2}{\partial s} - \bar{b}_2 \frac{\partial Y_2}{\partial s} - \bar{b}_3 X_2 - \bar{b}_4 Y_2$$

$$= -2\omega_1 \frac{\partial^2 Y_1}{\partial s^2} + \bar{b}_1 \omega_1 \frac{\partial X_1}{\partial s} + \bar{b}_2 \omega_1 \frac{\partial Y_1}{\partial s} + \frac{1}{2} \bar{b}_5 X_1^2 + \frac{1}{2} \bar{b}_6 Y_1^2$$

$$+ \bar{b}_7 X_1 Y_1 + \bar{b}_8 X_1 \frac{\partial X_1}{\partial s} + \bar{b}_9 Y_1 \frac{\partial Y_1}{\partial s} + \bar{b}_{10} X_1 \frac{\partial Y_1}{\partial s} + \bar{b}_{11} Y_1 \frac{\partial X_1}{\partial s} \qquad (6.39b)$$

Order (δ^3)

$$\frac{\partial^2 X_3}{\partial s^2} - \bar{a}_1 \frac{\partial X_3}{\partial s} - \bar{a}_2 \frac{\partial Y_3}{\partial s} - \bar{a}_3 X_3 - \bar{a}_4 Y_3$$

$$= -2\omega_1 \frac{\partial^2 X_2}{\partial s^2} - 2\omega_2 \frac{\partial^2 X_1}{\partial s^2} - 2 \frac{\partial^2 X_1}{\partial s \, \partial \tau^*} - \omega_1^2 \frac{\partial^2 X_1}{\partial s^2} + \bar{a}_1 \left(\frac{\partial X_1}{\partial \tau^*} + \omega_2 \frac{\partial X_1}{\partial s} + \omega_1 \frac{\partial X_2}{\partial s} \right)$$

$$+ \bar{a}_2 \left(\frac{\partial Y_1}{\partial \tau^*} + \omega_2 \frac{\partial Y_1}{\partial s} + \omega_1 \frac{\partial Y_2}{\partial s} \right) + \left(-2 \frac{a_1}{\bar{\omega}_{th}^3} + \frac{1}{\bar{\omega}_{th}^2} \frac{da_1}{d\varepsilon_s} \frac{d\varepsilon_s}{d\bar{\omega}} \right) \frac{\partial X_1}{\partial s}$$

$$+ \left(-2 \frac{a_2}{\bar{\omega}_{th}^3} + \frac{1}{\bar{\omega}_{th}^2} \frac{da_2}{d\varepsilon_s} \frac{d\varepsilon_s}{d\bar{\omega}} \right) \frac{\partial Y_1}{\partial s} + \left(-2 \frac{a_3}{\bar{\omega}_{th}^3} + \frac{1}{\bar{\omega}_{th}^2} \frac{da_3}{d\varepsilon_s} \frac{d\varepsilon_s}{d\bar{\omega}} \right) X_1$$

$$+\left(-\frac{2a_4}{\omega_{th}^3}+\frac{1}{\omega_{th}^2}\frac{da_4}{d\varepsilon_s}\frac{d\varepsilon_s}{d\omega}\right)Y_1+\bar{a}_5X_1X_2+\bar{a}_6Y_1Y_2+\bar{a}_7(X_1Y_2+Y_1X_2)$$

$$+\bar{a}_8\left\{X_1\left(\omega_1\frac{\partial X_1}{\partial s}+\frac{\partial X_2}{\partial s}\right)+X_2\frac{\partial X_1}{\partial s}\right\}+\bar{a}_9\left\{Y_1\left(\omega_1\frac{\partial Y_1}{\partial s}+\frac{\partial Y_2}{\partial s}\right)+Y_2\frac{\partial Y_1}{\partial s}\right\}$$

$$+\bar{a}_{10}\left\{X_1\left(\omega_1\frac{\partial Y_1}{\partial s}+\frac{\partial Y_2}{\partial s}\right)+X_2\frac{\partial Y_1}{\partial s}\right\}+\bar{a}_{11}\left\{Y_1\left(\omega_1\frac{\partial X_1}{\partial s}+\frac{\partial X_2}{\partial s}\right)+Y_2\frac{\partial X_1}{\partial s}\right\}$$

$$+\frac{1}{6}\bar{a}_{15}X_1^3+\frac{1}{6}\bar{a}_{16}Y_1^3+\frac{1}{2}\bar{a}_{17}X_1^2Y_1+\frac{1}{2}\bar{a}_{18}X_1^2\frac{\partial X_1}{\partial s}+\frac{1}{2}\bar{a}_{19}X_1^2\frac{\partial Y_1}{\partial s}$$

$$+\frac{1}{2}\bar{a}_{20}Y_1^2X_1+\frac{1}{2}\bar{a}_{21}Y_1^2\frac{\partial X_1}{\partial s}+\frac{1}{2}\bar{a}_{22}Y_1^2\frac{\partial Y_1}{\partial s}+\bar{a}_{23}X_1Y_1\frac{\partial X_1}{\partial s}+\bar{a}_{24}X_1Y_1\frac{\partial Y_1}{\partial s} \qquad (6.40a)$$

$$\frac{\partial^2Y_3}{\partial s^2}-\bar{b}_1\frac{\partial X_3}{\partial s}-\bar{b}_2\frac{\partial Y_3}{\partial s}-\bar{b}_3X_3-\bar{b}_4Y_3$$

$$=-2\omega_1\frac{\partial^2Y_2}{\partial s^2}-2\omega_2\frac{\partial^2Y_1}{\partial s^2}-2\frac{\partial^2Y_1}{\partial s\partial\tau^*}-\omega_1^2\frac{\partial^2Y_1}{\partial s^2}+\bar{b}_1\left(\frac{\partial X_1}{\partial\tau^*}+\omega_2\frac{\partial X_1}{\partial s}+\omega_1\frac{\partial X_2}{\partial s}\right)$$

$$+\bar{b}_2\left(\frac{\partial Y_1}{\partial\tau^*}+\omega_2\frac{\partial Y_1}{\partial s}+\omega_1\frac{\partial Y_2}{\partial s}\right)+\left(-2\frac{b_1}{\bar{\omega}_{th}^3}+\frac{1}{\bar{\omega}_{th}^2}\frac{db_1}{d\varepsilon_s}\frac{d\varepsilon_s}{d\bar{\omega}}\right)\frac{\partial X_1}{\partial s}+\left(-2\frac{b_2}{\bar{\omega}_{th}^3}+\frac{1}{\bar{\omega}_{th}^2}\frac{db_2}{d\varepsilon_s}\frac{d\varepsilon_2}{d\bar{\omega}}\right)\frac{\partial Y_1}{\partial s}$$

$$+\left(-\frac{2}{\bar{\omega}_{th}^3}b_3+\frac{1}{\bar{\omega}_{th}^2}\frac{db_3}{d\varepsilon_s}\frac{d\varepsilon_s}{d\bar{\omega}}\right)X_1+\left(-\frac{2}{\bar{\omega}_{th}^3}b_4+\frac{1}{\bar{\omega}_{th}^2}\frac{db_4}{d\varepsilon_s}\frac{d\varepsilon_s}{d\bar{\omega}}\right)Y_1+\bar{b}_5X_1X_2+\bar{b}_6Y_1Y_2$$

$$+\bar{b}_7(X_1Y_2+Y_1X_2)+\bar{b}_8\left\{X_1\left(\omega_1\frac{\partial X_1}{\partial s}+\frac{\partial X_2}{\partial s}\right)+X_2\frac{\partial X_1}{\partial s}\right\}+\bar{b}_9\left\{Y_1\left(\omega_1\frac{\partial Y_1}{\partial s}+\frac{\partial Y_2}{\partial s}\right)+Y_2\frac{\partial Y_1}{\partial s}\right\}$$

$$+\bar{b}_{10}\left\{X_1\left(\omega_1\frac{\partial Y_1}{\partial s}+\frac{\partial Y_2}{\partial s}\right)+X_2\frac{\partial Y_1}{\partial s}\right\}+\bar{b}_{11}\left\{Y_1\left(\omega_1\frac{\partial X_1}{\partial s}+\frac{\partial X_2}{\partial s}\right)+Y_2\frac{\partial X_1}{\partial s}\right\}$$

$$+\frac{1}{6}\bar{b}_{15}X_1^3+\frac{1}{6}\bar{b}_{16}Y_1^3+\frac{1}{2}\bar{b}_{17}X_1^2Y_1+\frac{1}{2}\bar{b}_{18}X_1^2\frac{\partial X_1}{\partial s}+\frac{1}{2}\bar{b}_{19}X_1^2\frac{\partial Y_1}{\partial s}+\frac{1}{2}\bar{b}_{20}Y_1^2X_1$$

$$+\frac{1}{2}\bar{b}_{21}Y_1^2\frac{\partial X_1}{\partial s}+\frac{1}{2}\bar{b}_{22}Y_1^2\frac{\partial Y_1}{\partial s}+\bar{b}_{23}X_1Y_1\frac{\partial X_1}{\partial s}+\bar{b}_{24}X_1Y_1\frac{\partial Y_1}{\partial s} \qquad (6.40b)$$

where $\bar{a}_1=\frac{a_1}{\bar{\omega}_{th}^2}$, $\bar{b}_1=\frac{b_1}{\bar{\omega}_{th}^2}$ etc.

Neglecting transients the solution to equations (6.38) is:

$$X_1(s,\tau^*) = A_1(\tau^*)e^{i\bar{\Omega}_{th}s} + c.c. \qquad (6.41)$$
$$Y_1(s,\tau^*) = \lambda A_1(\tau^*)e^{i\bar{\Omega}_{th}s} + c.c.$$

Substituting these expressions into the right hand side of equations (6.39) it is evident that the elimination of secular terms requires $\omega_1 = 0$. The right hand side of equations (6.39) may then be written in the form:

$$A_1^2(\tau^*)m_1 e^{2i\bar{\Omega}_{th}s} + |A_1|^2\frac{n_1}{2} + c.c.$$

$$A_1^2(\tau^*)m_2 e^{2i\bar{\Omega}_{th}s} + |A_1|^2\frac{n_2}{2} + c.c. \quad \text{(see equations 6.30)}$$

The solution to equations (6.39) is:

$$X_2(s,\tau^*) = A_2(\tau^*)\, e^{i\bar{\Omega}_{th}s} + A_1^2(\tau^*)u_1 e^{2i\bar{\Omega}_{th}s} + |A_1(\tau^*)|^2\frac{v_1}{2} + c.c. \qquad (6.42)$$

$$Y_2(s,\tau^*) = \lambda A_2(\tau^*)e^{i\bar{\Omega}_{th}s} + A_1^2(\tau^*)u_2 e^{2i\bar{\Omega}_{th}s} + |A_1(\tau^*)|^2\frac{v_2}{2} + c.c.$$

where $\begin{pmatrix} u_1 \\ u_2 \end{pmatrix} = \begin{pmatrix} B_5 & B_6 \\ B_7 & B_8 \end{pmatrix}\begin{pmatrix} m_1 \\ m_2 \end{pmatrix}\begin{pmatrix} v_1 \\ v_2 \end{pmatrix} = \begin{pmatrix} B_9 & B_{10} \\ B_{11} & B_{12} \end{pmatrix}\begin{pmatrix} n_1 \\ n_2 \end{pmatrix}$ (see equations 6.32)

Consider now the right hand side of equations (6.40). It is not necessary to write down the solution, but merely to suppress secular terms which will come from the "$e^{i\bar{\Omega}_{th}s}$" terms on the right hand side of equations (6.40). Substituting equations (6.42) into equations (6.40) the coefficient of the $e^{i\bar{\Omega}_{th}s}$ term on the right hand side of equation (6.40) may be written in the form;

$$\gamma_1\frac{dA_1}{d\tau^*} + A_1(\gamma_2+\gamma_3|A_1|^2) = q_1$$

$$\gamma_4\frac{dA_1}{d\tau^*} + A_1(\gamma_5+\gamma_6|A_1|^2) = q_2 \quad \text{(see equations 6.30)}$$

Referring to equation (6.33) it is seen that the elimination of secular terms requires:

$$B_1\left\{\gamma_1\frac{dA_1}{d\tau^*} + A_1(\gamma_2+\gamma_3|A_1|^2)\right\} + B_2\left\{\gamma_4\frac{dA_1}{d\tau^*} + A_1(\gamma_5+\gamma_6|A_1|^2)\right\} = 0$$

which leads to a complex amplitude equation of the form:

$$\frac{dA_1}{d\tau^*} = A_1(\eta_2-\eta_3|A_1|^2) \tag{6.43}$$

Separating out the real and imaginary parts by writing:

$$A(\tau^*) = R(\tau^*)e^{i\theta(\tau^*)} \quad \eta_2=\eta_{2r}+i\eta_{2i} \quad \eta_3=\eta_{3r}+i\eta_{3i}$$

yields:

$$\frac{dR}{d\tau^*} = R(\eta_{2r}-\eta_{3r}R^2) \qquad \text{Amplitude equation} \tag{6.44a}$$

$$\frac{d\theta}{d\tau^*} = \eta_{2i}-\eta_{3i}R^2 \qquad \text{Phase shift equation} \tag{6.44b}$$

Consider now the amplitude equation (6.44a). The coefficient of R in the equation is positive and is equal to the linear growth rate $(d\bar{\alpha}/d\bar{\omega})_{\bar{\omega}_{th}}$. The sign of the coefficient of $R^3(-\eta_{3r})$ determines whether or not the equation will have periodic solutions. This is most easily seen by writing down the solution of equation (6.44a) which is:

$$R^2(\tau^*) = \frac{\eta_{2r}/\eta_{3r}}{1+Ce^{-2\eta_{2r}\tau^*}} \qquad C \text{ constant; } R^2(0) = \frac{\eta_{2r}/\eta_{3r}}{1+C} \tag{6.45}$$

There are two cases to consider:

i) $\underline{\eta_{3r} > 0}$ $\Rightarrow R(\tau^*) \to (\eta_{2r}/\eta_{3r})^{1/2}$ as $\tau^* \to \infty$ and hence equations (6.37) show an approach to a limit cycle of the form:

$$\left.\begin{aligned}\Delta X(\tau) &= 2\left(\frac{\eta_{2r}}{\eta_{3r}}\right)^{1/2}(\bar{\omega}-\bar{\omega}_{th})^{1/2}\cos\left\{\bar{\Omega}_{th}(1+O(\bar{\omega}-\bar{\omega}_{th}))\tau\right\} + O(\bar{\omega}-\bar{\omega}_{th})\\ \Delta Y(\tau) &= 2|\lambda|\left(\frac{\eta_{2r}}{\eta_{3r}}\right)^{1/2}(\bar{\omega}-\bar{\omega}_{th})^{1/2}\sin\left\{\bar{\Omega}_{th}(1+O(\bar{\omega}-\bar{\omega}_{th}))\tau+\psi_1\right\} + O(\bar{\omega}-\bar{\omega}_{th})\end{aligned}\right\} \text{ as } \bar{\omega}\to\bar{\omega}_{th} \tag{6.46}$$

where $\psi_1 = \tan^{-1}(-\lambda_r/\lambda_i)$ $\quad \lambda = \lambda_r + i\lambda_i$

The stability of the periodic orbit follows immediately from equation (6.44a). For R less (greater) than $(\eta_{2r}/\eta_{3r})^{1/2}$, $dR/d\tau^*$ is greater (less) than zero which implies motion towards the periodic orbit (ie. stability). The period of the limit cycle is:

$$\frac{2\pi}{\bar{\Omega}_{th}}\left(1 + O(\bar{\omega}-\bar{\omega}_{th})\right) \text{ as } \bar{\omega} \to \bar{\omega}_{th} \qquad (6.47)$$

ii) $\underline{\eta_{3r} < 0}$. Equation (6.44a) implies that $dR/d\tau^* > 0 \; \forall \tau^*$ and there is no evolution towards a periodic orbit. The system is therefore unstable (at least as far as this scaling is concerned).

In a similar way to the method described previously, the existence of periodic orbits in the subcritical region may also be investigated. This is achieved by substituting:

$$\bar{\omega} = \bar{\omega}_{th} - \delta^2 \qquad (6.48)$$

into equations (6.27). This approach yields precisely the same amplitude equation as equation (6.44a) except the coefficient of R now has opposite sign. In this case $\eta_{2r} = -(d\bar{\alpha}/d\bar{\omega})_{\bar{\omega}_{th}} < 0$. There are two additional cases to consider:

iii) $\underline{\eta_{3r} > 0 \; \eta_{2r} < 0}$. Equation (6.45) implies that $R^2(\tau^*) \to 0$ as $\tau^* \to \infty$ ie. all states approach the equilibrium solution.

iv) $\underline{\eta_{3r} < 0 \; \eta_{2r} < 0}$. The most interesting case since the final solution depends upon the initial value of R(R(0)). A periodic solution is theoretically possible:

$$\text{ie. } R^2(\tau^*) \equiv \eta_{2r}/\eta_{3r} \quad \text{provided } R^2(0) = \eta_{2r}/\eta_{3r}$$

However, the orbit is unstable, since for $R^2(0) > \eta_{2r}/\eta_{3r}$, $dR/d\tau^*$ is always positive indicating movement away from the periodic orbit, whereas for $R^2(0) < \eta_{2r}/\eta_{3r}$, $dR/d\tau^*$ is always negative indicating movement away from the periodic orbit towards the equilibrium position.

The four possibilities for the amplitude equation are illustrated in Figure 6.2.

Having analysed the theoretical possibilities it remains to determine the value of the functions η_{2r}, η_{3r} for a particular value of ε_s. This was done by following the procedure outlined in the preceding pages. Although the calculation of η_{2r}, η_{3r} is rather tedious, it is relatively straightforward (the details are omitted for this reason).

6.4. RESULTS and DISCUSSION.

The calculated values of η_{2r},η_{3r} are shown in Table 6.1 for a range of values of ε_s. It may be seen that, once again, there are three regions of parameter space corresponding to the regions identified by bifurcation theory.

i) Region I ($0 < \varepsilon_s \leqslant 0.14$). Throughout this region $\eta_{3r} < 0$ and thus from the preceding discussion of the amplitude equation an unstable limit cycle exists for $\bar{\omega} < \bar{\omega}_{th}$ of the form:

$$\left.\begin{aligned}\Delta X(\tau) &= 2\left(\frac{\eta_{2r}}{\eta_{3r}}\right)^{1/2}(\bar{\omega}_{th}-\bar{\omega})^{1/2}\cos\left\{\bar{\Omega}_{th}\left(1+O(\bar{\omega}_{th}-\bar{\omega})\right)\tau\right\} + O(\bar{\omega}_{th}-\bar{\omega})\\ \Delta Y(\tau) &= 2|\lambda|\left(\frac{\eta_{2r}}{\eta_{3r}}\right)^{1/2}(\bar{\omega}_{th}-\bar{\omega})^{1/2}\sin\left\{\bar{\Omega}_{th}\left(1+O(\bar{\omega}_{th}-\bar{\omega})\right)\tau+\psi_1\right\}+O(\bar{\omega}_{th}-\bar{\omega})\end{aligned}\right\}\ \text{as}\ \bar{\omega}\to\bar{\omega}_{th} \qquad (6.49)$$

As far as this scaling is concerned, no periodic orbits may exist for $\bar{\omega} > \bar{\omega}_{th}$.

ii) Region II ($0.15 \leqslant \varepsilon_s \leqslant 0.74$). Throughout this region $\eta_{3r} > 0$ which implies that a stable periodic orbit of the form (6.46) bifurcates from $(\underline{X}, \bar{\omega}) = (\underline{X}_s, \bar{\omega}_{th})$ for $\bar{\omega} > \bar{\omega}_{th}$. For $\bar{\omega} < \bar{\omega}_{th}$ all states approach the equilibrium state.

iii) Region III ($0.75 \leqslant \varepsilon_s < 0.795$). Identical to region I; $\eta_{3r} < 0$ which implies that an unstable periodic orbit of the form (6.49) bifurcates from $(\underline{X},\bar{\omega}) = (\underline{X}_s,\bar{\omega}_{th})$ for $\bar{\omega} < \bar{\omega}_{th}$.

It is apparent that the method of multiple scaling as developed in this Chapter may be used to investigate the existence of periodic solu-

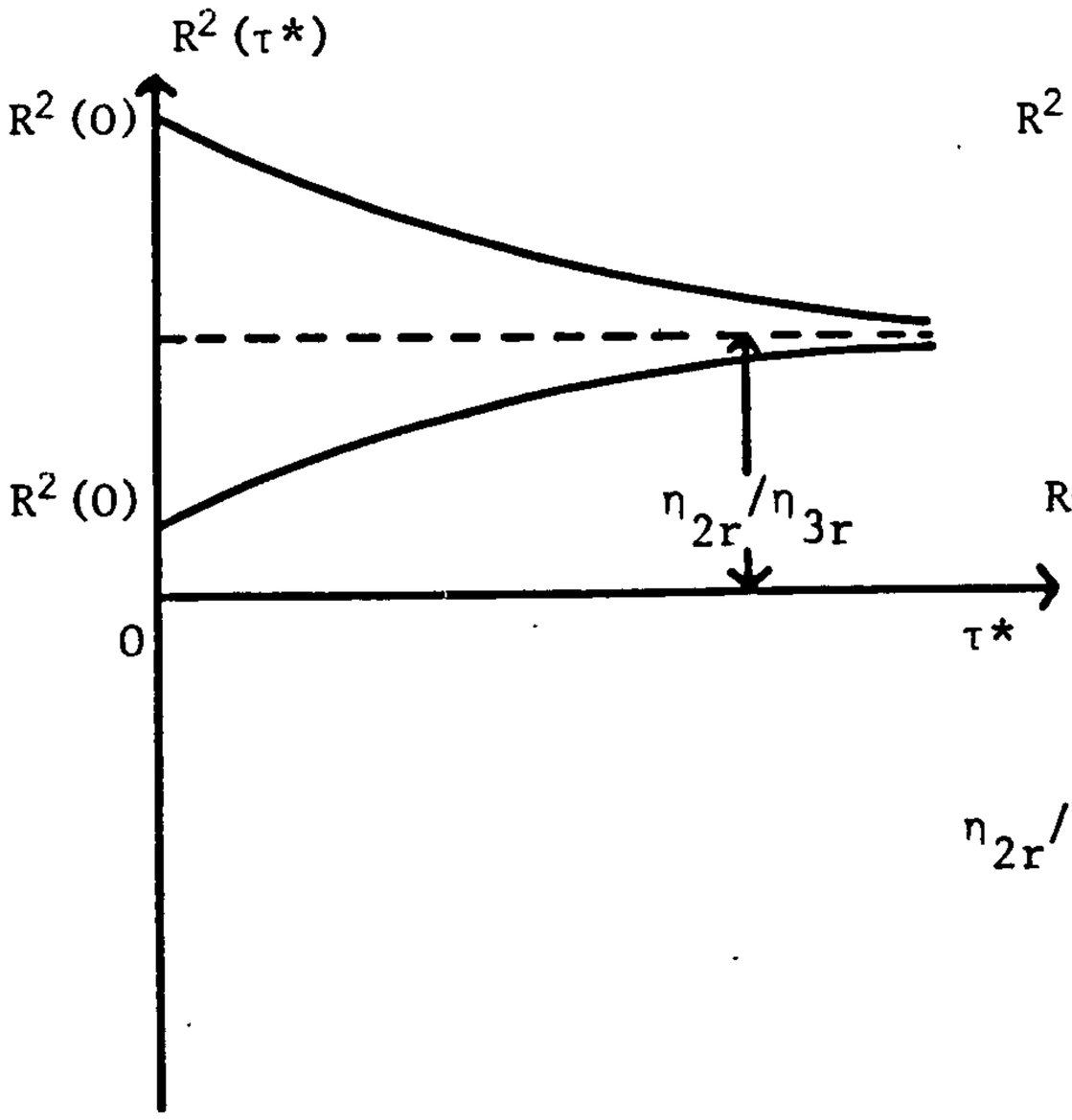

6.2(i) $\eta_{2r} > 0 \quad \eta_{3r} > 0$

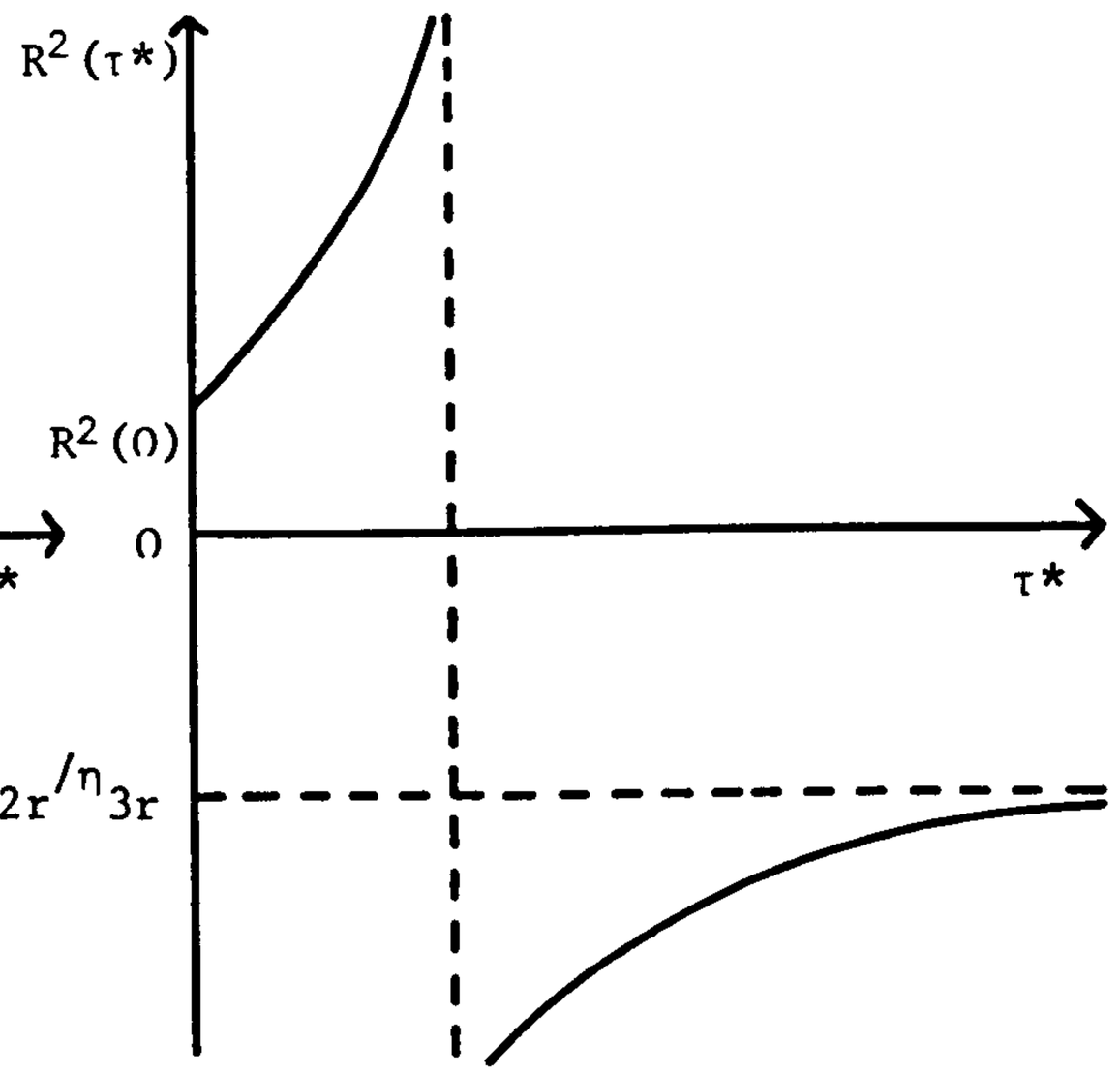

6.2(ii) $\eta_{2r} > 0 \quad \eta_{3r} < 0$

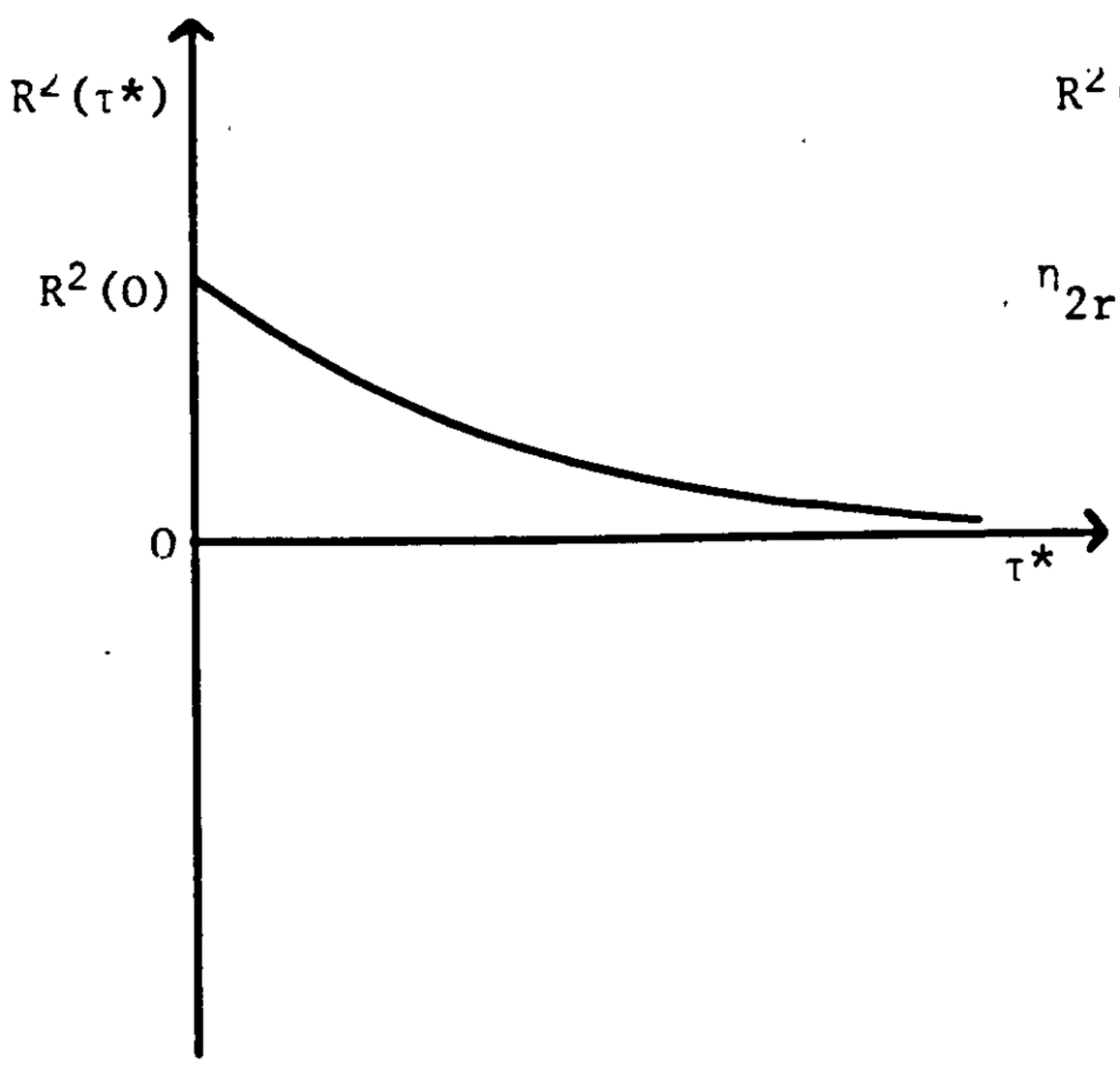

6.2(iii) $\eta_{2r} < 0 \quad \eta_{3r} > 0$

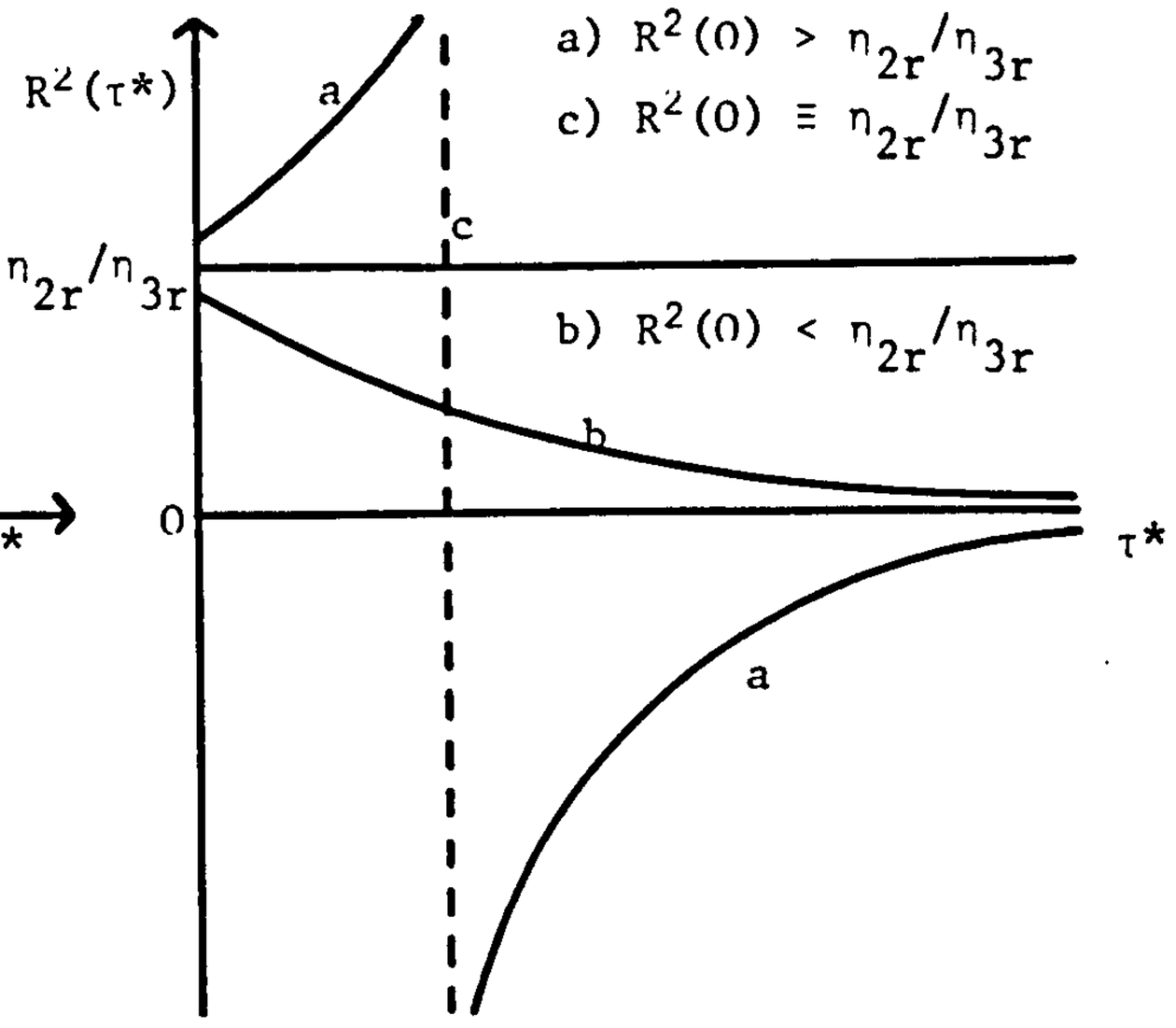

6.2(iv) $\eta_{2r} < 0 \quad \eta_{3r} < 0$

Figure 6.2. Different solutions of the amplitude equation.

ε_s	$\bar{\omega}_{th}$	$\bar{\Omega}_{th}$	$\pm\eta_{2r}$	η_{3r}	$\left\|\frac{\eta_{2r}}{\eta_{3r}}\right\|^{\frac{1}{2}}$	λ_r	λ_i	Remarks
0.01	0.94	1.15	0.04	-159.1	0.02	-0.0	-2.30	Unstable
0.05	0.94	1.15	0.19	-87.0	0.05	-0.01	-2.29	whirl orbits
0.10	0.95	1.14	0.35	-22.2	0.13	-0.01	-2.28	exist for
0.14	0.96	1.13	0.45	-2.66	0.17	-0.01	-2.26	$\bar{\omega} < \bar{\omega}_{th}$
0.15	0.96	1.13	0.47	0.41	1.03	-0.01	-2.26	
0.20	0.98	1.11	0.54	8.41	0.25	-0.02	-2.23	Stable
0.30	1.03	1.07	0.55	13.53	0.20	-0.03	-2.13	whirl
0.40	1.10	1.02	0.46	11.35	0.20	-0.04	-1.98	orbits
0.50	1.21	0.96	0.35	8.01	0.21	-0.05	-1.76	exist for
0.60	1.37	0.88	0.23	4.71	0.22	-0.09	-1.45	$\bar{\omega} > \bar{\omega}_{th}$
0.70	1.73	0.72	0.10	1.42	0.27	-0.16	-1.01	
0.74	2.13	0.60	0.05	0.09	0.75	-0.21	-0.77	
0.75	2.31	0.55	0.04	-0.22	0.43	-0.22	-0.70	Unstable
0.76	2.57	0.50	0.03	-0.50	0.24	-0.24	-0.61	whirl orbits
0.77	2.98	0.43	0.02	-0.72	0.17	-0.25	-0.52	exist for
0.78	3.77	0.35	0.01	-0.81	0.11	-0.27	-0.40	$\bar{\omega} < \bar{\omega}_{th}$
0.79	6.43	0.20	0.0	-0.54	0.0	-0.29	-0.23	

Table 6.1. Results obtained from the method of multiple scaling.

tions of the equations which describe the motion of a journal supported in fluid film journal bearings. It is interesting to note that the results obtained in this Chapter are in agreement with those obtained using bifurcation theory. The Hopf bifurcation theorem is a more rigorous mathematical method, since it is primarily an existence theorem. However, the method of multiple scaling is spectacularly successful here, if only for its simplicity. The method also describes the evolution from the equilibrium position to the periodic orbit through an amplitude equation. The stability of the orbit is easily deduced from the amplitude equation. The amount of algebra involved in calculating the terms in the amplitude equation is roughly equivalent to using Poore's bifurcation formula (see Chapter 5).

6.5. CONCLUSIONS.

i) The method of multiple scaling, as described in this Chapter, may be used to establish the existence of small amplitude periodic solutions to equations which describe the motion of a rotor supported in fluid film journal bearings.

ii) The evolution from the equilibrium position to the periodic orbit is governed by an amplitude equation. It is easily deduced from the amplitude equation that whirl orbits which exist above the threshold speed are stable, whereas whirl orbits below the threshold speed are unstable. It is also apparent that both types of orbit cannot occur simultaneously.

iii) For the particular model studied, it was found that the type of orbit which occurs is dependent upon the value of the steady state eccentricity ratio. The regions of parameter space identified by this method correspond exactly to those obtained using bifurcation theory.

CHAPTER 7

THE METHOD OF AVERAGING AND ITS APPLICATION TO THE EQUATIONS GOVERNING OIL WHIRL IN FLUID FILM JOURNAL BEARINGS.

The method of averaging has been developed by Lund (1966), and Lund and Saibel (1967) to solve the equations governing oil whirl in short journal bearings. In this Chapter Lund's technique is used to solve the equations of motion for a long bearing assumed to be operating with a half film. The results are compared with those derived in the previous two Chapters. There then follows a discussion on the validity of this method and an analysis of Lund's results for the short bearing.

7.1 THE PRINCIPLE of the METHOD of AVERAGING.

To discuss briefly the principle of the method of averaging consider the general weakly nonlinear second order equation:

$$\frac{d^2x}{dt^2} + \omega_o^2 x = \bar{\mu} f\left(x, \frac{dx}{dt}\right) \tag{7.1}$$

in which $\bar{\mu}$ is a small parameter and ω_o is a constant. The solution of the equation for $\bar{\mu} = 0$ is:

$$x = a\cos(\omega_o t+\theta) \qquad a,\theta \text{ constant} \tag{7.2}$$

To determine an approximate solution for $\bar{\mu}$ small, but non-zero, assume a solution of the form (7.2), but with a,θ now time dependent.

$$\text{ie.} \quad x = a(t)\cos(\omega_o t+ \theta(t)) \tag{7.3}$$

and subject to the condition that:

$$\frac{dx}{dt} = -\omega_o a(t)\sin(\omega_o t+\theta(t)) \tag{7.4}$$

$$\Rightarrow \frac{da}{dt}\cos(\omega_o t+\theta(t)) - a\frac{d\theta}{dt}\sin(\omega_o t+\theta(t)) = 0 \tag{7.5}$$

Differentiating equation (7.4), making use of equation (7.5) and substituting into equation (7.1) yields:

$$\omega_o \frac{da}{dt} \sin s + a\omega_o \frac{d\theta}{dt} \cos s = -\bar{\mu} f(a \cos s, -a\omega_o \sin s) \qquad (7.6)$$

$$(s=\omega_o t+\theta(t))$$

Equation (7.6) may be combined with equation (7.5) to yield:

$$\frac{da}{dt} = -\frac{\bar{\mu}}{\omega_o} \sin s \, f(a \cos s, -a\omega_o \sin s) \qquad (7.7)$$

$$\frac{d\theta}{dt} = -\frac{\bar{\mu}}{a\omega_o} \cos s \, f(a \cos s, -a\omega_o \sin s)$$

Equations (7.7) represent two first order ordinary differential equations for the amplitude a and the phase θ. The right hand sides of these equations are periodic in s:

$$\Rightarrow \frac{da}{dt} = O(\bar{\mu}), \quad \frac{d\theta}{dt} = O(\bar{\mu})$$

Therefore, a and θ are slowly varying functions of time which implies that they will change very little over the period $0 \leq s \leq 2\pi$. Averaging equations (7.7) over a cycle and taking a and θ to be constant on the right hand side (as a first approximation) yields:

$$\frac{da}{dt} = -\frac{\bar{\mu}}{2\pi\omega_o} \int_o^{2\pi} \sin s \, f(a \cos s, -a\omega_o \sin s) ds \qquad (7.8)$$

$$\frac{d\theta}{dt} = -\frac{\bar{\mu}}{2\pi\omega_o a} \int_o^{2\pi} \cos s \, f(a \cos s, -a\omega_o \sin s) ds \qquad (7.9)$$

As an example consider Duffing's equation:

$$\frac{d^2x}{dt^2} + \omega_o^2 x = -\bar{\mu} x^3 \qquad \Rightarrow f(x,\dot{x}) = -x^3 \qquad (7.10)$$

Equations (7.8) and (7.9) imply that:

$$\frac{da}{dt} = 0 \Rightarrow a = a_o \text{(constant)} \text{ and } \frac{d\theta}{dt} = \frac{3a^2}{8\omega_o}\bar{\mu} \Rightarrow \theta = \frac{3a^2}{8\omega_o}\bar{\mu}t$$

$$\Rightarrow x(t,\bar{\mu}) = a_o \cos\left\{\omega_o\left(1 + \frac{3a^2}{8\omega_o^2}\bar{\mu}\right)t\right\} + O(\bar{\mu})$$

The basic technique for the method of averaging is due to Krylov and Bogoliubov (1947). A more recent and formal approach was developed by Bogoliubov and Mitropolsky (1961). The method has been discussed comprehensively by Nayfeh (1972).

7.2 APPLICATION TO OIL WHIRL.

With the co-ordinate system as described in Chapter 5 the equations of motion are (see equations 5.7):

$$\ddot{X} = \frac{S}{\bar{\omega}^2}\bar{F}_X(X,Y,\dot{X},\dot{Y},S) \qquad \ddot{Y} = \frac{S}{\bar{\omega}^2}\bar{F}_Y(X,Y,\dot{X},\dot{Y},S) \tag{7.11}$$

$$\text{with } S = S(\varepsilon_s) = \sigma\bar{\omega}$$

To apply the method of averaging to equations (7.11) it is necessary to write them in a suitable form and to consider briefly the linearised equations. Transforming the origin of the X-Y co-ordinate system from the bearing centre to the steady state equilibrium position (Figure 7.1) and replacing $\bar{\omega}^2$ by the non-dimensional mass $\bar{m}$ the equations of motion become:

$$\bar{m}\Delta\ddot{X} = S\bar{F}_X(\Delta X,\Delta Y,\Delta\dot{X},\Delta\dot{Y},S) \qquad \bar{m}\Delta\ddot{Y} = S\bar{F}_Y(\Delta X,\Delta Y,\Delta\dot{X},\Delta\dot{Y},S) \tag{7.12}$$

$$\text{where } \bar{m} = \frac{mc\omega^2}{F} = \varpi^2 \qquad \Delta X = X - X_s \qquad \Delta Y = Y - Y_s$$

The linearised form of the equations are:

$$\bar{m}\Delta\ddot{X} + B_{XXs}\Delta\dot{X} + B_{XYs}\Delta\dot{Y} + K_{XXs}\Delta X + K_{XYs}\Delta Y = 0 \tag{7.13}$$

$$\bar{m}\Delta\ddot{Y} + B_{YXs}\Delta\dot{X} + B_{YYs}\Delta\dot{Y} + K_{YXs}\Delta X + K_{YYs}\Delta Y = 0$$

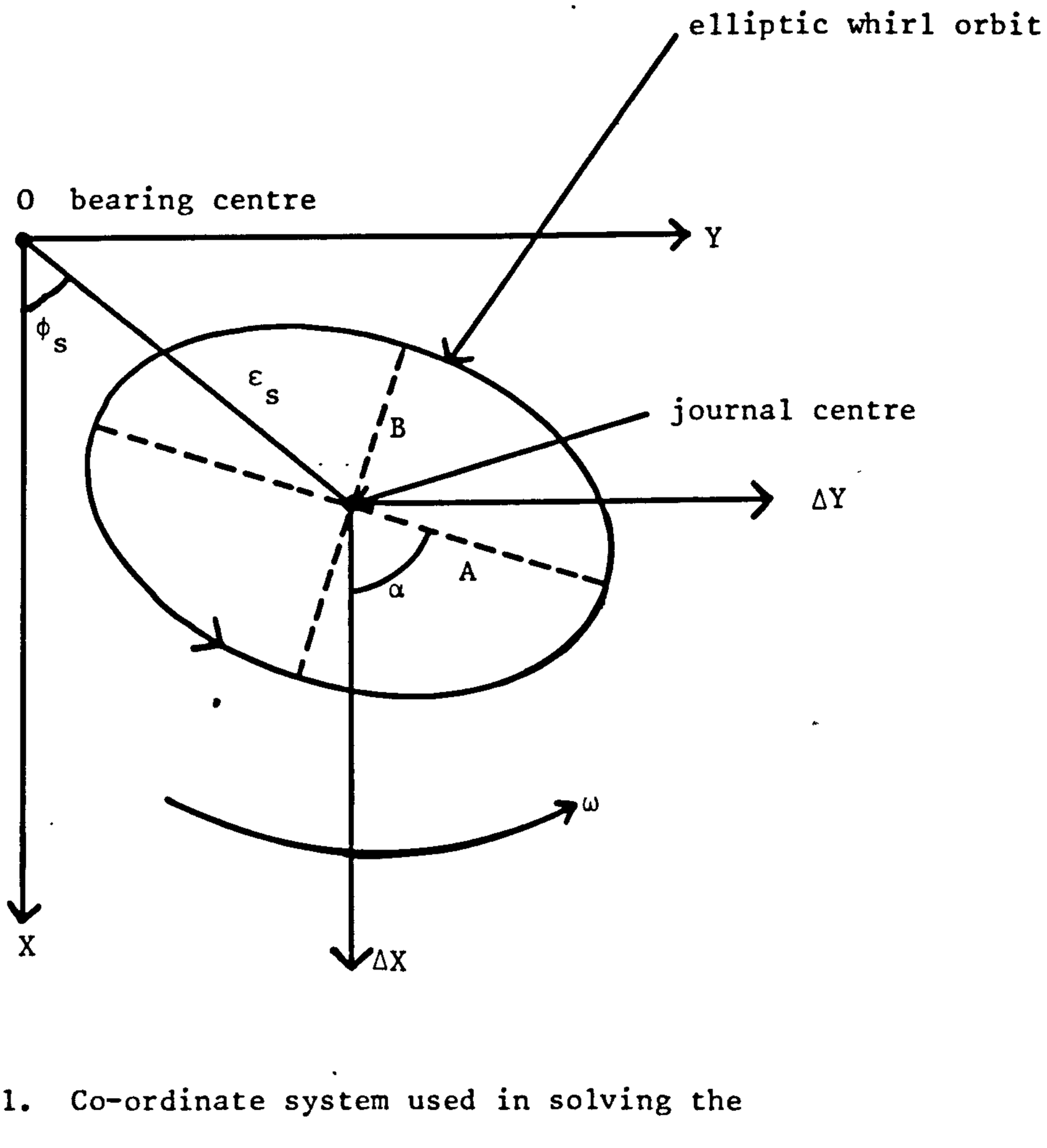

Figure 7.1. Co-ordinate system used in solving the averaged equations of motion.

nb. Nondimensional co-ordinate system is shown

$$\text{ie. } \varepsilon = \frac{e}{c} \qquad X = \frac{X^1}{c} \qquad Y = \frac{Y^1}{c} \qquad \Delta X = \frac{\Delta X^1}{c} \qquad \Delta Y = \frac{\Delta Y^1}{c}$$

The subscript s is included in the force derivatives to emphasize that they are evaluated at the steady state equilibrium position. At the threshold of instability the solution of equations (7.13) has the form:

$$\Delta X = (X_r + iX_i)e^{i\bar{\Omega}_{th}\tau} \qquad \Delta Y = (Y_r + iY_i)e^{i\bar{\Omega}_{th}\tau} \tag{7.14}$$

Substituting into equations (7.13):

$$\begin{bmatrix} (K_{XXs} - \kappa_{th} + i\bar{\Omega}_{th}B_{XXs}) & (K_{XYs} + i\bar{\Omega}_{th}B_{XYs}) \\ K_{YXs} + i\bar{\Omega}_{th}B_{YXs} & K_{YYs} - \kappa_{th} + i\bar{\Omega}_{th}B_{YYs} \end{bmatrix} \begin{bmatrix} \Delta X \\ \Delta Y \end{bmatrix} = 0 \tag{7.15}$$

$$\text{where } \kappa_{th} = \bar{m}_{th}\bar{\Omega}^2_{th} \tag{7.16}$$

κ is a spring coefficient introduced to define the oscillatory nature of the solution. A non-trivial solution to equations (7.15) implies that:

$$\kappa_{th} = \frac{\left(K_{XXs}B_{YYs} + K_{YYs}B_{XXs} - K_{XYs}B_{YXs} - K_{YXs}B_{XYs}\right)}{\left(B_{XXs} + B_{YYs}\right)} \tag{7.17}$$

$$\bar{\Omega}^2_{th} = \frac{\left\{(K_{XXs} - \kappa_{th})(K_{YYs} - \kappa_{th}) - K_{XYs}K_{YXs}\right\}}{\left(B_{XXs}B_{YYs} - B_{XYs}B_{YXs}\right)} \tag{7.18}$$

$$\bar{m}_{th} = \kappa_{th}/\bar{\Omega}^2_{th} \tag{7.19}$$

The preceding analysis of the linearised equations is equivalent to using Routh's criterion. The mode of the self-excited oscillation described by equations (7.14) may be written in the form:

$$\Delta X = X_r \cos\bar{\Omega}_{th}\tau \text{ (putting } X_i = 0) \qquad \Delta Y = Y_r \cos\bar{\Omega}_{th}\tau - Y_i \sin\bar{\Omega}_{th}\tau \tag{7.20}$$

$$\text{where } \frac{Y_r}{X_r} = -\left\{\frac{(K_{XXs} - \kappa_{th})K_{XYs} + \bar{\Omega}^2_{th}B_{XXs}B_{XYs}}{\left(K^2_{XYs} + \bar{\Omega}^2_{th}B^2_{XYs}\right)}\right\} \tag{7.21}$$

$$\frac{Y_i}{X_r} = \bar{\Omega}_{th} \left\{ \frac{(K_{XXs} - \kappa_{th})B_{XYs} - K_{XYs}B_{XXs}}{(K^2_{XYs} + \bar{\Omega}^2_{th}B^2_{XYs})} \right\} \qquad (7.22)$$

Equations (7.20) describe an elliptic whirl orbit centred at the steady state equilibrium position. Let the major semi-axis be A, the minor semi-axis be B and the angle of rotation be α, measured from the ΔX axis to the major semi-axis, positive in the direction of rotation (Figure 7.1). After some co-ordinate geometry it may be shown that:

$$\frac{A}{X_r} = \left[\frac{1}{2}\left[1+\left(\frac{Y_r}{X_r}\right)^2 + \left(\frac{Y_i}{X_r}\right)^2\right] + \left[\frac{1}{4}\left(1-\left(\frac{Y_r}{X_i}\right)^2 - \left(\frac{Y_i}{X_i}\right)^2\right)^2 + \left(\frac{Y_r}{X_r}\right)^2\right]^{1/2}\right]^{1/2} \qquad (7.23)$$

$$\frac{B}{X_r} = \pm\frac{Y_i/X_r}{A/X_r} \qquad \tan 2\alpha = \frac{2Y_r/X_r}{\left[1-\left(\frac{Y_r}{X_r}\right)^2 - \left(\frac{Y_i}{X_r}\right)^2\right]}$$

Information about the linearised whirl orbit is given in Table 7.1 for the long bearing operating with a half film.

Return now to the full equations of motion (equations 7.12) and assume that the equations admit an oscillatory solution with frequency $\bar{\Omega}$. Define a spring coefficient $\kappa = \bar{m}\bar{\Omega}^2$ and rewrite the equations as:

$$\bar{m}\Delta\bar{X}'' + \kappa\Delta X - (S\bar{F}_X + \bar{m}\bar{\Omega}^2\Delta X) = 0 \qquad (7.24)$$

$$\bar{m}\Delta\bar{Y}'' + \kappa\Delta Y - (S\bar{F}_Y + \bar{m}\bar{\Omega}^2\Delta Y) = 0$$

Comparing these equations with equation (7.1) it can be seen that it is necessary to introduce a small parameter $\bar{\mu}$ into the equations. Let the assumed oscillatory solution to equations (7.24) be:

$\Delta X = X_o$, $\Delta Y = Y_o$, $\bar{\Omega} = \bar{\Omega}_o$ and define:

$$||S\bar{F}_X|| = \frac{1}{2\pi\bar{m}\bar{\Omega}^2_o}\int_o^{2\pi} |S\bar{F}_X(X_o, Y_o, \bar{X}'_o, \bar{Y}'_o, S) + \bar{m}\bar{\Omega}^2_o X_o|\ d(\bar{\Omega}\tau) \qquad (7.25)$$

ε_s	S	$\bar{\omega}_{th}$	$\bar{\Omega}_{th}$	Y_r/X_r	Y_i/X_r	A/X_r	B/X_r	α
0.10	1.0588	0.9520	1.140	-0.0099	-2.2810	2.2810	1.0	-89.9^o
0.20	0.5258	0.9811	1.1143	-0.0146	-2.2597	2.2597	1.0	-89.8^o
0.30	0.3457	1.0306	1.0744	-0.0266	-2.1330	2.1332	0.9999	-89.6^o
0.40	0.2530	1.1028	1.0229	-0.0352	-1.9819	1.9823	0.9998	-89.3^o
0.50	0.1941	1.2053	0.9598	-0.0510	-1.760	1.7611	0.9994	-88.6^o
0.60	0.1506	1.3661	0.8752	-0.0859	-1.4492	1.4540	0.9967	-85.6^o
0.70	0.1143	1.7308	0.7210	-0.1603	-1.0121	1.0896	0.9289	-49.4^o
0.75	0.0972	2.3111	0.5541	-0.2224	-0.6964	1.0436	0.6673	-21.8^o

Table 7.1. Table of values for the linearised whirl orbit.

$$||S\bar{F}_Y|| = \frac{1}{2\pi\bar{m}\bar{\Omega}_o^2}\int_o^{2\pi}|S\bar{F}_Y(X_o,Y_o,\dot{X}_o,\dot{Y}_o,S)+\bar{m}\bar{\Omega}_o^2 Y_o|\ d(\bar{\Omega}\tau)$$

$$\bar{\mu} = (||S\bar{F}_X||^2+||S\bar{F}_Y||^2)^{1/2} \qquad (7.26)$$

The equations of motion may now be written:

$$\bar{m}\Delta\ddot{X} + \kappa\Delta X + \bar{\mu}\left\{\frac{-S\bar{F}_X-\bar{m}\bar{\Omega}^2\Delta X}{(||S\bar{F}_X||^2+||S\bar{F}_Y||^2)^{1/2}}\right\} = 0 \qquad (7.27)$$

$$\bar{m}\Delta\ddot{Y} + \kappa\Delta Y + \bar{\mu}\left\{\frac{-S\bar{F}_Y-\bar{m}\bar{\Omega}^2\Delta Y}{(||S\bar{F}_X||^2+||S\bar{F}_Y||^2)^{1/2}}\right\} = 0$$

The introduction of the small parameter $\bar{\mu}$ defined by equation (7.26) is due to Lund (1966). It is most easily understood from the following physical explanation. The assumed oscillatory solution may be written in the form:

$$X_o = a\cos\bar{\Omega}_o\tau \qquad \Rightarrow \ddot{X}_o = -\bar{\Omega}_o^2 X_o$$

$$Y_o = b\sin(\bar{\Omega}_o\tau+\xi) \qquad \Rightarrow \ddot{Y}_o = -\bar{\Omega}_o^2 Y_o$$

$$\Rightarrow |S\bar{F}_X(X_o,Y_o,\dot{X}_o,\dot{Y}_o,S) + \bar{m}_o\bar{\Omega}_o^2 X_o| = |S\bar{F}_X-\bar{m}\ddot{X}_o|$$

which represents the absolute error with which the assumed solution satisfies equations (7.12). The error is averaged over a cycle and normalised with respect to $\bar{m}\bar{\Omega}_o^2$ to conform with the overall strategy of the method of averaging. The smallness of the parameter $\bar{\mu}$ can be measured by comparing its value to the amplitude of the motion. Conversely, the error in the calculated results for the amplitudes will be of order $\bar{\mu}$. Having established an error criterion it is possible to solve the equations of motion approximately by using the method of averaging. Define the co-ordinate transformation:

$$\Delta X = c + X_r(\tau)\cos\bar{\Omega}\tau - X_i(\tau)\sin\bar{\Omega}\tau \qquad (7.28)$$

$$\Delta Y = d + Y_r(\tau)\cos\bar{\Omega}\tau - Y_i(\tau)\sin\bar{\Omega}\tau$$

with $$\Delta\dot{X} = -\bar{\Omega}X_r(\tau)\sin\bar{\Omega}\tau - \bar{\Omega}X_i(\tau)\cos\bar{\Omega}\tau \qquad (7.29)$$

$$\Delta\dot{Y} = -\bar{\Omega}Y_r(\tau)\sin\bar{\Omega}\tau - \bar{\Omega}Y_i(\tau)\cos\bar{\Omega}\tau$$

Comparing equations (7.28) and (7.29) leads to the compatibility conditions:

$$\dot{X}_r\cos\bar{\Omega}\tau - \dot{X}_i\sin\bar{\Omega}\tau = 0 \qquad (7.30)$$

$$\dot{Y}_r\cos\bar{\Omega}\tau - \dot{Y}_i\sin\bar{\Omega}\tau = 0$$

Using equations (7.28) and (7.29) the equations of motion (7.12) become:

$$-\bar{\Omega}^2X_r\cos\bar{\Omega}\tau + \bar{\Omega}^2X_i\sin\bar{\Omega}\tau - \bar{\Omega}\dot{X}_r\sin\bar{\Omega}\tau - \bar{\Omega}\dot{X}_i\cos\bar{\Omega}\tau = \frac{\bar{S}}{\bar{m}}\bar{F}_X \qquad (7.31)$$

$$-\bar{\Omega}^2Y_r\cos\bar{\Omega}\tau + \bar{\Omega}^2Y_i\sin\bar{\Omega}\tau - \bar{\Omega}\dot{Y}_r\sin\bar{\Omega}\tau - \bar{\Omega}\dot{Y}_i\cos\bar{\Omega}\tau = \frac{\bar{S}}{\bar{m}}\bar{F}_Y$$

Combining equations (7.31) with (7.30) produces a system of four first order ordinary differential equations:

$$\dot{X}_r = -\bar{\Omega}X_r\cos\bar{\Omega}\tau\sin\bar{\Omega}\tau + \bar{\Omega}X_i\sin^2\bar{\Omega}\tau - \frac{\bar{S}}{\bar{m}\bar{\Omega}}\bar{F}_X\sin\bar{\Omega}\tau$$

$$\dot{X}_i = -\bar{\Omega}X_r\cos^2\bar{\Omega}\tau + \bar{\Omega}X_i\cos\bar{\Omega}\tau\sin\bar{\Omega}\tau - \frac{\bar{S}}{\bar{m}\bar{\Omega}}\bar{F}_X\cos\bar{\Omega}\tau \qquad (7.32)$$

$$\dot{Y}_r = -\bar{\Omega}Y_r\cos\bar{\Omega}\tau\sin\bar{\Omega}\tau + \bar{\Omega}Y_i\sin^2\bar{\Omega}\tau - \frac{\bar{S}}{\bar{m}\bar{\Omega}}\bar{F}_Y\sin\bar{\Omega}\tau$$

$$\dot{Y}_i = -\bar{\Omega}Y_r\cos^2\bar{\Omega}\tau + \bar{\Omega}Y_i\cos\bar{\Omega}\tau\sin\bar{\Omega}\tau - \frac{\bar{S}}{\bar{m}\bar{\Omega}}\bar{F}_Y\cos\bar{\Omega}\tau$$

Assuming that the equations permit a stationary periodic motion with period $2\pi/\bar{\Omega}$, then the requirement that the motion be stationary implies that:

$$X_r(\tau) = X_r\left(\tau + \frac{2\pi}{\bar{\Omega}}\right) \text{ and similarly for } X_i, Y_r, Y_i.$$

Thus, the averaged values of $\dot{X}_r, \dot{Y}_r, \dot{X}_i, \dot{Y}_i$ must vanish over a cycle:

$$\text{ie. } \bar{\dot{X}}_r = \frac{1}{2\pi}\int_0^{2\pi} \dot{X}_r\, d(\bar{\Omega}\tau) = 0 \text{ etc.} \qquad (7.33)$$

Since the righthand sides of equations (7.32) are proportional to $\bar{\mu}$ (see equations 7.25 and 7.26), it follows that $\dot{X}_r, \dot{X}_i, \dot{Y}_r, \dot{Y}_i$ are small quantities such that X_r, X_i, Y_r, Y_i are slowly varying functions of time during the period $2\pi/\bar{\Omega}$. As a first approximation, therefore, they may be considered constant. Thus:

$$\bar{X}_r = \frac{1}{2}\bar{\Omega}X_i - \frac{1}{2\pi\bar{m}\bar{\Omega}}\int_0^{2\pi} S\bar{F}_X \sin s \, ds = 0 \text{ where } s = \bar{\Omega}\tau \qquad (7.34)$$

(and similarly for $\bar{X}_i, \bar{Y}_r, \bar{Y}_i$).

It is seen from equation (7.28) that the journal motion describes an ellipse with centre (c,d). Thus, an allowance is made in the theory for the centre of the elliptic whirl orbit to move away from the equilibrium position.

Analagous to requiring the averaged values of the velocities $\Delta\bar{X}'$ and $\Delta\bar{Y}'$ to be zero over a cycle in order for the whirl orbit to be stationary, a similar requirement may be imposed on the averaged values of $\Delta\bar{X}''$, $\Delta\bar{Y}''$.

$$\text{ie. } \overline{\Delta\bar{X}''} = \frac{1}{2\pi}\int_0^{2\pi} \Delta\bar{X}'' ds = \frac{1}{2\pi\bar{m}}\int_0^{2\pi} S\bar{F}_X ds = 0 \qquad (7.35)$$

(and similarly for $\bar{Y}''$).

Thus, there are six equations in seven unknowns:- $X_r, X_i, Y_r, Y_i, \bar{\Omega}, c, d$. The missing equation is a relationship removing the arbitrariness in defining the origin of the time scale. For convenience put $X_i = 0$.

The six equations are:

$$(\bar{X}_r = 0) \qquad \frac{1}{\pi}\int_0^{2\pi} S\bar{F}_X \sin s \, ds = 0 \qquad (7.36i)$$

$$(\bar{X}_i = 0) \quad \bar{m}\bar{\Omega}^2 X_r + \frac{1}{\pi}\int_0^{2\pi} S\bar{F}_X \cos s \, ds = 0 \qquad (7.36ii)$$

$$(\bar{Y}_r = 0) \quad -\bar{m}\bar{\Omega}^2 Y_i + \frac{1}{\pi}\int_0^{2\pi} S\bar{F}_Y \sin s \, ds = 0 \qquad (7.36iii)$$

$$(\bar{Y}_i' = 0) \quad \bar{m}\bar{\Omega}^2 Y_r + \frac{1}{\pi}\int_0^{2\pi} S\bar{F}_Y \cos s \, ds = 0 \qquad (7.36iv)$$

$$(\overline{\Delta\bar{X}''} = 0) \qquad \frac{1}{\pi}\int_0^{2\pi} S\bar{F}_X ds = 0 \qquad (7.36v)$$

$$(\overline{\Delta\bar{Y}''} = 0) \qquad \frac{1}{\pi}\int_0^{2\pi} S\bar{F}_Y ds = 0 \qquad (7.36vi)$$

The six unknowns are:

$$X_r, Y_r, Y_i, \bar{\Omega}, c, d \qquad (7.37)$$

Method of Solution.

Equations (7.36) are a system of six nonlinear algebraic equations. They were solved using Newton's iterative procedure. An initial trial solution was estimated; $X_r = X_{r1}$, $Y_r = Y_{r1}$, $\bar{\Omega} = \bar{\Omega}_1$, $c = c_1$, $d = d_1$, $Y_i = Y_{i1}$. The functions in equations (7.36) were then expanded as a first order Taylor series about the initial estimate (by substituting $X_r = X_{r1} + \delta X_{r1}$, $Y_r = Y_{r1} + \delta Y_{r1}$, $Y_i = Y_{i1} + \delta Y_{i1}$, $\bar{\Omega} = \bar{\Omega}_1 + \delta\bar{\Omega}_1$, $c = c_1 + \delta c_1$, $d = d_1 + \delta d_1$). Consider, for example, the first equation of equations (7.36), which becomes an expanding about the initial estimate:

$$-\left\{\delta X_{r1}\frac{\partial}{\partial X_r} + \delta Y_{r1}\frac{\partial}{\partial Y_r} + \delta Y_{i1}\frac{\partial}{\partial Y_i} + \delta\bar{\Omega}_1\frac{\partial}{\partial\bar{\Omega}} + \delta c_1\frac{\partial}{\partial c} + \delta d_1\frac{\partial}{\partial d}\right\}$$

$$\left(\frac{1}{\pi}\int_o^{2\pi} S\bar{F}_X \sin s\, ds\right)_1 = \left(\frac{1}{\pi}\int_o^{2\pi} S\bar{F}_X \sin s\, ds\right)_1$$

Introduce the following notition:

$$K_{XX1} = \frac{1}{\pi}\int_o^{2\pi} K_{XX}\cos^2 s\, ds \qquad K_{XX2} = \frac{1}{\pi}\int_o^{2\pi} K_{XX}\sin^2 s\, ds$$

$$K_{XX3} = \frac{1}{\pi}\int_o^{2\pi} K_{XX}\cos s \sin s\, ds \qquad K_{XX4} = \frac{1}{\pi}\int_o^{2\pi} K_{XX}\cos s\, ds \quad (7.38)$$

$$K_{XX5} = \frac{1}{\pi}\int_o^{2\pi} K_{XX}\sin s\, ds \qquad K_{XX6} = \frac{1}{\pi}\int_o^{2\pi} K_{XX}\, ds$$

(and similarly for B_{XX} etc.)

Using equations (7.28) and (7.29) the equation may be written in the form:

$$(K_{XX3}-\bar{\Omega}B_{XX2})_1\delta X_r + (K_{XY3}-\bar{\Omega}B_{XY2})_1\delta Y_r - (K_{XY2}+\bar{\Omega}B_{XY3})_1\delta Y_i$$

$$-(X_r B_{XX2}+Y_r B_{XY2}+Y_i B_{XY3})_1\delta\bar{\Omega} + (K_{XX5})_1\delta c + (K_{XY5})_1\delta d = \left(\frac{1}{\pi}\int_o^{2\pi} S\bar{F}_X \sin s\, ds\right)_1$$

The remaining five equations were treated similarly and yield:

$$(-\bar{m}\bar{\Omega}^2 + K_{XX1} - \bar{\Omega}B_{XX3})_1\delta X_r + (K_{XY1}-\bar{\Omega}B_{XY3})_1\delta Y_r - (K_{XY3}+\bar{\Omega}B_{XY1})_1\delta Y_i$$

$$-(2\bar{m}\bar{\Omega}X_r + X_r B_{XX3} + Y_r B_{XY3} + Y_i B_{XY1})_1\delta\bar{\Omega} + (K_{XX4})_1\delta c + (K_{XY4})_1\delta d$$

$$= (\bar{m}\bar{\Omega}^2 X_r)_1 + \left(\frac{1}{\pi}\int_o^{2\pi} S\bar{F}_X \cos s\, ds\right)_1$$

$$(K_{YX3}-\bar{\Omega}B_{YX2})_1\delta X_r + (K_{YY3}-\bar{\Omega}B_{YY2})_1\delta Y_r + (\bar{m}\bar{\Omega}^2-K_{YY2}-\bar{\Omega}B_{YY3})_1\delta Y_i$$

$$+ (2\bar{m}\bar{\Omega}Y_i-X_rB_{YX2}-Y_rB_{YY2}-Y_iB_{YY3})_1\delta\bar{\Omega} + (K_{YX5})_1\delta c + (K_{YY5})_1\delta d$$

$$= (-\bar{m}\bar{\Omega}^2Y_i)_1 + \left(\frac{1}{\pi}\int_o^{2\pi} S\bar{F}_Y \sin s\, ds\right)_1 \qquad (7.39)$$

$$(K_{YX1}-\bar{\Omega}B_{YX3})_1\delta X_r + (-\bar{m}\bar{\Omega}^2+K_{YY1}-\bar{\Omega}B_{YY3})_1\delta Y_r - (K_{YY3}+\bar{\Omega}B_{YY1})_1\delta Y_i$$

$$- (2\bar{m}\bar{\Omega}Y_r+X_rB_{YX3}+Y_rB_{YY3}+Y_iB_{YY1})\delta\bar{\Omega} + (K_{YX4})_1\delta c + (K_{YY4})_1\delta d$$

$$= (\bar{m}\bar{\Omega}^2Y_r)_1 + \left(\frac{1}{\pi}\int_o^{2\pi} S\bar{F}_Y \cos s\, ds\right)_1$$

$$(K_{XX4}-\bar{\Omega}B_{XX5})_1\delta X_r + (K_{XY4}-\bar{\Omega}B_{XY5})_1\delta Y_r - (K_{XY5}+\bar{\Omega}B_{XY4})_1\delta Y_i$$

$$- (X_rB_{XX5}+Y_rB_{XY5}+B_{XY4})_1\delta\bar{\Omega} + (K_{XX6})_1\delta c + (K_{XY6})_1\delta d$$

$$= \frac{1}{\pi}\left(\int_o^{2\pi} S\bar{F}_X ds\right)_1$$

$$(K_{YX4}-\bar{\Omega}B_{YX5})_1\delta X_r + (K_{YY4}-\bar{\Omega}B_{YY5})_1\delta Y_r - (K_{YY5}+\bar{\Omega}B_{YY4})_1\delta Y_i$$

$$- (X_rB_{YX5}+Y_rB_{YY5}+Y_iB_{YY4})_1\delta\bar{\Omega} + (K_{YX6})_1\delta c + (K_{YY6})_1\delta d$$

$$= \frac{1}{\pi}\left(\int_o^{2\pi} S\bar{F}_Y ds\right)_1$$

Equations (7.39) are six homogeneous linear equations which were solved for δX_{r1}, δY_{r1}, δY_{i1}, $\delta\bar{\Omega}_1$, δc_1, δd_1. The process was then repeated with $X_r = X_{r2} = X_{r1} + \delta X_{r1}$, etc. The iteration procedure was terminated when

$$\frac{|\delta X_r|+|\delta Y_r|+|\delta Y_i|+|\delta\bar{\Omega}|+|\delta c|+|\delta d|}{|X_r|+|Y_r|+|Y_i|+|\bar{\Omega}|+|c|+|d|} < 10^{-5}.$$

To solve the equations it was necessary to specify the Sommerfeld number S and the non-dimensional mass $\bar{m}$. The initial estimate for the solution had to be reasonably close to the actual solution for the scheme to be successful. The initial estimate was either based upon the solution to the linearised equations (equations 7.21 and 7.22), or by extrapolating results obtained for a slightly different value

of $\bar{m}$. Usually only 4-5 iterations were required to obtain a solution to the required accuracy.

The integrals in equation (7.39) were evaluated by numerical integration using the Trapezoidal rule:

$$\int_a^b f(x)dx \sim h\left\{\frac{1}{2}f(a)+f(a+h)+f(a+2h)+\ldots+f(a+(n-1)h)+\frac{1}{2}f(b)\right\} \qquad (7.40)$$

$$\text{where } h = \frac{(b-a)}{n}$$

The forces $\bar{F}_X$, $\bar{F}_Y$ were evaluated from the expressions:

$$\bar{F}_X = \frac{1}{S} + \bar{F}_r\cos\phi - \bar{F}_t\sin\phi \qquad \bar{F}_Y = \bar{F}_r\sin\phi + \bar{F}_t\cos\phi \qquad (7.41)$$

and the co-ordinate transformation defined by:

$$\Delta X = \varepsilon\cos\phi - \varepsilon_s\cos\phi_s \qquad \Delta Y = \varepsilon\sin\phi - \varepsilon_s\sin\phi_s \qquad \text{(Figure 7.1)}$$

$$\Rightarrow \varepsilon^2 = (\Delta X+X_s)^2 + (\Delta Y+Y_s)^2 \quad (X_s=\varepsilon_s\cos\phi_s,\ Y_s=\varepsilon_s\sin\phi_s) \qquad (7.42)$$

$$\cos\phi = \frac{\Delta X+X_s}{\varepsilon} \qquad \sin\phi = \frac{\Delta Y+Y_s}{\varepsilon}$$

$$\varepsilon' = \Delta X'\cos\phi+\Delta Y'\sin\phi \qquad \varepsilon\phi' = \Delta Y'\cos\phi-\Delta X'\sin\phi$$

Equations (7.41) and (7.42) define the forces $\bar{F}_X, \bar{F}_Y$ as functions of ΔX, ΔY, $\Delta X'$, $\Delta Y'$. In evaluating the integrals in equations (7.39) which involve $\bar{F}_X, \bar{F}_Y$, the four arguments ΔX, ΔY, $\Delta X'$, $\Delta Y'$ are given by equations (7.28) and (7.29). The force derivatives K_{XX}, B_{XX} etc. are calculated by differentiating equations (7.41) with respect to X, Y, X', Y' and using the relationships between the co-ordinate derivatives given in Appendix III (equations III.(4)). The procedure yields the following expressions:

$$B_{XX} = -S\frac{\partial\bar{F}_X}{\partial X'} = S\left\{-\frac{\partial\bar{F}_r}{\partial\varepsilon}\cos^2\phi - \frac{1}{\varepsilon}\frac{\partial\bar{F}_t}{\partial\phi}\sin^2\phi + \left(\frac{\partial\bar{F}_t}{\partial\varepsilon}+\frac{1}{\varepsilon}\frac{\partial\bar{F}_r}{\partial\phi}\right)\sin\phi\cos\phi\right\}$$

$$B_{XY} = -S\frac{\partial\bar{F}_X}{\partial Y'} = S\left\{-\frac{1}{\varepsilon}\frac{\partial\bar{F}_r}{\partial\phi}\cos^2\phi + \frac{\partial\bar{F}_t}{\partial\varepsilon}\sin^2\phi + \left(-\frac{\partial\bar{F}_r}{\partial\varepsilon}+\frac{1}{\varepsilon}\frac{\partial\bar{F}_t}{\partial\phi}\right)\sin\phi\cos\phi\right\}$$

$$B_{YX} = -S\frac{\partial\bar{F}_X}{\partial X'} = S\left\{-\frac{\partial\bar{F}_t}{\partial\varepsilon}\cos^2\phi + \frac{1}{\varepsilon}\frac{\partial\bar{F}_r}{\partial\phi}\sin^2\phi + \left(-\frac{\partial\bar{F}_r}{\partial\varepsilon}+\frac{1}{\varepsilon}\frac{\partial\bar{F}_t}{\partial\phi}\right)\sin\phi\cos\phi\right\}$$

$$B_{YY} = -S\frac{\partial \bar{F}_Y}{\partial Y'} = S\left\{-\frac{1}{\epsilon}\frac{\partial \bar{F}_t}{\partial \phi'}\cos^2\phi - \frac{\partial \bar{F}_r}{\partial \epsilon'}\sin^2\phi - \left(\frac{1}{\epsilon}\frac{\partial \bar{F}_r}{\partial \phi'} + \frac{\partial \bar{F}_t}{\partial \epsilon'}\right)\sin\phi\cos\phi\right\} \quad (7.43)$$

$$K_{XX} = -S\frac{\partial \bar{F}_X}{\partial X} = S\left\{-\frac{\partial \bar{F}_r}{\partial \epsilon}\cos^2\phi + \frac{1}{\epsilon}\left(-\bar{F}_r + \frac{\epsilon'}{\epsilon}\frac{\partial \bar{F}_t}{\partial \phi'}\right)\sin^2\phi\right.$$

$$\left. + \left(\frac{\partial \bar{F}_t}{\partial \epsilon} - \frac{1}{\epsilon}\left(\bar{F}_t + \frac{\epsilon'}{\epsilon}\frac{\partial \bar{F}_r}{\partial \phi'}\right)\right)\sin\phi\cos\phi\right\} - B_{XY}\phi'$$

$$K_{XY} = -S\frac{\partial \bar{F}_X}{\partial Y} = S\left\{\frac{1}{\epsilon}\left(\bar{F}_t + \frac{\epsilon'}{\epsilon}\frac{\partial \bar{F}_r}{\partial \phi'}\right)\cos^2\phi + \frac{\partial F_t}{\partial \epsilon}\sin^2\phi\right.$$

$$\left. + \left(-\frac{\partial \bar{F}_r}{\partial \epsilon} + \frac{1}{\epsilon}\left(\bar{F}_r - \frac{\epsilon'}{\epsilon}\frac{\partial \bar{F}_t}{\partial \phi'}\right)\right)\sin\phi\cos\phi\right\} + B_{XX}\phi'$$

$$K_{YX} = -\frac{\partial \bar{F}_Y}{\partial X} = S\left\{-\frac{\partial \bar{F}_t}{\partial \epsilon}\cos^2\phi - \frac{1}{\epsilon}\left(\bar{F}_t + \frac{\epsilon'}{\epsilon}\frac{\partial \bar{F}_r}{\partial \phi'}\right)\sin^2\phi\right.$$

$$\left. - \left(\frac{\partial \bar{F}_r}{\partial \epsilon} - \frac{1}{\epsilon}\left(\bar{F}_r - \frac{\epsilon'}{\epsilon}\frac{\partial \bar{F}_t}{\partial \phi'}\right)\right)\sin\phi\cos\phi\right\} - B_{YY}\phi'$$

$$K_{YY} = -S\frac{\partial \bar{F}_Y}{\partial Y} = S\left\{-\left(\bar{F}_r - \frac{\epsilon'}{\epsilon}\frac{\partial \bar{F}_t}{\partial \phi'}\right)\cos^2\phi + \frac{\partial F_r}{\partial \epsilon}\sin^2\phi\right.$$

$$\left. - \left(\frac{\partial \bar{F}_t}{\partial \epsilon} - \frac{1}{\epsilon}\left(\bar{F}_t + \frac{\epsilon'}{\epsilon}\frac{\partial \bar{F}_r}{\partial \phi'}\right)\right)\sin\phi\cos\phi\right\} + B_{YX}\phi'$$

The hydrodynamic forces are:

$$\bar{F}_r = -\frac{12\epsilon^2(1-2\phi')}{(2+\epsilon^2)(1-\epsilon^2)} - 6\frac{(\pi^2(2+\epsilon^2)-16)\epsilon'}{\pi(2+\epsilon^2)(1-\epsilon^2)^{3/2}} \quad (7.44)$$

$$\bar{F}_t = \frac{6\pi\epsilon(1-2\phi')}{(1-\epsilon^2)^{1/2}(2+\epsilon^2)} + \frac{24\epsilon\epsilon'}{(1-\epsilon^2)(2+\epsilon^2)} \quad \text{(see equation 3.3)}$$

and the required force derivatives are:

$$\frac{\partial \bar{F}_r}{\partial \epsilon'} = -6\frac{(\pi^2(2+\epsilon^2)-16)\epsilon'}{\pi(2+\epsilon^2)(1-\epsilon^2)^{3/2}} \qquad \frac{\partial \bar{F}_t}{\partial \epsilon'} = \frac{1}{\epsilon}\frac{\partial \bar{F}_r}{\partial \phi'} = \frac{24\epsilon}{(1-\epsilon^2)(2+\epsilon^2)}$$

$$\frac{1}{\epsilon}\frac{\partial \bar{F}_t}{\partial \phi'} = \frac{-12\pi}{(1-\epsilon^2)^{1/2}(2+\epsilon^2)} \quad (7.45)$$

$$\frac{\partial \bar{F}_r}{\partial \varepsilon} = \frac{24\varepsilon(1-2\phi')(2+\varepsilon^4)}{(2+\varepsilon^2)^2(1-\varepsilon^2)^2} + \frac{6\varepsilon\left\{(12\pi^2-64)+(12\pi^2-80)\varepsilon^2+3\pi^2\varepsilon^4\right\}\varepsilon'}{\pi(2+\varepsilon^2)^2(1-\varepsilon^2)^{5/2}}$$

$$\frac{\partial \bar{F}_t}{\partial \varepsilon} = \frac{6\pi(1-2\phi')(2-\varepsilon^2+2\varepsilon^4)}{(2+\varepsilon^2)^2(1-\varepsilon^2)^{3/2}} + \frac{24(2+\varepsilon^2+3\varepsilon^4)\varepsilon'}{(2+\varepsilon^2)^2(1-\varepsilon^2)^2}$$

A flowchart of the computer program which was written to solve equations (7.36) is given in Figure 7.2.

Stability of the Whirl Orbit.

Once a solution to the equations had been found it was necessary to determine whether or not the whirl orbit was stable. The quantities; X_r, Y_r, Y_i define the size and orientation of the elliptic whirl orbit. The stability of the orbit may be examined by forming the variational equations from equations (7.36(i),(iii),(iv)). Let $X_r = X_{ro}, Y_r = Y_{ro}$, $Y_i = Y_{io}$ satisfy equations (7.36(i),(iii),(iv)) and expand the three equations as a first order Taylor series about $X_r = X_{ro}, Y_r = Y_{ro}, Y_i = Y_{io}$ (ie. substitute $X_r = X_{ro}+\delta X_r, Y_r = Y_{ro}+\delta Y_r, Y_i = Y_{io}+\delta Y_i$). Consider, for example, equations (7.36(i)) which becomes:

$$\delta X_r' = -\frac{1}{2\pi m\bar{\Omega}}\left\{\delta X_r \frac{\partial}{\partial X_r} + \delta Y_r \frac{\partial}{\partial Y_r} + \delta Y_i \frac{\partial}{\partial Y_i}\right\}\left(\int_o^{2\pi} S\bar{F}_X \sin s \, ds\right)_o$$

$$\Rightarrow 2m\bar{\Omega}\delta X_r' = (K_{XX3}-\bar{\Omega}B_{XX2})\delta X_r + (K_{XY3}-\bar{\Omega}B_{XY2})\delta Y_r - (K_{XY2}+\bar{\Omega}B_{XY3})\delta Y_i$$

The two remaining equations are treated similarly and yield:

$$2m\bar{\Omega}\delta X_r' = (K_{YX3}-\bar{\Omega}B_{YX2})\delta X_r + (K_{YY3}-\bar{\Omega}B_{YY2})\delta Y_r - (K_{YY2}+\bar{\Omega}B_{YY3}-\bar{m}\bar{\Omega}^2)\delta Y_i$$

$$2m\bar{\Omega}\delta Y_i' = (K_{YX1}-\bar{\Omega}B_{YX3})\delta X_r + (K_{YY1}-\bar{\Omega}B_{YY3}-\bar{m}\bar{\Omega}^2)\delta Y_r - (K_{YY3}+\bar{\Omega}B_{YY1})\delta Y_i$$

The three variational equations above may be written in the form:

$$\delta X_r' = a_{11}\delta X_r + a_{12}\delta Y_r + a_{13}\delta Y_i$$

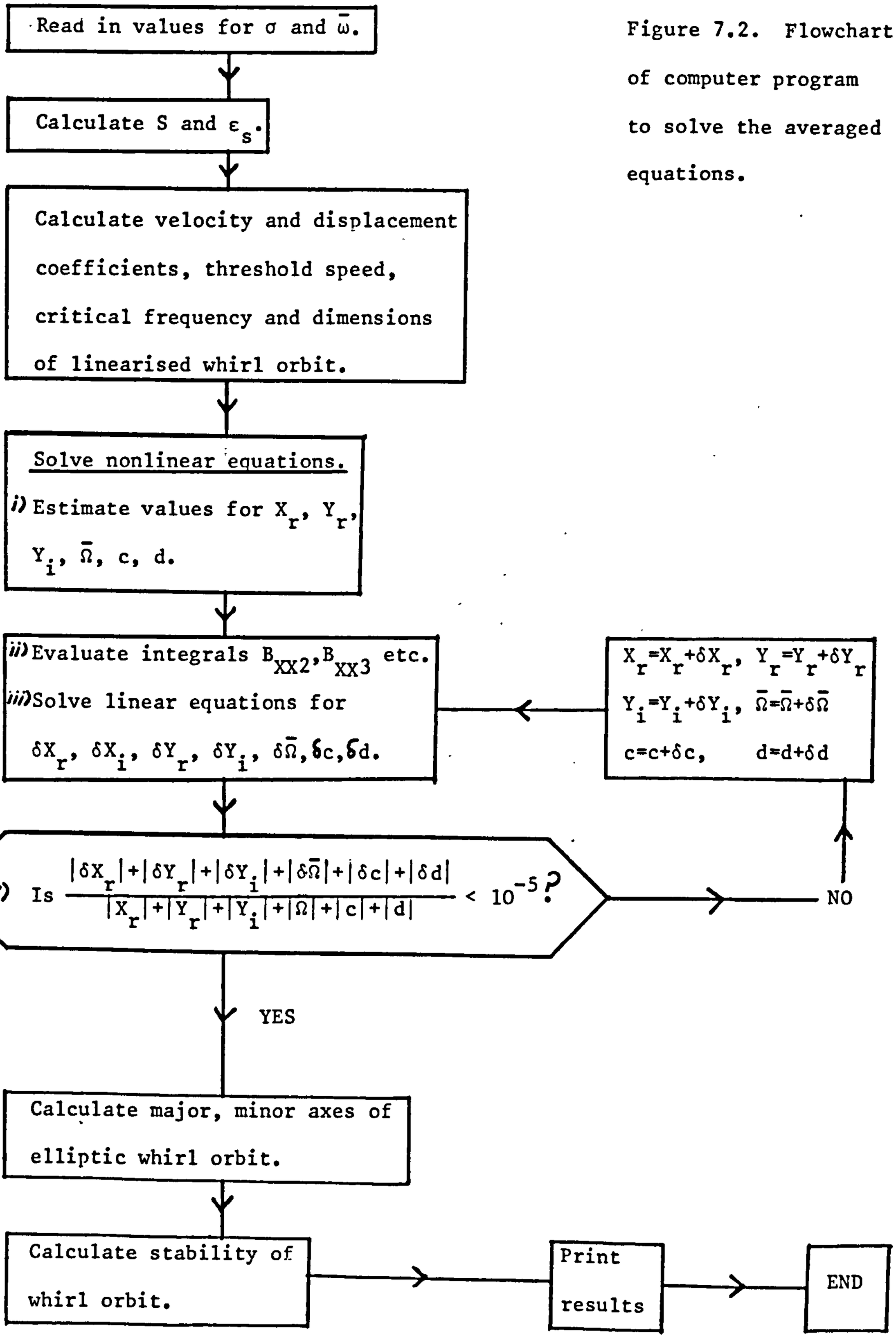

Figure 7.2. Flowchart of computer program to solve the averaged equations.

$$\delta\dot{Y}_r = a_{21}\delta X_r + a_{22}\delta Y_r + a_{23}\delta Y_i \qquad (7.46)$$

$$\delta\dot{Y}_i = a_{31}\delta X_r + a_{32}\delta Y_r + a_{33}\delta Y_i$$

The variational equations have a characteristic equation which is cubic:

$$\bar{\lambda}^3 + A_2\bar{\lambda}^2 + A_1\bar{\lambda} + A_o = 0 \qquad (7.47)$$

where $A_2 = -(a_{11}+a_{22}+a_{33})$

$$A_1 = \{(a_{11}a_{22}-a_{12}a_{21}) + (a_{11}a_{33}-a_{13}a_{31}) + (a_{22}a_{33}-a_{23}a_{32})\} \qquad (7.48)$$

$$A_o = -\{a_{11}(a_{22}a_{33}-a_{23}a_{32}) - a_{12}(a_{21}a_{33}-a_{23}a_{31}) + a_{13}(a_{21}a_{32}-a_{31}a_{22})\}$$

For the whirl orbit to be stable the perturbed solution must vanish asymptotically with time. This means the roots of the characteristic equation must have negative real parts. A necessary and sufficient condition for this to be so is provided by an application of Routh's criterion, which for a cubic equation is (Hartog (1947)):

$$A_o, A_1, A_2 > 0; \qquad R = A_1A_2 - A_o > 0 \qquad (7.49)$$

7.3 RESULTS and DISCUSSION.

In Chapter 5 a numerical investigation of three different rotor systems was carried out by introducing a system parameter σ, independent of the rotor speed defined by:

$$S = \sigma\bar{\omega}.$$

The equations were solved for σ = 0.035,0.2,2.0 (Figures 5.5,5.6,5.7) and a range of rotor speeds. To make a comparison between the method of averaging and the results obtained by numerical integration equations (7.36) were also solved for σ = 0.035,0.2,2.0. For each value of σ the equations were solved for a range of rotor speeds. The results are shown in graphic form (Figure 7.3), which illustrates the relationship between the amplitude of the elliptic whirl orbit and the rotor speed.

Figure 7.3 may be compared with the bifurcation diagrams shown in Figure 5.8. The calculated values of $X_r, Y_r, Y_i, \bar{\Omega}$, c, d etc. are given in Tables 7.2,7.3,7.4. For all three rotor systems no whirl orbits were found which were unstable. The quantity A_o, defined in equations (7.48), is included in the tables of results to represent the stability calculation.

The behaviour of a rotor with a system parameter equal to 0.035 is shown in Figure 7.3(i). A stable whirl orbit was found to exist below the threshold speed ($\bar{\omega}_{th} \approx 2.655$). The amplitude of the orbit increased (from zero) as the rotor speed was decreased away from the threshold speed. The frequency of the whirl orbit increased from its threshold value of 0.484 as the speed was decreased. It is apparent, therefore, that the whirl orbit corresponds to the subcritical bifurcated periodic orbit established in Chapter 5. This implies that there is an anomaly in the measurement of the orbit's stability (subcritical bifurcation is unstable). The stability argument used here corresponds to the one used by Lund (1966). It is discussed more fully in section 7.5.

No whirl orbits were found below a rotor speed of 2.35 (apart from the equilibrium solution). Numerical integration of the equations of motion indicated that this value was approximately 2.45 (Figure 5.8(i)). No whirl orbits were found for rotor speeds in excess of the threshold speed. The parameter $\bar{\mu}$ was zero at the threshold speed and increased gradually as the speed was reduced below the threshold speed (Table 7.2). An increase in $\bar{\mu}$ implies an increase in the error of the calculated solution.

Figure 7.3(ii) shows the whirl orbits which were found for a rotor with a system parameter equal to 0.2. No solutions were found below the threshold speed ($\bar{\omega}_{th} = 1.138$). As soon as the threshold speed was exceeded, a stable whirl orbit was found increasing in amplitude (from

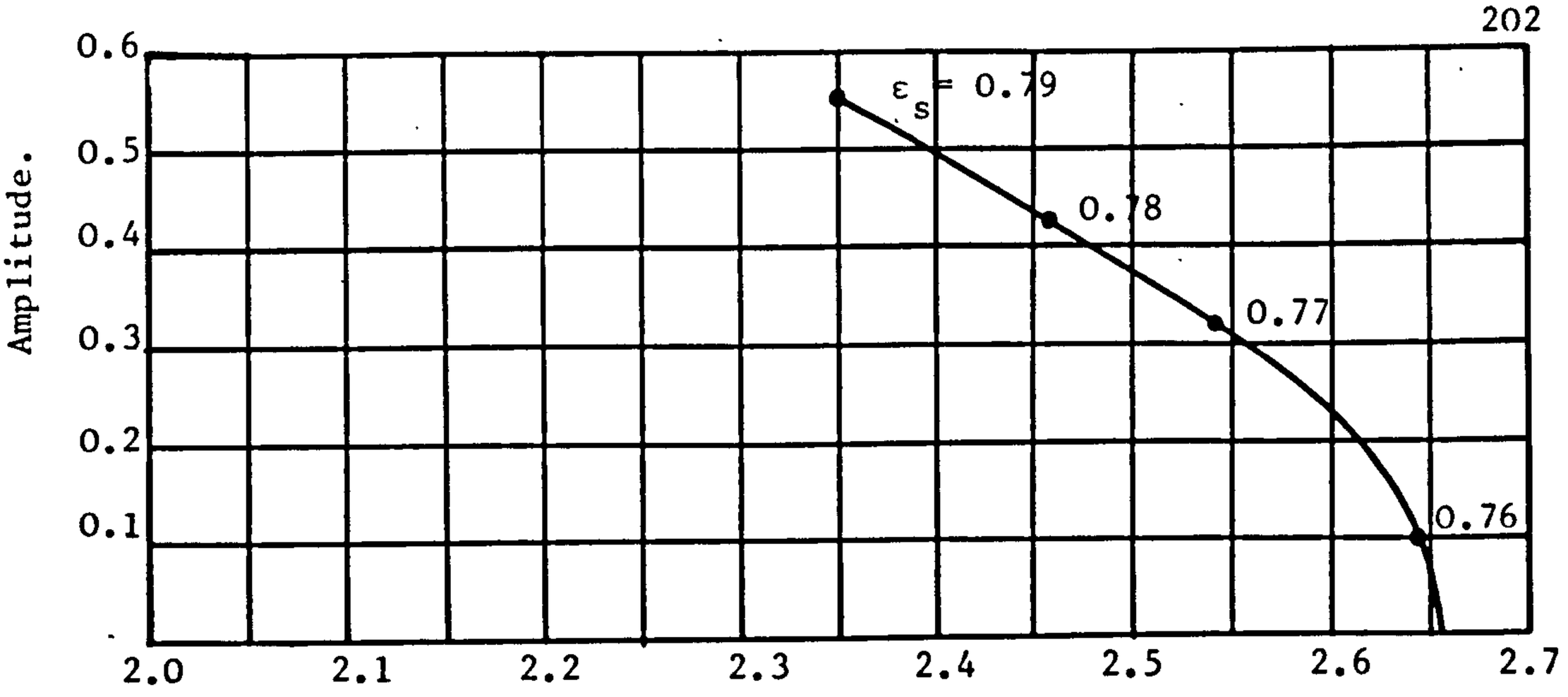

Normalised rotor speed $\bar{\omega}$.

7.3(i). System parameter = 0.035.

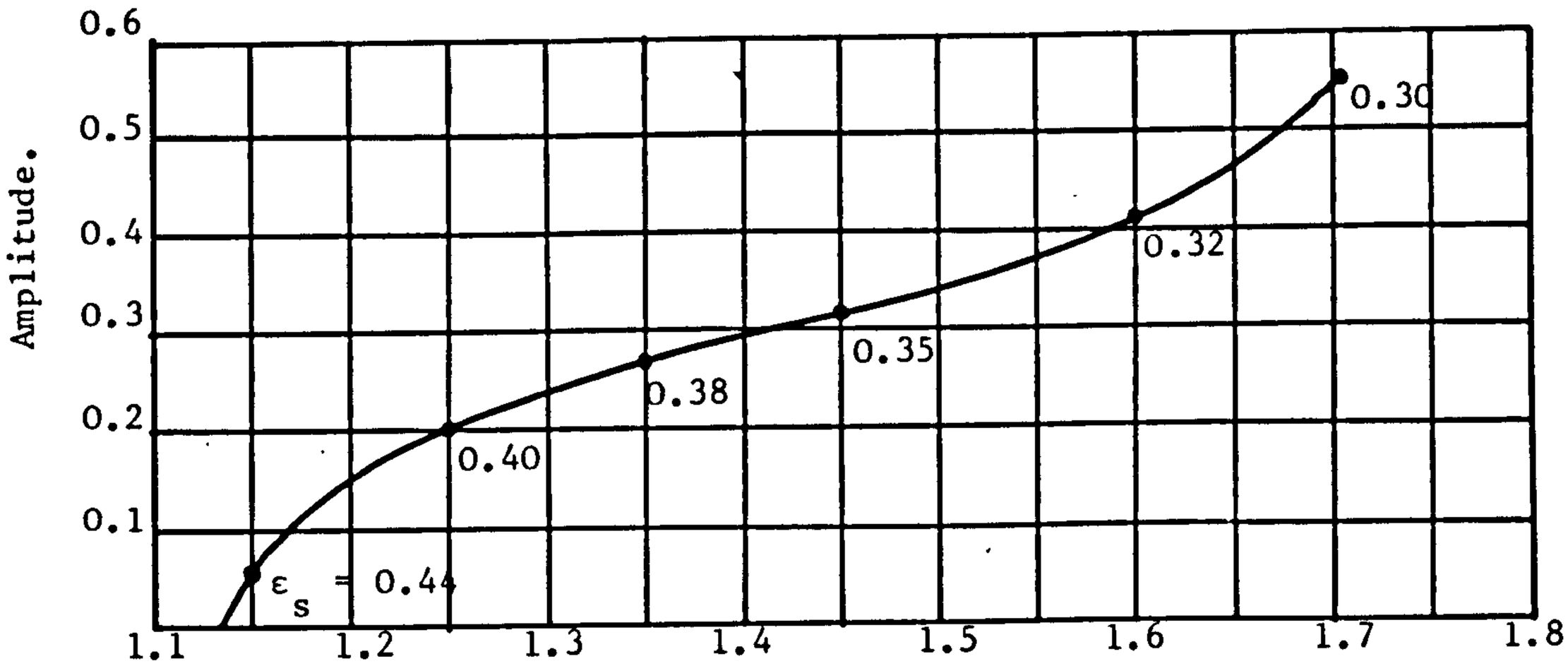

Normalised rotor speed $\bar{\omega}$.

7.3(ii). System parameter = 0.2.

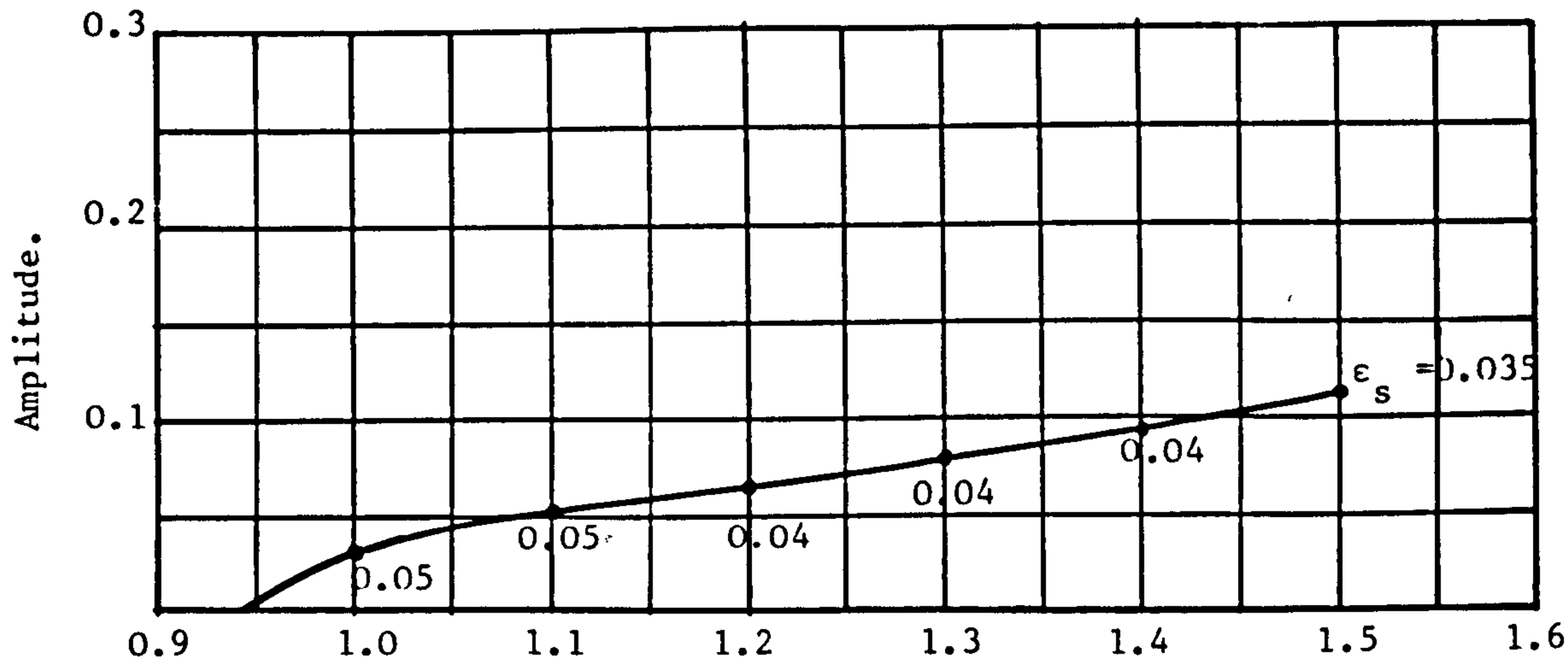

Normalised rotor speed $\bar{\omega}$.

7.3(iii). System parameter = 2.0.

Figure 7.3. Whirl amplitude as a function of the rotor speed for three different rotor-bearing systems.

$\bar{\omega}$	S	ε_s	X_r	Y_r	Y_i	$\bar{\Omega}$	c	d	A	B	α	$\bar{\mu}$	A_o
2.65	0.0927	0.7631	0.0717	-0.0177	-0.0423	0.4858	-0.0028	-0.0018	0.0748	0.0406	-19.9^o	0.0055	0.0001
2.60	0.0910	0.7682	0.2182	-0.0624	-0.1273	0.4887	-0.0257	-0.0154	0.2307	0.1204	-22.4^o	0.0488	0.0018
2.55	0.0892	0.7733	0.2926	-0.0936	-0.1698	0.4936	-0.0458	-0.0257	0.3131	0.1587	-24.4^o	0.0849	0.0045
2.50	0.0875	0.7784	0.3493	-0.1221	-0.2027	0.5003	-0.0651	-0.0345	0.3780	0.1873	-26.1^o	0.1183	0.0091
2.45	0.0857	0.7835	0.3983	-0.1495	-0.2325	0.5088	-0.0846	-0.0431	0.4358	0.2125	-27.7^o	0.1524	0.0176
2.40	0.0840	0.7886	0.4449	-0.1768	-0.2627	0.5196	-0.1054	-0.0528	0.4916	0.2378	-29.1^o	0.1931	0.0343
2.35	0.0822	0.7937	0.4937	-0.2047	-0.2980	0.5334	-0.1293	-0.0660	0.5505	0.2672	-30.4^o	0.2485	0.0733

Table 7.2. Table of results showing solutions of the averaged equations of motion for $\sigma = 0.035$

$\bar{\omega}$	S	ϵ_s	X_r	Y_r	Y_i	$\bar{\Omega}$	c	d	A	B	α	$\bar{\mu}$	A_o
1.138	0.2276	0.5486	0.0	0.0	0.0	-	0.0	0.0	0.0	0.0	-	0.0	0.0
1.15	0.230	0.4347	0.0367	-0.0016	-0.0688	0.9920	0.0010	0.0032	0.0688	0.0367	-89.0^{o}	0.010	0.0090
1.20	0.240	0.4190	0.0876	-0.005	-0.1527	0.9595	0.0051	0.0171	0.1528	0.0875	-88.3^{o}	0.0536	0.0466
1.25	0.250	0.4042	0.1238	-0.0095	-0.2007	0.9287	0.0087	0.0312	0.2011	0.1236	-87.3^{o}	0.094	0.0853
1.30	0.260	0.3904	0.1569	-0.0144	-0.2366	0.8993	0.0115	0.0455	0.2373	0.1564	-85.9^{o}	0.1328	0.1255
1.35	0.270	0.3773	0.1898	-0.0199	-0.2657	0.8712	0.0133	0.0599	0.2672	0.1887	-83.9^{o}	0.1690	0.1676
1.40	0.280	0.3651	0.2238	-0.0259	-0.2906	0.8442	0.0138	0.0742	0.2933	0.2217	-80.8^{o}	0.2026	0.2117
1.45	0.290	0.3535	0.2601	-0.0321	-0.3127	0.8183	0.0125	0.0884	0.3177	0.2560	-75.9^{o}	0.2334	0.2584
1.50	0.30	0.3427	0.30	-0.0380	-0.3331	0.7934	0.0088	0.1024	0.3423	0.2919	-67.3^{o}	0.2608	0.3098
1.60	0.320	0.3227	0.3978	-0.0445	-0.3724	0.7457	-0.0104	0.1414	0.3601	0.3601	-31.8^{o}	0.3015	0.4572
1.70	0.340	0.3048	0.5449	-0.0216	-0.4205	0.6985	-0.0641	0.1464	0.5460	0.4197	-5.6^{o}	0.3355	1.0779

Table 7.3. Table of results showing solutions of the averaged equations of motion for $\sigma = 0.2$

$\bar{\omega}$	S	ε_s	X_r	Y_r	Y_i	$\bar{\Omega}$	c	d	A	B	α	$\bar{\mu}$	A_o
0.95	1.90	0.0558	0.0043	-0.0	-0.0098	1.1429	0.0	0.0007	0.0098	0.0043	-89.9^o	0.0075	3.1275
1.0	2.00	0.0530	0.0158	-0.0	-0.0323	1.1068	0.0002	0.0079	0.0323	0.0158	-89.6^o	0.0775	48.45
1.05	2.10	0.0505	0.0235	-0.0007	-0.0433	1.0678	0.0003	0.0147	0.0433	0.0235	-89.3^o	0.1319	106.02
1.10	2.20	0.0482	0.0309	-0.0011	-0.0516	1.0290	0.0004	0.0212	0.0516	0.0309	-88.9^o	0.1731	160.6
1.20	2.40	0.0442	0.0446	-0.0021	-0.0655	0.9583	0.0002	0.0336	0.0655	0.0465	-87.4^o	0.2190	190.7
1.30	2.60	0.0408	0.646	-0.0031	-0.0786	0.9026	-0.0007	0.0460	0.0788	0.0648	-84.4^o	0.2159	212.7
1.40	2.80	0.0379	0.0872	-0.004	-0.0938	0.8598	-0.0027	0.0599	0.0943	0.0867	-75.0^o	0.1632	173.9
1.50	3.00	0.0354	0.1111	-0.0039	-0.1088	0.8254	-0.0064	0.0725	0.1122	0.1077	-30.0^o	0.1030	254.0

Table 7.4. Solutions of the averaged equations of motion for $\sigma = 2.0$

zero) with increasing speed. Above a rotor speed of 1.8 no closed orbit solution could be found - the journal approached the bearing side ($\varepsilon \to 1$). Numerical integration suggested that this value was close to 1.9 (Figure 5.8(ii)). The frequency of the whirl orbit decreased from its threshold value of 1.10 as the speed was increased. Comparing these results with those obtained in Chapter 5 (Figures 5.6,5.8(ii)) it may be seen that there is very good agreement between bifurcation theory (which predicts supercritical bifurcation), numerical integration and the method of averaging.

Comparing Figure 7.3(iii) with the results obtained in Chapter 5 for a rotor with a system parameter = 2.0 (Figures 5.7,5.8(iii)) it can be seen that there is a discrepancy in the results (bifurcation theory predicts subcritical bifurcation and numerical integration establishes that a stable whirl orbit surrounds the unstable solution). On solving the averaged equations no solutions were found below the threshold speed (Figure 7.3(iii)), but a stable whirl orbit was found above the threshold speed ($\bar{\omega}_{th} \approx 0.945$), over the speed range $0.945 \leqslant \bar{\omega} \leqslant 1.55$. The frequency of the orbit decreased from its threshold value of 1.14. In this case $\bar{\mu}$ is larger than the amplitude of the orbit (eg. at $\bar{\omega} = 1.0, A = 0.0323, \bar{\mu} = 0.0775$) and thus, there is a large error in the solution. This is one possible explanation of why there is a discrepancy, in the results for rotor speeds close to the threshold speed.

7.4 DISCUSSION OF LUND'S RESULTS.

The application of the method of averaging to the equations governing oil whirl was developed by Lund (1966), who used the technique to analyse a short bearing operating with a half film Lund also presented results in terms of a system parameter (denoted here by σ_s), which was defined as:

$$\sigma_s = \left(\frac{\bar{\omega}}{S_s}\right)^2 \qquad S_s = \text{modified Sommerfeld number.}$$

Results were shown for four different rotor systems (σ_s = 0.2,6.0, 35,200). The results are summarised in Figure 7.4 which shows the amplitude of the elliptic whirl orbit as a function of the rotor speed.

In two cases; σ_s = 6.0,35 stable whirl orbits were found for rotor speeds in excess of the threshold speed, the amplitude increasing with increasing speed. For these two rotor systems no whirl orbits were found below the threshold speed. For the two remaining systems; σ_s = 0.2,200 stable whirl orbits were found to exist just below the threshold speed. This effect is referred to by Lund as a hysteresis effect.

The fact that whirl orbits were only found either above or below the threshold speed confirms the bifurcation character of the onset of oil whirl. Lund's results suggest that a rotor supported on short journal bearings with a system parameter equal to 6.0 or 35 will exhibit supercritical bifurcation, whereas subcritical bifurcation will occur for a rotor with a system parameter equal to 0.2 or 200. It would be extremely interesting to analyse the short bearing using, either bifurcation theory, or the method of multiple scaling to determine rigorously the direction of bifurcation. This remains an area for future work.

Lund found that the whirl orbits were confined to a relatively small speed range around the threshold speed: eg. for a rotor with σ_s = 6.0 whirl orbits were found only over the speed range $2.64 \leqslant \bar{\omega} \leqslant 2.70$. This is not true of the long bearing where the whirl orbits appear to exist over a greater speed range: eg. for a rotor with σ = 0.2 whirl orbits were found over the speed range $1.14 \leqslant \bar{\omega} \leqslant 1.8$.

As for the long bearing Lund found that whirl orbits above and below the threshold speed were stable. However, as discussed in Chapter 5, subcritical bifurcation to periodic orbits is unstable.

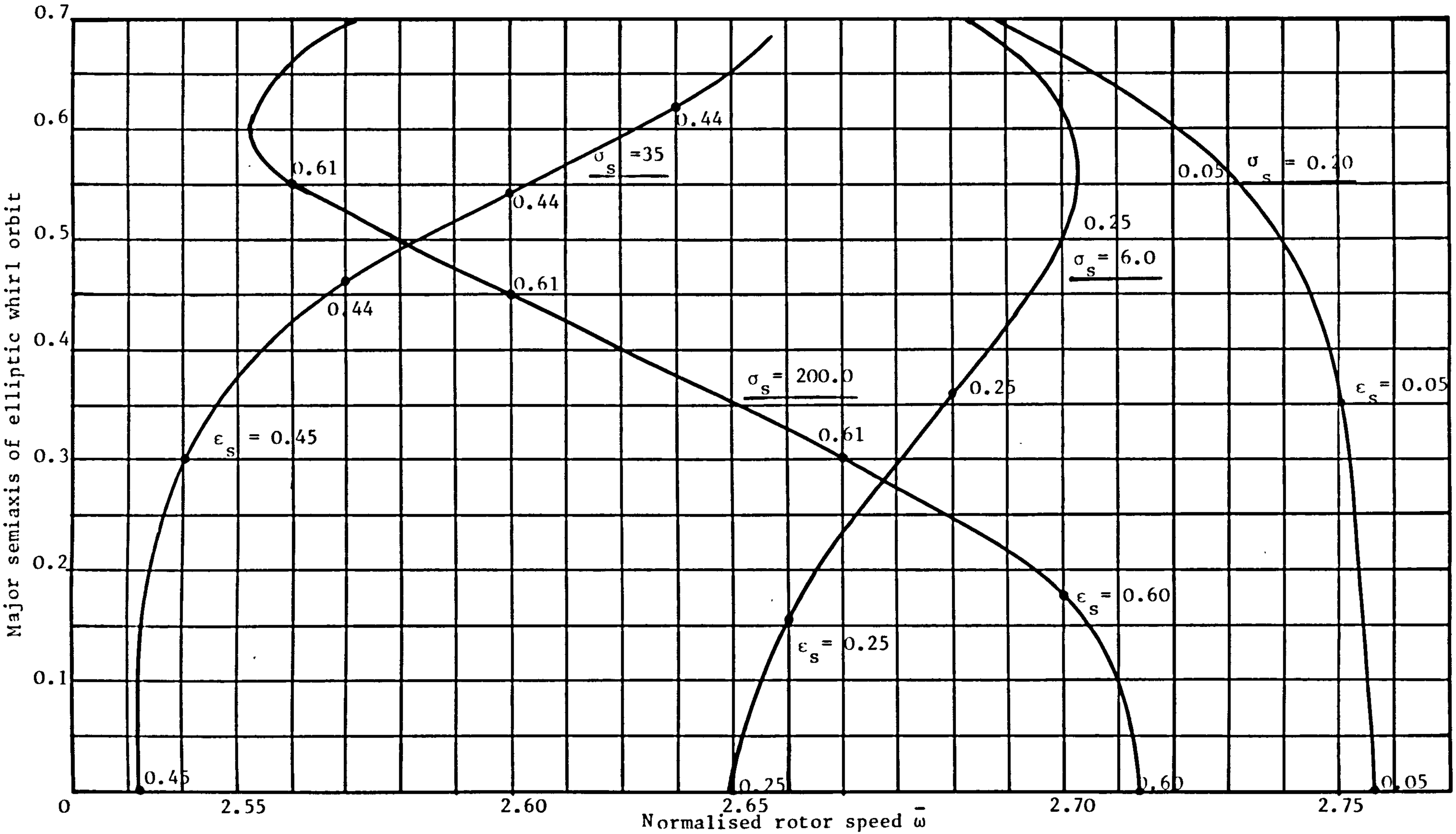

Figure 7.4. Summary of Lund's results for the short bearing.

Thus, under certain conditions, the stability argument used in the method of averaging gives incorrect results.

7.5 DISCUSSION of the STABILITY ARGUMENT.

The stability of the whirl orbit was found by forming the variational equations from the averaged equations (equations 7.36(i),(iii) (iv)). This approach yields three linear equations with constant coefficients (equation 7.46). Using this approach leads to anomaly as far as the stability of any subcritical bifurcation is concerned.

An alternative approach is to return to the original equations of motion (equations 7.11). Let the obtained solution be given by $\Delta X = X_o, \Delta Y = Y_o$. The stability of the whirl motion may be examined by forming the variational equations from equations (7.11). Substituting $\Delta X = X_o + \delta X, \Delta Y = Y_o + \delta Y$ into equations (7.11) and retaining only first order terms yields:

$$\bar{m}\delta\ddot{X} = S\bar{F}_X(X,Y,\dot{X},\dot{Y}) - S\bar{F}_X(X_o,Y_o,\dot{X}_o,\dot{Y}_o) \tag{7.50}$$

$$= S\left(\frac{\partial\bar{F}_X}{\partial X}\right)_o \delta X + S\left(\frac{\partial\bar{F}_X}{\partial Y}\right)_o \delta Y + S\left(\frac{\partial\bar{F}_X}{\partial\dot{X}}\right)_o \delta\dot{X} + S\left(\frac{\partial\bar{F}_X}{\partial\dot{Y}}\right)_o \delta\dot{Y}$$

and analogously for the $\delta\ddot{Y}$ equations. Since the force derivatives are functions of X_o and Y_o they are periodic in s with period 2π and may therefore be expanded as a Fourier series:

$$\begin{aligned}
&\bar{m}\delta\ddot{X} + \left\{\tfrac{1}{2}A_{XXO} + \sum_{n=1}^{\infty} A_{XXn}\cos(ns) + A^1_{XXn}\sin(ns)\right\}\delta X \\
&+ \left\{\tfrac{1}{2}A_{XYO} + \sum_{n=1}^{\infty} A_{XYn}\cos(ns) + A^1_{XYn}\sin(ns)\right\}\delta Y \\
&+ \left\{\tfrac{1}{2}B_{XXO} + \sum_{n=1}^{\infty} B_{XXn}\cos(ns) + B^1_{XXn}\sin(ns)\right\}\delta\dot{X} \\
&+ \left\{\tfrac{1}{2}B_{XYO} + \sum_{n=1}^{\infty} B_{XYn}\cos(ns) + B^1_{XYn}\sin(ns)\right\}\delta\dot{Y} = 0
\end{aligned} \tag{7.51}$$

where the Fourier coefficients are given by:

$$A_{XXn} = \frac{1}{\pi}\int_{o}^{2\pi} (K_{XX})_0 \cos(ns)ds \qquad A^{1}_{XXn} = \frac{1}{\pi}\int_{o}^{2\pi} (K_{XX})_0 \sin(ns)ds \quad (7.52)$$

and similarly for the remaining coefficients. This approach means that the coefficients of the $\delta X, \delta Y$ terms in equation (7.51) retain their time dependence. These equations are alternative variational equations to the ones used in this work. It is felt that an analysis of these equations may resolve the stability anomalies which have been discovered in this Chapter. One approach, which was adopted by Lund (1980) was to include only the terms (n=0,1) in the Fourier expansion and seek a series solution.

7.6. CONCLUSIONS.

i) The method of averaging is an alternative technique which may be used to solve the equations governing oil whirl in plain, cylindrical journal bearings. The whirl orbit is assumed to be elliptic and is calculated directly, not as a result of transient growth or decay. The error in the solution may also be calculated and if this error becomes large it is reasonable to assume that the whirl orbit is no longer elliptic.

ii) When the results for a long bearing obtained using the method of averaging were compared with the results derived using other methods some discrepancies were uncovered. Since the method of averaging is an important technique in this field (see (iii) below), the resolution of these discrepancies is an area for future work. It is probable that improvements can be made in the application of the method of averaging (for example in the method used to determine the stability of the whirl orbit).

iii) The method of averaging is an important technique in the investigation of the vibrational characteristics of oil lubricated journal bearings because:

a) it is relatively simple to apply the technique to a more complicated model (for example by using a more accurate boundary condition at film rupture, or by incorporating additional features into the model such as rotor flexibility, mass unbalance).

b) it is possible to pursue the development of the whirl orbit for rotor speeds away from the threshold speed (provided the error lies within acceptable limits).

SUMMARY OF PART 2.

The use of four different techniques to solve the equations of motion provides a very comprehensive examination of the phenomenon of oil whirl in fluid film journal bearings. Of particular importance in Part 2, was the use of bifurcation theory to establish the existence of periodic solutions of the equations of motion for rotor speeds close to the threshold speed. Both bifurcation theory and multiple scaling were then used to investigate the form and structure of the periodic solutions. The features which were identified by these techniques were illustrated by integrating the equation numerically. An investigation of the use of the method of averaging to solve the equations governing oil whirl was also carried out. A summary of the four techniques is given in the Table on the following page.

	BIFURCATION THEORY	MULTIPLE SCALING	METHOD OF AVERAGING	NUMERICAL INTEGRATION
DESCRIPTION	i) Rigorous mathematical technique. ii) Existence theorem which establishes the existence of small amplitude whirl orbits for rotor speeds close to the threshold speed. iii) Poore's algebraic formula determines the direction of bifurcation (ie. subcritical or supercritical). iv) Amplitude of whirl orbit. $\alpha \lvert \bar{\omega} - \bar{\omega}_{th} \rvert^{\frac{1}{2}}$ as $\bar{\omega} \to \bar{\omega}_{th}$	i) Singular perturbation technique. ii) Series solution based upon physical insite. iii)Evolution from ≡bm position to periodic solution is described by an amplitude growth equation. iv) The direction of bifurcation is determined through the sign of the terms in the amplitude equation. v) Reproduces results obtained from bifurcation theory.	i) Developed by Lund (1966). ii) Combination of numerical/analytic technique to solve the equations of motion approximately. iii) Whirl orbit is assumed to be elliptic. iv) Size and orientation of the ellipse is calculated, together with the error in the solution.	Straightforward step by step integration of the equations of motion on a digital computer.
ADVANTAGES	i) Mathematical rigour. ii) Theory provides detailed information about the structure of periodic solutions close to the threshold speed.	i)Method is simple and spectacularly successful. ii) Stability of the periodic orbit is easily deduced from the amplitude equation.	i) Whirl orbit is calculated directly, not as a result of transient growth or decay. ii) Method is adaptable. iii) Method is valid at rotor speeds away from threshold speed (but error increases).	i) Pictorial representation of journal motion. ii) Valuable for checking feature established theoretically and also in complementing theoretical work. iii) Can be used for any bearing model.
DISADVANTAGES	i) Limited to fairly simple models. ii) Algebraic formula is rather tedious to apply. iii) Theory is valid only for rotor speeds close to the threshold speed.	i) Limited to fairly simple models. ii) Method is rather tedious to apply iii) Theory is valid only for rotor speeds close to the threshold speed.	i) Method is approximate. ii) Discrepancies exist between results obtained from methods 1 and 2 and those obtained by averaging the equations.	i) Fairly expensive in computing time. ii) Errors may accumulate significantly over many time steps. iii) Without analytic methods, there is no identification of the important regions of parameter space.

Table summarising non linear techniques employed in Part 2.

CHAPTER 8.

CONCLUSIONS AND RECOMMENDATIONS FOR FUTURE WORK.

8.1 CONCLUSIONS.

1. Plain cylindrical journal bearings operating with complete lubricating fluid films are inherently unstable at all rotor speeds. As whirling proceeds the journal spirals outwards towards the bearing surface with a frequency approaching half the rotational speed.

2. When cavitation is incorporated in the bearing model, linear stability theory has shown that the journal is stable below its threshold speed. Thus, although cavitation is commonly regarded as an undesirable feature of journal bearings (for example, due to a reduced load capacity), cavitation is a stabilising mechanism, crucial to the smooth operation of the bearing.

3. The threshold speed is sensitive to:

   i) different cavitation boundary conditions at film rupture.

   ii) oil film behaviour during journal vibration.

An accurate model must, therefore, incorporate precise boundary conditions at film rupture (and film reformation) and also account correctly for the behaviour of the oil film during journal vibration. These details are often overlooked in the analysis of rotor-bearing systems.

4. Increasing the steady state eccentricity ratio has a stabilising effect on the journal by raising the threshold speed. An important point to bear in mind, however, is that, although the journal may be stable theoretically, the stability may be marginal, such that vibrations are only weakly damped. This effect is most pronounced at low and high eccentricity ratios.

5. Two factors which influence the vibrational characteristics of the single axial groove journal bearing are:

   i) the groove position

   ii) the oil supply pressure

In theory, it is possible to maximise the threshold speed, thus minimising vibrational problems, by selecting the optimum groove position.

6. The onset of oil whirl in plain journal bearings is a bifurcation phenomenon, which may be examined by using the Hopf bifurcation theorem. It has been established that the equations of motion have small amplitude periodic solutions for rotor speeds close to the threshold speed. Two distinct types of bifurcation are possible, depending on the operating parameters of the rotor-bearing system:

   i) supercritical bifurcation. The journal is stable below its threshold speed (the journal spirals into its equilibrium position when displaced from it). As the threshold speed is exceeded, the equilibrium point bifurcates to a stable limit cycle, whose amplitude increases (from zero) as the speed is increased further above the threshold speed. There is a gradual transition from stability to complete instability and thus it is feasible to operate the machine above its threshold speed.

   ii) subcritical bifurcation. Bifurcation to unstable whirl orbits occurs below the threshold speed. Large amplitude stable whirl orbits may exist outside the unstable limit cycle and, in general, the orbit of the journal is dependent on its initial conditions. Above the threshold speed the journal may, or may not be completely unstable. Since there is no gradual transition from stability to complete instability in this case it is not feasible to operate the machine above its threshold speed.

7. A detailed analysis of the structure of periodic solutions at rotor speeds close to the threshold speed can only be obtained by using nonlinear mathematical analysis (eg. bifurcation theory and multiple scaling). Although, it is not possible to apply these techniques to complicated models, their importance lies in describing the qualitative features of oil whirl in simple models and in identifying regions of parameter space where different behaviour occurs.

8. Three nonlinear techniques were used to investigate the equations of

motion. Two of these methods, namely bifurcation theory and multiple scaling produced identical results, but are suitable only for simple models primarily because both methods require the calculation of the second and third order partial derivatives of the hydrodynamic force components. The third method, the method of averaging, is a more adaptable technique, but a detailed comparison of results obtained from the method of averaging with those derived from bifurcation theory and multiple scaling has indicated some areas of discrepancy which are worthy of further investigation.

9. The importance of numerical integration lies in complementing the theoretical work by checking features obtained theoretically and in widening the investigation to cover regions of parameter space in which existing theories are invalid. An entirely numerical investigation is not only expensive in computing time, but limited, because there are large parameter ranges to cover with no identification of the regions where different behaviour occurs.

10. This thesis has investigated some of the features of oil whirl which are due to the nonlinearity of the hydrodynamic forces. The limitations of a purely linearised approach have been exposed. This is not to say that bearing calculations should always include nonlinear effects, but there should be a greater awareness of the role which the nonlinear terms play in the phenomenon of oil whirl.

8.2 RECOMMENDATIONS FOR FUTURE WORK.

1. There is a need for more carefully controlled experiments in the examination of the vibrational characteristics of oil lubricated journal bearings and in relating theoretical work to experimental results. It is envisaged that experimental work could be carried out in three main areas:

i) The determination of the behaviour of the oil film during journal vibration. At present, there is little experimental evidence to suggest whether the oil film remains static during journal vibration, or swings round with the whirling motion. An important additional factor is the extent of the cavitating region during whirling. An experimental project specifically designed to investigate these effects would be important since it has been shown in this thesis that such factors have a significant influence on the vibrational characteristics of the bearing.

ii) The investigation of the significance of groove position and oil supply pressure on the vibrational characteristics of the single axial groove journal bearing and the comparison of the results with the theoretical predictions made in Chapter 4. A test apparatus has already been designed and built for this purpose (see Appendix IV).

iii) The examination of the onset of oil whirl in a simple rotor-bearing system. Much of the theoretical work described in Part 2 of this thesis was concerned with the onset of instability and the different whirling motions which were possible once whirling was initiated. It would be interesting to carry out an experimental project to determine whether these different features actually occurred in a real rotor-bearing system. It would be necessary to design the apparatus so that the system parameter could be altered - this could be achieved by using oils of different viscosities.

2. This work has emphasised the importance of incorporating accurate boundary conditions at film rupture and film reformation, which is essential in providing a quantitative description of the vibrational characteristics of the bearing. Future work should be directed towards a more comprehensive understanding of film rupture and film reformation in journal bearings under both steady state and dynamic conditions.

3. A significant extension of the present work would be to carry out an investigation of the short bearing (half film) similar to the analysis of the long bearing made in Part 2. Either bifurcation theory or multiple scaling could be used and the results contrasted with those from a numerical investigation and with Lund's results obtained from the method of averaging.

4. Future work should also be directed towards improving the application of the method of averaging to the equations governing oil whirl. The method of averaging is an important technique in the investigation of oil whirl because it is more adaptable than the other nonlinear techniques (the method of averaging requires only the calculation of the first order partial derivatives of the hydrodynamic force components). However, there is a need to resolve the present discrepancies which exist between results obtained from the method of averaging and those obtained from bifurcation theory and multiple scaling.

5. The model used throughout this work was a simple one. Future work could be carried out in a similar manner to that described here, but the model could be extended in various ways by incorporating:

i) rotor flexibility

ii) journal misalignment

iii) mass unbalance

iv) different bearing geometries.

Of the most theoretical interest, is the analysis of a simple model which includes the effect of mass unbalance. Some mass unbalance in the rotor

is inevitable due to limitations in the manufacturing accuracy and introduces periodic forcing terms into the equations. Under these conditions the steady state solution is no longer an equilibrium point, but a closed orbit. The effect of mass unbalance on oil whirl has not been widely studied (some recent work was carried out by Lund (1980)). It is envisaged that an initial investigation could be made by using the method of multiple scaling.

It is evident that there are many interesting aspects of oil whirl in fluid film journal bearings which remain to be examined. These problems are a challenge to the applied mathematician and engineer alike.

REFERENCES

ALLAIRE, P.E. (1980). Private communication.

BADGLEY, R.H. and BOOKER, J.F. (1969). Turborotor instability: effect of initial transients on plane motion. Trans. ASME., J. Lubr. Tech., Vol.91, p625.

BIRKHOFF, G. and HAYS, D.F. (1963). Free boundaries in partial lubrication. J. Maths. Phys., Vol.42, p126.

BOEKER, G.F. and STERNLICHT, B. (1956). Investigation of translatory fluid whirl in vertical machines. Trans. ASME, Vol.78, p13.

BOGOLIUBOV, N.N. and MITROPOLSKY, Y.A. (1961). Asymptotic methods in the theory of non-linear oscillations. Gordon and Breach Science Publishers, New York.

BRETHERTON, F.P. (1960). The motion of long bubbles in tubes. J. Fluid Mech., Vol.10, p166.

CAMERON, A. (1955). Oil whirl in bearings - Theoretical deduction of a further criterion. Engineering, London, p 237.

CAMERON, A. and SOLOMON, P.J.B. (1957). Vibrations in journal bearings: Preliminary observations. Proc. Inst. Mech. Eng. Conf. Lubr. and Wear, Paper 103, p191.

CAPRIZ, G. (1963). On some dynamical problems arising in the theory of lubrication. Rivista di Matematica, Univ. Parma, Vol.4, p1.

COHEN, D.S. (1972). Nonlinear problems in the physical sciences and biology. Proc. Bottelle Summer Inst., Seattle, July 3-28, lecture notes in mathematics, p15, Springer-Verlag, N. York.

COYNE, J.C. and ELROD, H.G. (1970). Conditions for the rupture of a lubricating film, Part I: Theoretical model. Trans. ASME, J. Lubr. Tech., Vol.92, p451.

COYNE, J.C. and ELROD, H.G. (1971). Conditions for the rupture of a lubricating film, Part II: New boundary conditions for Reynolds' equation. Trans. ASME, J. Lubr. Tech., Vol.93, p156.

CRAIGHEAD, I.A. (1976). A study of the dynamics of rotor-bearing systems and related fluid-film bearing characteristics. Ph.D. thesis, Univ. Leeds, U.K.

DOWSON, D. (1957). Cavitation in lubricating films supporting small loads. Proc. Inst. Mech. Eng. Conf. Lubr. Wear, p93.

DOWSON, D. and TAYLOR, C.M. (1979). Cavitation in bearings. Ann. Rev. Fluid Mech., Vol.11, p35.

FLOBERG, L. (1975). Cavitation boundary conditions with regard to the number of streamers and tensile strength of the liquid. 1st. Leeds-Lyon Symp. Cavitation Relat. Phenom. Lubr., p31, London, N. York: Mech. Eng. Publ. Ltd.

FRIEDRICHS, K.O. (1965). Advanced ordinary differential equations. Gordon and Breach, N. York.

GUMBEL, L.K.R. (1921). Vergleich der Ergebrusse der rectinerischen Behandling der Lagerschmierangsproblem mit neueren Veisuch-sergebrussen. Monatsbl. Berliner Berz. Ver. Dtsch. Ing., p125.

HAGG, A.C. (1946). The influence of oil-film journal bearings on the stability of rotating machines. Trans. ASME, J. Appl. Mech., Vol.68, p211.

HAGG, A.C. and WARNER, P.C. (1953). Oil whip of flexible rotors. Trans. ASME, Vol.75, No. 7, p1339.

HAHN, E.J. (1975). The excitability of flexible rotors in short sleeve bearings. Trans. ASME, J. Lubr. Tech., p105.

HALL, G. and WATT, J.M. (1976). Modern numerical methods for ordinary differential equations. Clarendon Press, Oxford.

HARRISON, W.J. (1919). The hydrodynamical theory of the lubrication of a cylindrical bearing under variable load, and of a pivot bearing. Trans. Edinburgh Phil. Soc., Vol.22, p373.

HARTOG, D. (1947). Mechanical vibrations. McGraw-Hill Book Company, New York.

HASSARD, B.D., KAZARINOFF, N.D. and WAN, Y.H. (1981). Theory and applications of Hopf bifurcation. London Math. Soc. Lecture Note Series,

No.41, Cambridge University Press, New York.

HOLMES, R. (1960). The vibration of a rigid shaft on short sleeve bearings. J. Mech. Eng. Sci., Vol.2, No.4, p337.

HOLMES, R. (1963). Oil-whirl characteristics of a rigid rotor in 360-degree journal bearings. Proc. Inst. Mech. Eng, Vol.177, No.11, p291.

HOLMES, R. (1965). See Mitchell, Holmes and Byrne (1965-66).

HOLMES, R. (1966). Instability phenomena due to circular bearing oil films. J. Mech. Eng. Sci., Vol.8, No.4, p419.

HOPF, E. (1942). Abzweigung einer periodischen Lösung von einer stationären Lösung eines Differentialsystems. Ber. Verh. Sachs. Akad. Wiss. Leipsig Math-Nat., Vol.94, p3. For translation to English with commentary by L. Howard and N. Kopell see Marsden, J.E. and McCracken, M. (1976).

HOPKINS, M.R. (1957). Viscous flow between rotating cylinders and a sheet moving between them. Brit. J. Appl. Phys. Vol.8, p442.

HORI, Y. (1959). A theory of oil whip. Trans. ASME, J. Appl. Mech, Vol.81, p189.

HSÜ, I.D. and KAZARINOFF, N.D. (1976). An applicable Hopf bifurcation formula and instability of small periodic solutions of the Field-Noyes model. J. Math. Anal. and Applic., Vol.55, p61.

HUGGINS, N.J. (1963-64). Non-linear modes of vibration of a rigid rotor in short journal bearings. Proc. Inst. Mech. Eng. Conf. Lubr. and Wear, Paper 18, London.

HUMMEL, C. (1926). Kritische Drehzohlen als Folge der Nachgiebigkeit des Schmiermittels im Lager, VDI-Forsch Hft, Vol. 287.

JENNINGS, U.D. (1960). An investigation of oil bearing whirl by electronic-analog computer techniques. Ph.D. thesis, Cornell Univ, U.S.A.

KRYLOV, N.M. and BOGOLIUBOV, N.N. (1947). Introduction to non-linear mechanics. Annals of Maths. Study, No.11, Princeton University Press.

LUND, J.W. (1966). Self-excited, stationary whirl orbits of a journal in a sleeve bearing. Ph.D. thesis, Rensselaer Polytechnic Inst., U.S.A.

LUND, J.W. (1980). Instability threshold of an unbalanced, rigid rotor in short journal bearings. Inst. Mech. Eng. Vibrations Conf., Cambridge, Sept, No. C263.

LUND, J.W. and Saibel, E. (1967). Oil whip whirl orbits of a rotor in sleeve bearings. Trans. ASME, J. Eng. Ind., Vol.89, p813.

LUND, J.W. and THOMSEN, K.K. (1978). A calculation method and data for the dynamic coefficients of oil-lubricated journal bearings. Topics in Fluid Film Bearing and Rotor Bearing System Design Optimisation, ASME.

LUND, J.W. and TONNESEN, J. (1978). Some experiments on instability of rotors supported in fluid-film bearings. Trans. ASME. J. Mech. Design, Vol.100, p147.

LUNDHOLM, G. (1969). The circumferential groove journal bearing considering cavitation and dynamic stability. Acta Poly. Scandinavica, Mech. Eng. Ser., No.42, Stockholm.

LUNDHOLM, G. (1971). The axial groove journal bearing considering cavitation and dynamic stability. Acta Poly. Scandinavica, Mech. Eng. Ser., No.58, Stockholm.

LUNDHOLM, G. (1973). On whirl frequencies and stability borderlines for journal bearings. Trans. of Machine Elements Division, Lund Univ., Sweden.

MARSDEN, J.E. and McCRACKEN, M. (1976). The Hopf bifurcation and its applications. Appl. Math. Sciences, Vol.19, Springer-Verlag, N. York.

MARSH, H. (1965). The stability of aerodynamic gas bearings. Mech. Eng. Sci., Monograph no.2, Inst. Mech. Eng.

McKAY, J.T. (1981). Fluid flow and whirl orbits in a whirling rotor bearing. Ph.D. thesis, Univ. Leeds, U.K.

MITCHELL, J.R., HOLMES, R. and BYRNE, J. (1965-66). Oil whirl of a rigid rotor in 360° journal bearings: Further characteristics. Proc. Inst. Mech. Eng., Vol.180, p593.

MURRAY, J.D. (1976). Lectures on nonlinear-differential-equation models in biology. Oxford University Press, Oxford.

NAYFEH, A. (1972). Perturbation methods. Series in pure and applied mathematics, A Wiley-Interscience publication, J. Wiley and Sons, N. York.

NEWKIRK, B.L. (1924). Shaft whipping. Gen. Elect. Review, p169.

NEWKIRK, B.L. (1930). Whirling of balanced shafts. Third Intern. Cong. of Appl. Mech., Sweden.

NEWKIRK, B.L. (1956). Varieties of shaft disturbances due to fluid films in journal bearings. Trans. ASME, Vol.78, p985.

NEWKIRK, B.L. (1957). Journal bearing instability. Inst. Mech. Eng.-ASME Intern. Conf. on Lubr. and Wear, London, Rev. Paper, Session 1, no. 2.

NEWKIRK, B.L. and GROBEL, L.P. (1934). Oil-film whirl - A non-whirling bearing, Trans. ASME, Vol.56, p607.

NEWKIRK, B.L. and LEWIS, J.F. (1956). Oil-film whirl - An investigation of disturbances due to oil films in journal bearings. Trans. ASME, Vol.78, p21.

NEWKIRK, B.L. and TAYLOR, H.D. (1925). Shaft whipping due to Oil Action in Journal Bearings. Gen. Elect. Review, p559.

OCVIRK, F.W. (1953). Short-bearing approximation for full journal bearings. NACA Tech. Note 2808.

PINKUS, O. (1956). Experimental investigation of resonant whip. Trans. ASME, Vol.78, p975.

PINKUS, O. and STERNLICHT, B. (1961). Theory of Hydrodynamic Lubrication. McGraw-Hill Book Co., New York.

POORE, A.B. (1976). On the theory and application of the Hopf-Friedrichs bifurcation theory. Arch. Rat. Mech. and Anal., Vol.60, p371.

PORITSKY, H. (1953). Contribution to the theory of oil whip. Trans. ASME, Vol.75, p1153.

REDDI, M.M. and TRUMPLER, P.R. (1962). Stability of the high-speed journal bearing under steady load. Trans. ASME., J. Eng. Ind., Vol.84, p351.

REYNOLDS, O. (1886). On the theory of lubrication and its application to Beauchamp Tower's experiments, including an experimental determination of the viscosity of olive oil. Phil. Trans. R.Soc. London, Ser. A, Vol.177, p157-233.

RIEGER, N.F. and THOMAS, C.B. (1976). Some recent computer studies on the stability of rotors in fluid-film bearings. Intern. Union of Theor. and Appl. Mech.,Proc. Dyn. of Rotors Symp., Lyngby, Denmark, p436.

ROBERTSON, D. (1933). Whirling of a journal in a sleeve bearing. Phil. Mag., Ser.7, Vol.15, p113.

RUDDY, A.V. (1980). The dynamics of rotor-bearing systems with particular reference to the influence of fluid film journal bearings and the modelling of flexible rotors. Ph.D. thesis. Univ. Leeds, U.K.

RUDDY, A.V. (1981). Private communication.

SAVAGE, M.D. (1977). Cavitation in lubrication. Pt.I. On boundary conditions and cavity-fluid interferences. Pt.II. Analysis of wavy interfaces. J. Fluid. Mech., Vol.80. p743.

SMALLEY, A.J. and MALANOSKI, S.B. (1978). The use of the computer in the design of rotor-bearing systems. Topics in Fluid Film Bearing and Rotor Bearing System Design and Optimisation, ASME.

SMITH, D.M. (1963). Dynamic characteristics of turbine journal bearings. Inst. Mech. Eng. Conv. on Lubr. and Wear, p72.

SMITH, D.M. (1970). Journal bearings in turbomachinery. Chapman and Hull Ltd.

SMITH, E.H. (1975). A study of film rupture in hydrodynamic lubrication. Ph.D. thesis. Univ. Leeds, U.K.

SOMEYA, T. (1963-64). Stability of a balanced shaft running in cylindrical

journal bearings.Proc. Inst. Mech. Engrs., Vol.178(Pt.3N), p196.

SOMMERFELD, A. (1904). Zur hydrodynamiscien theorie der schmiermittehreibung. Z. Math. Phys., Vol.50, p97.

STERNLICHT, B. (1959). Elastic and damping properties of cylindrical journal bearings. Trans. ASME, J. Basic Eng., Vol.81, p101.

STERNLICHT, B. (1962). Stability and dynamics of rotors supported on fluid-film bearings. ASME paper 62-WA-190.

STERNLICHT, B. and RIEGER, N.F. (1967-68). Rotor stability. Proc. Inst. Mech. Eng., Vol.182 (Pt.3A), p82.

STODOLA, A. (1925). Kritische Wellenstorung Infolge der Nachgiebigkeit des Oelpolsters im Lager. Schweizerische Bauzeitung, Vol.85, p265.

TAYLOR, G.I. (1963). Cavitation of a viscous fluid in narrow passages. J. Fluid Mech., Vol.16, p595.

TONDL, A. (1961). Experimental investigation of self-excited vibrations of rotors due to the action of whirling oil film in journal bearings. Monographs and Memoranda No.1.

TONDL, A. (1965). Some problems of rotor dynamics. Publishing House of the Czechoslovak Academy of Sciences, Prague.

TOLLE, G.C. and MUSTER. D. (1969). An analytic solution for whirl in a finite journal bearing with a continuous lubricating film. Trans. ASME, J. Eng. Ind., Vol.91, p1189.

WARNER, P.C. (1963). Static and dynamic properties of partial journal bearings. Trans. ASME, J. Basic Eng., Vol.85, p247.

WEISSMAN, M.A. (1979). Nonlinear wave packets in the Kelvin-Helmholtz instability. Phil. Trans. R. Soc. London, Ser. A, Vol.290, p639.

WOODCOCK, J.S. and HOLMES, R. (1969-70). The determination and application of the dynamic properties of a turborotor bearing oil film. Proc. Inst. Mech. Engs., Vol.184, (Pt.3L).

APPENDIX I: THE SOMMERFELD SUBSTITUTION.

Integrals of the form $\int_{\theta_1}^{\theta_2} \frac{\cos\theta d\theta}{(1+\varepsilon\cos\theta)^3}$ which occur frequently when solving the Reynolds equation may be evaluated by using the substitution:

$$1 - \varepsilon\cos\psi = \frac{1-\varepsilon^2}{1+\varepsilon\cos\theta}$$

It is commonly referred to as the Sommerfeld substitution with ψ the Sommerfeld angle. A list of the integrals which have been used throughout this work appears below.

$$\int_{\theta_1}^{\theta_2} \frac{d\theta}{(1+\varepsilon\cos\theta)^3} = \frac{1}{4(1-\varepsilon^2)^{5/2}} \{\varepsilon^2(\sin2\psi_2-\sin2\psi_1)-8\varepsilon(\sin\psi_2-\sin\psi_1) +2(2+\varepsilon^2)(\psi_2-\psi_1)\} \quad \text{I1}$$

$$\int_{\theta_1}^{\theta_2} \frac{\sin\theta d\theta}{(1+\varepsilon\cos\theta)^3} = \frac{1}{4(1-\varepsilon^2)^2} \{\varepsilon(\cos2\psi_2-\cos2\psi_1)-4(\cos\psi_2-\cos\psi_1)\} \quad \text{I2}$$

$$\int_{\theta_1}^{\theta_2} \frac{\cos\theta d\theta}{(1+\varepsilon\cos\theta)^3} = \frac{1}{4(1-\varepsilon^2)^{5/2}} \{4(1+\varepsilon^2)(\sin\psi_2-\sin\psi_1)-6\varepsilon(\psi_2-\psi_1) -\varepsilon(\sin2\psi_2-\sin2\psi_1)\} \quad \text{I3}$$

$$\int_{\theta_1}^{\theta_2} \frac{\sin\theta\cos\theta d\theta}{(1+\varepsilon\cos\theta)^3} = \frac{1}{4(1-\varepsilon^2)^2} \{4\varepsilon(\cos\psi_2-\cos\psi_1)-(\cos2\psi_2-\cos2\psi_1)\} \quad \text{I4}$$

$$\int_{\theta_1}^{\theta_2} \frac{\sin^2\theta d\theta}{(1+\varepsilon\cos\theta)^3} = \frac{1}{4(1-\varepsilon^2)^{3/2}} \{2(\psi_2-\psi_1)-(\sin2\psi_2-\sin2\psi_1)\} \quad \text{I5}$$

$$\int_{\theta_1}^{\theta_2} \frac{\cos^2\theta d\theta}{(1+\varepsilon\cos\theta)^3} = \frac{1}{4(1-\varepsilon^2)^{5/2}} \{(\sin2\psi_2-\sin2\psi_1)-8\varepsilon(\sin\psi_2-\sin\psi_1) +2(1+2\varepsilon^2)(\psi_2-\psi_1)\} \quad \text{I6}$$

where ψ_2,ψ_1 are the Sommerfeld angles corresponding to θ_2,θ_1 respectively. Note that ψ coincides with θ at 0, π and 2π.

APPENDIX II. DETAILS OF THE LINEARISATION FOR VARIOUS MODELS.

II(i) A LONG BEARING OPERATING WITH A STATIC HALF FILM.

Integrating the Reynolds equation for a long bearing twice (equation 2.1) with the boundary conditions:

$$p(-\gamma) = p(\pi-\gamma) = 0 \quad \text{(see Figure 3.1)} \tag{II.1}$$

$$\Rightarrow \left(\frac{c}{R}\right)^2 \frac{p}{\mu\omega} = \frac{\varepsilon(1-2\phi')}{4(1-\varepsilon^2)^{5/2}} \left\{ \begin{array}{l} 4(1+\varepsilon^2)(\sin\psi-\sin\psi_1) - 6\varepsilon(\psi-\psi_1) - \varepsilon(\sin2\psi-\sin2\psi_1) \\ + C1\left[\varepsilon^2(\sin2\psi-\sin2\psi_1)-8\varepsilon(\sin\psi-\sin\psi_1)+2(2+\varepsilon^2)(\psi-\psi_1)\right] \end{array} \right\}$$

$$+ \frac{\varepsilon'}{2(1-\varepsilon^2)^2} \left\{ \varepsilon(\cos2\psi-\cos2\psi_1) - 4(\cos\psi-\cos\psi_1) \right\} \tag{II.2}$$

where ψ_1, ψ_2 are the Sommerfeld angles corresponding to $-\gamma$, $\pi-\gamma$ respectively.

$$\text{and } C1 = -\frac{I3}{I1} - \frac{2\varepsilon'(1-\varepsilon^2)^{1/2}}{\varepsilon(1-2\phi')} \frac{I2}{I1} \quad \text{(see Appendix I)} \tag{II.3}$$

The hydrodynamic forces are:

$$-\left(\frac{c}{R}\right)^2 \frac{F_r}{LR\omega\mu} = 6\varepsilon(1-2\phi')(I4+C1.I2) + 12.I5\varepsilon' \tag{II.4}$$

$$\left(\frac{c}{R}\right)^2 \frac{F_t}{LR\omega\mu} = 6\varepsilon(1-2\phi')(I6+C1.I3) + 12.I4\varepsilon'$$

The equations of motion are:

$$\ddot{\varepsilon} - \varepsilon\dot{\phi}^2 = \nu(\cos\phi+S\bar{F}_r) \quad \varepsilon\ddot{\phi} + 2\dot{\varepsilon}\dot{\phi} = -\nu(\sin\phi-S\bar{F}_t) \tag{II.5}$$

During a small amplitude vibration of the journal about its equilibrium position γ will be << 1. Hence the following relationships can be derived from the Sommerfeld substitution (Appendix I):

$$\sin\psi_2 - \sin\psi_1 = \frac{2\gamma}{(1-\varepsilon_s^2)^{1/2}} \quad \cos\psi_2 - \cos\psi_1 = -2 \quad \cos 2\psi_2 - \cos 2\psi_1 = 0$$

$$\sin 2\psi_2 - \sin 2\psi_1 = -\frac{4\gamma\varepsilon_s}{(1-\varepsilon_s^2)^{1/2}} \quad \psi_2 - \psi_1 = \pi - \frac{2\gamma\varepsilon_s}{(1-\varepsilon_s^2)^{1/2}} \tag{II.6}$$

The procedure for linearising the equations of motion is:

i) Substitute $\varepsilon = \varepsilon_s + \delta$, $\phi = \phi_s + \gamma$.

ii) Use the above relationships to eliminate ψ_2, ψ_1.

iii) Retain only first order terms.

iv) Collect like terms and convert to Cartesian co-ordinates by putting $\delta = x$, $\varepsilon_s\gamma = y$.

This procedure yields the eight velocity and displacement coefficients given in Chapter 3 for this model (equations 3.13).

II(ii) THE AXIAL GROOVE JOURNAL BEARING. (including the work on the Reynolds boundary condition described in Chapter 3).

a) Film Start at the Groove Position.

For this model the boundary conditions are:

$$p = p_g \text{ at } \theta = \theta_1, \quad \text{the groove position.} \tag{II.7}$$

$$p = \frac{dp}{d\theta} = 0 \text{ at } \theta = \theta_2, \quad \text{the film rupture position.}$$

Integrating the Reynolds equation for the long bearing:

$$\Rightarrow \frac{dp}{d\theta} = 6\mu\left(\frac{R}{c}\right)^2 \left\{ \frac{\varepsilon(\omega-2\dot{\phi})(\cos\theta - \cos\theta_2) + 2\dot{\varepsilon}(\sin\theta - \sin\theta_2)}{(1+\varepsilon\cos\theta)^3} \right\}$$

which satisfies $\left(\frac{dp}{d\theta}\right) = 0$ at $\theta = \theta_2$.

Integrating again:

$$\left(\frac{c}{R}\right)^2 \frac{(p-p_g)}{\mu\omega} = \frac{3\varepsilon(1-2\dot{\phi}')F(\varepsilon,\psi,\psi_1,\psi_2)}{2(1-\varepsilon^2)^{3/2}(1-\varepsilon\cos\psi_2)} + \frac{3\varepsilon' Q(\varepsilon,\psi,\psi_1,\psi_2)}{(1-\varepsilon^2)^2(1-\varepsilon\cos\psi_2)} \tag{II.8}$$

which satisfies $p(\theta_1) = p_g$. ψ_1 and ψ_2 are the Sommerfeld angles corresponding to θ_1 and θ_2 respectively. θ_2, the film rupture position is determined by solving the equation $p(\theta_2) = 0$:

$$\Rightarrow \varepsilon(1-2\dot{\phi}')(1-\varepsilon^2)^{1/2}F(\varepsilon,\psi_1,\psi_2) + 2\varepsilon' Q(\varepsilon,\psi_1,\psi_2) + \frac{2}{3}\bar{p}_g(1-\varepsilon^2)^2(1-\varepsilon\cos\psi_2) = 0 \tag{II.9}$$

For the functions F,Q etc. see equations (II.19).

The hydrodynamic forces are:

$$F_r = LR\int_{\theta_1}^{\theta_2} p(\theta)\cos\theta d\theta = LR\left|p(\theta)\sin\theta\right|_{\theta_1}^{\theta_2} - LR\int_{\theta_1}^{\theta_2}\frac{dp}{d\theta}\sin\theta d\theta$$

$$F_t = LR\int_{\theta_1}^{\theta_2} p(\theta)\sin\theta d\theta = -LR\left|p(\theta)\cos\theta\right|_{\theta_1}^{\theta_2} + LR\int_{\theta_1}^{\theta_2}\frac{dp}{d\theta}\cos\theta d\theta$$

$$\Rightarrow \bar{F}_r = -\bar{p}_g\sin\theta_1 - \frac{3\varepsilon(1-2\phi')(\cos\psi_2-\cos\psi_1)^2}{(1-\varepsilon^2)(1-\varepsilon\cos\psi_2)} - \frac{3T(\varepsilon,\psi_1,\psi_2)\varepsilon'}{(1-\varepsilon^2)^{3/2}(1-\varepsilon\cos\psi_2)} \quad \text{(II.10)}$$

$$\bar{F}_t = \bar{p}_g\cos\theta_1 + \frac{3\varepsilon(1-2\phi')A(\varepsilon,\psi_1,\psi_2)}{2(1-\varepsilon^2)^{3/2}(1-\varepsilon\cos\psi_2)} + \frac{3V(\varepsilon,\psi_1,\psi_2)\varepsilon'}{(1-\varepsilon^2)^2(1-\varepsilon\cos\psi_2)}$$

Steady State Expressions.

$$\bar{p}_s = \bar{p}_g + \frac{3\varepsilon_s}{2(1-\varepsilon_s^2)^{3/2}(1-\varepsilon_s\cos\psi_{2s})}\left\{\begin{array}{l} 4(1+\varepsilon_s\cos\psi_{2s})(\sin\psi-\sin\psi_{1s}) \\ -2(\varepsilon_s+2\cos\psi_{2s})(\psi-\psi_{1s})-\varepsilon_s(\sin2\psi-\sin2\psi_{1s}) \end{array}\right\}$$

ψ_{2s} satisfies the equation:

$$\varepsilon_s F(\varepsilon_s,\psi_{1s},\psi_{2s}) + \frac{2}{3}\bar{p}_g(1-\varepsilon_s^2)^{3/2}(1-\varepsilon_s\cos\psi_{2s}) = 0 \quad \text{(II.12)}$$

which may be solved for ψ_{2s}, after specifying ε_s,ψ_{1s} and $\bar{p}_g$, by the Newton-Raphson technique.

$$\bar{F}_{rs} = -\bar{p}_g\sin\theta_{1s} - \frac{3\varepsilon_s(\cos\psi_{2s}-\cos\psi_{1s})^2}{(1-\varepsilon_s^2)(1-\varepsilon_s\cos\psi_{2s})} \cdot \bar{F}_{ts} = \bar{p}_g\cos\theta_{1s} + \frac{3\varepsilon_s A(\varepsilon_s,\psi_{1s},\psi_{2s})}{2(1-\varepsilon_s^2)^{3/2}(1-\varepsilon_s\cos\psi_{2s})}$$

$$\tan\phi_s = \left(\frac{\bar{F}_{ts}}{-\bar{F}_{rs}}\right) \qquad S(\varepsilon_s) = \frac{1}{(\bar{F}_{rs}^2+\bar{F}_{ts}^2)^{1/2}} \quad \text{(II.13)}$$

Linearised Equations of Motion.

The full equations of motion are:

$$\varepsilon'' - \varepsilon\phi'^2 = \nu(\cos\phi+S\bar{F}_r) \qquad \varepsilon\phi'' + 2\varepsilon'\phi' = -\nu(\sin\phi-S\bar{F}_t) \quad \text{(II.14)}$$

with $\bar{F}_r,\bar{F}_t$ given by equations (II.10) and ψ_2 specified by equation(II.9). During journal vibration about the equilibrium position:

$$\varepsilon \to \varepsilon_s + \delta,\ \phi \to \phi_s + \gamma,\ \psi_2 \to \psi_{2s} + \delta\psi_2,\ \psi_1 \to \psi_{1s} + \delta\psi_1 \qquad \text{(II.15)}$$

$$\text{where } \delta\psi_1 = -\frac{\sin\psi_{1s}}{(1-\varepsilon_s^2)}\delta - \frac{(1-\varepsilon_s\cos\psi_{1s})\gamma}{(1-\varepsilon_s^2)^{1/2}} \qquad \text{(II.16)}$$

since $\psi_1 = \psi_1(\varepsilon)$, since $\theta_1 \to \theta_{1s} - \gamma$ during journal vibration

Substituting these expressions into equation (II.9) and retaining only first order terms yields an equation of the form:

$$\delta\psi_2 = 2\varepsilon_s\dot{\gamma}(1-\varepsilon_s^2)^{1/2}\ \bar{F}_s - 2\dot{\delta}\bar{Q}_s - \bar{F}_{6s}\delta + \bar{F}_{4s}\gamma \qquad \text{(II.17)}$$

The equations of motion are linearised by substituting equations (II.15), (II.16) and (II.17) into equations (II.14), using the steady state expressions and retaining only first order terms. The eight velocity and displacements coefficients obtained by this procedure are:

$$B_{xx} = \frac{3ST_s}{(1-\varepsilon_s^2)^{3/2}(1-\varepsilon_s\cos\psi_{2s})} + \frac{6S\bar{Q}_s\varepsilon_s(\cos\psi_{2s}-\cos\psi_{1s})(2-\varepsilon_s\cos\psi_{2s}-\varepsilon_s\cos\psi_{1s})\sin\psi_{2s}}{(1-\varepsilon_2^2)(1-\varepsilon_s\cos\psi_{2s})^2}$$

$$B_{xy} = \frac{-6S(\cos\psi_{2s}-\cos\psi_{1s})^2}{(1-\varepsilon_2^2)(1-\varepsilon_s\cos\psi_{2s})} - \frac{6S\varepsilon_s\bar{F}_s(\cos\psi_{2s}-\cos\psi_{1s})(2-\varepsilon_s\cos\psi_{2s}-\varepsilon_s\cos\psi_{1s})\sin\psi_{2s}}{(1-\varepsilon_s^2)^{1/2}(1-\varepsilon_s\cos\psi_{2s})^2}$$

$$B_{yx} = \frac{-3SV_s}{(1-\varepsilon_s^2)^2(1-\varepsilon_s\cos\psi_{2s})} + \frac{3S\varepsilon_s\left\{(\partial A/\partial\psi_2)_s(1-\varepsilon_s\cos\psi_{2s})-A_s\varepsilon_s\sin\psi_{2s}\right\}\bar{Q}_s}{(1-\varepsilon_s^2)^{3/2}(1-\varepsilon_s\cos\psi_{2s})^2}$$

$$B_{yy} = \frac{3SA_s}{(1-\varepsilon_s^2)^{3/2}(1-\varepsilon_s\cos\psi_{2s})} - \frac{3S\varepsilon_s\left\{(\partial A/\partial\psi_2)_s(1-\varepsilon_s\cos\psi_{2s})-A_s\varepsilon_s\sin\psi_{2s}\right\}\bar{F}_s}{(1-\varepsilon_s^2)(1-\varepsilon_s\cos\psi_{2s})^2}$$

$$K_{xx} = \frac{3S(\cos\psi_{2s}-\cos\psi_{1s})^2\ (1+\varepsilon_s^2-2\varepsilon_s^3\cos\psi_{2s})}{(1-\varepsilon_2^2)^2(1-\varepsilon_s\cos\psi_{2s})^2} - \frac{6S\varepsilon_s(\cos\psi_{2s}-\cos\psi_{1s})\sin^2\psi_{1s}}{(1-\varepsilon_s^2)^2(1-\varepsilon_s\cos\psi_{2s})}$$

$$+ \frac{3S\bar{F}_{6s}\varepsilon_s(\cos\psi_{2s}-\cos\psi_{1s})(2-\varepsilon_s\cos\psi_{2s}-\varepsilon_s\cos\psi_{1s})\sin\psi_{2s}}{(1-\varepsilon_2^2)(1-\varepsilon_s\cos\psi_{2s})^2} \qquad \text{(II.18)}$$

$$K_{xy} = \frac{S}{\varepsilon_s}(\bar{F}_{ts}-\bar{p}_g\cos\theta_{1s}) - \frac{3\bar{F}_{4s}S(\cos\psi_{2s}-\cos\psi_{1s})(2-\varepsilon_s\cos\psi_{2s}-\varepsilon_s\cos\psi_{1s})\sin\psi_{2s}}{(1-\varepsilon_s^2)(1-\varepsilon_s\cos\psi_{2s})^2}$$

$$- \frac{6S(\cos\psi_{2s}-\cos\psi_{1s})\sin\psi_{1s}(1-\varepsilon_s\cos\psi_{1s})}{(1-\varepsilon_s^2)^{3/2}(1-\varepsilon_s\cos\psi_{2s})}$$

$$K_{yx} = \frac{3S\varepsilon_s(\partial A/\partial\psi_1)_s \sin\psi_{1s}}{2(1-\varepsilon_s^2)^{5/2}(1-\varepsilon_s\cos\psi_{2s})} - \frac{3S\left\{A_s(1+2\varepsilon_s^2-3\varepsilon_s^3\cos\psi_{2s})+\varepsilon_s(\partial A/\partial\varepsilon)_s(1-\varepsilon_s^2)(1-\varepsilon_s\cos\psi_{2s})\right\}}{2(1-\varepsilon_s^2)^{5/2}(1-\varepsilon_s\cos\psi_{2s})^2}$$

$$+ \frac{3S\varepsilon_s\left\{(\partial A/\partial\psi_2)_s(1-\varepsilon_s\cos\psi_{2s})-\varepsilon_s\sin\psi_{2s}A_s\right\}\bar{F}_{6s}}{2(1-\varepsilon_s^2)^{3/2}(1-\varepsilon_s\cos\psi_{2s})^2}$$

$$K_{yy} = -\frac{S}{\varepsilon_s}(\bar{F}_{rs}+\bar{p}_g\sin\theta_{1s}) + \frac{3S(\partial A/\partial\psi_1)_s(1-\varepsilon_s\cos\psi_{1s})}{2(1-\varepsilon_s^2)^2(1-\varepsilon_s\cos\psi_{2s})}$$

$$- \frac{3S\left\{(\partial A/\partial\psi_2)_s(1-\varepsilon_s\cos\psi_{2s})-\varepsilon_s\sin\psi_{2s}A_s\right\}\bar{F}_{4s}}{2(1-\varepsilon_s^2)^{3/2}(1-\varepsilon_s\cos\psi_{2s})^2}$$

where:

$$F(\varepsilon,\psi,\psi_1,\psi_2) = 4(1+\varepsilon\cos\psi_2)(\sin\psi-\sin\psi_1)-2(\varepsilon+2\cos\psi_2)(\psi-\psi_1)$$

$$-\varepsilon(\sin2\psi-\sin2\psi_1)$$

$$Q(\varepsilon,\psi,\psi_1,\psi_2) = \left[\varepsilon(\cos2\psi-\cos2\psi_1)-4(\cos\psi-\cos\psi_1)\right](1-\varepsilon\cos\psi_2)$$

$$-\sin\psi_2\left[\varepsilon^2(\sin2\psi-\sin2\psi_1)-8\varepsilon(\sin\psi-\sin\psi_1)+2(2+\varepsilon^2)(\psi-\psi_1)\right]$$

$$T(\varepsilon,\psi_1,\psi_2) = 2(1-\varepsilon\cos\psi_2)(\psi_2-\psi_1)-(1-\varepsilon\cos\psi_2)(\sin2\psi_2-\sin2\psi_1)$$

$$-\varepsilon\sin\psi_2(\cos2\psi_2-\cos2\psi_1)+4\sin\psi_2(\cos\psi_2-\cos\psi_1)$$

$$V(\varepsilon,\psi_1,\psi_2) = 4\varepsilon(1-\varepsilon\cos\psi_2)(\cos\psi_2-\cos\psi_1)-(1-\varepsilon\cos\psi_2)(\cos2\psi_2-\cos2\psi_1)$$

$$-4\ (1+\varepsilon^2)(\sin\psi_2-\sin\psi_1)\sin\psi_2+6\varepsilon\sin\psi_2(\psi_2-\psi_1)+\varepsilon\sin\psi_2(\sin2\psi_2-\sin2\psi_1)$$

$$A(\varepsilon,\psi_1,\psi_2) = (\sin2\psi_2-\sin2\psi_1)+2(1+2\varepsilon\cos\psi_2)(\psi_2-\psi_1)-4(\sin\psi_2-\sin\psi_1)(\varepsilon+\cos\psi_2) \qquad \text{(II.19)}$$

$$\left(\frac{\partial F}{\partial\varepsilon}\right)_s = \sin2\psi_{2s}+\sin2\psi_{1s}-4\cos\psi_{2s}\sin\psi_{1s}-2(\psi_{2s}-\psi_{1s})$$

$$\left(\frac{\partial F}{\partial\psi_2}\right)_s = 4\left\{(\psi_{2s}-\psi_{1s})\sin\psi_{2s}+\varepsilon_s\sin\psi_{2s}\sin\psi_{1s}-\varepsilon_s\sin^2\psi_{2s}\right\}$$

$$\left(\frac{\partial F}{\partial\psi_1}\right)_s = 2(\varepsilon_s+2\cos\psi_{2s})+2\varepsilon_s\cos2\psi_{1s}-4\cos\psi_{1s}(1+\varepsilon_s\cos\psi_{2s})$$

$$F_{4s} = \varepsilon_s \left(\frac{\partial F}{\partial \psi_1}\right)_s (1-\varepsilon_s \cos\psi_{1s})$$

$$F_{5s} = \varepsilon_s (1-\varepsilon_s^2)^{1/2} \left(\frac{\partial F}{\partial \psi_2}\right)_s + \frac{2}{3} \bar{p}_g \varepsilon_s (1-\varepsilon_s^2)^2 \sin\psi_{2s}$$

$$F_{6s} = \varepsilon_s (1-\varepsilon_s^2)^{1/2} \left(\frac{\partial F}{\partial \varepsilon}\right)_s + \frac{(1-2\varepsilon_s^2)}{(1-\varepsilon_s^2)^{1/2}} F_s - \frac{2}{3} \bar{p}_g (1-\varepsilon_s^2)(4\varepsilon_s + (1-5\varepsilon_s^2)\cos\psi_{2s})$$

$$- \frac{\varepsilon_s \sin\psi_{1s}}{(1-\varepsilon_s^2)^{1/2}} \left(\frac{\partial F}{\partial \psi_1}\right)_s$$

$$\bar{F}_s = F_s/F_5 \qquad \bar{Q}_s = Q_s/F_{5s} \qquad \bar{F}_{4s} = F_{4s}/F_{5s} \qquad \bar{F}_{6s} = F_{6s}/F_{5s}$$

$$\left(\frac{\partial A}{\partial \varepsilon}\right)_s = 4\left[(\psi_{2s}-\psi_{1s})\cos\psi_{2s} + \sin\psi_{1s} - \sin\psi_{2s}\right]$$

$$\left(\frac{\partial A}{\partial \psi_2}\right)_s = 4\left[\sin^2\psi_{2s} - \varepsilon_s(\psi_{2s}-\psi_{1s})\sin\psi_{2s} - \sin\psi_{1s}\sin\psi_{2s}\right]$$

$$\left(\frac{\partial A}{\partial \psi_1}\right)_s = 4\left[\cos\psi_{1s}\cos\psi_{2s} - \cos^2\psi_{1s} + \varepsilon_s\cos\psi_{1s} - \varepsilon_s\cos\psi_{2s}\right]$$

To obtain the eight velocity and displacement coefficients for the model with the Reynolds condition at film rupture described in Chapter 3 substitute $\bar{p}_g = 0$ and $\theta_1 = \theta_{1s} = 0$ into the preceding expressions. The values obtained correspond to those for the static film where the film forms at the maximum film thickness in equilibrium and remains there during journal vibration. To model the oscillating film also described in Chapter 3 the procedure is identical except that equation (II.16) reduces to:

$$\delta\psi_1 = -\frac{\sin\psi_{1s}\delta}{(1-\varepsilon_s^2)} = 0 \text{ for } \theta_{1s} = \psi_{1s} = 0 \qquad \text{(II.20)}$$

$$\Rightarrow \delta\psi_2 = 2\varepsilon_s \dot{\gamma}(1-\varepsilon_s^2)^{1/2}\bar{F}_s - 2\bar{Q}_s\dot{\delta} - \bar{F}_{6s}\delta$$

Only two of the eight bearing coefficients (K_{xy} and K_{yy}) are altered. For

this model the expressions are:

$$K_{xy} = \frac{S}{\varepsilon_s} \bar{F}_{ts} \qquad K_{yy} = -\frac{S}{\varepsilon_s} \bar{F}_{rs}. \tag{II.21}$$

b) Film Termination at the Groove Position.

For this model the boundary conditions are:

$$p = p_g \quad \theta = \theta_2 \quad \text{Film rupture} \tag{II.22}$$
$$p = 0 \quad \theta = \theta_1 \quad \text{Film start}$$

Integrating the Reynolds equation for the long bearing twice with the boundary conditions:

$$p = p_g \quad \text{at} \quad \theta = \theta_2,\ \theta_2 + 2\pi$$

$$\Rightarrow \left(\frac{c}{R}\right)^2 (p-p_g)\frac{1}{\mu\omega} = \frac{3\varepsilon(1-2\phi')}{(1-\varepsilon^2)^{3/2}(2+\varepsilon^2)}\left\{2(2-\varepsilon^2)(\sin\psi-\sin\psi_2)-\varepsilon(\sin 2\psi-\sin 2\psi_2)\right\}$$
$$+\frac{3\varepsilon'}{(1-\varepsilon^2)^2}\left\{\varepsilon(\cos 2\psi-\cos 2\psi_2)-4(\cos\psi-\cos\psi_2)\right\} \tag{II.23}$$

Let $p = 0$ at $\theta = \theta_1$; $\quad p > 0$ for $\theta_1 < \theta < \theta_2$.

θ_1 satisfies the equation:

$$\frac{(1-\varepsilon^2)^2(2+\varepsilon^2)}{3}\bar{p}_g + \varepsilon(1-\varepsilon^2)^{1/2}(1-2\phi')F_1(\varepsilon,\psi_1,\psi_2) + \varepsilon' F_2(\varepsilon,\psi_1,\psi_2) = 0 \tag{II.24}$$

For the expressions F_1, F_2 etc. see equations (II.30).

The hydrodynamic forces are;

$$\bar{F}_r = \bar{p}_g \sin\theta_2 - \frac{3\varepsilon(1-2\phi')\left\{(\cos 2\psi_1-\cos 2\psi_2)+2\varepsilon(\cos\psi_1-\cos\psi_2)\right\}}{(1-\varepsilon^2)(2+\varepsilon^2)} \tag{II.25}$$
$$-\frac{3\varepsilon'}{(1-\varepsilon^2)^{3/2}}\left\{2(\psi_2-\psi_1)-(\sin 2\psi_2-\sin 2\psi_1)\right\}$$

$$\bar{F}_t = -\bar{p}_g \cos\theta_2 + \frac{3\varepsilon(1-2\phi')\left\{(\sin 2\psi_2-\sin 2\psi_1)-2\varepsilon(\sin\psi_2-\sin\psi_1)+2(1-\varepsilon^2)(\psi_2-\psi_1)\right\}}{(1-\varepsilon^2)^{3/2}(2+\varepsilon^2)}$$

$$+ \frac{3\varepsilon'}{(1-\varepsilon^2)^2}\left\{4\varepsilon(\cos\psi_2-\cos\psi_1) - (\cos 2\psi_2-\cos 2\psi_1)\right\}$$

Steady State Expressions.

$$\bar{p}_s = \bar{p}_g + \frac{3\varepsilon_s}{(1-\varepsilon_s^2)^{3/2}(2+\varepsilon_s^2)}\left\{2(2-\varepsilon_s^2)(\sin\psi-\sin\psi_{2s})-\varepsilon_s(\sin 2\psi-\sin 2\psi_{2s})\right\} \quad \text{(II.26)}$$

ψ_{1s} is the solution of the equation:

$$\frac{(1-\varepsilon_s^2)^{3/2}(2+\varepsilon_s^2)}{3}\bar{p}_g + \varepsilon_s F_1(\varepsilon_s,\psi_{1s},\psi_{2s}) = 0 \quad \text{(II.27)}$$

$$\bar{F}_{rs} = \bar{p}_g\sin\theta_{2s} - \frac{3\varepsilon_s\left\{(\cos 2\psi_{1s}-\cos 2\psi_{2s})+2\varepsilon_s(\cos\psi_{1s}-\cos\psi_{2s})\right\}}{(1-\varepsilon_s^2)(2+\varepsilon_s^2)} \quad \text{(II.28)}$$

$$\bar{F}_{ts} = -\bar{p}_g\cos\theta_{2s} + \frac{3\varepsilon_s\left\{(\sin 2\psi_{2s}-\sin 2\psi_{1s})-2\varepsilon_s(\sin\psi_{2s}-\sin\psi_{1s})+2(1-\varepsilon_s^2)(\psi_{2s}-\psi_{1s})\right\}}{(1-\varepsilon_s^2)^{3/2}(2+\varepsilon_s^2)}$$

Linearised Equations of Motion.

The equations of motion are then formulated and linearised following a similar procedure to case (a). The eight velocity and displacement coefficients so obtained are:

$$B_{xx} = \frac{3S(2(\psi_{2s}-\psi_{1s})-(\sin 2\psi_{2s}-\sin 2\psi_{1s}))}{(1-\varepsilon_s^2)^{3/2}} + \frac{6S\bar{F}_{2s}\varepsilon_s(\sin 2\psi_{1s}+\varepsilon_s\sin\psi_{1s})}{(1-\varepsilon_s^2)(2+\varepsilon_s^2)}$$

$$B_{xy} = -\frac{6S(A_s+B_s\varepsilon_s)}{(1-\varepsilon_s^2)(2+\varepsilon_s^2)} - \frac{12S\varepsilon_s(\sin 2\psi_{1s}+\varepsilon_s\sin\psi_{1s})\bar{F}_{1s}}{(1-\varepsilon_s^2)^{1/2}(2+\varepsilon_s^2)}$$

$$B_{yx} = -\frac{3S(A_s-2B_s\varepsilon_s)}{(1-\varepsilon_s^2)^2} + \frac{3S\varepsilon_s(\partial G/\partial\psi_1)_s\bar{F}_{2s}}{(1-\varepsilon_s^2)^{3/2}(2+\varepsilon_s^2)}$$

$$B_{yy} = \frac{6SG_s}{(1-\varepsilon_s^2)^{3/2}(2+\varepsilon_s^2)} - \frac{6S(\partial G/\partial\psi_1)_s\bar{F}_{1s}\varepsilon_s}{(1-\varepsilon_s^2)(2+\varepsilon_s^2)} \quad \text{(II.29)}$$

$$K_{xx} = \frac{3S\left\{(A_s+2B_s\varepsilon_s)(1-\varepsilon_s^2)(2+\varepsilon_s^2)+2\varepsilon_s^2(A_s+B_s\varepsilon_s)(1+2\varepsilon_s^2)\right\}}{(1-\varepsilon_s^2)^2(2+\varepsilon_s^2)^2}$$

$$- \frac{6S\epsilon_s \sin\psi_{2s}\left\{\sin 2\psi_{2s}+\epsilon_s \sin\psi_{2s}\right\}}{(1-\epsilon_s^2)^2(2+\epsilon_s^2)} + \frac{6S\bar{F}_{4s}\epsilon_s\left\{\sin 2\psi_{1s}+\epsilon_s \sin\psi_{1s}\right\}}{(1-\epsilon_s^2)(2+\epsilon_s^2)}$$

$$K_{xy} = \frac{S}{\epsilon_s}\left\{\bar{F}_{ts} + \bar{p}_g \cos\theta_{2s}\right\} - \frac{6S\left\{\sin 2\psi_{2s}+\epsilon_s \sin\psi_{2s}\right\}(1-\epsilon_s \cos\psi_{2s})}{(1-\epsilon_s^2)^{3/2}(2+\epsilon_s^2)}$$

$$- \frac{6S\left\{\sin 2\psi_{1s}+\epsilon_s \sin\psi_{1s}\right\}\epsilon_s \bar{\bar{F}}_{3s}}{(1-\epsilon_s^2)(2+\epsilon_s^2)}$$

$$K_{yx} = - \frac{3S\left\{(G_s+\epsilon_s(\partial G/\partial\epsilon)_s)(1-\epsilon_s^2)(2+\epsilon_s^2)+\epsilon_s^2 G_s(4+5\epsilon_s^2)\right\}}{(1-\epsilon_s^2)^{5/2}(2+\epsilon_s^2)^2}$$

$$+ \frac{3S\epsilon_s(\partial G/\partial\psi_2)_s \sin\psi_{2s}}{(1-\epsilon_s^2)^{5/2}(2+\epsilon_s^2)} + \frac{3S\epsilon_s(\partial G/\partial\psi_1)_s \bar{F}_{4s}}{(1-\epsilon_s^2)^{3/2}(2+\epsilon_s^2)}$$

$$K_{yy} = \frac{S}{\epsilon_s}\left\{-\bar{F}_{rs}+\bar{p}_g \sin\theta_{2s}\right\} + \frac{3S(\partial G/\partial\psi_2)_s(1-\epsilon_s \cos\psi_{2s})}{(1-\epsilon_s^2)^2(2+\epsilon_s^2)}$$

$$- \frac{3S(\partial G/\partial\psi_1)_s \bar{F}_{3s}\epsilon_s}{(1-\epsilon_s^2)^{3/2}(2+\epsilon_s^2)}$$

where:

$$F_1(\epsilon,\psi_1,\psi_2) = 2(2-\epsilon^2)(\sin\psi_1-\sin\psi_2) - \epsilon(\sin 2\psi_1-\sin^2\psi_2)$$

$$F_2(\epsilon,\psi_1,\psi_2) = (2+\epsilon^2)\left\{\epsilon(\cos 2\psi_1-\cos 2\psi_2) - 4(\cos\psi_1-\cos\psi_2)\right\}$$

$$\left(\frac{\partial F_1}{\partial\epsilon}\right)_s = (\sin 2\psi_{2s}-\sin 2\psi_{1s}) + 4\epsilon_s(\sin\psi_{2s}-\sin\psi_{1s})$$

$$\left(\frac{\partial F_1}{\partial\psi_2}\right)_s = 2\epsilon_s \cos 2\psi_{2s} - 2(2-\epsilon_s^2)\cos\psi_{2s}$$

$$\left(\frac{\partial F_1}{\partial\psi_1}\right)_s = 2(2-\epsilon_s^2)\cos\psi_{1s} - 2\epsilon_s \cos 2\psi_{1s} \qquad \text{(II.30)}$$

$$F_{3s} = \left(\frac{\partial F}{\partial\psi_2}\right)_s (1-\epsilon_s \cos\psi_{2s})$$

$$F_{4s} = \left\{ \epsilon_s (1-\epsilon_s^2)^{1/2} \left(\frac{\partial F_1}{\partial \epsilon}\right)_s + \frac{(1-2\epsilon_s^2)F_{1s}}{(1-\epsilon_s^2)^{1/2}} - \epsilon_s \left(\frac{\partial F_1}{\partial \psi_2}\right)_s \frac{\sin\psi_{2s}}{(1-\epsilon_s^2)^{1/2}} \right.$$

$$\left. + \bar{p}_{g3} \frac{1}{2} \left(2\epsilon_s (1-\epsilon_s^2)^2 - 4\epsilon_s (1-\epsilon_s^2)(2+\epsilon_s^2)\right) \right\}.$$

$$\bar{F}_{1s} = \frac{F_{1s}}{\epsilon_s (1-\epsilon_s^2)^{1/2} (\partial F_1/\partial \psi_1)_s} \qquad \text{similarly for } \bar{F}_{2s},\ \bar{F}_{3s},\ \bar{F}_{4s}$$

$$A_s = \cos 2\psi_{1s} - \cos 2\psi_{2s} \qquad B_s = 2(\cos\psi_{1s} - \cos\psi_{2s})$$

$$G_s = (\sin 2\psi_{2s} - \sin 2\psi_{1s}) - 2\epsilon_s (\sin\psi_{2s} - \sin\psi_{1s}) + 2(1-\epsilon_s^2)(\psi_{2s} - \psi_{1s})$$

$$\left(\frac{\partial G}{\partial \epsilon}\right)_s = -2(\sin\psi_{2s} - \sin\psi_{1s}) - 4\epsilon_s (\psi_{2s} - \psi_{1s})$$

$$\left(\frac{\partial G}{\partial \psi_1}\right)_s = -2\cos 2\psi_{1s} + 2\epsilon_s \cos\psi_{1s} - 2(1-\epsilon_s^2)$$

$$\left(\frac{\partial G}{\partial \psi_2}\right)_s = 2\cos 2\psi_{2s} - 2\epsilon_s \cos\psi_{2s} + 2(1-\epsilon_s^2)$$

ε_s	S	ϕ_s^o	θ_{1s}^o	θ_{2s}^o	B_{xx}	B_{xy}	B_{yx}	B_{yy}	K_{xx}	K_{xy}	K_{yx}	K_{yy}	ν_{crit}	$\bar{\Omega}_{crit}$
0.10	34.75	19.94	130.1	204.3	86.74	-18.80	-18.80	6.82	11.88	42.09	-4.30	-8.86	1.2863	0.5610
0.20	13.30	19.82	130.2	203.7	43.55	-9.41	-9.41	3.39	7.44	20.38	-2.67	-4.12	1.4583	0.6217
0.30	6.60	19.67	130.3	203.0	29.21	-6.28	-6.28	2.24	6.19	13.06	-2.19	-2.50	1.6111	0.6827
0.40	3.56	19.46	130.5	202.2	22.10	-4.71	-4.71	1.67	5.81	9.33	-2.03	-1.65	1.7374	0.7439
0.50	1.96	19.18	130.8	201.2	17.93	-3.78	-3.78	1.31	5.89	7.02	-2.01	-1.11	1.8254	0.8048
0.60	1.06	18.77	131.2	199.8	15.28	-3.16	-3.16	1.07	6.35	5.39	-2.10	-0.70	1.8554	0.8630
0.70	0.53	18.15	131.9	198.1	13.60	-2.71	-2.71	0.89	7.33	4.12	-2.31	-0.35	1.7903	0.9116
0.80	0.24	17.10	132.9	195.6	12.78	-2.39	-2.39	0.74	9.41	3.01	-2.71	-0.01	1.5469	0.9277
0.90	0.08	14.95	135.1	191.6	13.47	-2.15	-2.15	0.57	15.35	1.91	-3.64	0.37	0.8341	0.7744

II. 1(a). Non-dimensional oil supply pressure = 0.0.

Table II. 1. Data for the axial groove journal bearing. Groove position 30^o before the load line.

ε_s	S	ϕ_s^o	θ_{1s}^o	θ_{2s}^o	B_{xx}	B_{xy}	B_{yx}	B_{yy}	K_{xx}	K_{xy}	K_{yx}	K_{yy}	ν_{crit}	$\bar{\Omega}_{crit}$
0.10	1.39	1.96	148.04	262.74	9.43	3.92	3.92	2.58	-2.76	5.39	-1.79	2.10	∞	-
0.20	1.20	20.89	129.11	231.70	9.80	0.06	0.06	0.56	-0.05	5.49	-0.50	0.03	∞	-
0.30	1.04	24.59	125.41	220.10	9.31	-1.01	-1.01	0.57	1.03	4.89	-0.61	-0.45	7.7202	0.7624
0.40	0.88	25.05	124.95	213.04	9.18	-1.48	-1.48	0.64	1.83	4.44	-0.82	-0.56	4.5318	0.8114
0.50	0.71	24.22	125.78	207.88	9.33	-1.74	-1.74	0.69	2.68	4.06	-1.07	-0.53	3.4099	0.8583
0.60	0.53	22.73	127.27	203.70	9.69	-1.91	-1.91	0.71	3.78	3.69	-1.38	-0.42	2.7696	0.9022
0.70	0.35	20.83	129.17	199.99	10.23	-2.02	-2.02	0.70	5.35	3.26	-1.79	-0.24	2.2781	0.9381
0.80	0.19	18.58	131.42	196.30	11.03	-2.06	-2.06	0.65	8.01	2.69	-2.37	0.01	1.7607	0.9443
0.90	0.07	15.50	134.50	191.79	12.80	-2.04	-2.04	0.55	14.52	1.85	-3.47	0.36	0.8879	0.7854

II. 1(b). Non-dimensional oil supply pressure = 1.0.

Table II. 1. continued. Data for the axial groove journal bearing. Groove position 30^o before the loadline.

ϵ_s	S	ϕ_s^o	θ_{1s}^o	θ_{2s}^o	B_{xx}	B_{xy}	B_{yx}	B_{yy}	K_{xx}	K_{xy}	K_{yx}	K_{yy}	ν_{crit}	$\bar{\Omega}_{crit}$
0.10	3.27	39.40	80.60	225.03	37.44	-15.46	-15.46	12.69	8.71	17.45	-7.04	-6.40	0.4424	0.5285
0.20	1.48	38.50	81.50	221.86	19.25	-7.83	-7.83	6.23	5.04	8.26	-3.87	-2.56	0.4716	0.5526
0.30	0.88	37.43	82.57	218.54	13.33	-5.29	-5.29	4.05	3.95	5.18	-2.86	-1.25	0.4901	0.5719
0.40	0.57	36.14	83.86	215.07	10.51	-4.04	-4.04	2.95	3.57	3.63	-2.40	-0.59	0.4956	0.5857
0.50	0.39	34.58	85.42	211.42	8.98	-3.29	-3.29	2.27	3.54	2.68	-2.19	-0.17	0.4848	0.5923
0.60	0.27	32.65	87.35	207.52	8.16	-2.81	-2.81	1.80	3.81	2.03	-2.12	0.13	0.4513	0.5875
0.70	0.17	30.18	89.82	203.29	7.88	-2.47	-2.47	1.44	4.50	1.53	-2.19	0.35	0.3815	0.5597
0.80	0.10	26.80	93.20	198.54	8.22	-2.23	-2.23	1.13	6.10	1.12	-2.45	0.55	0.2351	0.4610
0.90	0.05	21.47	98.53	192.71	10.01	-2.07	-2.07	0.81	11.13	0.73	-3.21	0.74	0.0000	0.0000

II. 2(a). Non-dimensional oil supply pressure = 0.0.

Table II. 2. Data for the axial groove journal bearing. Groove position 60^o before the loadline.

ε_s	S	ϕ_s^o	θ_{1s}^o	θ_{2s}^o	B_{xx}	B_{xy}	B_{yx}	B_{yy}	K_{xx}	K_{xy}	K_{yx}	K_{yy}	ν_{crit}	$\bar{\Omega}_{crit}$
0.10	0.60	52.32	67.68	258.39	13.37	-2.84	-2.84	3.90	1.65	7.10	-2.39	-1.29	2.2251	0.5808
0.20	0.46	50.93	69.07	239.32	9.10	-2.94	-2.94	2.94	1.90	4.48	-1.93	-1.04	1.1767	0.6001
0.30	0.37	48.07	71.93	229.28	7.42	-2.64	-2.64	2.36	1.95	3.30	-1.70	-0.66	0.9383	0.6140
0.40	0.30	45.04	74.96	221.87	6.60	-2.40	-2.40	1.97	2.08	2.59	-1.60	-0.36	0.8101	0.6225
0.50	0.24	41.85	78.15	215.64	6.24	-2.22	-2.22	1.67	2.34	2.10	-1.58	-0.11	0.7083	0.6241
0.60	0.19	38.36	81.64	209.99	6.20	-2.10	-2.10	1.43	2.80	1.71	-1.65	0.10	0.6046	0.6149
0.70	0.14	34.38	85.62	204.57	6.49	-2.02	-2.02	1.23	3.63	1.38	-1.82	0.30	0.4772	0.5835
0.80	0.09	29.53	90.47	199.06	7.30	-1.98	-1.98	1.02	5.35	1.07	-2.18	0.50	0.2823	0.4835
0.90	0.04	22.78	97.22	192.83	9.49	-1.96	-1.96	0.78	10.52	0.73	-3.05	0.71	0.0000	0.0000

II. 2(b). Non-dimensional oil supply pressure = 1.0.

Table II. 2. continued. Data for the axial groove journal bearing. Groove position 60^o before the loadline.

ε_s	S	ϕ^o_s	θ^o_{1s}	θ^o_{2s}	B_{xx}	B_{xy}	B_{yx}	B_{yy}	K_{xx}	K_{xy}	K_{yx}	K_{yy}	ν_{crit}	$\bar{\Omega}_{crit}$
0.10	1.13	57.61	32.39	240.91	21.14	-10.71	-10.71	16.89	5.60	10.08	-8.38	-4.04	0.3505	0.5027
0.20	0.58	55.30	34.70	234.31	11.25	-5.69	-5.69	8.22	3.20	5.00	-4.14	-1.47	0.3369	0.5022
0.30	0.38	52.76	37.24	228.05	8.19	-4.03	-4.03	5.31	2.52	3.28	-2.79	-0.59	0.3194	0.4992
0.40	0.28	49.93	40.07	222.07	6.80	-3.22	-3.22	3.83	2.31	2.39	-2.18	-0.12	0.2983	0.4936
0.50	0.22	46.76	43.24	216.33	6.15	-2.74	-2.74	2.91	2.37	1.84	-1.90	0.17	0.2725	0.4841
0.60	0.16	43.12	46.88	210.75	5.94	-2.43	-2.43	2.28	2.68	1.44	-1.80	0.38	0.2375	0.4657
0.70	0.12	38.80	51.20	205.19	6.11	-2.23	-2.23	1.79	3.37	1.13	-1.86	0.55	0.1812	0.4215
0.80	0.08	33.34	56.66	199.45	6.83	-2.09	-2.09	1.37	4.92	0.86	-2.13	0.69	0.0658	0.2657
0.90	0.04	25.51	64.49	192.98	8.99	-2.01	-2.01	0.96	9.92	0.58	-2.94	0.83	0.0000	0.0000

II. 3(a). Non-dimensional oil supply pressure = 0.0.

Table II. 3. Data for the axial groove journal bearing. Groove position 90^o before the loadline.

ε_s	S	ϕ_s^o	θ_{1s}^o	θ_{2s}^o	B_{xx}	B_{xy}	B_{yx}	B_{yy}	K_{xx}	K_{xy}	K_{yx}	K_{yy}	ν_{crit}	$\bar{\Omega}_{crit}$
0.10	0.40	79.76	10.24	267.34	10.98	-3.58	-3.58	8.73	1.94	5.89	-4.70	-1.49	1.2094	0.5456
0.20	0.28	71.51	18.49	248.02	6.98	-2.88	-2.88	5.29	1.67	3.53	-2.82	-0.84	0.7137	0.5417
0.30	0.22	65.89	24.11	236.54	5.53	-2.43	-2.43	3.78	1.55	2.55	-2.05	-0.41	0.5543	0.5340
0.40	0.18	61.00	29.00	227.55	4.90	-2.17	-2.17	2.91	1.57	1.98	-1.67	-0.12	0.4591	0.5239
0.50	0.15	56.15	33.85	219.82	4.68	-2.00	-2.00	2.33	1.73	1.60	-1.50	0.11	0.3851	0.5105
0.60	0.12	50.93	39.07	212.84	4.76	-1.91	-1.91	1.91	2.09	1.31	-1.47	0.29	0.3148	0.4893
0.70	0.10	44.96	45.04	206.31	5.17	-1.86	-1.86	1.57	2.80	1.07	-1.58	0.46	0.2300	0.4443
0.80	0.07	37.68	52.32	199.92	6.12	-1.86	-1.86	1.26	4.36	0.84	-1.91	0.61	0.0888	0.2953
0.90	0.04	27.79	62.21	193.09	8.52	-1.90	-1.90	0.92	9.28	0.59	-2.79	0.78	0.0000	0.0000

II. 3(b). Non-dimensional oil supply pressure = 1.0.

Table II. 3. continued. Data for the axial groove journal bearing. Groove position 90^o before the loadline.

ε_s	S	ϕ_s^o	θ_{1s}^o	θ_{2s}^o	B_{xx}	B_{xy}	B_{yx}	B_{yy}	K_{xx}	K_{xy}	K_{yx}	K_{yy}	ν_{crit}	$\bar{\Omega}_{crit}$
0.10	0.59	79.87	-34.87	256.02	15.11	-3.52	-3.52	19.69	2.08	7.59	-9.48	-1.41	0.6489	0.4915
0.20	0.31	76.59	-31.59	246.49	7.82	-2.32	-2.32	9.73	1.52	3.82	-4.46	-0.66	0.4875	0.4738
0.30	0.22	72.75	-27.75	237.39	5.62	-1.98	-1.98	6.37	1.40	2.58	-2.80	-0.32	0.3624	0.4500
0.40	0.17	68.30	-23.30	228.85	4.74	-1.85	-1.85	4.65	1.44	1.95	-2.01	-0.07	0.2696	0.4240
0.50	0.14	63.14	-18.14	220.94	4.44	-1.81	-1.81	3.57	1.61	1.57	-1.61	0.14	0.2023	0.3983
0.60	0.12	57.17	-12.17	213.61	4.51	-1.81	-1.81	2.80	1.96	1.28	-1.46	0.33	0.1496	0.3691
0.70	0.09	50.16	-5.16	206.76	4.94	-1.83	1.83	2.19	2.65	1.05	-1.52	0.51	0.0942	0.3139
0.80	0.07	41.65	3.35	200.14	5.90	-1.87	-1.87	1.66	4.17	0.82	-1.83	0.68	0.0000	0.0000
0.90	0.04	30.27	14.73	193.16	8.33	-1.92	-1.92	1.12	9.03	0.57	-2.71	0.83	0.0000	0.0000

II. 4(a). Non-dimensional oil supply pressure = 0.0.

Table II. 4. Data for the axial groove journal bearing. Groove position 135^o before the loadline.

ε_s	S	ϕ^o_s	θ^o_{1s}	θ^o_{2s}	B_{xx}	B_{xy}	B_{yx}	B_{yy}	K_{xx}	K_{xy}	K_{yx}	K_{yy}	ν_{crit}	$\bar{\Omega}_{crit}$
0.10	0.38	109.66	-64.66	275.75	13.31	-0.60	-0.60	14.23	0.41	7.13	-7.62	-0.29	4.5235	0.5357
0.20	0.22	95.10	-50.10	257.04	6.73	-1.10	-1.10	7.73	0.82	3.54	-3.95	-0.39	1.2001	0.5180
0.30	0.16	87.33	-42.33	244.22	4.81	-1.22	-1.22	5.28	0.97	2.40	-2.56	-0.27	0.6732	0.4900
0.40	0.13	80.86	-35.86	233.47	4.06	-1.29	-1.29	3.97	1.10	1.83	-1.84	-0.11	0.4293	0.4574
0.50	0.11	74.33	-29.33	224.00	3.82	-1.37	-1.37	3.12	1.31	1.49	-1.47	0.06	0.2884	0.4245
0.60	0.10	67.09	-22.09	215.52	3.94	-1.47	-1.47	2.50	1.65	1.25	-1.32	0.24	0.1967	0.3899
0.70	0.08	58.56	-13.56	207.81	4.41	-1.57	-1.57	2.01	2.32	1.04	-1.37	0.42	0.1191	0.3336
0.80	0.06	48.02	-3.02	200.59	5.45	-1.70	-1.70	1.56	3.82	0.83	-1.69	0.61	0.0049	0.0738
0.90	0.04	33.88	11.12	193.27	8.00	-1.84	-1.84	1.09	8.64	0.59	-2.60	0.79	0.0000	0.000

II. 4(b). Non-dimensional oil supply pressure = 1.0.

Table II . 4. continued. Data for the axial groove journal bearing. Groove position 135^o before the loadline.

ε_s	S	ϕ_s^o	θ_{1s}^o	θ_{2s}^o	B_{xx}	B_{xy}	B_{yx}	B_{yy}	K_{xx}	K_{xy}	K_{yx}	K_{yy}	ν_{crit}	$\bar{\Omega}_{crit}$
0.10	0.53	89.78	-89.78	261.31	19.28	-0.08	-0.08	20.00	0.12	9.49	-9.99	-0.04	6.2237	0.4960
0.20	0.27	89.02	-89.02	252.44	9.51	-0.17	-0.17	10.00	0.26	4.47	-4.96	-0.07	2.5894	0.4828
0.30	0.18	87.51	-87.51	243.44	6.41	-0.29	-0.25	6.66	0.43	2.79	-3.25	-0.10	1.3278	0.4595
0.40	0.14	84.89	-84.89	234.37	5.01	-0.45	-0.45	4.98	0.66	1.95	-2.38	-0.11	0.7015	0.4255
0.50	0.11	80.63	-80.63	225.37	4.36	-0.65	-0.65	3.95	0.98	1.47	-1.84	-0.07	0.3596	0.3815
0.60	0.09	73.99	-73.99	216.63	4.19	-0.92	-0.92	3.20	1.45	1.19	-1.53	0.05	0.1732	0.3267
0.70	0.08	64.40	-64.40	208.40	4.50	-1.23	-1.23	2.58	2.22	1.00	-1.44	0.25	0.0661	0.2431
0.80	0.06	51.72	-51.72	200.79	5.49	-1.55	-1.55	1.96	3.79	0.83	-1.68	0.51	0.0000	0.0000
0.90	0.04	35.43	-35.43	193.30	8.04	-1.81	-1.81	1.29	8.68	0.60	-2.59	0.78	0.0000	0.0000

II. 5(a). Non-dimensional oil supply pressure = 0.0.

Table II. 5. Data for the axial groove journal bearing. Groove position 180^o before the loadline.

ε_s	S	ϕ_s^o	θ_{1s}^o	θ_{2s}^o	B_{xx}	B_{xy}	B_{yx}	B_{yy}	K_{xx}	K_{xy}	K_{yx}	K_{yy}	ν_{crit}	$\bar{\Omega}_{crit}$
0.10			Iterative scheme did not converge for these values of ε_s.											
0.20														
0.30	0.17	98.98	-98.98	248.46	6.69	-0.09	-0.09	6.27	0.17	3.13	-3.36	-0.04	4.1110	0.5007
0.40	0.12	94.82	-94.82	238.05	5.10	-0.24	-0.24	4.68	0.43	2.12	-2.46	-0.08	1.3916	0.4661
0.50	0.10	89.96	-89.96	228.07	4.34	-0.44	-0.44	3.72	0.77	1.56	-1.91	-0.08	0.5993	0.4191
0.60	0.08	83.09	-83.09	218.49	4.10	-0.71	-0.71	3.05	1.25	1.22	-1.57	-0.00	0.2576	0.3588
0.70	0.07	72.97	-72.97	209.49	4.35	-1.06	-1.06	2.49	2.04	1.03	-1.44	0.18	0.0924	0.2708
0.80	0.06	58.73	-58.73	201.27	5.32	-1.44	-1.44	1.93	3.62	0.86	-1.64	0.45	0.0000	0.0000
0.90	0.03	39.55	-39.55	193.41	7.93	-1.77	-1.77	1.28	8.52	0.63	-2.55	0.75	0.0000	0.0000

II. 5(b). Non-dimensional oil supply pressure = 1.0.

Table II. 5. continued. Data for the axial groove journal bearing. Groove position 180^o before the loadline.

ε_s	S	ϕ_s^o	θ_{1s}^o	θ_{2s}^o	B_{xx}	B_{xy}	B_{yx}	B_{yy}	K_{xx}	K_{xy}	K_{yx}	K_{yy}	ν_{crit}	$\bar{\Omega}_{crit}$
0.10	0.97	86.65	-4.52	183.35	20.53	-1.17	26.13	19.97	1.17	10.12	-10.11	14.17	0.2551	0.4893
0.20	0.45	83.93	-11.14	186.07	11.15	-1.06	13.58	9.94	1.07	5.29	-5.25	7.72	0.2517	0.4797
0.30	0.27	81.88	-20.51	188.12	8.57	-0.94	9.50	6.60	0.95	3.85	-3.75	5.50	0.2563	0.4746
0.40	0.18	80.52	-33.37	189.48	7.86	-0.82	7.49	4.93	0.80	3.29	-3.13	4.31	0.2734	0.4767
0.50	0.13	79.88	-50.40	190.12	8.07	-0.70	6.18	3.94	0.61	3.12	-2.89	3.50	0.3068	0.4869
0.60	0.10	79.94	-71.65	190.06	8.93	-0.58	5.08	3.28	0.36	3.14	-2.85	2.81	0.3595	0.5050
0.70	0.08	80.60	-96.06	189.40	10.43	-0.47	3.98	2.82	0.09	3.24	-3.00	2.17	0.4364	0.5324
0.80	0.06	81.76	-121.61	188.24	13.22	-0.36	2.90	2.47	-0.18	3.37	-3.56	1.58	0.5562	0.5771
0.90	0.02	89.81	-158.95	180.19	16.74	-0.01	0.09	2.22	-0.15	1.28	-5.26	0.05	9.0089	0.4246

II. 6(a). Non-dimensional oil supply pressure = 0.0.

Table II. 6. Data for the axial groove journal bearing. Groove position 270^o before the loadline.

ε_s	S	ϕ_s^o	θ_{1s}^o	θ_{2s}^o	B_{xx}	B_{xy}	B_{yx}	B_{yy}	K_{xx}	K_{xy}	K_{yx}	K_{yy}	ν_{crit}	$\overline{\Omega}_{crit}$
0.10	0.35	90.00	-180.00	180.00	13.27	0.00	0.0	13.07	-0.00	6.53	-6.64	0.0	∞	-
0.20	0.28	93.78	-60.55	176.22	11.83	-2.00	5.37	5.75	1.29	5.76	-2.71	3.24	0.4162	0.4732
0.30	0.21	88.45	-53.23	181.55	9.14	-1.24	5.46	4.47	0.93	4.23	-2.24	3.35	0.3308	0.4637
0.40	0.16	85.43	-56.95	184.57	8.19	-0.99	5.07	3.78	0.79	3.55	-2.10	3.11	0.3046	0.4616
0.50	0.12	83.57	-67.02	186.43	8.16	-0.84	4.62	3.30	0.68	3.26	-2.11	2.79	0.3100	0.4697
0.60	0.10	82.56	-82.23	187.44	8.82	-0.70	4.09	2.95	0.53	3.19	-2.26	2.41	0.3432	0.4891
0.70	0.07	82.27	-101.56	187.73	10.24	-0.56	3.45	2.66	0.34	3.24	-2.58	1.98	0.4087	0.5213
0.80	0.06	82.62	-123.64	187.38	13.08	-0.42	2.70	2.42	0.09	3.38	-3.32	1.52	0.5260	0.5725
0.90	0.02	89.89	-159.75	180.11	16.72	-0.01	0.09	2.22	-0.12	1.28	-5.25	0.05	7.6210	0.4244

II. 6(b). Non-dimensional oil supply pressure = 1.0.

Table II. 6. continued. Data for the axial groove journal bearing. Groove position 270^o before the loadline.

APPENDIX III. An Outline of the Bifurcation Calculation.

i) Note on the Co-ordinate Transformation.

With the origin of the X-Y co-ordinate system at the bearing centre O (Figure 5.2) the relationship between the Cartesian and polar co-ordinates is:

$$X = \varepsilon\cos\phi, \qquad Y = \varepsilon\sin\phi \qquad \text{III(1)}$$

$$\Rightarrow \varepsilon^2 = X^2+Y^2 \qquad \cos\phi = \frac{X}{\varepsilon} \qquad \sin\phi = \frac{Y}{\varepsilon}$$

Differentiating equation III(1) with respect to τ:

$$\dot{X} = \dot{\varepsilon}\cos\phi - \varepsilon\dot{\phi}\sin\phi \qquad \dot{Y} = \dot{\varepsilon}\sin\phi + \varepsilon\dot{\phi}\cos\phi$$

$$\Rightarrow \dot{\varepsilon} = \dot{X}\cos\phi + \dot{Y}\sin\phi \qquad \varepsilon\dot{\phi} = \dot{Y}\cos\phi - \dot{X}\sin\phi \qquad \text{III(2)}$$

Referring to Figure 5.2:

$$\bar{F}_X = \frac{1}{S} + \bar{F}_r\cos\phi - \bar{F}_t\sin\phi \qquad \bar{F}_Y = \bar{F}_r\sin\phi + \bar{F}_t\cos\phi \qquad \text{III(3)}$$

Equations III(1),III(2),III(3) define the force components $\bar{F}_X$ and $\bar{F}_Y$ as functions of $X, \dot{X}, Y, \dot{Y}$. To calculate the force derivatives $(\partial\bar{F}_X/\partial X)_s$ etc. the relationship between the co-ordinate derivatives is required. They are derived from equations III(1) and III(2) and are:

$$\frac{\partial\varepsilon}{\partial X} = \cos\phi \qquad \frac{\partial\varepsilon}{\partial Y} = \sin\phi \qquad \frac{\partial\varepsilon}{\partial\dot{X}} = \frac{\partial\varepsilon}{\partial\dot{Y}} = \frac{\partial\phi}{\partial\dot{X}} = \frac{\partial\phi}{\partial\dot{Y}} = 0$$

$$\frac{\partial\phi}{\partial X} = -\frac{1}{\varepsilon}\sin\phi \qquad \frac{\partial\phi}{\partial Y} = \frac{1}{\varepsilon}\cos\phi \qquad \frac{\partial\dot{\varepsilon}}{\partial X} = -\dot{\phi}\sin\phi \qquad \frac{\partial\dot{\varepsilon}}{\partial Y} = \dot{\phi}\cos\phi \qquad \text{III(4)}$$

$$\frac{\partial\dot{\phi}}{\partial X} = \frac{1}{\varepsilon^2}\{\dot{\varepsilon}\sin\phi - \varepsilon\dot{\phi}\cos\phi\} \qquad \frac{\partial\dot{\phi}}{\partial Y} = -\frac{1}{\varepsilon^2}\{\dot{\varepsilon}\cos\phi + \varepsilon\dot{\phi}\sin\phi\}$$

$$\frac{\partial\dot{\varepsilon}}{\partial\dot{X}} = \cos\phi \qquad \frac{\partial\dot{\phi}}{\partial\dot{X}} = -\frac{1}{\varepsilon}\sin\phi \qquad \frac{\partial\dot{\varepsilon}}{\partial\dot{Y}} = \sin\phi \qquad \frac{\partial\dot{\phi}}{\partial\dot{Y}} = \frac{1}{\varepsilon}\cos\phi$$

The eight first order force derivatives may now be calculated by differentiating equations III(3) with respect to $X, \dot{X}, Y, \dot{Y}$ and using equations III(4). For the model investigated in Chapter 5 (ie. a long bearing

operating with a half film) the eight coefficienrs are:

$$B_{XX} = \frac{2\{2\varepsilon_s(\pi^2(2+\varepsilon_s^2)-16)+\pi^2(1-\varepsilon_s^2)(\pi^2(1+\varepsilon_s^2)+8\varepsilon_s^2)\}}{\pi\varepsilon_s(1-\varepsilon_s^2)^{1/2}\{\pi^2(1-\varepsilon_s^2)+4\varepsilon_s^2\}^{3/2}}$$

$$B_{XY} = B_{YX} = \frac{2(2+\varepsilon_s^2)(\pi^2-8)}{\{\pi^2(1-\varepsilon_s^2)+4\varepsilon_s^2\}^{3/2}} \qquad B_{YY} = \frac{\pi(1-\varepsilon_s^2)^{1/2}(2+\varepsilon_s^2)(\pi^2-8)}{\varepsilon_s\{\pi^2(1-\varepsilon_s^2)+4\varepsilon_s^2\}^{3/2}}$$

$$K_{XX} = \frac{2\{8\varepsilon_s^2(2+\varepsilon_s^4)+\pi^2(1-\varepsilon_s^2)(2-\varepsilon_s^2+2\varepsilon_s^4)\}}{(2+\varepsilon_s^2)(1-\varepsilon_s^2)\{\pi^2(1-\varepsilon_s^2)+4\varepsilon_s^2\}^{3/2}} \qquad \text{III(5)}$$

$$K_{XY} = \frac{\pi\{8\varepsilon_s^2(2+\varepsilon_s^4)+\pi^2(1-\varepsilon_s^2)(2-\varepsilon_s^2+2\varepsilon_s^4)\}}{(2+\varepsilon_s^2)(1-\varepsilon_s^2)^{1/2}\{\pi^2(1-\varepsilon_s^2)+4\varepsilon_s^2\}^{3/2}}$$

$$K_{YX} = \frac{\pi\{4\varepsilon_s^4-\pi^2(1-\varepsilon_s^2)^2\}}{\varepsilon_s(1-\varepsilon_s^2)^{1/2}\{\pi^2(1-\varepsilon_s^2)+4\varepsilon_s^2\}^{3/2}} \qquad K_{YY} = \frac{2\{4\varepsilon_s^2+\pi^2(2-\varepsilon_s^2)\}}{\{\pi^2(1-\varepsilon_s^2)+4\varepsilon_s^2\}^{3/2}}$$

ii) <u>The Calculation of $(d\bar{\alpha}/d\bar{\omega})_{\bar{\omega}_{th}}$ and $(d\bar{\Omega}/d\bar{\omega})_{\bar{\omega}_{th}}$</u>

The characteristic equation (equation 5.15) may be written in the form:

$$\bar{\lambda}^4 + \frac{1}{\bar{\omega}^2}A(\varepsilon_s)\bar{\lambda}^3 + \frac{1}{\bar{\omega}^2}\left(B(\varepsilon_s)+\frac{1}{\bar{\omega}^2}C(\varepsilon_s)\right)\bar{\lambda}^2 + \frac{1}{\bar{\omega}^4}D(\varepsilon_s)\bar{\lambda} + \frac{1}{\bar{\omega}^4}E(\varepsilon_s) = 0$$

where: $A(\varepsilon_s) = B_{XX}+B_{YY}$ $\quad B(\varepsilon_s) = K_{XX}+K_{YY}$ $\quad C(\varepsilon_s) = B_{XX}B_{YY}-B_{XY}B_{YX}$

$D(\varepsilon_s) = B_{XX}K_{YY}+B_{YY}K_{XX}-B_{XY}K_{YX}-B_{YX}K_{XY}$ $\quad E(\varepsilon_s) = K_{XX}K_{YY}-K_{XY}K_{YX}$

The Sommerfeld number is a function of the steady state eccentricity ratio: $S = S(\varepsilon_s)$

Since $S = \sigma\bar{\omega} \Rightarrow \sigma\bar{\omega} = S(\varepsilon_s)$ (σ constant)

Differentiating with respect to $\varepsilon_s \Rightarrow \frac{d\bar{\omega}}{d\varepsilon_s} = \frac{1}{\sigma}\frac{dS(\varepsilon_s)}{d\varepsilon_s}$ $\qquad$ III(6)

At the threshold speed $\bar{\omega} = \bar{\omega}_{th}$, $\bar{\lambda}_{th} = +i\bar{\Omega}_{th}$

$$\text{at } \bar{\omega} = \bar{\omega}_{th} + \delta\bar{\omega} \qquad \bar{\lambda} = i\bar{\Omega}_{th} + \left(\frac{d\bar{\alpha}}{d\bar{\omega}}\right)_{\bar{\omega}_{th}}^{\delta\bar{\omega}} + i\left(\frac{d\bar{\Omega}}{d\bar{\omega}}\right)_{\bar{\omega}_{th}}^{\delta\bar{\omega}} = \bar{\lambda}_{th}+\delta\bar{\lambda}$$

Substituting the above expressions into the characteristic equation and retaining only first order terms yields:

$$\left\{4(i\bar{\Omega}_{th})^3 - \frac{3}{\bar{\omega}^2_{th}} A\,\bar{\Omega}^2_{th} + \frac{2}{\bar{\omega}^2_{th}} i\left(B + \frac{1}{\bar{\omega}^2_{th}} C\right)\bar{\Omega}_{th} + \frac{D}{\bar{\omega}^4_{th}}\right\}\delta\bar{\lambda}$$

$$+\left\{\left(\frac{1}{\bar{\omega}^2_{th}}\frac{dA}{d\epsilon_s}\frac{d\epsilon_s}{d\bar{\omega}} - \frac{1}{\bar{\omega}^3_{th}} A\right)(i\bar{\Omega}_{th})^3 - \left[\left(\frac{1}{\bar{\omega}^2_{th}}\frac{dB}{d\epsilon_s} + \frac{1}{\bar{\omega}^4_{th}}\frac{dC}{d\epsilon_s}\right)\frac{d\epsilon_s}{d\bar{\omega}} - \frac{2B}{\bar{\omega}^3_{th}} - \frac{4C}{\bar{\omega}^5_{th}}\right]\bar{\Omega}^2_{th}\right.$$

$$\left. + i\left(\frac{1}{\bar{\omega}^4_{th}}\frac{dD}{d\epsilon_s}\frac{d\epsilon_s}{d\bar{\omega}} - \frac{4D}{\bar{\omega}^5_{th}}\right)\bar{\Omega}_{th} + \left(\frac{1}{\bar{\omega}^4_{th}}\frac{dE}{d\epsilon_s}\frac{d\epsilon_s}{d\bar{\omega}} - \frac{4E}{\bar{\omega}^5_{th}}\right)\right\}\delta\bar{\omega} = 0 \qquad \text{III(7)}$$

from which the derivative $(d\bar{\lambda}/d\bar{\omega})_{\bar{\omega}_{th}}$ may be determined. Separating out the real and imaginary parts of the expression yields the required derivatives:

$$\left(\frac{d\bar{\alpha}}{d\bar{\omega}}\right)_{\bar{\omega}_{th}} \quad \text{and} \quad \left(\frac{d\bar{\Omega}}{d\bar{\omega}}\right)_{\bar{\omega}_{th}}$$

iii) The Calculation of the Eigenvectors $\underline{u}$ and $\underline{v}$.

Let $\underline{v}$ denote the right eigenvector of $\underline{A}^{\bar{\omega}}_{th}$ of the eigenvalue $+i\bar{\Omega}_{th}$, then by definition:

$$(\underline{A}^{\bar{\omega}}_{th} - i\bar{\Omega}_{th}\underline{I})\,\underline{v} = \underline{0} \qquad \text{with } \underline{v} = \begin{pmatrix} v_1 \\ v_2 \\ v_3 \\ v_4 \end{pmatrix} \qquad \text{III(8)}$$

and $\underline{A}^{\bar{\omega}}_{th}$ defined by equation (5.14). Equation III(8) represents 4 equations, one of which is redundant. Taking the first three equations and omitting the subscript th:

$$\begin{aligned} -i\bar{\Omega}v_1 + v_2 &= 0 \\ \frac{1}{\bar{\omega}^2}K_{XX}v_1 + \left(\frac{1}{\bar{\omega}^2}B_{XX} + i\bar{\Omega}\right)v_2 + \frac{1}{\bar{\omega}^2}K_{XY}v_3 + \frac{1}{\bar{\omega}^2}B_{XY}v_4 &= 0 \qquad \text{III(9)} \\ -i\Omega v_3 + v_4 &= 0 \end{aligned}$$

Let $v_1 = \tau = \tau_1 + i\tau_2$, a complex parameter then:

the first equation of equation III(9) $\Rightarrow$ $V_2 = i\bar{\Omega}\tau$

the second equation $\Rightarrow$ $$V_3 = \left\{ \frac{\bar{\Omega}^2\bar{\omega}^2 - K_{XX} - i\bar{\Omega}B_{XX}}{K_{XY} + i\bar{\Omega}B_{XY}} \right\}\tau \qquad \text{III(10)}$$

the third equation $\Rightarrow$ $V_4 = i\bar{\Omega}V_3$

Let $\underline{u}$ denote the left eigenvector of $A^{\bar{\omega}}$th for the eigenvalue $+i\bar{\Omega}_{th}$

then by definition:

$$\underline{u}\ (\underline{A}^{\bar{\omega}}\text{th} - i\bar{\Omega}_{th}\underline{I}) = \underline{0} \text{ with } \underline{u} = (u_1\ u_2\ u_3\ u_4) \qquad \text{III(11)}$$

Again considering the first three equations:

$$\begin{aligned} i\bar{\Omega}u_1 + \frac{1}{\bar{\omega}^2}K_{XX}u_2 + \frac{1}{\bar{\omega}^2}K_{YX}u_4 &= 0 \\ u_1 - \left(\frac{1}{\bar{\omega}^2}B_{XX} + i\bar{\Omega}\right)u_2 - \frac{1}{\bar{\omega}^2}B_{YX}u_4 &= 0 \qquad \text{III(12)} \\ \frac{1}{\bar{\omega}^2}K_{XY}u_2 + i\bar{\Omega}u_3 + \frac{1}{\bar{\omega}^2}K_{YY}u_4 &= 0 \end{aligned}$$

Taking $u_4 = 1$ and eliminating u_1 from the first two equations of equations III(12):

$$\Rightarrow u_2 = \frac{(K_{YX} + i\bar{\Omega}B_{YX})}{\{(\bar{\Omega}^2\bar{\omega}^2 - K_{XX}) - i\bar{\Omega}B_{XX}\}}$$

Substituting into the second and third equations of equation III(12):

$$\Rightarrow u_1 = \frac{1}{\bar{\omega}^2}B_{YX} + \left(\frac{1}{\bar{\omega}^2}B_{XX} + i\bar{\Omega}\right)\left\{ \frac{K_{YX} + i\bar{\Omega}B_{YX}}{(\bar{\omega}^2\bar{\Omega}^2 - K_{XX}) - i\bar{\Omega}B_{XX}} \right\} \qquad \text{III(13)}$$

$$\text{and } u_3 = -\frac{1}{i\bar{\Omega}\bar{\omega}^2}\left\{ K_{YY} + \frac{K_{XY}(K_{YX} + i\bar{\Omega}B_{YX})}{(\bar{\omega}^2\bar{\Omega}^2 - K_{XX}) - i\bar{\Omega}B_{XX}} \right\}$$

In the bifurcation calculation it is necessary to calculate the real and imaginary parts of the components of $\underline{u}$ and $\underline{v}$. This is a straightforward, but tedious process. τ, the complex parameter, is chosen to satisfy the normalisation requirement $\underline{u}\,\underline{v} = \underline{1}$

$$\Rightarrow u_1v_1 + u_2v_2 + u_3v_3 + u_4v_4 = 1$$

iv) The Inverse of the Matrices $\underline{A}^{\bar{\omega}}th$ and $(\underline{A}^{\bar{\omega}}th - 2i\bar{\Omega}_{th}\underline{I})$.

It is easily verified that the inverse of $\underline{A}^{\bar{\omega}}th$ is:

$$(\underline{A}^{\bar{\omega}}th)^{-1} = \frac{1}{\text{Det } \underline{A}} \begin{pmatrix} \frac{1}{\bar{\omega}^4}(B_{YX}K_{XY}-B_{XX}K_{YY}) & -\frac{1}{\bar{\omega}^2}K_{YY} & \frac{1}{\bar{\omega}^4}(B_{YY}K_{XY}-B_{XY}K_{YY}) & \frac{1}{\bar{\omega}^2}K_{XY} \\ -\frac{1}{\bar{\omega}^4}(K_{XY}K_{YX}-K_{XX}K_{YY}) & 0 & 0 & 0 \\ \frac{1}{\bar{\omega}^4}(K_{YX}B_{XX}-K_{XX}B_{YX}) & \frac{1}{\bar{\omega}^2}K_{YX} & \frac{1}{\bar{\omega}^4}(B_{XY}K_{YX}-K_{XX}B_{YY}) & -\frac{1}{\bar{\omega}^2}K_{XX} \\ 0 & 0 & -\frac{1}{\bar{\omega}^4}(K_{YX}K_{XY}-K_{XX}K_{YY}) & 0 \end{pmatrix} \quad \text{III(14)}$$

where $\text{Det } \underline{A} = \frac{1}{\bar{\omega}^4}(K_{XX}K_{YY}-K_{XY}K_{YX})$

In fact only four non-zero elements of $\underline{A}^{-1}$ are required in the calculation:

they are $(\underline{A}^{-1})_{12}$ $(\underline{A}^{-1})_{32}$ $(\underline{A}^{-1})_{14}$ $(\underline{A}^{-1})_{34}$

Let $\underline{C} = \underline{A}^{\bar{\omega}}th - 2i\bar{\Omega}_{th}\underline{I}$

$$\Rightarrow \underline{C} = \begin{pmatrix} -2i\bar{\Omega} & 1 & 0 & 0 \\ -\frac{1}{\bar{\omega}^2}K_{XX} & -\frac{1}{\bar{\omega}^2}B_{XX}-2i\bar{\Omega} & -\frac{1}{\bar{\omega}^2}K_{XY} & -\frac{1}{\bar{\omega}^2}B_{XY} \\ 0 & 0 & -2i\bar{\Omega} & 1 \\ -\frac{1}{\bar{\omega}^2}K_{YX} & -\frac{1}{\bar{\omega}^2}B_{YX} & -\frac{1}{\bar{\omega}^2}K_{YY} & -\frac{1}{\bar{\omega}^2}B_{YY}-2i\bar{\Omega} \end{pmatrix} \quad \text{III(15)}$$

The elements of $\underline{C}^{-1}$ which are required in the calculation are:

$(\underline{C}^{-1})_{12}$, $(\underline{C}^{-1})_{22}$, $(\underline{C}^{-1})_{32}$ $(\underline{C}^{-1})_{42}$ $(\underline{C}^{-1})_{14}$ $(\underline{C}^{-1})_{24}$ $(\underline{C}^{-1})_{34}$ $(\underline{C}^{-1})_{44}$

These elements are calculated following the usual procedure for matrix inversion:

$$(C^{-1})_{12} = \frac{(4\bar{\Omega}^2\bar{\omega}^2-K_{YY})-2i\bar{\Omega}B_{YY}}{\bar{\omega}^2 \text{ Det } C} \qquad (C^{-1})_{22} = \frac{4\bar{\Omega}^2B_{YY}+2i\bar{\Omega}(4\bar{\Omega}^2\bar{\omega}^2-K_{YY})}{\bar{\omega}^2 \text{ Det } C}$$

$$(C^{-1})_{32} = \frac{K_{YX} + 2i\bar{\Omega}B_{YX}}{\bar{\omega}^2 \text{ Det } C} \qquad (C^{-1})_{42} = \frac{-4\bar{\Omega}^2 B_{YX} + 2i\bar{\Omega}K_{YX}}{\bar{\omega}^2 \text{ Det } C} \qquad \text{III(16)}$$

$$(C^{-1})_{14} = \frac{K_{XY} + 2i\bar{\Omega}B_{XY}}{\bar{\omega}^2 \text{ Det } C} \qquad (C^{-1})_{24} = \frac{-4\bar{\Omega}^2 B_{XY} + 2i\bar{\Omega}K_{XY}}{\bar{\omega}^2 \text{ Det } C}$$

$$(C^{-1})_{34} = \frac{(4\bar{\Omega}^2\bar{\omega}^2 - K_{XX}) - 2i\bar{\Omega}B_{XX}}{\bar{\omega}^2 \text{ Det } C} \qquad (C^{-1})_{44} = \frac{4\bar{\Omega}^2 B_{XX} + 2i\bar{\Omega}(4\bar{\Omega}^2\bar{\omega}^2 - K_{XX})}{\bar{\omega}^2 \text{ Det } C}$$

where $\text{Det } C = 16\bar{\Omega}^4 - 4\frac{\bar{\Omega}^2}{\bar{\omega}^2}\left\{(K_{XX}+K_{YY}) + \frac{1}{\bar{\omega}^2}(B_{XX}B_{YY} - B_{XY}B_{YX})\right\} + \frac{1}{\bar{\omega}^4}(K_{XX}K_{YY} - K_{XY}K_{YX})$

$$- 6i\frac{\bar{\Omega}^3}{\bar{\omega}^2}(B_{XX}+B_{YY})$$

It is necessary to calculate the real and imaginary parts of the above expressions.

v) The Calculation of $\partial^2 F^{\ell}/\partial x_j \partial x_k$, $\partial^3 F^{\ell}/\partial x_i \partial x_j \partial x_k$ $(i,j,k,\ell = 1,2,3,4)$

Referring to equation (5.11):

$$\underline{F}(\underline{X},\bar{\omega},S) = \begin{pmatrix} X_2 \\ \frac{S}{\bar{\omega}^2}\bar{F}_X \quad (X_1,X_2,X_3,X_4,S) \\ X_4 \\ \frac{S}{\bar{\omega}^2}\bar{F}_Y \quad (X_1,X_2,X_3,X_4,S) \end{pmatrix} \qquad \text{III(17)}$$

(where $X = X_1, \dot{X} = X_2, Y = X_3, \dot{Y} = X_4$)

$$\text{Since } \dot{F}^1 = X_2 \Rightarrow \frac{\partial^2 F^1}{\partial X_j \partial X_k} = \frac{\partial^3 F^1}{\partial X_j \partial X_k \partial X_p} \equiv 0 \ \forall_{j,k,p} \qquad \text{III(18)}$$

$$\text{and} \quad F^3 = X_4 \Rightarrow \frac{\partial^2 F^3}{\partial X_j \partial X_k} = \frac{\partial^3 F^3}{\partial X_j \partial X_k \partial X_p} \equiv 0 \ \forall_{j,k,p} \qquad \text{III(19)}$$

$$F^2 = \frac{S}{\bar{\omega}^2}\bar{F}_X \Rightarrow \frac{\partial^2 F^2}{\partial X_j \partial X_k} = \frac{S}{\bar{\omega}^2}\frac{\partial^2 \bar{F}_X}{\partial X_j \partial X_k}\ ; \ \frac{\partial^3 F^2}{\partial X_j \partial X_k \partial X_p} = \frac{S}{\bar{\omega}^2}\frac{\partial^3 \bar{F}_X}{\partial X_j \partial X_k \partial X_p} \qquad \text{III(20)}$$

and similarly for $F^4 = \frac{S}{\bar{\omega}^2}\bar{F}_Y$ etc.

The derivatives of $\bar{F}_X$ and $\bar{F}_Y$ are calculated be differentiating equations III(3) and using equations III(4). For the model under

investigation the hydrodynamic forces $\bar{F}_r$, $\bar{F}_t$ are given by equations (5.16). For the purpose of calculating the derivatives they are most conveniently written in the form:

$$-\bar{F}_r = (1-2\dot{\phi})\,A(\varepsilon) + B(\varepsilon)\dot{\varepsilon} \qquad \text{III(21)}$$
$$F_t = (1-2\dot{\phi})\,C(\varepsilon) + D(\varepsilon)\dot{\varepsilon}$$

$$\text{where } A(\varepsilon) = \frac{12\varepsilon^2}{(2+\varepsilon^2)(1-\varepsilon^2)} \qquad B(\varepsilon) = \frac{6(\pi^2(2+\varepsilon^2)-16)}{\pi(2+\varepsilon^2)(1-\varepsilon^2)^{3/2}} \qquad \text{III(22)}$$

$$C(\varepsilon) = \frac{6\pi\varepsilon}{(1-\varepsilon^2)^{1/2}(2+\varepsilon^2)} \quad D(\varepsilon) = \frac{24\varepsilon}{(2+\varepsilon^2)(1-\varepsilon^2)} = \frac{2A(\varepsilon)}{\varepsilon}$$

The derivatives are all evaluated at the steady state equilibrium position and with $\bar{\omega} = \bar{\omega}_{th}$ in equation III(20).

The derivatives are:

$$a_5 = S\frac{\partial^2\bar{F}_x}{\partial X^2} = S\Big\{-A^{11}\cos^3\phi_s + 3\left(\frac{A}{\varepsilon_s^2} - \frac{A^1}{\varepsilon_s}\right)\sin^2\phi_s\cos\phi_s - C^{11}\sin\phi_s\cos^2\phi_s$$
$$+\left(\frac{C^1}{\varepsilon_s} - \frac{C}{\varepsilon_s^2}\right)(2\cos^2\phi_s - \sin^2\phi_s)\sin\phi_s\Big\}$$

$$a_6 = S\frac{\partial^2\bar{F}_X}{\partial Y^2} = S\Big\{\left(\frac{A}{\varepsilon_s^2} - \frac{A^1}{\varepsilon_s}\right)(\cos^2\phi_s - 2\sin^2\phi_s)\cos\phi_s - A^{11}\cos\phi_s\sin^2\phi_s$$
$$- C^{11}\sin^3\phi_s + 3\left(\frac{C}{\varepsilon_s^2} - \frac{C^1}{\varepsilon_s}\right)\cos^2\phi_s\sin\phi_s\Big\}$$

$$a_7 = S\frac{\partial^2\bar{F}_X}{\partial X\partial Y} = S\Big\{-A^{11}\cos^2\phi_s\sin\phi_s - \left(\frac{A}{\varepsilon_s^2} - \frac{A^1}{\varepsilon_s}\right)(2\sin\phi_s\cos^2\phi_s - \sin^3\phi_s)$$
$$- C^{11}\cos\phi_s\sin^2\phi_s + \left(\frac{C}{\varepsilon_s^2} - \frac{C^1}{\varepsilon_s}\right)(\cos^2\phi_s - 2\sin^2\phi_s)\cos\phi_s\Big\}$$

$$a_8 = S\frac{\partial^2\bar{F}_X}{\partial X\partial X} = -S\Big\{B^1\cos^3\phi_s + 2\left(\frac{B}{\varepsilon_s} + \frac{C^1}{\varepsilon_s} - 3\frac{C}{\varepsilon_s^2}\right)\sin^2\phi_s\cos\phi_s$$
$$+\left(D^1 - \frac{D}{\varepsilon_s} + 2\frac{A^1}{\varepsilon_s} - 4\frac{A}{\varepsilon_s^2}\right)\sin\phi_s\cos^2\phi_s + \left(\frac{D}{\varepsilon_s} + 2\frac{A}{\varepsilon_s^2}\right)\sin^3\phi_s\Big\}$$

$$a_9 = S\frac{\partial^2\bar{F}_X}{\partial Y\partial Y} = S\left\{2\left(\frac{A^1}{\varepsilon_s} - \frac{A}{\varepsilon_s^2}\right)\cos^2\phi_s\sin\phi_s - D^1\sin^3\phi_s - 2\left(2\frac{A}{\varepsilon_s^2} + \frac{D}{\varepsilon_s}\right)\sin\phi_s\cos^2\phi_s\right.$$
$$\left. + \left(2\frac{C^1}{\varepsilon_s} - 4\frac{C}{\varepsilon_s^2} - B^1 + \frac{B}{\varepsilon_s}\right)\sin^2\phi_s\cos\phi_s + \left(2\frac{C}{\varepsilon_s^2} - \frac{B}{\varepsilon_s}\right)\cos^3\phi_s\right\}$$

$$a_{10} = S\frac{\partial^2\bar{F}_X}{\partial X\partial Y} = S\left\{2\left(\frac{A^1}{\varepsilon_s} - \frac{A}{\varepsilon_s^2}\right)\cos^3\phi_s + \left(4\frac{A}{\varepsilon_s^2} + 2\frac{D}{\varepsilon_s} - D^1\right)\sin^2\phi_s\cos\phi_s\right.$$
$$\left. + \left(2\frac{C^1}{\varepsilon_s} - 4\frac{C}{\varepsilon_s^2} - B^1 + \frac{B}{\varepsilon_s}\right)\sin\phi_s\cos^2\phi_s + \left(2\frac{C}{\varepsilon_s^2} - \frac{B}{\varepsilon_s}\right)\sin^3\phi_s\right\}$$

$$a_{11} = S\frac{\partial^2\bar{F}_X}{\partial Y\partial X} = -S\left\{\left(B^1 - 2\frac{B}{\varepsilon_s} + 4\frac{C}{\varepsilon_s^2}\right)\sin\phi_s\cos^2\phi_s + 2\left(\frac{C^1}{\varepsilon_s} - \frac{C}{\varepsilon_s^2}\right)\sin^3\phi_s\right.$$
$$\left. + \left(D^1 - \frac{D}{\varepsilon_s} + 2\frac{A^1}{\varepsilon_s} - 4\frac{A}{\varepsilon_s^2}\right)\sin^2\phi_s\cos\phi_s + \left(\frac{D}{\varepsilon_s} + 2\frac{A}{\varepsilon_s^2}\right)\cos^3\phi_s\right\}$$

$$a_{12} = S\frac{\partial^2\bar{F}_X}{\partial X^2} = 0 \qquad a_{13} = S\frac{\partial^2\bar{F}_X}{\partial X\partial Y} = 0$$

$$a_{14} = S\frac{\partial^2\bar{F}_X}{\partial Y^2} = 0$$

$$a_{15} = S\frac{\partial^3\bar{F}_X}{\partial X^3} = S\left\{-A^{111}\cos^4\phi_s - 6\left(\frac{A^{11}}{\varepsilon_s} - 2\frac{A^1}{\varepsilon_s^2} + 2\frac{A}{\varepsilon_s^3}\right)\sin^2\phi_s\cos^2\phi_s\right.$$
$$- 3\left(\frac{A^1}{\varepsilon_s^2} - \frac{A}{\varepsilon_s^3}\right)\sin^4\phi_s - \left(C^{111} - 3\frac{C^{11}}{\varepsilon_s} + 6\frac{C^1}{\varepsilon_s^2} - 6\frac{C}{\varepsilon_s^3}\right)\sin\phi_s\cos^3\phi_s$$
$$\left. - 3\left(\frac{C^{11}}{\varepsilon_s} - 3\frac{C^1}{\varepsilon_s^2} + 3\frac{C}{\varepsilon_s^3}\right)\sin^3\phi_s\cos\phi_s\right\}$$

$$a_{16} = S\frac{\partial^3\bar{F}_X}{\partial Y^3} = S\left\{-\left(A^{111} - 3\frac{A^{11}}{\varepsilon_s} + 6\frac{A^1}{\varepsilon_s^2} - 6\frac{A}{\varepsilon_s^3}\right)\sin^3\phi_s\cos\phi_s - C^{111}\sin^4\phi_s\right.$$
$$- 3\left(\frac{A^{11}}{\varepsilon_s} - 3\frac{A^1}{\varepsilon_s^2} + 3\frac{A}{\varepsilon_s^3}\right)\cos^3\phi_s\sin\phi_s + 3\left(\frac{C}{\varepsilon_s^3} - \frac{C^1}{\varepsilon_s^2}\right)\cos^4\phi_s$$
$$\left. - 6\left(\frac{C^{11}}{\varepsilon_s} - 2\frac{C^1}{\varepsilon_s^2} + 2\frac{C}{\varepsilon_s^3}\right)\cos^2\phi_s\sin^2\phi_s\right\}$$

$$a_{17} = S\frac{\partial^3 \bar{F}_X}{\partial X^2 \partial Y} = -S\left\{\left(A^{111} - 3\frac{A^{11}}{\varepsilon_s} + 6\frac{A^1}{\varepsilon_s^2} - 6\frac{A}{\varepsilon_s^3}\right)\sin\phi_s\cos^3\phi_s\right.$$

$$+ 3\left(\frac{A^{11}}{\varepsilon_s} - 3\frac{A^1}{\varepsilon_s^2} + 3\frac{A}{\varepsilon_s^3}\right)\sin^3\phi_s\cos\phi_s - \left(C^{111} - 4\frac{C^{11}}{\varepsilon_s} + 11\frac{C^1}{\varepsilon_s^2} - 11\frac{C}{\varepsilon_s^3}\right)\sin^2\phi_s\cos^2\phi_s$$

$$\left. + \left(\frac{C^{11}}{\varepsilon_s} - 2\frac{C^1}{\varepsilon_s^2} + 2\frac{C}{\varepsilon_s^3}\right)(\sin^4\phi_s + \cos^4\phi_s)\right\}$$

$$a_{18} = S\frac{\partial^3 \bar{F}_X}{\partial X^2 \partial X} = -S\left\{B^{11}\cos^4\phi_s + \left(5\frac{B^1}{\varepsilon_s} - 6\frac{B}{\varepsilon_s^2} + 2\frac{C^{11}}{\varepsilon_s} - 12\frac{C^1}{\varepsilon_s^2} + 24\frac{C}{\varepsilon_s^3}\right)\sin^2\phi_s\cos^2\phi_s\right.$$

$$+ 2\left(\frac{B}{\varepsilon_s^2} + \frac{C^1}{\varepsilon_s^2} - 3\frac{C}{\varepsilon_s^3}\right)\sin^4\phi_s + \left(D^{11} - 2\frac{D^1}{\varepsilon_s} + 2\frac{D}{\varepsilon_s^2} + 2\frac{A^{11}}{\varepsilon_s} - 8\frac{A^1}{\varepsilon_s^2} + 12\frac{A}{\varepsilon_s^3}\right)\cos^3\phi_s\sin\phi_s$$

$$\left. + 3\left(\frac{D^1}{\varepsilon_s} - 2\frac{D}{\varepsilon_s^2} + 2\frac{A^1}{\varepsilon_s^2} - 6\frac{A}{\varepsilon_s^3}\right)\sin^3\phi_s\cos\phi_s\right\}$$

$$a_{19} = S\frac{\partial^3 \bar{F}_X}{\partial X^2 \partial Y} = S\left\{2\left(\frac{A^{11}}{\varepsilon_s} - 2\frac{A^1}{\varepsilon_s^2} + 2\frac{A}{\varepsilon_s^3}\right)\cos^4\phi_s + \left(10\frac{A^1}{\varepsilon_s^2} - 22\frac{A}{\varepsilon_s^3} - D^{11} + 4\frac{D^1}{\varepsilon_s} - 6\frac{D}{\varepsilon_s^2}\right)\sin^2\phi_s\cos^2\phi_s\right.$$

$$+ \left(4\frac{A}{\varepsilon_s^3} + 2\frac{D}{\varepsilon_s^2} - \frac{D^1}{\varepsilon_s}\right)\sin^4\phi_s + \left(2\frac{C^{11}}{\varepsilon_s} - 8\frac{C^1}{\varepsilon_s^2} + 12\frac{C}{\varepsilon_s^3} - B^{11} + 2\frac{B^1}{\varepsilon_s} - 2\frac{B}{\varepsilon_s}\right)\sin\phi_s\cos^3\phi_s$$

$$\left. + \left(6\frac{C^1}{\varepsilon_s^2} - 18\frac{C}{\varepsilon_s^3} - 3\frac{B^1}{\varepsilon_s} + 6\frac{B}{\varepsilon_s^2}\right)\sin^3\phi_s\cos\phi_s\right\}$$

$$a_{20} = S\frac{\partial^3 \bar{F}_X}{\partial Y^2 \partial X} = -S\left\{\left(A^{111} - 4\frac{A^{11}}{\varepsilon_s} + 11\frac{A^1}{\varepsilon_s^2} - 11\frac{A}{\varepsilon_s^3}\right)\sin^2\phi_s\cos^2\phi_s + \left(C^{111} - 3\frac{C^{11}}{\varepsilon_s} + 6\frac{C^1}{\varepsilon_s^2} - 6\frac{C}{\varepsilon_s^3}\right)\right.$$

$$\sin^3\phi_s\cos\phi_s$$

$$\left. + \left(\frac{A^{11}}{\varepsilon_s} - 2\frac{A^1}{\varepsilon_s^2} + 2\frac{A}{\varepsilon_s^3}\right)(\cos^4\phi_s + \sin^4\phi_s)\right.$$

$$\left. + 3\left(\frac{C^{11}}{\varepsilon_s} - 3\frac{C^1}{\varepsilon_s^2} + 3\frac{C}{\varepsilon_s^3}\right)\cos^3\phi_s\sin\phi_s\right\}$$

$$a_{21} = S\frac{\partial^3 \bar{F}_X}{\partial Y^2 \partial X} = -S\left\{\left(B^{11} - 4\frac{B^1}{\varepsilon_s} + 6\frac{B}{\varepsilon_s^2} + 10\frac{C^1}{\varepsilon_s^2} - 22\frac{C}{\varepsilon_s^3}\right)\sin^2\phi_s\cos^2\phi_s\right.$$

$$+ 2\left(\frac{C^{11}}{\varepsilon_s} - 2\frac{C^1}{\varepsilon_s^2} + 2\frac{C}{\varepsilon_s^3}\right)\sin^4\phi_s + \left(\frac{B^1}{\varepsilon_s} - 2\frac{B}{\varepsilon_s^2} + 4\frac{C}{\varepsilon_s^3}\right)\cos^4\phi_s$$

$$+\left(D^{11}-2\frac{D^1}{\varepsilon_s}+2\frac{D}{\varepsilon_s^2}+2\frac{A^{11}}{\varepsilon_s}-8\frac{A^1}{\varepsilon_s^2}+12\frac{A}{\varepsilon_s^3}\right)\sin^3\phi_s\cos\phi_s+3\left(\frac{D^1}{\varepsilon_s}-2\frac{D}{\varepsilon_s^2}+2\frac{A^1}{\varepsilon_s^2}-6\frac{A}{\varepsilon_s^3}\right)\Bigg\}$$

$\cos^3\phi_s\sin\phi_s$

$$a_{22}=S\frac{\partial^3\bar{F}_X}{\partial Y^2\partial Y}=S\Bigg\{\left(2\frac{A^{11}}{\varepsilon_s}-12\frac{A^1}{\varepsilon_s^2}+24\frac{A}{\varepsilon_s^3}-5\frac{D^1}{\varepsilon_s}+6\frac{D}{\varepsilon_s^2}\right)\sin^2\phi_s\cos^2\phi_s-D^{11}\sin^4\phi_s$$

$$+2\left(\frac{A^1}{\varepsilon_s^2}-3\frac{A}{\varepsilon_s^3}-\frac{D}{\varepsilon_s^2}\right)\cos^4\phi_s+\left(2\frac{C^{11}}{\varepsilon_s}-8\frac{C^1}{\varepsilon_s^2}+12\frac{C}{\varepsilon_s^3}-B^{11}+2\frac{B^1}{\varepsilon_s}-2\frac{B}{\varepsilon_s^2}\right)\sin^3\phi_s\cos\phi_s$$

$$+3\left(2\frac{C^1}{\varepsilon_s^2}-6\frac{C}{\varepsilon_s^3}-\frac{B^1}{\varepsilon_s^2}+2\frac{B}{\varepsilon_s^2}\right)\sin\phi_s\cos^3\phi_s\Bigg\}$$

$$a_{23}=S\frac{\partial^3\bar{F}_X}{\partial X\partial Y\partial X}=-S\Bigg\{\left(B^{11}-3\frac{B^1}{\varepsilon_s}+4\frac{B}{\varepsilon_s^2}-4\frac{C^1}{\varepsilon_s^2}+12\frac{C}{\varepsilon_s^3}\right)\sin\phi_s\cos^3\phi_s$$

$$+2\left(\frac{B^1}{\varepsilon_s}-2\frac{B}{\varepsilon_s^2}+\frac{C^{11}}{\varepsilon_s}-5\frac{C^1}{\varepsilon_s^2}+9\frac{C}{\varepsilon_s^3}\right)\sin^3\phi_s\cos\phi_s+\left(D^{11}-3\frac{D^1}{\varepsilon_s}+6\frac{D}{\varepsilon_s^2}+2\frac{A^{11}}{\varepsilon_s}-10\frac{A^1}{\varepsilon_s^2}+22\frac{A}{\varepsilon_s^3}\right)$$

$\sin^2\phi_s\cos^2\phi_s$

$$+\left(\frac{D^1}{\varepsilon_s}-\frac{D}{\varepsilon_s^2}+2\frac{A^1}{\varepsilon_s^2}-4\frac{A}{\varepsilon_s^3}\right)\sin^4\phi_s+\left(\frac{D^1}{\varepsilon_s}-\frac{D}{\varepsilon_s^2}+2\frac{A^1}{\varepsilon_s^2}-4\frac{A}{\varepsilon_s^3}\right)\cos^4\phi_s\Bigg\}$$

$$a_{24}=S\frac{\partial^3\bar{F}_X}{\partial X\partial Y\partial Y}=S\Bigg\{2\left(\frac{A^{11}}{\varepsilon_s}-5\frac{A^1}{\varepsilon_s^2}+9\frac{A}{\varepsilon_s^3}-\frac{D^1}{\varepsilon_s}+2\frac{D}{\varepsilon_s^3}\right)\sin\phi_s\cos^3\phi_s$$

$$-\left(D^{11}-3\frac{D^1}{\varepsilon_s}+4\frac{D}{\varepsilon_s^2}-4\frac{A^1}{\varepsilon_s^2}+12\frac{A}{\varepsilon_s^3}\right)\sin^3\phi_s\cos\phi_s$$

$$+\left(2\frac{C^{11}}{\varepsilon_s}-10\frac{C^1}{\varepsilon_s^2}+22\frac{C}{\varepsilon_s^3}-B^{11}+3\frac{B^1}{\varepsilon_s}-6\frac{B}{\varepsilon_s^2}\right)\cos^2\phi_s\sin^2\phi_s$$

$$+\left(2\frac{C^1}{\varepsilon_s^2}-4\frac{C}{\varepsilon_s^3}-\frac{B^1}{\varepsilon_s}+\frac{B}{\varepsilon_s^2}\right)(\sin^4\phi_s+\cos^4\phi_s)\Bigg\}$$

$$a_{25}=S\frac{\partial^3\bar{F}_X}{\partial X\partial X^2}=0 \qquad a_{26}=S\frac{\partial^3\bar{F}_X}{\partial Y\partial X^2}=0$$

$$a_{27}=S\frac{\partial^3\bar{F}_X}{\partial X\partial Y^2}=0 \qquad a_{28}=S\frac{\partial^3\bar{F}_X}{\partial Y\partial Y^2}=0$$

$$a_{29}=S\frac{\partial^3\bar{F}_X}{\partial X\partial X\partial Y}=0 \qquad a_{30}=S\frac{\partial^3\bar{F}_X}{\partial Y\partial X\partial Y}=0$$

$$a_{31} = S\,\frac{\partial^3 \bar{F}_X}{\partial X^2 \partial Y} = 0 \qquad a_{32} = S\,\frac{\partial^3 \bar{F}_X}{\partial Y^2 \partial X} = 0$$

$$a_{33} = S\,\frac{\partial^3 \bar{F}_X}{\partial X^3} = 0 \qquad a_{34} = S\,\frac{\partial^3 \bar{F}_X}{\partial Y^3} = 0$$

where:
$$A^1 = \left.\frac{dA}{d\varepsilon}\right|_{\varepsilon_s} = \frac{4\varepsilon_s(2+\varepsilon_s^4)}{(2+\varepsilon_s^2)^2(1-\varepsilon_s^2)^2}$$

$$A^{11} = \left.\frac{d^2A}{d\varepsilon^2}\right|_{\varepsilon_s} = \frac{4(4+6\varepsilon_s^2+24\varepsilon_s^4-\varepsilon_s^6+3\varepsilon_s^8)}{(2+\varepsilon_s^2)^3(1-\varepsilon_s^2)^3}$$

$$A^{111} = \left.\frac{d^3A}{d\varepsilon^3}\right|_{\varepsilon_s} = \frac{24\varepsilon_s(8+44\varepsilon_s^2+16\varepsilon_s^4+40\varepsilon_s^6-2\varepsilon_s^8+2\varepsilon_s^{10})}{(2+\varepsilon_s^2)^4(1-\varepsilon_s^2)^4}$$

$$B^1 = \left.\frac{dB}{d\varepsilon}\right|_{\varepsilon_s} = \frac{\varepsilon_s(a+b\varepsilon_s^2+c\varepsilon_s^4)}{\pi(2+\varepsilon_s^2)^2(1-\varepsilon_s^2)^{5/2}} \quad a = 12\pi^2 - 64,\ b = 12\pi^2 - 80,\ c = 3\pi^2.$$

$$B^{11} = \left.\frac{d^2B}{d\varepsilon^2}\right|_{\varepsilon_s} = \frac{\{2a+(5a+6b)\varepsilon_s^2+(8a+3b+10c)\varepsilon_s^4+(6b+c)\varepsilon_s^6+4c\varepsilon_s^8\}}{\pi(2+\varepsilon_s^2)^3(1-\varepsilon_s^2)^{7/2}}$$

$$C^1 = \left.\frac{dC}{d\varepsilon}\right|_{\varepsilon_s} = \frac{\pi(2-\varepsilon_s^2+2\varepsilon_s^4)}{(1-\varepsilon_s^2)^{3/2}(2+\varepsilon_s^2)^2} \qquad C^{11} = \left.\frac{d^2C}{d\varepsilon^2}\right|_{\varepsilon_s} = \frac{3\pi\varepsilon_s^3(10-3\varepsilon_s^2+2\varepsilon_s^4)}{(1-\varepsilon_s^2)^{5/2}(2+\varepsilon_s^2)^3}$$

$$C^{111} = \left.\frac{d^3C}{d\varepsilon^3}\right|_{\varepsilon_s} = \frac{3\pi\varepsilon_s^2(60-20\varepsilon_s^2+111\varepsilon_s^4-24\varepsilon_s^6+8\varepsilon_s^8)}{(1-\varepsilon_s^2)^{7/2}(2+\varepsilon_s^2)^4}$$

$$D^1 = \left.\frac{dD}{d\varepsilon}\right|_{\varepsilon_s} = \frac{4(2+\varepsilon_s^2+3\varepsilon_s^4)}{(1-\varepsilon_s^2)^2(2+\varepsilon_s^2)^2}$$

$$D^{11} = \left.\frac{d^2D}{d\varepsilon^2}\right|_{\varepsilon_s} = \frac{24\varepsilon_s(2+7\varepsilon_s^2+\varepsilon_s^4+2\varepsilon_s^6)}{(1-\varepsilon_s^2)^3(2+\varepsilon_s^2)^3}$$

The derivatives of $\bar{F}_Y$ ($b_5 \to b_{34}$) are obtained from the corresponding derivatives of $\bar{F}_X$ by replacing A by -C, B by -D, C by A and D by B (this fact may be deduced from equations III(3) and III(21)).

Note that:

$$\frac{\partial^2 \bar{F}_Y}{\partial X \partial X} = \frac{\partial^2 \bar{F}_X}{\partial X \partial Y} \quad (\text{ie. } b_8 = a_{10}) \qquad \frac{\partial^2 \bar{F}_Y}{\partial Y \partial X} = \frac{\partial^2 \bar{F}_X}{\partial Y \partial Y} \quad (\text{ie. } b_{11} = a_9)$$

$$\frac{\partial^3 \bar{F}_Y}{\partial X^2 \partial X} = \frac{\partial^3 \bar{F}_X}{\partial X^2 \partial Y} \quad (\text{ie. } b_{18} = a_{19}) \qquad \frac{\partial^3 \bar{F}_Y}{\partial X \partial Y \partial X} = \frac{\partial^3 \bar{F}_X}{\partial X \partial Y \partial Y} \quad (\text{ie. } b_{23} = a_{24})$$

$$\frac{\partial^3 \bar{F}_Y}{\partial Y^2 \partial X} = \frac{\partial^3 \bar{F}_X}{\partial Y^2 \partial Y} \quad (\text{ie. } b_{21} = a_{22})$$

Thus all the quantities required to use Poore's bifurcation formula (equation (5.4)) have been determined. The calculation is completed by writing out equation (5.4) in full (ie. summing over the repeated indices from 1 to 4) and separating out the real and imaginary parts. The sign of the quantities $\delta^1(0)$, $\eta^1(0)$ may then be determined.

APPENDIX IV. DESIGN OF TEST APPARATUS.

ACKNOWLEDGEMENTS.

The author would like to express his thanks to Dr. A. V. Ruddy, Research Fellow in the Department of Mechanical Engineering, University of Leeds, for his help with the design of the test apparatus. Thanks are also due to Mr. R. T. Harding of the same department and his technical staff, who were responsible for the detailed drawings, manufacture and construction of the apparatus.

IV.1. INTRODUCTION.

This appendix describes the initial stages of an experimental project, which had the following objectives:

i) to test the theoretical predictions of this work regarding the influence of groove location and oil supply pressure on the vibrational characteristics of the single axial groove journal bearing (see Chapter 4).

ii) to provide, in the longer term, a basic test apparatus for examining the stability of a rotor supported in oil lubricated journal bearings.

Unfortunately, owing to a shortage of time and problems which were encountered with the instrumentation, it was only possible to design and construct the test apparatus. A description of the test apparatus is given, together with theoretical predictions of shaft behaviour and a discussion of the problems which were encountered.

IV. 2. DESCRIPTION OF THE APPARATUS.

The apparatus consisted of a steel rotor mounted horizontally on two, plain, cylindrical, oil lubricated journal bearings. The dimensions of the rotor are as shown in Figure IV.1. A photograph of the complete apparatus is shown in Figure IV. 2. For a more detailed specification of the test apparatus, the reader is referred to the detailed drawings in the Mechanical Engineering Department of Leeds University (drawing numbers A1 - 3911, 3912, 3914).

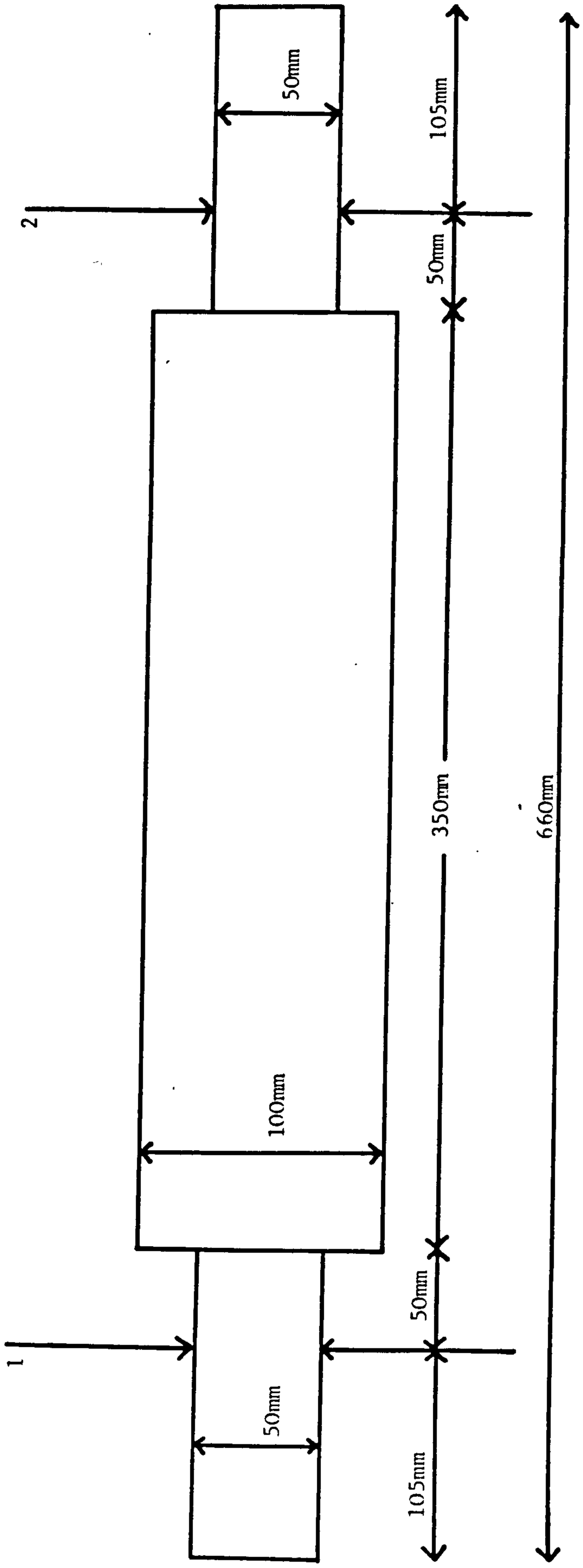

Figure IV.1. Dimensions of the rotor.

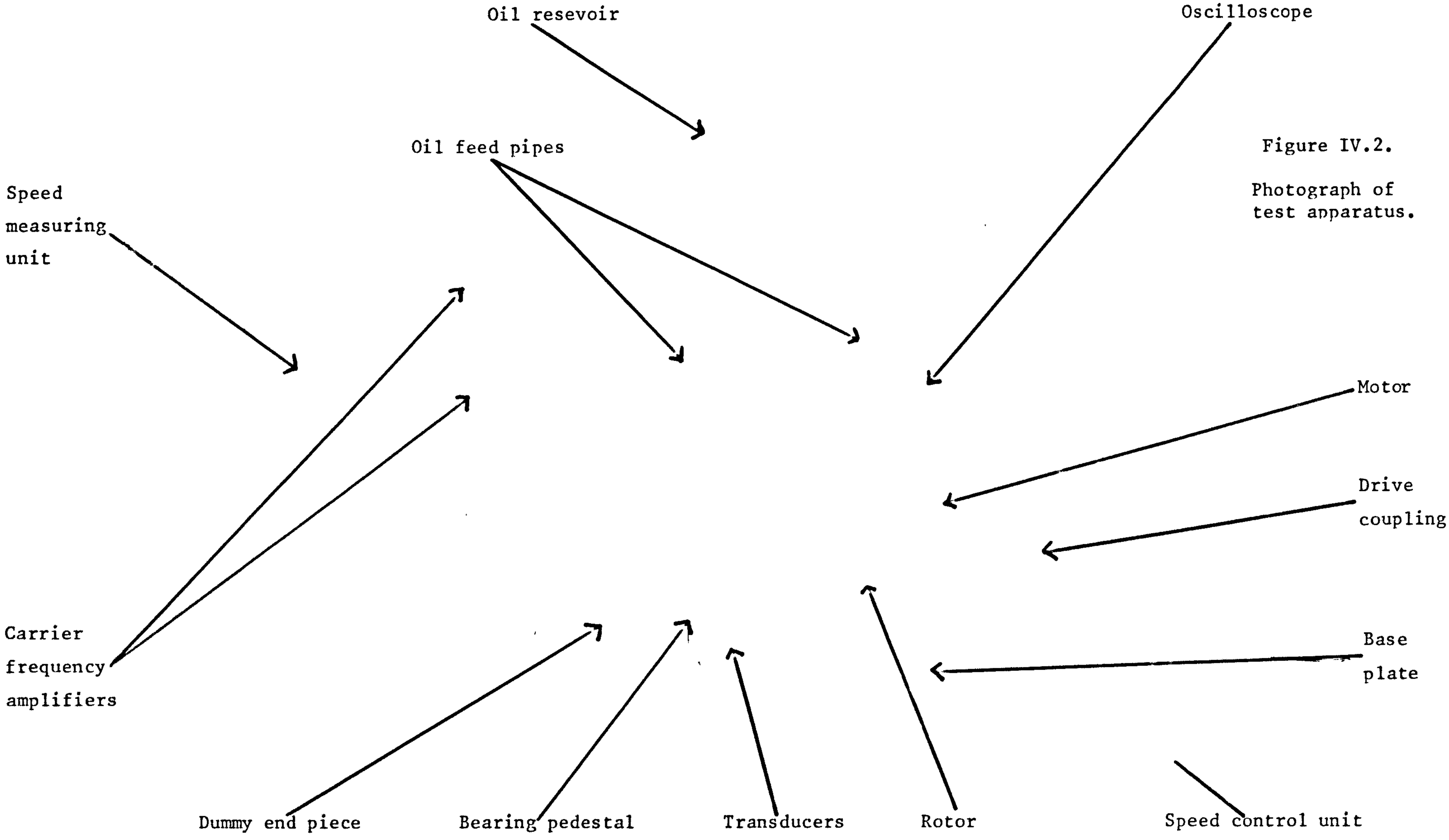

Figure IV.2.

Photograph of test apparatus.

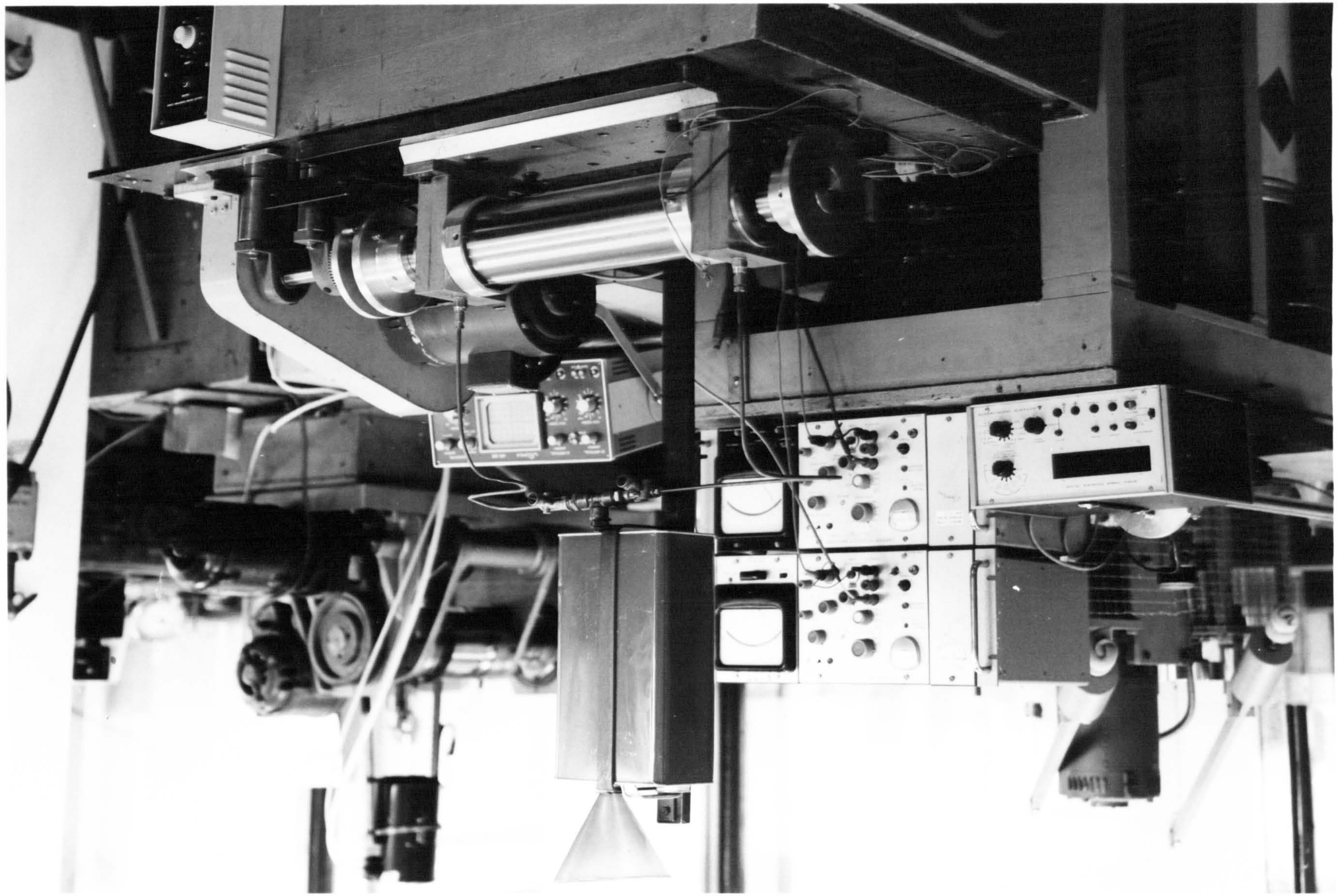

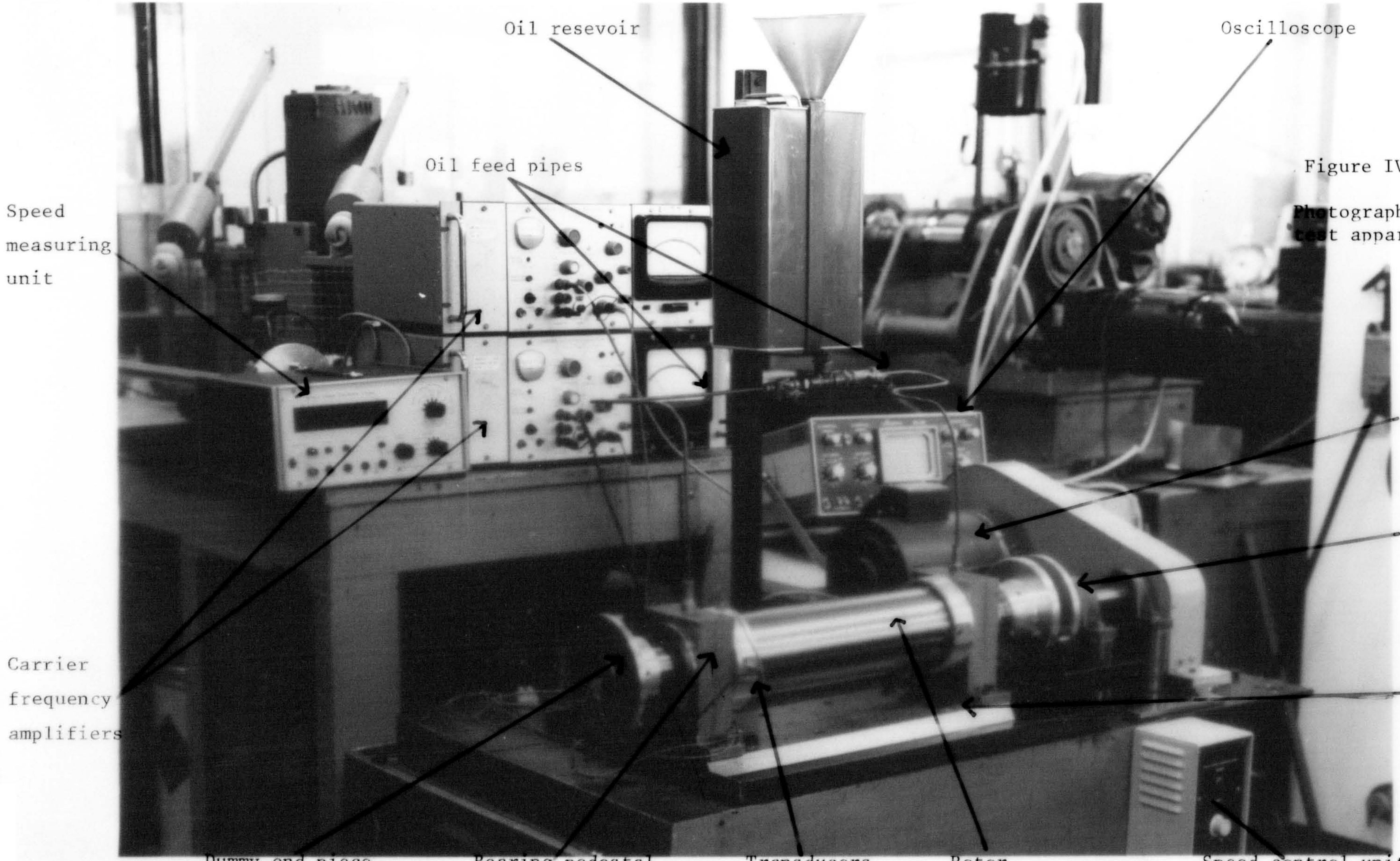

Figure IV.2.

Photograph of test apparatus.

The system was designed initially, by employing the results of Chapter 4 to predict the load capacity, steady state eccentricity ratio, attitude angle and the instability threshold speed of the rotor in the support bearings. When the basic dimensions of the rotor had been decided, a more comprehensive investigation of the rotor-bearing model was undertaken with the assistance of Dr. A. V. Ruddy (1981). A computer program, developed by Dr. Ruddy, was used to calculate the damped natural frequencies, critical speeds and response to mass unbalance of the rotor-bearing system. The theoretical behaviour of the rotor is discussed in section IV. 4.

The rotor was driven by an induction motor, attached to the rotor through a belt-coupling arrangement, such that the shaft could vibrate with minimal interference from the motor. The rotor speed could be continuously varied up to a maximum speed of 6500rpm.

The bearings were identical, plain, cylindrical journal bearings with the following dimensions:

axial length 50mm.

diameter 50mm. (L/D = 1)

radial clearance 0.14mm.

The lubricant used was a very light viscosity oil, Tellus R5 (μ = 0.004 Pas at 55^{o}C), which was fed into the bearing through an axial groove located in the bearing sleeve. The oil was supplied to the bearings under gravity, from a resevoir mounted above the rotor (Figure IV.2) - the small supply pressure due to gravity was sufficient to force the oil into the bearings.

In order to model as closely as possible the long bearing model described in Chapter 4, rubber seals were attached to the rotor to restrict side leakage from the bearings. This meant that, unless removed, oil would be continually circulating round the bearing, getting

hotter and hotter. This situation was avoided by providing an outlet groove just upstream of the inlet groove, so that some oil was forced out of the bearing during each revolution. It was hoped that this would be sufficient to achieve a stable operating temperature.

The bearings were specifically designed so that the bearing sleeve and hence the axial groove, could be rotated relative to the bearing pedestal. Therefore, the axial groove could be placed in any position relative to the loadline. The groove was fixed by screws located around the bearing pedestal.

INSTRUMENTATION.

The instruments which were used to measure the shaft displacement were:

i) four contactless displacement transducers of the inductance type.

ii) two carrier frequency amplifiers and bridges.

iii) an oscilloscope to observe the shaft orbit.

A speed measuring control unit with a magnetic pick-up was used to determine the rotational speed of the rotor. Some time was spent becoming familiar with the instrumentation and it was here that problems were encountered. A major difficulty was the setting up and calibration of the transducers.

Transducers.

Two matched pairs of contactless inductance displacement transducers were used to measure the horizontal and vertical displacements of one end of the shaft. The arrangement was as shown in Figure IV. 3. Ideally it should have been possible to measure the displacement of both ends of the shaft simultaneously. This was not possible because of a shortage of suitable transducers and carrier frequency amplifiers (four matched pairs of transducers and four carrier frequency amplifiers would have been required for this purpose).

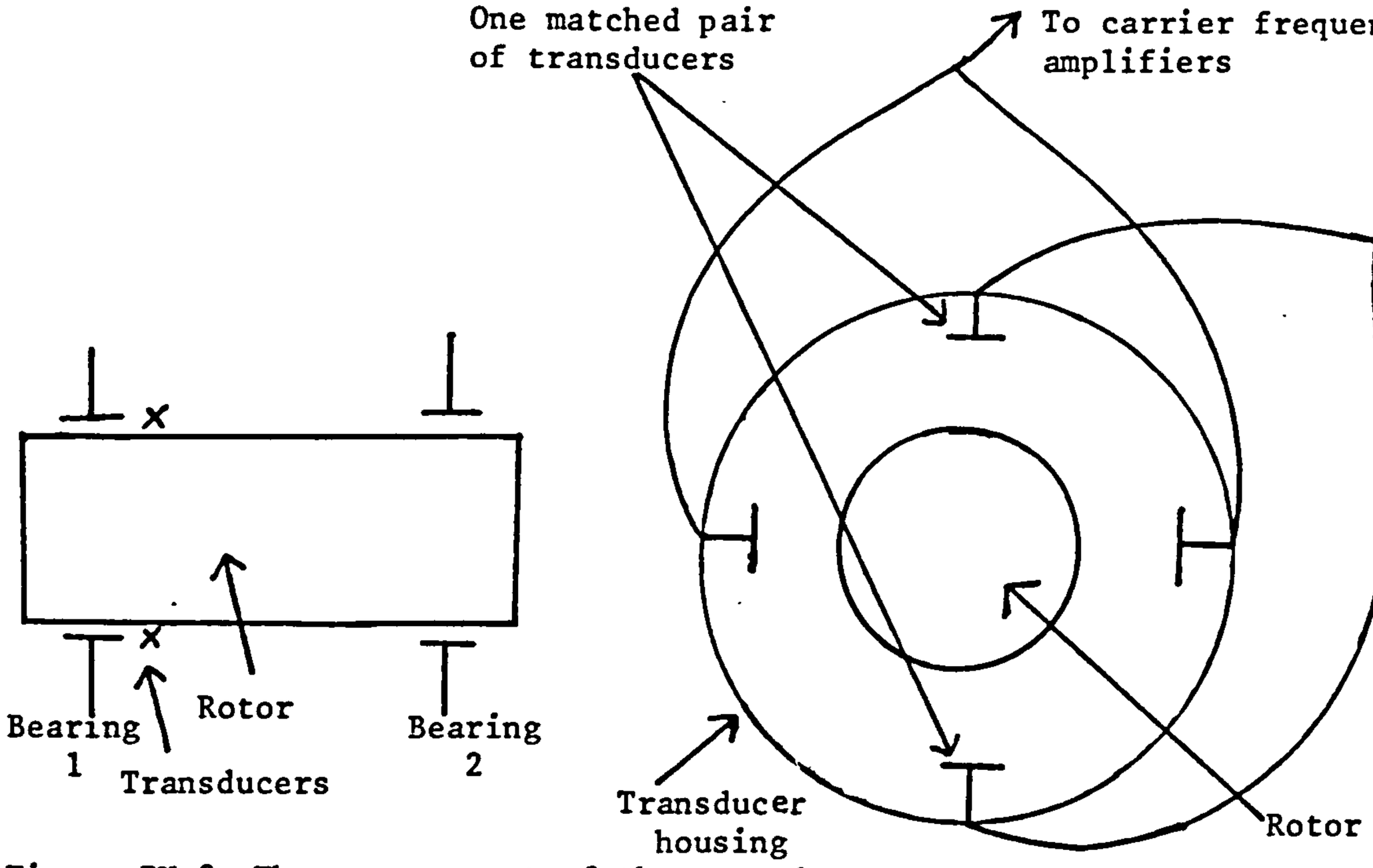

Figure IV.3. The arrangement of the transducers.

Initally, each transducer was set at a distance of 0.2mm from the rotor when it was central in its bearings. Special inserts were manufactured to enable this to be accomplished. The process also relied upon the careful design and manufacture of the apparatus, particularly in relation to the bearing pedestals.

Carrier Frequency Amplifier.

Each transducer pair was connected to a carrier frequency amplifier in a half bridge circuit, one for measuring the horizontal displacement and the other, the vertical displacement. The vibration levels were monitored by recording the linearised output of the amplifiers after demodulation on the accompanying meters. The two amplifiers were synchronised to avoid the phenomenon of beats.

The output signals were conected to the X and Y plates of an oscilloscope so that the shaft orbit could be observed directly.

IV.3. INITIAL TESTING, PROBLEM AREAS AND SUGGESTION FOR MODIFYING THE APPARATUS.

Having established the test apparatus and the instrumentation described in section IV.2, several major problems were encountered

when it was tried to carry out a meaningful experimental program.

The initial test procedure was:

i) The carrier frequency amplifiers were switched on and allowed to warm up:- this took approximately one hour. The oscilloscope was also switched on.

ii) The valves from the oil resevoir were opened to allow oil to flow into the bearings.

iii) The motor and speed measuring unit were turned on.

iv) The rotor speed was gradually increased to 1000rpm and the apparatus allowed to settle.

v) The meter readings showing the horizontal and vertical displacements of the rotor were recorded together with the rotor speed. The shaft orbit was observed on the oscilloscope.

vi) The rotor speed was increased by 500rpm and after a few minutes the same measurements were recorded. This was repeated up to a rotor speed of 6000rpm.

vii) The rotor speed was reduced gradually by 500rpm and the measurements again recorded.

A set of test results are shown in Table IV.1.

It was envisaged that a similar test program could be carried out for different groove positions and oil supply pressures. However, it became apparent that such a test program would only be meaningful if considerably more time than was available was spent on the instrumentation.

Various problems were encountered in the initial test stages.

i) When test runs were repeated, widely different results were obtained. This could have been due to "running in" of the machine, failure to allow the carrier frequency amplifiers to warm up sufficiently, or failure to set up the transducers properly (for example, by balancing them incorrectly). Another possibility was that the oil temperature was varying and hence altering the oil viscosity. It is clearly necessary to install thermocouples to measure the inlet and outlet temp-

Rotor speed rpm	Vibrometer readings Horizontal	Vertical	Rotor speed rpm	Vibrometer readings Horizontal	Vertical
1000	100	35	6000	53	20
1500	90	30	5500	50	20
2000	80	25	5000	50	20
2500	80	30	4500	55	22
3000	80	30	4000	55	20
3500	85	32	3500	55	20
4000	80	32	3000	80	35
4500	80	35	2500	82	35
5000	80	40	2000	82	30
5500	62	25	1500	90	35
6000	53	20	1000	100	35

Table IV.1. Some initial test results. Groove position 180°before loadline.

erature of the oil.

ii) No attempt was made to calibrate the instrumentation, owing to shortage of time. Vibrometer readings were merely recorded with no idea of the actual level of vibration. This is an important omission from the work and it is crucial that when the work is continued, considerable time and effort is spent on calibration. In theory, with the transducer arrangement described in the previous section, it is possible, after calibration, to measure actual journal displacements from the bearing centre.

iii) It was observed that the shaft orbit was not a simple closed orbit, but a series of loops. Typical orbits are shown below.

It is generally accepted that the occurence of double loop orbits is because the vibrations are made up of different frequency components eg. due to half frequency whirl and mass unbalance (full frequency whirl). The investigation could be simplified by filtering out any synchronous vibrations.

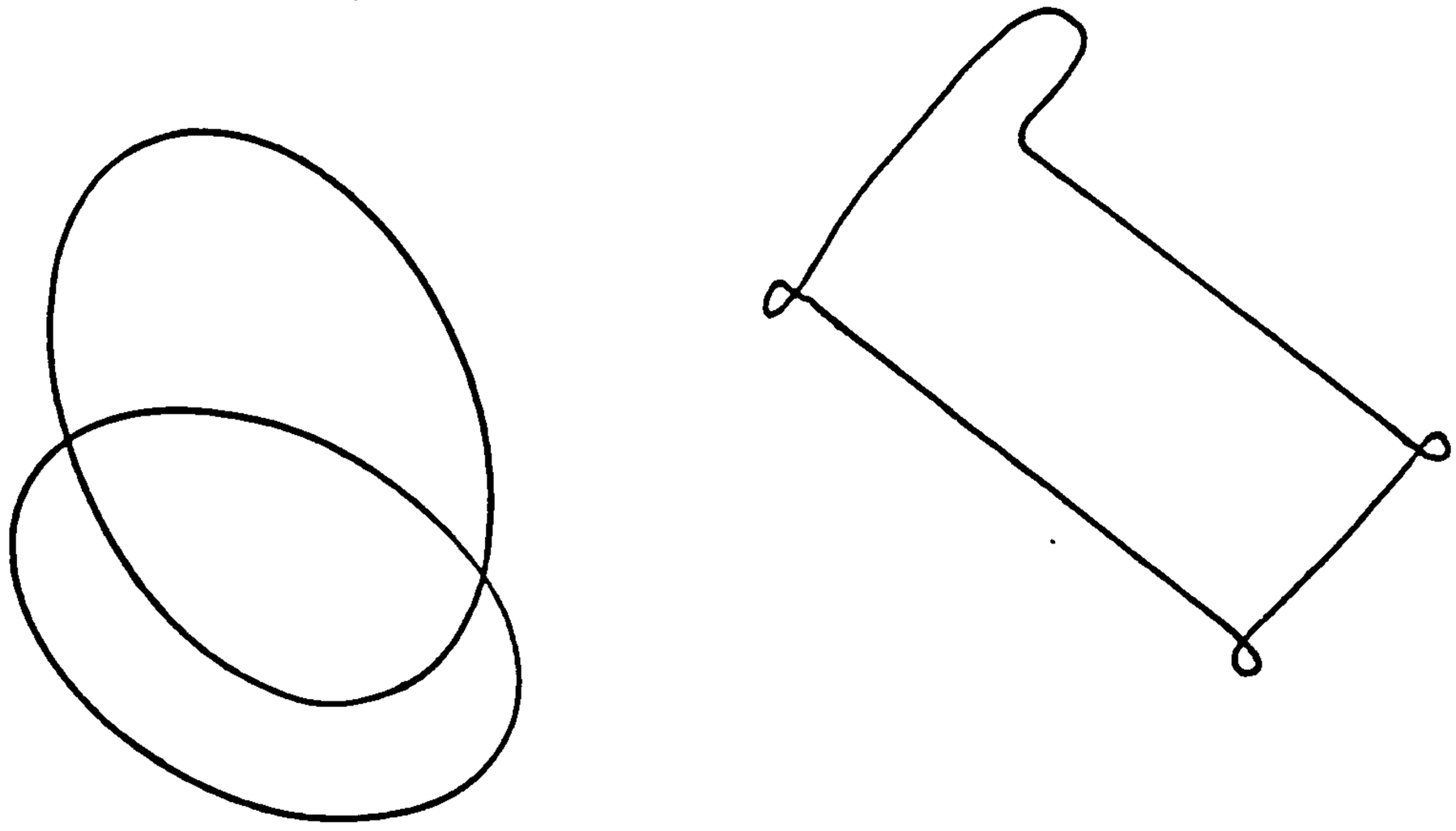

Figure IV.4. Typical orbits observed on the oscilloscope.

iv) Side seals were added to the bearings to restrict side leakage and so approximate to the long bearing model discussed theoretically in Chapter 4. At high speeds, it was noticed that oil was spraying from the seals. It is not possible to predict the effect of the rubber seals on the vibrational characteristics of the bearing. In future work, the side seals could be removed and a more comprehensive theory, which takes into account side leakage, could be used to predict the performance of the system.

IV.4. THEORETICAL PREDICTIONS OF THE ROTOR BEHAVIOUR.

Initially, in designing the test apparatus, the theoretical bearing characteristics reported in Chapter 4 were used to predict the behaviour of the rotor. A summary of this work is given in Table IV.2, which shows the Sommerfeld number, steady state eccentricity ratio, attitude angle and threshold speed for a range of rotor speeds and three different groove positions ($\beta = 30^{o}, 90^{o}, 180^{o}$). The threshold speed is predicted to be 1800rpm for $\beta = 180^{o}$, 4400rpm for $\beta = 90^{o}$ and 2100rpm for $\beta = 30^{o}$. This information was obtained from the stability chart shown in Figure 4.6.

A more comprehensive study of the theoretical behaviour was then

Groove position 30° before the loadline					Groove position 90° before the loadline					Groove position 180° before the loadline				
ω rpm	S	ε_s	ϕ_s^o	Stability?	ω rpm	S	ε_s	ϕ_s^o	Stability?	ω rpm	S	ε_s	ϕ_s^o	Stability?
500	0.06	0.92	14.0	Stable	500	0.06	0.85	29.9	Stable	500	0.06	0.79	52.5	Stable
1000	0.13	0.87	15.6	Stable	1000	0.13	0.69	39.1	Stable	1000	0.13	0.44	83.3	Stable
1500	0.19	0.83	16.5	Stable	1500	0.19	0.56	44 7	Stable	1500	0.19	0.29	87.7	Stable
2000	0.26	0.80	17.2	Stable	2000	0.26	0.45	48.3	Stable	2000	0.26	0.22	88.8	Un-stable
2500	0.32	0.77	17.6	Un-stable	2500	0.32	0.37	50.8	Stable	2500	0.32	0.17	89.3	Un-stable
3000	0.39	0.75	17.9	Un-stable	3000	0.39	0.31	52.4	Stable	3000	0.39	0.14	89.5	Un-stable
3500	0.45	0.73	18.1	Un-stable	3500	0.45	0.27	53.6	Stable	3500	0.45	0.12	89.7	Un-stable
4000	0.51	0.71	18.1	Un-stable	4000	0.51	0.24	54.4	Stable	4000	0.51	0.11	89.8	Un-stable
4500	0.58	0.70	18.2	Un-stable	4500	0.58	0.21	55.1	Un-stable	4500	0.58	0.09	89.9	Un-stable
5000	0.64	0.68	18.2	Un-stable	5000	0.64	0.19	55.6	Un-stable	5000	0.64	0.07	89.9	Un-stable
Threshold speed 2100rpm Whirl frequency 1800rpm (30Hz)					Threshold speed 4400rpm Whirl frequency 2200rpm (37Hz)					Threshold speed 1800rpm Whirl frequency 900rpm (15Hz)				

Table IV.2. Summary of theoretical predictions of the rotor-bearing system.

carried out by A. V. Ruddy (1981), who has developed a computer program to calculate the damped natural frequencies, normal modes, critical speeds and response to mass unbalance of a rotor-bearing system. The method used to perform the calculation is discussed fully by Ruddy (1980).

A summary of the investigation is shown in Figure IV.5., which shows the natural frequency curves as functions of the rotor speed for a groove position of 180^{o} before the loadline. The four lowest natural frequencies only are shown, corresponding to the four rigid body modes (two cylindrical and two conical whirling modes). The numbers on the curves indicate the logarithmic decrement of the vibration. When the logarithmic decrement changes sign from positive to negative, the stability threshold has been reached. It can be seen that the threshold speed is reached at a rotor speed of 1800rpm, when the mode corresponding to the lowest natural frequency becomes unstable. This result, as with those for the other groove positions, corresponds to the theoretical predictions made in Chapter 4.

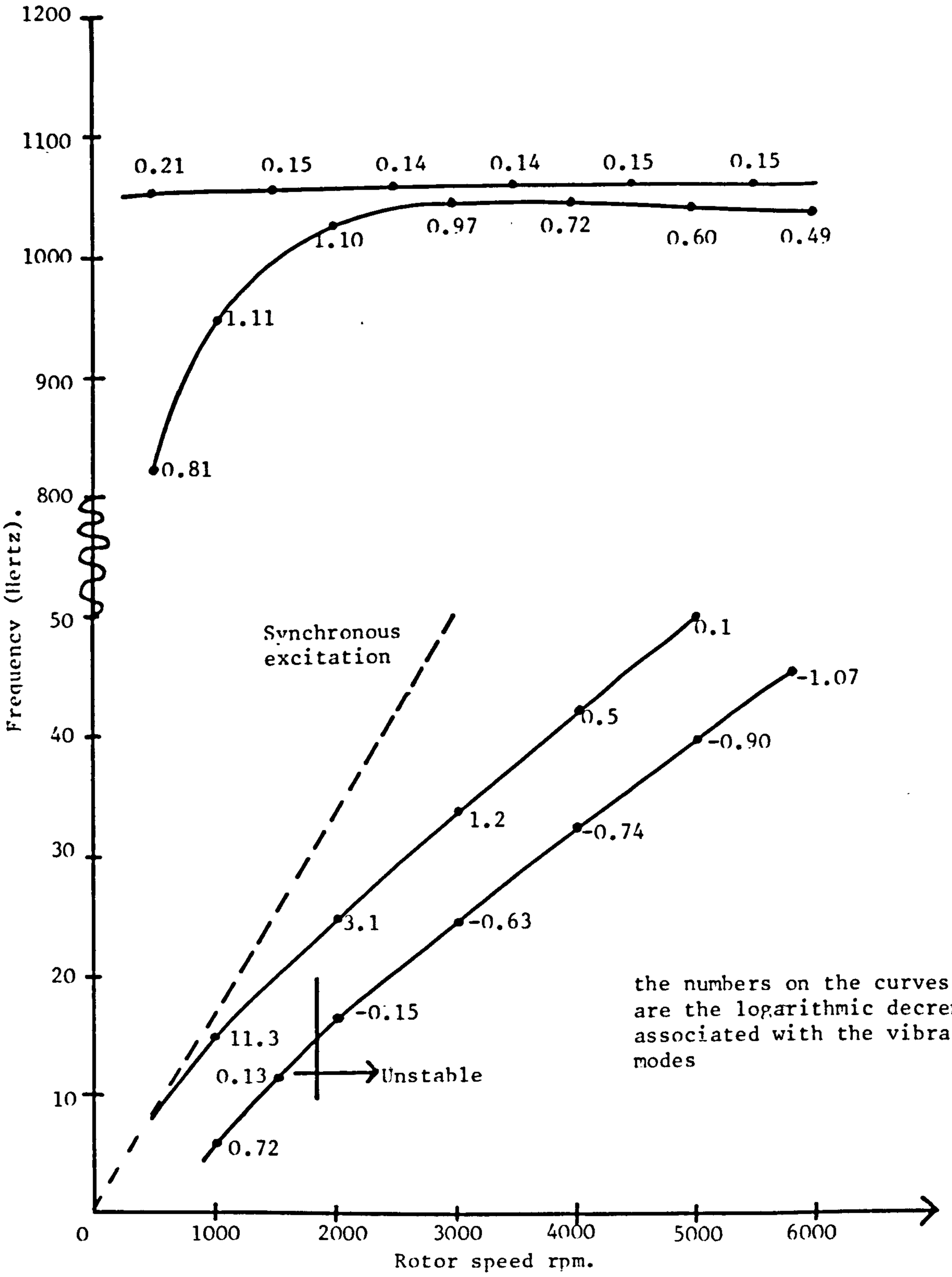

Figure IV.5. Damped natural frequencies of the rotor.